Zeitschrift: IABSE reports = Rapports AIPC = IVBH Berichte
Band: 73/1/73/2 (1995)

Rubrik: Poster Session 3: Bridges

Poster Session 3

Bridges
Ponts
Brücken

Leere Seite
Blank page
Page vide

Design of Togawa Bridge
Étude du pont de Togawa
Entwurf der Togawa-Brücke

Takeshi TSUYOSHI
Civil Engineer
East Japan Railway Co.
Tokyo, Japan

Takahiro KANNO
Civil Engineer
East Japan Railway Co.
Tokyo, Japan

Shuji TOMITA
Vice Chief
East Japan Railway Co.
Sendai, Japan

Yuki KOIWA
Civil Engineer
East Japan Railway Co.
Sendai, Japan

Shin'ichi SUZUKI
Civil Engineer
JR East Consultants Co.
Sendai, Japan

SUMMARY
Togawa Bridge is a three-span, continuous, partially prestressed, concrete through-girder bridge with an open floor for railways. This bridge is located in an area of much snowfall, so an open floor type with a mounted track is adopted for the first time in Japan for prestressed concrete girders. This paper reports on the outline of the design of this bridge.

RÉSUMÉ
Le pont de Togawa est un pont ferroviaire à plancher ouvert, formé de 3 travées continues et dont les poutres sont en béton partiellement précontraint. Il fallut, pour que le pont puisse être utilisé dans une zone fortement enneigée, adopter pour la première fois au Japon sur ce genre d'ouvrage, la technique de plancher ouvert. L'article présente le projet du pont.

ZUSAMMENFASSUNG
Die Togawa-Brücke ist eine teilweise vorgespannte Eisenbahn-Trogbrücke, die drei Felder durchläuft. Wegen dem vielen Schnee ist der Tafelträger teilweise geöffnet und die Schiene wird direkt mit den Tafelträger verbunden. Es ist das erste Mal in Japan, dass dieser Typ von Schienenverbindungen einer teilweise vorgespannten Brücke aufgenommen wird. Im Bericht wird der Entwurf vorgestellt.

1. INTRODUCTION

Togawa Bridge is a three span continuous partially prestressed concrete through girder with an open floor for railways. The total length of this bridge is 114.8 meter, the main span is 40.0 meter, and the height of the main girder is 2.5 to 3.0 meter. This bridge is constructed at the area where is famous to have much snow in winter, so the open floor type with a mounted track (Fig.1) is adopted in order to reduce snow on the bridge without maintenance works. Construction of this bridge is a part of river improvement works of the Togawa River. At first, the temporary track is executed adjacent to the present railway bridge, and next, the present bridge is withdrawn and the new bridge is constructed. The superstructures are executed on site by a staging with bent and girder during drought period.

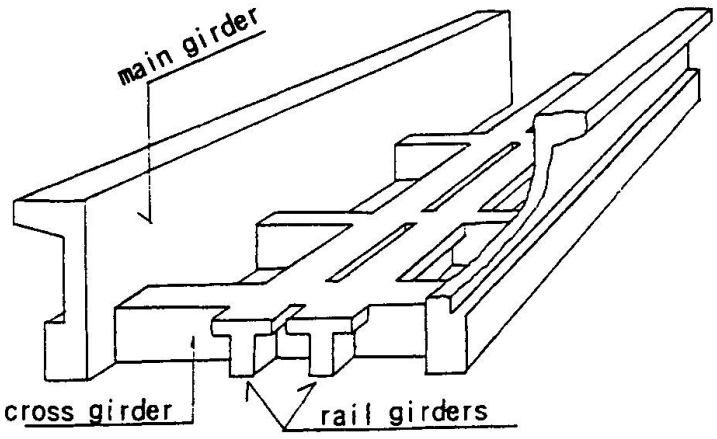

Fig. 1 Image of This Girder

Then, rubber bearings and damper stoppers are adopted for bearings. This combination is generally for railway concrete girders in Japan. Damper stoppers are not resistant against slowly horizontal movements by variations of temperature, creep, drying shrinkage and so on,and are resistant by viscosity of oils in dampers against abruptly horizontal movements by earthquakes.

2. PROCEDURES OF CONSTRUCTION OF SUPERSTRUCTURES

Table 1 shows the proceduresof construction of the superstructures of this bridge. For this structural type like this brige, more larger prestressing stresses are necessary for girders which support tracks directly (we call this girders rail girders in this report) than for main girders. So, if prestressing forces are introduced after completion of all members, too much prestressing strands are necessary to give enough prestressing stresses to rail girders.

Therefore, prestressing strands arranged in rail girders are planned to be tensioned before main girders are casted. Then, after completion of all members, because the concrete stress level are rather different in rail girders and main girders during permanent loads,large statically interminate forces occur by the influence of creep. Therefore, to make creep deformations as small as possible, prestressing strands arranged in rail are also planned to be tensioned just before the completion of connected parts with main girders and cross beams are executed.

Table 1 Procedures of Construction

1	Setting a Staging
2	Executing Rail Girders and Cross Beams
3	Introducing Prestressing Forces in Rail Girders
4	Executing Main Girders
5	Introducing Prestressing Forces in Two Cables in Cross Beam
6	Introducing Prestressing Forces in Three Cables in Main Girder
7	Introducing Prestressing Forces in Rest Cables in Cross Beam
8	Introducing Prestressing Forces in Rest Cables in Main Girder
9	Withdrawing a Staging
10	Executing the Second Part of Rail Girders

Then, because a mounted track is adopted in this bridge, in consideration of executed errors,unexpexted elastic deformations and so on, 5 cm height-part of rail girders are not structural members not but adjusting parts to keep the rail level.

3. OUTLINE OF DESIGN OF THIS BRIDGE

Fig.2 shows a general view of this bridge, Table 2 shows general design conditions, and Table 3 shows the material strength. Rail girders and cross beams, to which train live load act directly and which have the necessity to convey these load to main girders surely, are designed as prestressed concrete members. And main girders are design as partially prestressed concrete members which have low concrete compressive stresses by prestressing forces and small creep deformations in consideration that a mounted track is adopted in this bridge. For prestressed concrete members, design verifications are carried out to the ultimate limit state and the serviceability limit state. And, for partially prestressed concrete members, verifications are carried out to the ultimate limit state, the ultimate limit state of fatigue, and the serviceability limit state. Representative combinations of loads to each limit state are indicated in Table 4. For partially prestressed concrete members, concrete tensile stresses are restricted within the design tensile strength during the permanent

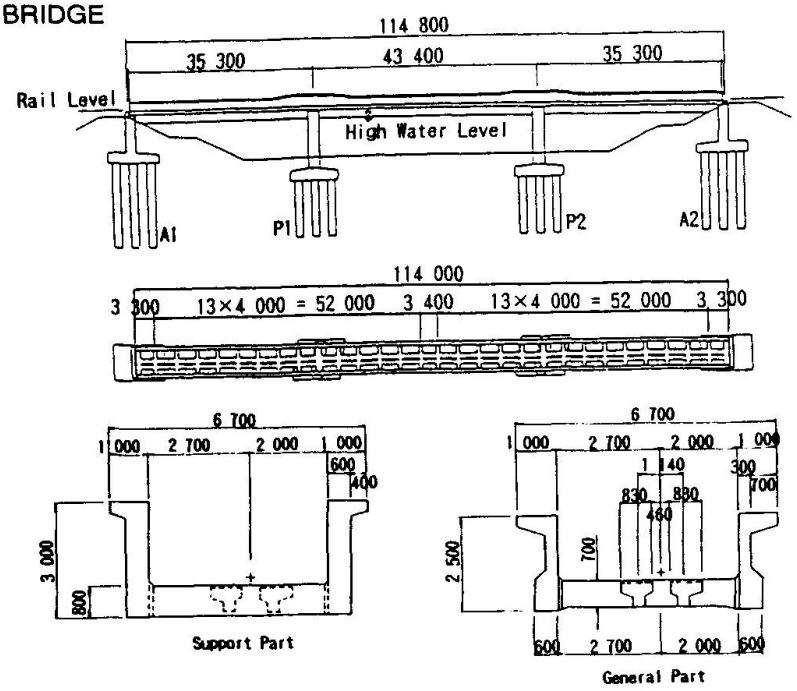

Fig.2 General View of This Bridge

Table 2 General Design Conditions

Length of Bridge (m)	114.8
Spans (m)	35.3+43.4+35.8
Alignment of Track	Straight
Track Type	Mounted Track
Design Horizontal Seismic Coefficient	Kh=0.2
Shoe Type	Rubber Shoe
Stopper Type	Damper Stopper

Table 3 Material Strength

Member	Design Compressive Strength of Concrete	Prestressing Strand Tensile Strength	Reinforcement Yield Strength
Main Girder	39.2 (MPa)	SWPR7B 12T12.7 1862 (MPa)	SD345 343 (MPa)
Cross Beam	44.1 (MPa)	SBPR 95/110φ32 1078 (MPa)	SD345 343 (MPa)
Rail Girder	44.1 (MPa)	SWPR7B 12T12.7 1862 (MPa)	SD345 343 (MPa)

Table 4 Main Combinations of Loads (Load Factor)

Verification		Dead Load	Train Load	Impact Load	* 2
Ultimate Limit State		1.7	1.7	1.7	1.0
* 1	Bending Tensile Stress of Concrete (PPC)	1.0	—	—	1.0
	Bending Tensile Stress of Concrete (PC)	1.0	1.0	1.0	1.0
	Bending Compressive Stress of Concrete	1.0	—	—	1.0
	Diagonal Tensile Stress of Concrete	1.0	1.0	1.0	1.0
	Bending Crack Width for Durability (PPC)	1.0	0.2	0.2	1.0
	Bending Crack Width for Appearance (PPC)	1.0	—	—	1.0
	Deformation	—	1.0	—	—
Ultimate Limit State of Fatigue		1.0	1.0	1.0	1.0

* 1 : Serviceability Limit State

* 2 : Statically Indeterminate Forces by Prestressing Forces, Creep and Shrinkage

PPC : Partially Prestressed Concrete Member

PC : Prestressed Concrete Member

loads in order that bending cracks do not occur until train live loads act. It is because the bending crack width becomes rather large by the influence of creep and local drying shrinkage, if cracks occur in younger concrete age. And then, also for partially prestressed concrete members, in the serviceability limit state, diagonal tensile stresses in concrete are restricted not to be occurred by shear cracks. This is because the design method to shear cracks can not be necessarily said to be cleared up.

Fig.3 shows the analysis model for completion. In the design works of concrete through girders, plane grid frame analysis is usually adopted, but in this design, grade grid frame analysis is adopted. The reason is that the axial forces in rail girders occurred by the bending deformations of main girders are not able to be estimated by plane analysis. Then, section forces are calculated by grade model in which centroids of main girders and rail girders are connected by virtual members. Infinite stiffnesses are given to these virtual members.

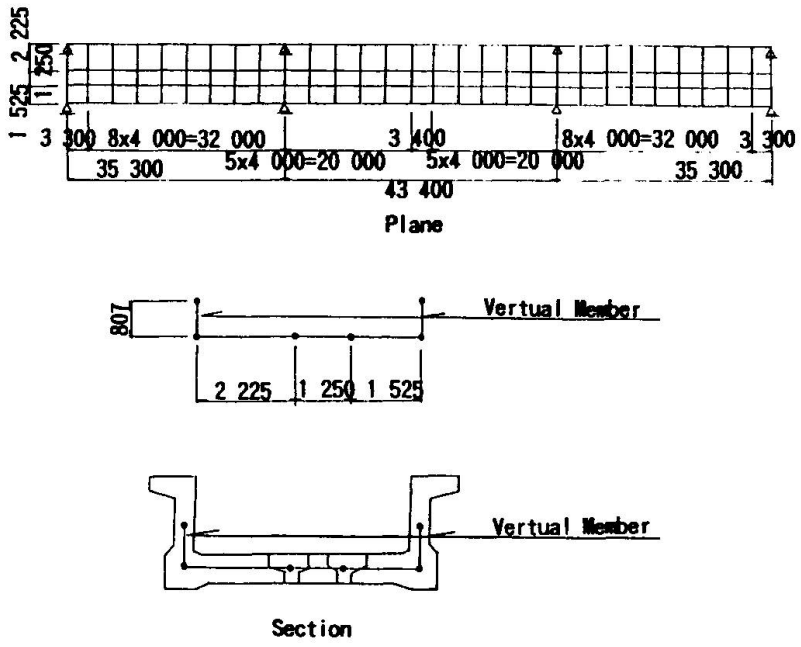

Fig.3 Analysis Model

4. DESIGN OF MEMBERS

4. 1 MAIN GIRDERS

In this bridge, rail girders are arranged eccentric in the cross direction, so section forces are different between the right and the left main girder. Design verifications are carried out only the larger section forces in the two main girders. As for prestressing cable system, Freyssinet 12T12.7 is adopted, and as for axial reinforcements to control bending cracks, deform 19 and 22 are arranged. Fig.4 shows the cable and axial rein-

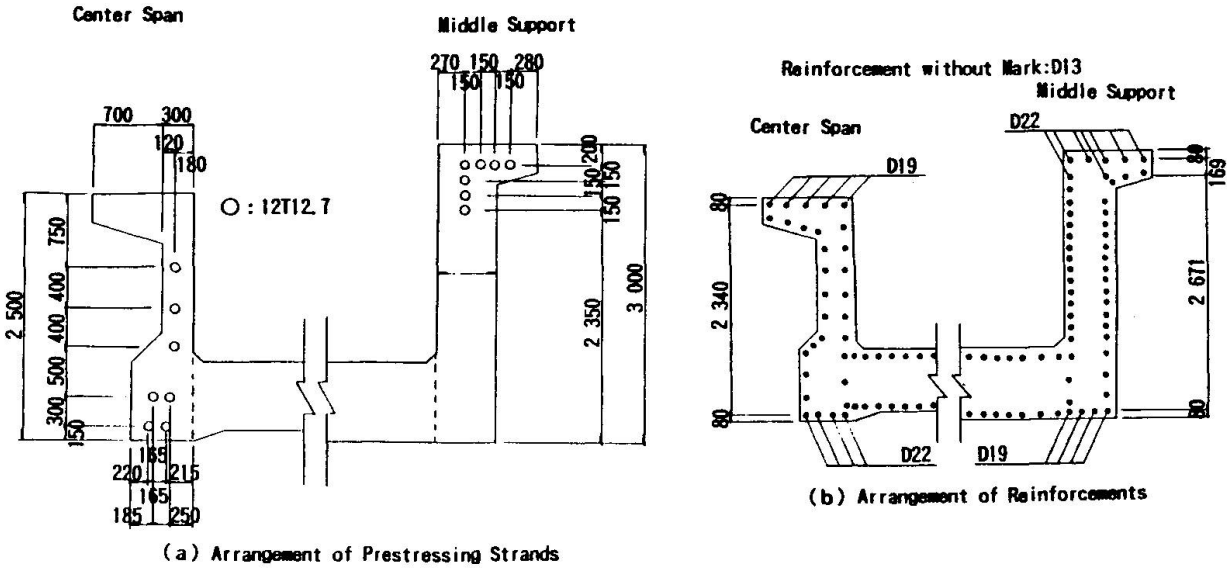

Fig.4 Arrangements of Prestressing Strands and Reinforcements

forcement arrangements at the center span section and the middle support section. As mentioned before, main girders are designed as partially prestressed concrete members, so axial reinforcements are much arranged than prestressed concrete members as usual. By this reasons, resistant forces in reinforcements are rather larger against deformations in the axial direction by prestressing forces, creep, drying shrinkage and so on. So, this influence are considered in this design. Table 5 shows design results of concrete stresses during permanent loads, the ultimate limit state, and the ultimate limit state of fatigue in main sections. Further, the verifications of the maximum bending crack width in the serviceavility limit state are carried out under the load conditions shown in Table 4, so, this time,agaist these loads' combinations, bending cracks do not occur. Next, the arrangements of stirrups are mensioned. In this bridge, diagonal tensile stresses inconcrete is restricted within the design tensile strength in the serviceability limit state not to be ocurred by shear cracks. Then, stirrups are arranged against the ultimate limit state. Generally, stirrups in the main girders are both as hanging reinforcements for lower slabs. In this bridge, assumed the punching shear failure surface in Fig.5, in these section, stirrups are calculated both as stirrups for shear forces and the punching forces by cross beams in the ultimate limit state.

Table 5 Design Results of Main Girders

			Center of Side Span	Middle Support	Center of Main Span
Number of Prestressing Cables			7	7	7
Number of Reinforcements		Upper Verge	D 1 9 × 5	D 2 2 × 7	D 1 9 × 5
		Upper Verge	D 2 2 × 4	D 1 9 × 4	D 2 2 × 4
Ultimate Limit State		Safety Ratio (Bending)	1.63	1.46	1.88
* 1	Concrete Stress at Parmanent Load (MPa)	Upper Verge	5.81	1.84	3.90
		Lower Verge	3.64	4.30	2.74
		Limit Value	−1.86~15.68		
	Bending Crack Width (mm)	Calculated Value	———	———	———
		Limit Value	0.004 c (c : covering)		
	Diagonal Tensile Stress of Concrete at Design Load (MPa)	Without Torsion	−0.10	−1.72	−0.02
		With Torsion	−0.10	−1.76	−0.02
		Limit Value	−2.06		
* 2	Prestressing Strand (MPa)	Stress Variation	37.85	43.82	40.73
		Strength of Fatigue	256.85	294.75	341.78
	Reinforcement (MPa)	Stress Variation	42.48	49.99	45.55
		Strength of Fatigue	343.00	343.00	343.00

* 1 : Serviceability Limit State

* 2 : Ulitimate Limit State of Fatigue

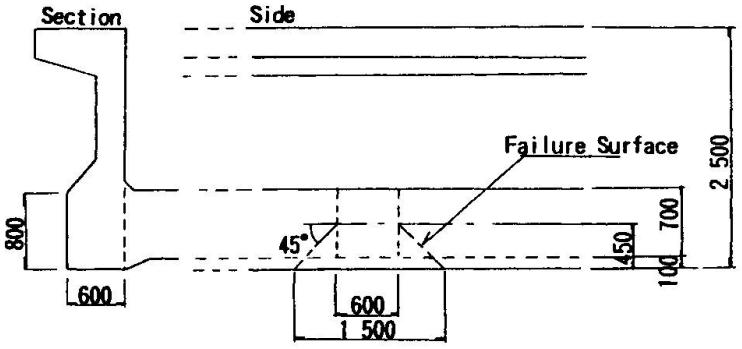

Fig.5 Assumption of Shear Failure Surface

4. 2 RAIL GIRDERS

This members are design as prestressed c oncrete members. In consideration of thes afety side, the bending moments are cal-c ulated by the 3 span continuous frame model assumed that connected parts with cross beams are hinge supports, and the d esign is carried out against this bending m oments and other section forces by

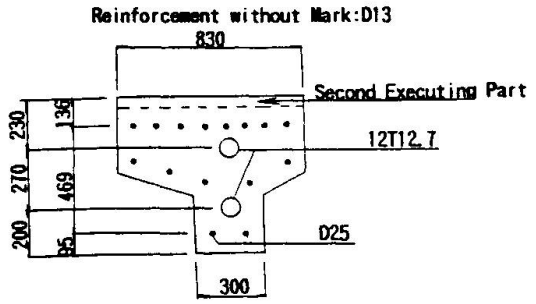

Fig.6 Arrangements of Prestressing Strands

grade grid frame analysis. Fig.6 shows the arrangements of prestressing cables.and axial reinforcements. Table 6 shows the design results of the ultimate limit state and the serviceability limit state.

Table 6 Design Results of Rail Girders

			Crossing Part with Cross Beam	Center between Cross Beams
Number of Prestressing Cables			2	2
Ultimate Limit State	Safety Ratio (Bending)		6.43	2.83
* 1	Concrete Stress at Parmanent Load (MPa)	Upper Verge	5.59	6.01
		Lower Verge	6.67	6.00
		Limit Value	0 ~ 17.64	
	Concrete Stress at Design Load (MPa)	Upper Verge	2.04	9.20
		Lower Verge	7.92	2.46
		Limit Value	−2.07	
	Diagonal Tensile Stress of Concrete at Design Load (MPa)	Without Torsion	−0.01	−0.04
		With Torsion	−0.11	−0.29
		Limit Value	−2.01	

* 1 : Serviceability Limit State

4. 3 CROSS BEAMS

Rather large out-of-plane forces by prestressing forces in main girders and the defference of axial deformations between main girders and rail gerders act to cross beams. So, verifications for safety are carried out to two directions. And, by grade grid frame analysis, minus bending forces scarecely occur at connected parts of cross beams and main girders mainly by vertical and torsional deformations in main girders. But, also in consideration of thesafety side, this parts are design minus moments equal to one-half of plus bending moments at the center span of cross beams by grade grid frame analysis. Then, cross beams have the same stiffness except ones on supports. Each cross beams has different section forces. But, this design, to make the design works simple, the design iscarried out reprezentative section forces.

5. CONSIDERATION FOR VERTICAL DEFORMATIONS

Because the mounted track type is adopted, it is very important to make vertical deformations by creep smaller for views of the maintenance works and the comfortness of train-running. So, special verifications are carried out for the vertical deformations in main girders which give much influences to deformations of the total structures. Then, concrete stresses at the upper verge and lower verge during permanent loads are design to be as ballanced as possible. By this considerations, vertical deformations by creep can be reduced, and if the errors of stifness and creep coefficient ocurr, these influence to rails can also be reduced.

6. CONCLUSION

This paper reports on the outline of the design of partially prestressed concrete through girder with open floors adopted first time in Japan. In areas where works of getting rid of snow are very hard in winter, this type seems to be much effective if only considerations for vertical deformations are taken adequately. We hope this report will of some use in the design of concrete bridges in which maintenance works are reduced.

Rebuilding of the Bridge Over the River Damuji in Cuba

Reconstruction du pont sur la rivière Damuji à Cuba

Wiederaufbau der Brücke über den Fluss Damuji in Kuba

José H. DIAS FERRER
Civil Engineer
E.P.O.T.
Havana, Cuba

José H. Días Ferrer, born in 1937, obtained his degree in civil engineering at the University of Havana, Cuba. He designs and constructs bridges and diverse structures. His research interests include the analysis of prestressed concrete by limit state method and applied soil mechanics. He is an engineer, consultant and specialist in bridge design.

SUMMARY

This paper deals with the reconstruction of a prestressed concrete Gerber bridge, partially collapsed due to the collision of a bus and a truck-mounted crane and the corrosion of the vertical anchoring cables of the deck in one of its abutments. Different studied alterna-tives are described here and a technical-economical comparison between them is also made, enumerating the difficulties of the most economical one, showing the adopted solutions in each case.

RÉSUMÉ

L'article présente la reconstruction d'un pont Gerber en béton précontraint qui a été partiellement détruit lors de la collision d'un autocar et d'une grue mobile et résultant de la corrosion des câbles d'ancrage verticaux du tablier dans l'une des culées. Différentes études sont décrites et une comparaison technique, économique est présentée énumérant les difficultés de la solution la plus économique et indiquant la solution retenue.

ZUSAMMENFASSUNG

Der Beitrag behandelt den Wiederaufbau einer vorgespannten Gerber-Brücke, die nach Anprall eines Busses und eines Kranwagens teilweise einstürzte, mitverursacht durch die Korrosion vertikaler Verankerungskabel in einem der Auflagen. Unterschiedliche Konstruktionsmöglichkeiten werden in technischer und wirtschaftlicher Hinsicht miteinander verglichen, die Schwierigkeiten der Bestvariante erläutert und die jeweils gewählten Lösungen dargestellt.

1. DESCRIPTIONS.

1.1. Schematic description.

This prestressed concrete bridge (12 ϕ 7mm.Freyssinet cables) with a (10.00 m. +65.00 m. + 10.00 m.) sketch has a principal structure or deck composed by two extreme Gerber 30.00 m. longs and a simply supported 25.00 m. beam. The 30.00 m. Gerber beams are distributed in 10.00 m. extreme spans and 20.00 m. cantilevers close to the central bay. Deck cross section (1.50 m.+ 6.00 m.+ 1.50 m.) has been achieved with box girders for the extreme 10.00 m. spans and for the first 5.00 m. cantilevers; for the 15.00 m. extreme cantilevers and the central simply supported beam, "T" sections have been used. Longitudinally, the height of the deck section varies between 1.25 and 3.00 m.

1.2. Functional description.

As can be appreciated, extreme 10.00 m. spans are not able, by themselves, to compensate or balance the central bay; consequently, these spans are anchored, in their extremes, to their respective massive abutments, by vertical cables pressing the deck against the top of the above mentioned abutments and guaranteeing the deck stability under dead and live loads. These anchoring cables were designed with a working force of 6 400 kN and a breaking force of 10 000 kN.

1.3. Collapse description.

Due to a defficiency in design, vertical cables to anchor the deck to the abutments had not enough anticorrosive protection; due to this fact, those cables were submitted to corrosion in the contact zone between the abutment and the deck in the side next to Abreus town, since there was penetration of moisture, in that zone, through the cavities due to the non coincidence of the different contact surfaces and due to the separation between those surfaces provoked by the crossing of great loads; this corrosion was weakening the cables' cross sections until the appearance of live loads (a truck-mounted crane and a bus) making these corroded cables reach to breaking stresses. When the cables were broken, occurred excessive surcharge to the adjacent cables, making them break as a chain action and reaction.

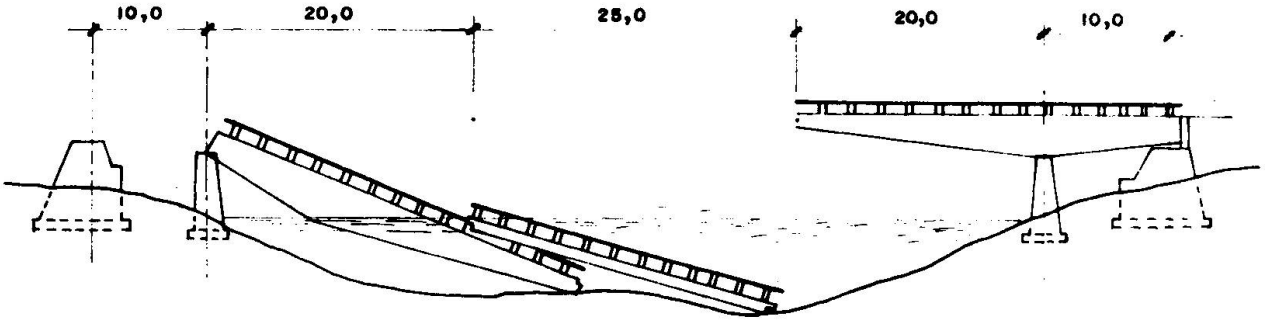

ELEVATION

FIG. 1

After collapsing, only one Gerber beam remained in place while the other sank in

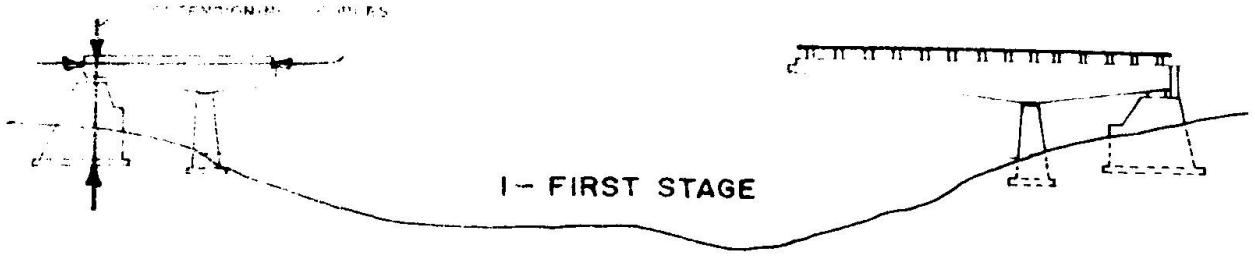
1 – FIRST STAGE

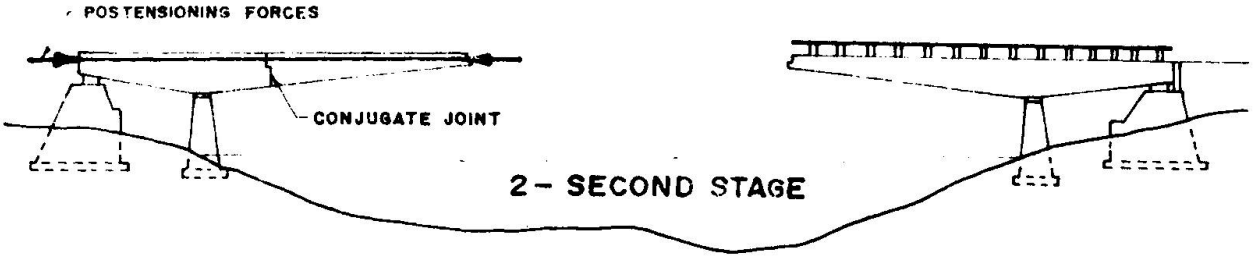
POSTENSIONING FORCES
CONJUGATE JOINT
2 – SECOND STAGE

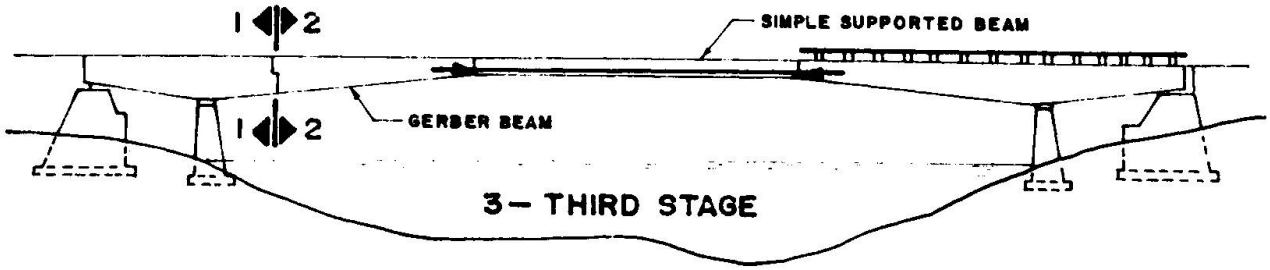
1
2
SIMPLE SUPPORTED BEAM
GERBER BEAM
3 – THIRD STAGE

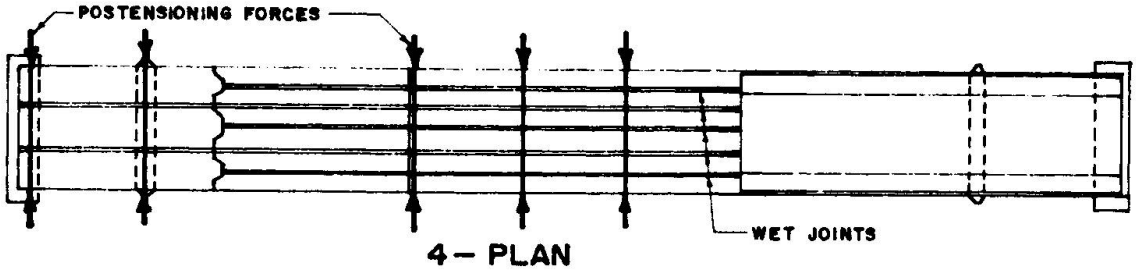
POSTENSIONING FORCES
WET JOINTS
4 – PLAN

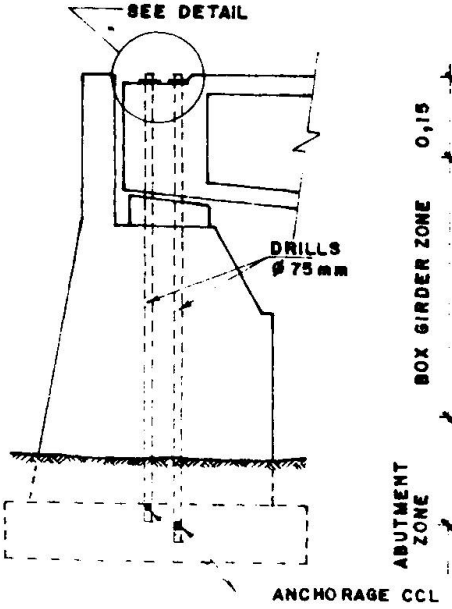
SEE DETAIL
DRILLS
ø 75 mm
ANCHORAGE CCL
5 – BOX GIRDER ANCHORING

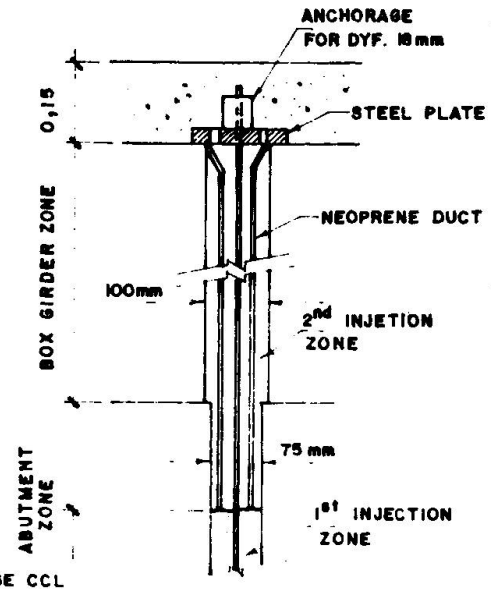
ANCHORAGE
FOR DYF. 18mm
STEEL PLATE
NEOPRENE DUCT
100mm
2nd INJETION
ZONE
75 mm
1st INJECTION
ZONE
0,15
BOX GIRDER ZONE
ABUTMENT
ZONE
6 – ANCHOR DETAIL

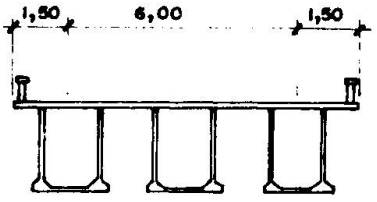
1,50
6,00
1,50
7 – SECTION 1–1

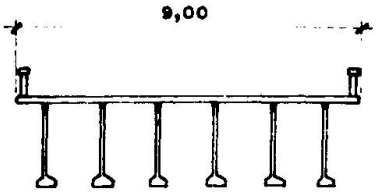
9,00
8 – SECTION 2–2

FIG. 2

an inclined position with its main part inside the river water.The single central simply supported 25.00 m. beam remained totally submerged in bent position too (see fig. 1).

2. STUDIED ALTERNATIVES.

2.1.Counting of the alternatives.

2.1.1. Bridge of single spans, utilizing the existing supports and creating new piers.
2.1.2. Bridge of single spans, changing its location.
2.1.3. Gerber bridge with a 65.00 m. central span and extreme compensation 53.00m. spans (to avoid vertical cables).
2.1.4. Repetition of the above mentioned sketch, keeping the non collapsed part (reconstruction).

3. COMMENT AND ECONOMICAL APPRAISAL OF THE STUDIED ALTERNATIVES.

3.1.Comment.

Alternatives 2.1.1 and 2.1.2 partly coincided, because both stated primarily to demolish part of the existing Gerber beam and a partial demolition of the collapsed Gerber beam that remained out of the water, with a cost of 10 000.00 Cuban pesos; secondly, creation of new supports was stated in order to create smaller spans; then, the bridge to construct would cost 204 000.00 Cuban pesos, and in case of 2.1.2 alternative, the road length to construct would cost 55 900.00 Cuban pesos. Summarizing, alternative 2.1.1 would cost 214 000.00 Cuban pesos, even without evaluating extra cost of foundations in the zone of submerged superstructure, and alternative 2.1.2 would cost 269 900.00 Cuban pesos. As for alternative 2.1.3, extreme 53.00 m. spans are necessary to compensate the central 65.00 m. span; so, this aternative will become a Gerber bridge with a length of 171.00 m. and taking into account demolitions, this alternative would cost 220 400.00 Cuban pesos. Analizing alternative 2.1.4, can be seen that the reason to build extreme 10.00 m. spans with vertical cables, anchored to the mass of the abutments, is to save 86.00 m.of bridge, that is, a bridgelength practically the same as the mentioned bridge (85.00 m.long) can be saved and taking into account that it would only be necessary to construct 55.00 m. of deck, without foundations and that it would not be necessary to demolish the non collapsed span, this alternative, 2.1.4, would only cost 68 000.00 Cuban pesos.

4. DIFFICULTIES FACED RESPECT TO THE ALTERNATIVE REPEATING THE EXISTING SKETCH AND KEEPING THE NON COLLAPSED PART.

4.1.Lack of confidence.

At the same time than distrust arisen with vertical cables, because this was not the first project where they have presented problems, there was the doubt about what could happen with the remaining in the non collapsed span, up to that moment.

4.2. How to conjugate joints, shortage of wood to make forms and limitations with the hoisting equipment.

At the time of the analysis of this topic, it was thought that deck concreting should be made directly on the site ("in situ") in order to solve the problem of conjugate joints in the transition section from box to precast "T"-shaped girders (see fig 2.7 and 2.8). At that time, there was no available wood for formwork, and precasting of the box-sectioned length would result in a huge member for which there was no joisting equipment.

5. SOLUTION OF THE PROBLEM WITH THE ALTERNATIVE OF THE REPETITION OF THE SKETCH, REMAINING THE NON COLLAPSED LENGTH.

5.1.Updating.

The first step was to check whether the non collapsed zone fulfilled the requirements of the Codes in force in Cuba (about critical sections); this turned out be satisfactory. The following was to undertake the solution of all the different problems (see fig 2.5).

5.2. Anticorrosive isolating sheaths.

In this case, it cannot only be relied on mortar grouting, because, in this section, it breaks and moisture can penetrate up the reinforcement; then, it is necessary to wrap the cables with a neoprene sheath and, afterwards, to inject the mortar.

5.3. Vertical anchoring holes and cable placing.

As this case is a postensioned structure, in the initial case cables were kept embedded in the mass of the abutment and anchored in the lower zone, reserving an upper zone for elongations; this was solved practicing vertical holes in the mass of the abutment and putting one cable in each one with fixed anchorage grips in their lower extremes. Later, cement gel was grouted, forming an embedding column for cables and of frictional force transference between the column and the drilled hole; the upper zone of the drills remained as elongation, anticorrosive or neoprene sheath zone, and final grouting (see fig 2.5 and 2.6).

5.4. Tests.

Though the heights of those mortar columns were calculated, as there was no previous experience, six test drillings were made, properly located in non interference zones. The outcomes of the tests were satisfactory, not being found slidings of the column until reached the breakage of the cables.

5.5. Vertical cable design.

According to the new analysis and using the standard loads in force, a total 8 000 kN anchoring force, for what 32 ϕ 18 mm. DYFORM cables were placed, working with an individual force of 250 kN and a 380 kN breaking force.

5.5.1. Reinforcing the non collapsed Gerber span.

In the presence of the uncertainty about what could happen with the non collapsed

length, it was treated exactly like the reconstructed one, placing on it the same 32 DYFORM cables.

6. TOTALLY PRECAST SOLUTION OF THE NEW DECK, KEEPING THE SAME EXTERNAL FEATURES.

6.1. Box section length in the Gerber beam.

The first 15.00 m. of the Gerber beam length were fractioned in three boxes with a weight of 800kN, and wet longitudinal joints. Transverse sitffness was achieved postensioning the supporting diaphragms (see fig. 2.1 and 2.4).

6.2. Conjugate joints.

For the transition from box sections to "T"-shaped beams, a conjugate joint was designed, able to constraint the three degrees of freedom of the dowels when assembled in an appendix form or as longitudinally precontraint bosses (see fig 2).

6.3. "T"-shaped length in Gerber beam.

The extreme 15.00 m. cantilever in Gerber beam were achieved with precast "T" -shaped dowels weighing 200 kN (two per eachbox), because they are the extension of the vertical box walls. The longitudinal assembly was made with wet joints and the transverse stiffness was achieved with transverse postensioning of the slab and the extreme diaphragm (see fig 2.2 and 2.4).

6.4. Central simply supported length.

Six precast "T"-shaped beams were placed, longitudinally assembled by wet joints and the transverse stiffness was achieved by transverse postensioning of the slab and diaphragms (see fig 2.3 and 2.4).

CONCLUSIONS.

A technical and economical appraisal of the different alternatives is shown in this paper, with an exhaustive analysis of all the pro's and con's of each one and the reasons that guided to the selected one, though the reluctance of some people, finally and fortunately overcome. This paper shows a way regarding the use, in damaged structures, of non collapsed parts of them, with all the advantages and savings this technique could bring.

REFERENCES.

1. GUYON,Y. Hormigón pretensado, estudio teórico y experimental. Ed. DOSSAT, Madrid, 1965 (in Spanish).
2. ABELES, P.W. and TURNER, F.H. Prestressed concrete designer's handbook. Concrete Publications, London, 1962.
3. DREUX,G. La práctica del hormigón pretensado. Editorial Blume, Madrid - Barcelona, 1970 (in Spanish).
4. GUYON-MASSONET-BARES. Le calcul des grillages de poutres et dalles orthotropes. Prague, 1966 (in French).
5. CUBAN CODE 53-125. Construction design elaboration. Bridges and sewers. Design specification and calculation methods. 1984.

Repair and Strengthening of the Blagnac Bridge in Toulouse

Réparation et renforcement du pont de Blagnac à Toulouse

Reparatur und Verstärkung der Blagnac-Brücke in Toulouse

Bernard GREZES
Civil Engineer
Ministère de l'Équipement
Saint-Médard en Jalles, France

Pierre BARRAS
Civil Engineer
Ministère de l'Équipement
Saint-Médard en Jalles, France

SUMMARY

The three-span bridge, prestressed concrete box beam constructed by the balanced cantilever method, presents insufficiences in the longitudinal prestressing and in the transversal passive reinforcement. Mainly in the central span, this insufficiency was evidenced as peripheral cracking of the bottom slab around the continuous prestressing zone. The repair has consisted in adding longitudinal prestressing and in removing the cracked zone.

RÉSUMÉ

L'ouvrage à trois travées, caisson précontraint construit par encorbellement, présentait une insuffisance de précontrainte longitudinale et de ferraillage passif transversal. Cette insuffisance se traduisait principalement en travée centrale par une fissuration périphérique du hourdis inférieur autour de la zone contenant la précontrainte de continuité. La réparation a consisté à ajouter de la précontrainte longitudinale et déposer la zone fissurée.

ZUSAMMENFASSUNG

Die vorgespannte Drei-Feld-Kastenbrücke weist eine ungenügende Vorspannung in Längsrichtung und eine ungenügende schlaffe Bewehrung in Querrichtung auf. Diese Mängel zeigten sich hauptsächlich im mittleren Feld, wo sich lokal Risse bildeten. Die Reparatur besteht in einer zusätzlichen Vorspannung in Längsrichtung und dem Ersetzen der gerissenen Zone.

1.PRESENTATION ET HISTORIQUE

Le pont de Blagnac franchit la Garonne à Toulouse. Il comporte un tablier en béton précontraint réalisé par encorbellements successifs. Sa longueur totale de 200 m se décompose en trois travées de 55,00 m - 90,00 m - 55,00 m.
Construit entre 1973 et 1975, il supportait avant travaux, une chaussée bidirectionnelle de 7,50 m et un trottoir aval de 2,00 m (cf. Fig 1).
Dès sa construction des fissures en « arêtes de poisson » sont apparues au voisinage des bossages d'ancrage des câbles de continuité, bossages implantés sur le hourdis inférieur. Les nombreuses inspections détaillées postérieures (annuelles) ont mis à jour l'évolution de la fissuration en nombre et en ouverture.
En 1987, compte-tenu de l'évolution des désordres, le Maître d'ouvrage a demandé le recalcul de l'ouvrage, préalable au diagnostic et au projet de réparation et de renforcement lié à la mise à trois voies dans le cadre de l'aménagement de la liaison aéroport. Parallèlement, et sans attendre, à titre de mesure conservatoire, le pont a été limité à 3.5 tonnes.

2.ETUDES DE DIAGNOSTIC

La flexion longitudinale a été étudiée en 1988 en fluage scientifique sur la base du calendrier de construction extrait du journal de chantier. Le calcul conduit à une contrainte minimale en zone clé de la travée centrale de l'ordre de -4 MPa sous combinaison rare. La réserve en moment fléchissant en travée centrale mesurée sur trois joints de voussoirs lors des essais de 1983 est située dans la fourchette de calcul (états à vide à la mise en service et à 50 000 jours). Ces essais indiquaient que l'ouvrage souffrait davantage de défauts locaux (diffusion, entraînement, poussée au vide) que d'une insuffisance caractérisée en flexion générale.

En section transversale, le calcul a été conduit de manière classique en cumulant , en un point donné, les armatures de :
-flexion transversale,
-effort tranchant général sous la même sollicitation que la combinaison retenue en flexion transversale,
-diffusion.
Ce calcul conduit à un manque d'armatures dans les zones fissurées (hourdis inférieur sur 20 m de part et d'autre de la clé et en particulier à la jonction hourdis inférieur âme) mais également dans les zones saines (à proximité des piles).

Au vu des résultats du recalcul, il a été décidé en 1989 de:
- procéder à des essais de chargement afin d'estimer la réserve de compression en fibre inférieure de la travée centrale pour dimensionner la précontrainte de renfort,
- de faire effectuer un nouveau calcul en section transversale où l'on vérifie, au droit des points remarquables du caisson l'intégrité du béton ou à défaut « la règle des coutures ».

Les essais réalisés en Avril ont montré que la réserve en compression se situait dans la fourchette des états à vide. Ils ont confirmé l'hétérogénéité transversale de la réserve sur la fibre inférieure; nulle dans l'axe du tablier, de l'ordre de la réserve de calcul au bas des âmes.
Ceci a conduit à dimensionner la précontrainte de renfort pour ne pas décomprimer la fibre inférieure dans les deux schémas de comportement suivants:

- un comportement d'ensemble où l'état avant renforcement est la moyenne des « réserves » locales des points de la fibre inférieure ; combinaison : « réserve moyenne » + précontrainte + 1,2 charges d'exploitation + gradient de 6°C;
- un comportement local, au milieu du hourdis inférieur, où la réserve est nulle; combinaison : précontrainte + 1,2 (une file de 2 camions Bc) + 8°C.

Il s'agit d'une combinaison fréquente destinée à prévenir la fatigue des câbles de continuité régnant dans le hourdis inférieur.

Le calendrier des études a été décalé car un autre ouvrage en béton précontraint géré par le maître d'ouvrage présentait des désordres en flexion très importants nécessitant une réparation rapide, effectuée aux 2e et 3e trimestres 1990.

Le nouveau calcul en section transversale effectué s'est avéré nettement plus satisfaisant. En effet :
- là où le calcul indiquait un béton intègre ou bien un respect de la règle des coutures, les inspections n'avaient pas relevé de fissures,
- là où le calcul conduisait à une insuffisance d'armatures pour respecter la règle des coutures régnait la fissuration.
Le principe de ce calcul a été retenu pour le dimensionnement de corsets dont le rôle au niveau des fissures est d'assurer la non-décompression en flexion transversale, et de rendre non nécessaire la présence d'armatures passives équilibrant les cisaillements.

3.PROJETS DE REPARATION ENVISAGES

L'avant-projet de réparation réalisé fin 1990 comprenait (cf. figure 2):
-un renforcement transversal à l'aide de corsets composés de barres « MACALLOY » Ø 32 classe 1230 Mpa et espacés de 50 cm en zone de clé;
-un renforcement longitudinal à l'aide d'une précontrainte extérieure composée « par âme » de 3 câbles 19T15,7 ancrés au niveau des culées et 3 câbles 15T15,7 ancrés en arrière des piles.

L'élaboration du projet a mis à jour plusieurs problèmes susceptibles de nuire à sa fiabilité et sa pérennité.
-le précédent d'un ouvrage similaire a révélé des problèmes technologiques liés à l'utilisation des barres.
-le faible espacement des corsets rend délicat la gestion des « conflits » câble de fléau en place-forage pour barre verticale et rend nécessaire l'utilisation d'ancrages par « chevilles »;
-le nombre et la taille des fissures à injecter peuvent nuire au monolithisme de l'ouvrage renforcé.

Ces doutes nous ont conduit à envisager une solution de démolition et reconstruction du tablier.
Des gammagraphies réalisées au cours du 2e trimestre 1991 ont confirmé l'existence de conflits câbles de fléau-corsets mais en nombre limité. C'est en fait le faible espacement des corsets qui s'est révélé pénalisant. En effet, l'implantation des ancrages en défoncé sur l'encorbellement nécessitait la coupure des 2/3 des armatures de flexion ce qui rendait nécessaire le renforcement à l'aide de plats collés transversaux.
La réparation fut estimée à 13,5 MF pour une durée de travaux de 9 mois et la démolition-reconstruction à 7 +15 MF, cette dernière solution nécessitant la construction préalable du doublement alors estimé à 25 MF.

4.PROJET DE REPARATION RETENU

Devant les difficultés et doutes posés par les solutions envisagées, a resurgi la boutade lancée à l'origine de notre intervention : « hourdis à découper selon le pointillé (les fissures) ». En d'autres termes pourquoi s'obstiner à reconstituer à tout prix le monolithisme du caisson. N'est-il pas préférable d'enlever sur 40 m en travée centrale la partie de hourdis inférieur dont le prédécoupage par la fissuration en fait peut-être autant un poids mort qu'une partie vraiment résistante ?
Une étude sur la base de cette idée a été menée lors du 3e trimestre 1991.

L'enlèvement du hourdis inférieur entraîne une diminution importante de a section résistante compensée par:
-une diminution du moment de poids propre dans la travée centrale,
-une plus grande efficacité de la précontrainte de renfort dont la majeure partie occupe la place du hourdis enlevé,
-une diminution des effets des charges d'exploitation en zone centrale,
-une diminution des effets du gradient thermique(par référence à un ouvrage réalisé sans hourdis inférieur dans la partie centrale).

La dépose nécessitait:
-la mise en oeuvre préalable de la part de précontrainte régnant au dessus des bossages du hourdis inférieur (câbles IV, V),
-l'adjonction de plats boulonnés en bas des âmes nécessaires au fonctionnement en classe II. Pendant cette opération, réalisée hors circulation mais de ce fait en Juillet-Août, l'ouvrage reste soumis aux efforts du gradient thermique pouvant atteindre 12° (mesuré).

Dans la zone où le hourdis est déposé, il est ajouté au milieu de chaque voussoir une entretoise pour compenser la perte de rigidité transversale créée par la dépose du hourdis inférieur (cf.fig 3).
La dépose du hourdis inférieur était prévue à l'aide d'un pont roulant, placé au dessus de l'élément préalablement découpé, permettant sa descente et sa dépose sur une barge assurant son évacuation.
Ce principe de renforcement fut validé en considérant:
-une meilleure fiabilité et une meilleure esthétique que le renforcement par corset
-un plus faible impact sur le public que la démolition
-la compatibilité avec le financement disponible (coût 13MF à comparer aux 25 MF TTC du doublement préalable à la démolition-reconstruction).

5.SURVEILLANCE DE L'OUVRAGE

Parallèlement, l'ouvrage fut placé sous surveillance en Février 1991. A l'aide d'une centrale de télémesure, six fissures caractéristiques des dégradations (diffusion, poussée au vide) ont été auscultées chaque jour.
Ces mesures étaient, pour chaque fissure, comparées à une courbe alarme déduite de la courbe moyenne établie à partir des mesures effectuées sur les six premiers mois.
L'objectif de cette surveillance était de pouvoir parer à une accélération des dégradations.

6.EXECUTION ET SUIVI DES TRAVAUX

Le marché a été attribué en Octobre 1992 pour un montant de 12,1 MF TTC, au groupement Bisseuil-VSL.
Les moyens de l'entreprise l'ont conduite à remplacer, pour la dépose, le pont roulant par une grue mobile. Cette technique applique sur le tablier une charge de chantier de 25 tonnes excentrées au lieu de 5 tonnes centrées du pont roulant.

Fig. 1
Ouvrage avant travaux

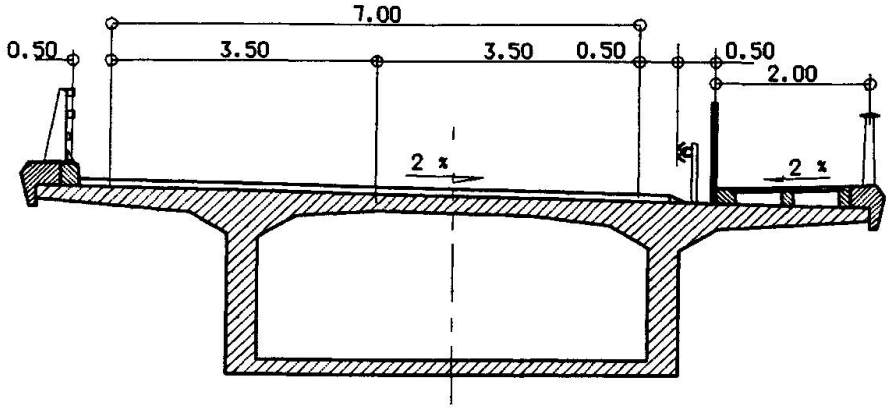

Fig. 2
Projet initial

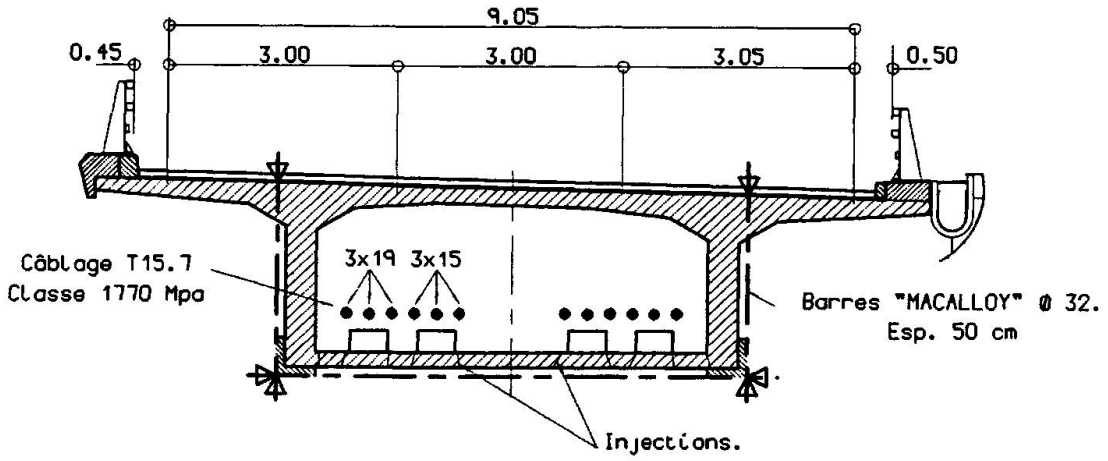

Fig. 3
Ouvrage réparé et renforcé

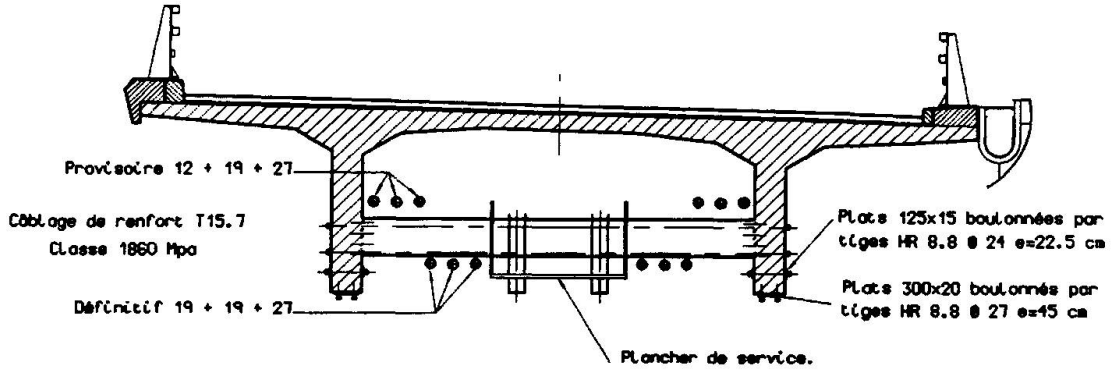

L'accroissement de charge n'étant pas admissible en flexion longitudinale, l'entreprise a proposé lors de la signature du marché de prendre à sa charge un complément de précontrainte provisoire constitué d'un câble de 10T15,7 par âme.

Les études d'exécution comprenaient un calcul aux éléments finis qui a permis:
-de valider le dimensionnement des entretoises en travée et de leur précontrainte,
-de valider la découpe en biseau aux abouts et de dimensionner l'entretoise extrême du voussoir
-de dimensionner les armatures et scellements des déviateurs (ce qui a permis d'éviter la fissuration systématique de la traverse inférieure sous les effets du retrait, fissure constatée sur d'autres ouvrages renforcés)
-de valider la méthode de dépose, les contraintes obtenues sous les effets de la grue excentrée étant admissibles.

Le complément de précontrainte provisoire est en fait passé de 10 à 34T15 dans le souci de ne pas fissurer le bas de l'âme lors de la dépose.
En effet, si la contrainte de traction est du même ordre de grandeur,en fibre inférieure, lors de la dépose et en service, la probabilité de l'atteindre est forte lors de la dépose (dépose de l'élément défavorable l'après-midi) alors qu'elle est faible en service (combinaison rare).
De plus, afin de limiter les conséquences du gradient thermique, l'enrobé a été peint en blanc pendant la phase de dépose et la présence de la grue sur le tablier exclue après 14h00. Il était escompté une diminution de 30% du gradient. En fait celle-ci a été de 85% au début à 60% en fin d'opération (salissure de la peinture). Cela a permis de lever la restriction d'utilisation de la grue. Le rythme de dépose a atteint deux éléments par jour (sciage par couronne diamantée, descente, remontée, évacuation).

Le déroulement des travaux a été à quelques détails près conforme au planning de l'avant-projet:
-Février à Juin 1993 :(une voie de circulation) changement des appareils d'appui, réalisation des pièces d'ancrage, des entretoises et mise en oeuvre des plats boulonnés,
-7 Juillet-9 Septembre 1993 :(coupure totale) câbles provisoires, dépose du hourdis, câbles définitfs et épreuves,
-9 au 16 Septembre 1993 :(une voie de circulation) finitions.

L'opération présentée comme la plus délicate(la dépose) s'est parfaitement déroulée et les plus grandes difficultés sont apparues pour le scellement des plats et l'emplacement des entretoises. Celles-ci, à l'origine identiques sont presque tous différentes compte-tenu de la géométrie réelle du caisson et du tracé des câbles de précontrainte extérieure qui doivent être dessus, dessous ou traverser avec un enrobage suffisant.

Le renforcement a fait l'objet d'un suivi métrologique à l'aide de jauges sur trois sections caractéristiques : avant découpe,dans le premier voussoir découpé,à proximité de la clé, et sur une entretoise.
A la mission traditionnelle des mesures lors d'un renforcement (comparaison avant après) s'est ajouté ici le suivi en temps réel de la transformation du tablier afin de comparer l'évolution réelle à celle prévue par le calcul.

7.CONCLUSIONS

Globalement le renforcement s'est déroulé conformément aux prévisions. Le point le plus délicat a été la mise au point des plats boulonnés et la limitation de la traction en fibre inférieure lors de la transformation. Le coût final est de 14.6 MF TTC (+ 20%) compte-tenu de toutes les mises aux points et travaux supplémentaires.

Maintenance of the Ponte Vecchio Historical Bridge in Florence

Restauration et entretien du pont historique Ponte Vecchio à Florence

Erneuerung der historischen Ponte-Vecchio-Brücke in Florenz

Andrea CHIARUGI
Professor
University degli Studi di Firenze
Firenze, Italy

Andrea Chiarugi, born 1937, received his civil engineering degree at the University of Bologna, Italy. He is Prof. in the Civil Engineering Department of the University of Florence, Italy.

Paolo FORABOSCHI
Dr. Eng.
Universita degli Studi di Bologna
Bologna, Italy

Paolo Foraboschi, born 1959, received his civil engineering degree at the Univ. of Bologna, and his Ph.D. at the University of Florence, Italy. He has now a fellowship at the University of Bologna.

SUMMARY

This paper presents a new maintenance procedure, proposed for existing buildings. It consists of the arrangement of a mechanical survey for historical bridges, i.e., old masonry bridges. The procedure is applied to "Ponte Vecchio", in Florence, one of the main Italian monuments. The bridge presents a great crack pattern and masonry is damaged. A nonlinear finite element model was updated referring to the crack pattern and the experimental natural frequencies. The safety of the bridge was assessed together with its residual strength.

RÉSUMÉ

Cet article présente une nouvelle procédure de contrôle pour des ouvrages existants. Elle consiste en une adaptation du contrôle mécanique pour des ponts historiques, par exemple les vieux ponts en maçonnerie. La procédure a été appliquée au Ponte Vecchio de Florence, l'un des plus importants monuments italiens. Le pont présente un réseau de fissures et les pierres sont très endommagées. Un modèle aux éléments finis non-linéaires a été réalisé en se référant au réseau de fissures et aux fréquences naturelles expérimentales. La sûreté et la résistance du pont ont été déterminées.

ZUSAMMENFASSUNG

Eine neue Entwicklung der Kontrolle bestehender Gebäude wird dargestellt. Sie wird als mechanische Aufnahme bezeichnet. Das neue Verfahren wird an den Ponte Vecchio, eines der wichtigsten italienischen Denkmäler, angewandt. Die Brücke zeigt eine grosse Rissverteilung und das Mauerwerk ist beschädigt. Ein nichtlineares Finite Elemente Modell wurde angepasst, um die Rissbildung zu berücksichtigen. Hierzu, wurde ein inverses Problem gelöst, so dass das wirkliche Verhalten der Brückenstruktur ermittelt werden konnte.

1. INTRODUCTION: MAINTAINANCE OF HISTORICAL BRIDGES

Most historical bridges are used in the infrastrucures. Thus, the load carrying capacity required, at the present time to historical bridges may be substantially larger than in the past. Moreover, the floods of most rivers are increased in centuries, since the urban areas are increased in number and extension. As a result of the larger loads, the damage rate has increased in time. Therefore, nowadays structural degeneration of historical bridges grows faster than in the past centuries. For the aformentioned reasons, the maintainance of historical bridges is a fundamental topic for structural engineering. The safety margins have to be periodically assessed with respect to both loadings and structural state existing at the moment at which the structural analysis is conducted. It follows that the bridges that are proved to be any longer safe must be rehabilitated, i.e. retrofitted.

In the case of existing buildings, the analized structures can be tested, wheras this is obviously not possible in the case of building yet to be built. Thus, observations provided by specific in situ tests of the analized building, hereafter named monitoring resuls, can be used to identify the structural behavior. Nevertheless, special procedures are necessary in order to gain profit from monitoring prospect, since ordinary structural analysis does not include a-posteriori information.

Aiming at analizing existing buildings on the basis of monitoring results, the authors had proposed a special procedure, named *mechanical survey* [1, 2]. All existing buildings can be treated within the framework of mechanical survey. Nevertheless, the special arrangements of the procedure need to be correlated to the type of building that is analized. This paper is concerned with the development of mechanical survey procedure in order to deal with historical bridges, i.e. with existing masonry bridges. The proposed procedure is applied to the *Ponte Vecchio*, in Florence.

2. DESCRIPTION OF THE STRUCTURE

Due to architectural worth and artistic value as well as historical significance, the masonry bridge named *Ponte Vecchio* (Fig. 1) represents one of the main Italian monuments. Despite this, it has never been studied extensively in the past.

2.1 Geometry of *Ponte Vecchio*

As seen from Fig. 1, the structure consists of: 1) three circular arches covering a 60 degree angle, respectively with span of: 26.35 m; 28.85; and 26.25, along with thickness of: 1.0 m; 1.05 m; and 1.0 m; 2) two piers; 3) the abutments (i.e. two bridge-seats). Longitudinal retaining walls at the sides of the arches contain spandrel fill. The spandrel fill results in a flat extrados of the deck.

2.2 Structural problems of the bridge

The present investigation was prompted by: 1) the visible and accentuated crack pattern; 2) the considerable level of damage of the structural material, especially of the masonry mortar joints; 3) and the total absence of any structural investigation on the bridge. The main focus of the present study was to assess the safety of the bridge. If an insufficient safety margin had resulted, the study was expected to point out how the bridge should be retrofitted.

3. MECHANICAL SURVEY OF THE BRIDGE

Motivated by the need to better comprehend the behavior of the bridge, as well as to assess the present strength and stiffness, a *mechanical survey* procedure was carried out [1, 2].

3.1 Mechanical survey: review of the procedure

The procedure of mechanical survey is based on the comparison between monitoring data (i.e. observed response quantities) and correspondent mathematical model predictions. A physical interpretative model, hereafter named *virtual model*, allows use to be made of all a priori information derived

from the geometric survey as well as the theory of structures. Thus a well-detailed description of the structural response can be guaranteed by the virtual model. Uncertainties regarding structural modeling can be restricted to the values of N parameters, denoted as the N-dimensional vector $\{\lambda\}$. Let the M-dimensional vector $\{\zeta\}$ denotes the results of M measurements, M > N, $\vartheta(\{\lambda\})$ denotes the mathematical model posed as a function of the N unknown parameters $\{\lambda\}$, i.e. M nonlinear, continuously differentiable functions of $\{\lambda\}$. The following relation between $\{\zeta\}$ and $\{\vartheta\}$ is assumed

$$\{\zeta\} = \{\vartheta(\{\lambda\})\} + \{\rho\} \tag{1}$$

where $\{\rho\}$ is a stochastic M-dimensional vector noise (assumed additive, independent on $\{\lambda\}$ and Gaussian). The procedure updates the initial estimate of parameters $\{\upsilon_\mu\}$ in order to optimize the differences between the predicted overall response and the monitoring data. The best estimation was found in the minimum of the following objective function $\Theta(\{\lambda\})$:

$$\Theta(\{\lambda\}) = \left\| \{\zeta\} - \{\vartheta(\{\lambda\})\} \right\|_{[\Delta]} + \left\| \{\lambda\} - \{\upsilon_\mu\} \right\|_{[\chi]} \tag{2}$$

in which $[\Delta] = [\Xi]^{-1}$ where the M·M matrix $[\Xi]$ denotes the covariance matrix of the noise $\{\rho\}$, and $[\chi] = [\Psi]^{-1}$ where the N·N matrix $[\Psi]$ denotes the covariance matrix of the initial estimate of parameters $\{\upsilon_\mu\}$, and where $\|\{\alpha\}\|_{[\beta]}$ is taked to denote $\{\alpha\}^T \cdot [\beta] \cdot \{\alpha\}$.

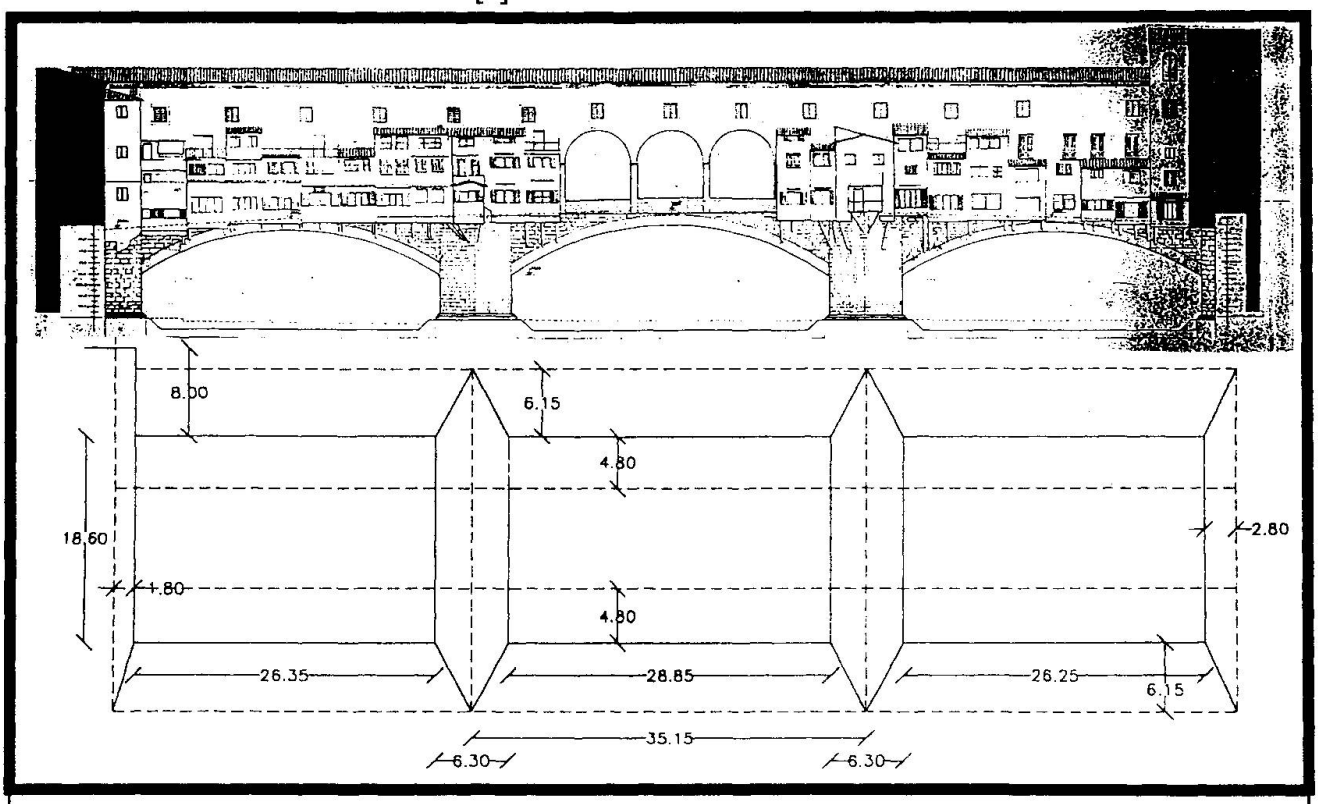

Fig. 1. Architectonic survey of the *Ponte Vecchio*, located in Florence, ITALY.

3.2 Historical information

Historical information about the bridge is necessary in order to obtain the virtual model. To this objective an extensive historical review of the bridge was carried out.

Ponte Vecchio was built to substitute the brigde that the 1333-river-Arno-flood destroyed. It should be noted that the thickness to span ratio is about 1/27, that corresponds to a low value and that the angle formed by the springing section to the horizontal is 30 degrees, that corresponds to an extremely large value. The heigth to span ratio is nearly 1/6, never built so little before.

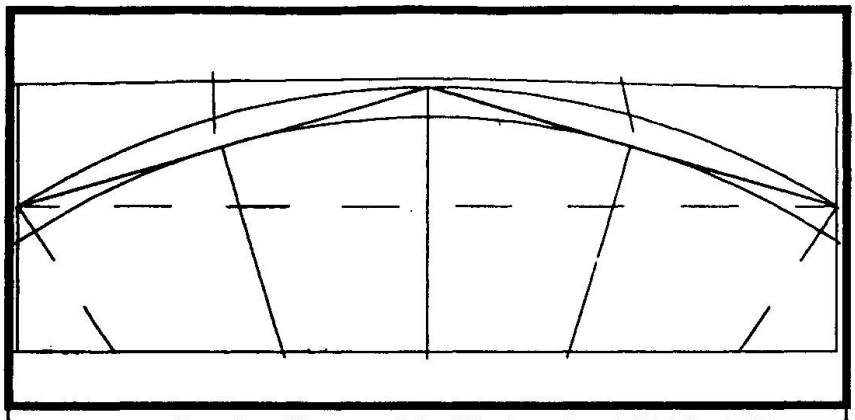

Fig. 2. Geometric rule used for the design

The reason of the dimensions was found in the rule explained in Fig. 2. Such a rule is attributed to Leonardo da Vinci, yet this study proved that the rule was known at least a century and an half before. Accordingly, it was possible to reduce both the hight of the crown to the springing, and the thickness. Nevertheless, this rule is not theoretically supported.

The bridge has been subjected to deep transformations. The shops have continuously grown in size. Moreover a gallery was built on the shops. As a result, the dead weights considerably increased. Arches and piers have never been modified, whereas piles (i.e. foundations columns) and diaphrams were built to support the existing foundations. In doing so, the bridge was upgraded so as to better withstand the periodical flood of the river Arno. As a result, the bridge was capable of resisting the flood of 1966, that corresponds to the largest flood of the river Arno.

3.3 Monitoring of the bridge

Maintaimance of historical bridges requires: 1) the prediction of the structural response to vehicles and floods; 2) and the assessement of the present safety margins. Aiming at these two targets, two different monitoring strategies were carried out.

3.3.1 Mechanical survey for predictive analyses

Predictive analyses were conducted by tuning the virtual model according to Eq. (2) in which experimental modal parameters were used in $\{\zeta\}$. To obtain $\{\zeta\}$, a vibrodyne composed of 4 masses fixed at the edge of two disks rotating with opposite spin, ω, was used. The vibrodyne was located at the midspan of a lateral arch (point v) and the response of the structure was measured by severals accelerometers located at the level of the deck (points r). The excitation, $f_v(t)$, and the response, $q_r(t)$, can be written as (i denotes the imaginary unit)

$$f_v(t) = F(\omega)\cdot e^{i\cdot\omega\cdot t} \quad ; \quad q_r(t) = Q(\omega)\cdot e^{i\cdot[\omega\cdot t + \theta(t)]} \quad . \tag{3}$$

Let $H_{rv}(\omega)$ denotes the transfer function with respect to the vibrodyne in v. One obtains

$$H_{rv}(\omega) = \frac{Q\cdot e^{i\cdot(\omega\cdot t + \theta)}}{F\cdot e^{i\cdot\omega\cdot t}} = \frac{Q(\omega)}{F(\omega)}\cdot e^{i\cdot\theta(\omega)} \rightarrow H_{rv}(\omega) = \frac{Q}{F}\cdot[\cos(\theta) + i\cdot\sin(\theta)] \tag{4}$$

Using the readings from the instrumentations (e.g. accelerometers and vibrodyne), F, Q and θ were available as a function of ω. Thus, $H_{rv}(\omega)$ was numerically camputed. The natural frequencies of the structure were pointed out by the peaks of the imaginary part of the H_{jv} (1^{st} = 4.92 Hz), while the *j-th* element of the *k-th* modal shape, denoted with Φ_j^k, was yielded by the following expression

$$\Phi_j^k = \frac{I\langle H_{jv}^k(\omega_k)\rangle}{I\langle H_{vv}^k(\omega_k)\rangle} \cong \frac{I\langle H_{jv}(\omega_k)\rangle}{I\langle H_{vv}(\omega_k)\rangle} \tag{5}$$

3.3.2 Mechanical survey for safety assessement

In order to tune the model for safety assessement purposes, monitoring was composed of 3 parts: *1)* analysis of the structural materials; *2)* survey of the crack pattern; *3)* strain-temperature monitoring. The material analysis revealed a stone masonry along with the absence of mortar joints for a depth of 0.1 m at the the intrados. Thus, the thickness of the arches is now about 0.9 times the original ones.

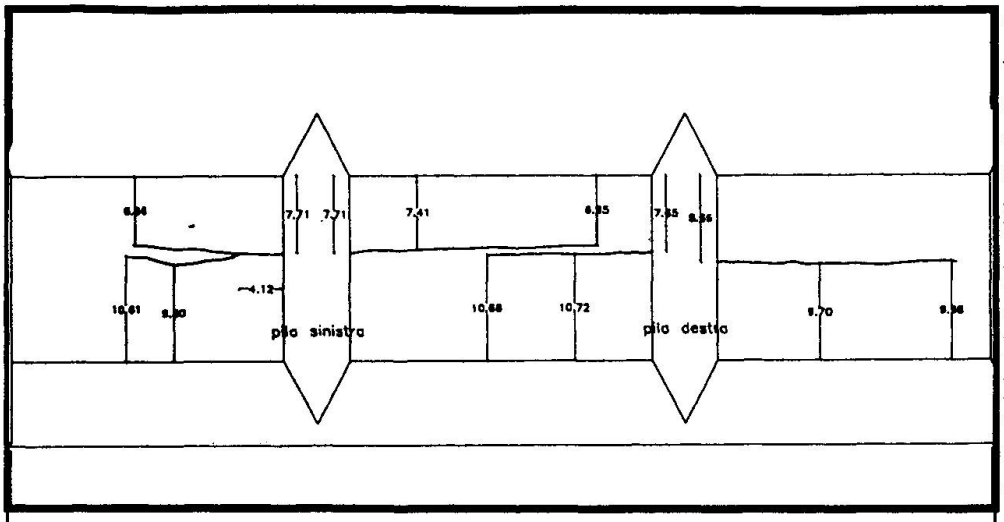

Fig. 3. Survey of the crack pattern

The crack pattern survey (Fig. 3) pointed out a longitudinal crack that split deck and piers into two parts. Thus, Ponte Vecchio resulted to be ideally composed of two ideal adjoining bridges. Strain-temperature monitoring correlated displacements of crack with temperature of air [3].

3.4 Virtual model

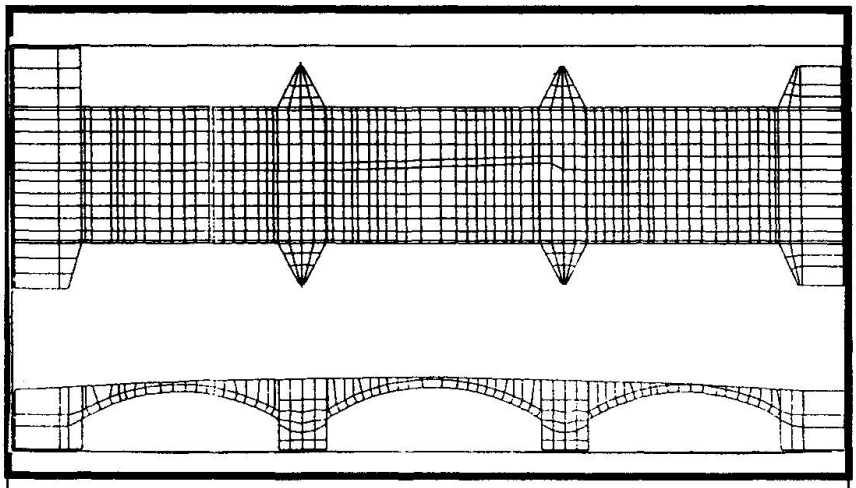

Fig. 4. Virtual model

A finite element model (Fig. 4) of the bridge was generated based on the geometrical survey. Brick element (eight-node element) was used. The virtual model exactly corresponds to the bridge in its first age. In fact, the shops were modelled with their original size, whereas the gallery was not modelled. The commercial program ANSYS version 4.4 installed in a 386 personal computer was used to perform the analysis.

4. ESTIMATION AND RESULTS

Two separate analyses were conducted, depending on the type of experimental data that are used.

4.1 Predictive analyses

The parameters were updated based on dynamic monitoring data, according to Eq. 2 [4]. The model tuned was used for simulating dynamic performances, including expected floods.

4.2 Safety margin

A new method was proposed for defining the safety margin of the bridge. A state-space description was used instead of a parameter-space one. Thus, a state-parameter vector was used for $\{\lambda\}$ in Eq. 2. To this objective, the following criteria were adopted for stresses and strains.

$$\sigma_3 < \sigma_2 < \sigma_1 < 0 \; ; \; [\varepsilon] = [\varepsilon]^e + [\varepsilon]^c \; ; \; \varepsilon_3^c < \varepsilon_2^c < \varepsilon_1^c > 0 \; ; [\sigma] \cdot [\varepsilon]^c = 0 \qquad (6)$$

in which σ_i and ε_i denote respectively principal stress and strain related to i-direction, apex "c" cracking strain, apex "e" elastic strain, $[\sigma]$ and $[\varepsilon]$ respectively the stress and strain tensors. A linear-elastic behavior is assumed. Denoting the elastic deformability tensor with [C], it follows:

$$[\varepsilon] = [C]\bullet[\sigma] + [\varepsilon]^c \qquad (7)$$

The matrices $[\sigma]$ and $[\varepsilon]_c$ were assumed as the process state variables, and the measured matrix $[\varepsilon]_m^c$ as measurement noise vector. Gap elements (i.e. interfaces) were used to obtain $[\varepsilon]^c$.

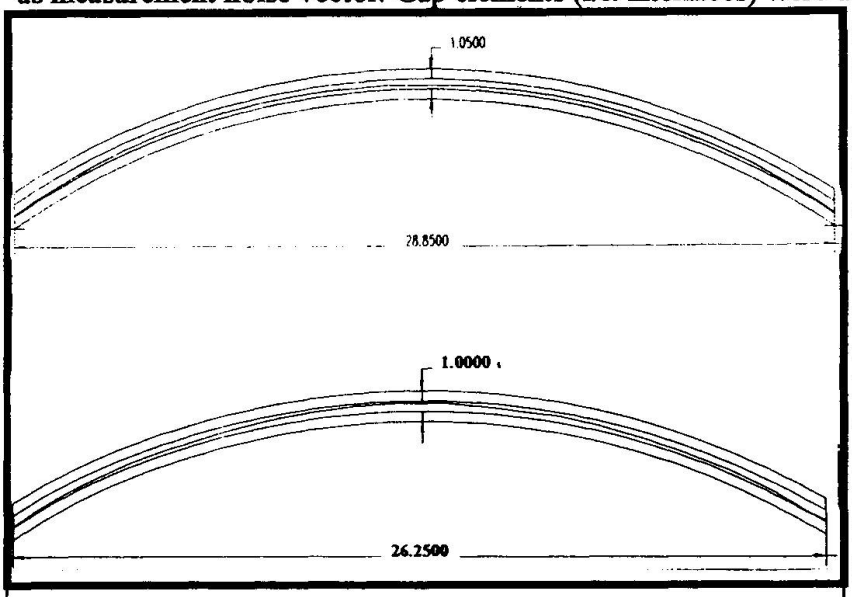

Starting from the virtual model, the aforementioned process defined a new model that reproduced the crack pattern of the bridge in its first age. Then, the present dead loads were simulated and the process was repeated. In so doing, the new model reproduced the observed crack pattern. Thus, the mechanical history of the bridge was defined. The final model represents the bridge in the present state. Thus, it can be used to reliably assess the safety and the strength of the bridge in the present structural conditions.

Fig. 5. Lines of thrust in the present configuration: maximum compressive stress σ_{max} = 6,2 N/mm^2

5. FINAL REMARKS

The proposed procedure permits to establish strength and stiffness of existing bridges and to assess the safety. The application of the procedure to *Ponte Vecchio* has demonstrated that: 1) The crack pattern is stable; 2) The lines of thrust of the arches are in accordance with the *"middle third rule"* both in the present dead load configuration (Fig. 5) and in the original one. 3) The bridge - as obvious - was well designed; 3) Cracks do not reduce the load carrying capacity, since crack occurring modified the transversal behavior but not the longitudinal behavior of the structure. 4) The arches are capable of carrying the present dead loads; 5) The level reached by compressive stresses (6.2 N/mm^2) requires the rehabilitation of the damaged mortar joints. 6) The new foundations make the bridge capable of withstanding the expected floods. 7) The structural behavior of the bridge was predicted to not alter in the future, provided that damage of masonry is prevented.

REFERENCES

1. Chiarugi A., Foraboschi P., The Arnolfo Tower: structural identification. «*Special Issue*: Numerical methods in architecture», International Journal from Computational Mechanics Publications. Editor C.A. Brebbia; Ashurst, Southampton (U.K.); April 1990. V. 6, N° 2, pp. 62-67.
2. Chiarugi A., Foraboschi P., Structural monitoring and identification. (in italian). *Structural Engineering Publication*, Editor. P.G. Malerba, C.I.S.M. - Udine, Italy, 1994.
3. Bartoli G., Blasi C., Chiarugi A., Foraboschi P., Gusella V., Preliminary analysis of the data recorded by actual monitoring system of the Brunelleschi's Dome in Florence. IV-ICCCBE, Japan Society of Civil Engineering and Architectural Institute; Tokyo (Japan), July 1991.
4. Gladwell G.M., Inverse problems in vibration. Martinus Nijhoff Publishers, Netherlands, 1986.

Stabilization of Double Leaf Bascules

Stabilité des ponts à bascules

Zur Stabilisierung doppelter Klappbrücken

Terry L. KOGLIN
Mechanical Engineer
Koglin & Colker
Hoboken, NJ, USA

Terry Koglin, BSME from the University of Wisconsin at Madison, has designed, inspected, built and rehabilitated many movable bridges. He was the Overall Project Engineer for the Culvert Street Bascule Bridge.

Sarah COLKER
Structural Engineer
Koglin & Colker
Hoboken, NJ, USA

Sarah Colker received her BS in Structural Engineering from Princeton University. She was Chief Structural Engineer for the Culvert Street bascule bridge design, and has worked on several other movable bridge projects.

SUMMARY

This paper describes the positive and negative aspects of selecting a double leaf bascule for a movable bridge application, and describes various defects that can be encountered in the load supporting system of double leaf bascules. Solutions to problems encountered in bascule bridges are outlined, as are ways of avoiding these problems.

RÉSUMÉ

L'article décrit les aspects positifs et négatifs de la sélection d'un pont à bascules doubles dans le cas d'un pont mobile et décrit divers défauts rencontrés dans le système de charges de ces ponts à bascules. Il présente les solutions aux problèmes rencontrés dans ce type de pont, ainsi que les possibilités d'éviter l'apparition de ces problèmes.

ZUSAMMENFASSUNG

Der Beitrag behandelt die Vor- und Nachteile bei der Ausgestaltung einer beweglichen Brücke als doppelte Klappbrücke und mögliche Schäden, die an den Klappenlagern auftreten können. Für diese Probleme werden Lösungen und vorbeugende Gegenmassnahmen erörtert.

1. INTRODUCTION

Most double leaf bascule bridges consist of two cantilever spans projected toward each other, connected at their tips by a suitable shear lock. They can open and close more quickly than other types of movable bridges, are less affected by wind loads than a single leaf bascule spanning the same channel width, and use slightly less structural steel than other types of movable bridges. Double leaf bascules are less susceptible to collision with vessels and are considered more aesthetically pleasing than other types of movable bridges. These advantages are balanced by complications, particularly in regard to stability of the structures under live load.

2. STABILIZATION

Double leaf bascule bridges frequently have problems with seating. The bridge may be carrying live loads larger than those designed for, overstressing the support system. The bridge stabilizing devices may have suffered deterioration so that they cannot contain the forces imposed on them. The bridge stabilizing devices may be improperly adjusted so that they do not perform their intended function. These devices include: live load shoes which form stops for each moving leaf as it attains its seated position; center or shear locks forming a vertical tie between the two leaves of a double leaf bascule bridge when in the closed position; live load anchors which are capable of exerting a downward force at the rear of the bridge counterweight; tail locks which form a shear connection at or near the rear of the bridge counterweight, and balance of the moving leaf.

2.1 Stabilizing Components

2.1.1 Live Load Supports

There are two common variations of basic live load support for double leaf bascule bridges:

- "Live Load Shoes" located under the bascule girder between trunnion or tracks and sea wall.

This type is used on most double leaf bascules because of the advantage in reducing the maximum trunnion or track loading. Live load shoes bolted to the bottom flange of the bascule girders make contact with castings anchored to the pier. This support is normally quite durable; the most common mode of deterioration is corrosion when debris is allowed to build up around the castings.

- "Live Load Anchorages" near the rear of the counterweights.

This type allows constructing a smaller pier, as the center of rotation can be placed close to the sea wall. The live load moment is taken to the pier near the rear of the counterweight. This requires a large superstructure element to act as a tiedown for the rear of the leaf, usually in conjunction with an approach roadway deck. Rear live load anchorages have the disadvantage of producing higher trunnion loads and span moments. They tend to be less accessible than forward live load shoes, and are thus more prone to maladjustment.

2.1.2 Anchors

Live load anchors are sometimes used in combination with forward live load shoes but are set up so that they have small clearances when the main live load shoes are firmly seated. As load is released at the trunnion columns, due to live load on the cantilever arm shifting the center of gravity toward the live load shoes, the anchors should come into contact. It is almost impossible to adjust these components precisely, so the anchors usually do no work until the main live load shoes become worn, when the anchors end up taking over the main live load support and become susceptible to structural failure.

2.1.3 Center Locks

Toe end support consists of shear center locks which transmit vertical loading to the toe of the mating leaf. When a live load is near the middle of the bridge, the center locks provide for the two leaves to share this load, forcing them to have equal deflection. After the center locks wear excessively, the equalization of deflection is lost, and the two leaves bounce as each live load passes from one leaf to the other. A new bridge with center locks

properly aligned and adjusted to the design clearances may develop excessive vertical play within a year or two of being opened to traffic.

Trunnion bascules generally use retractible lock bars. The retractible lock bars slide in guides and sockets, which are lubricated to minimize wear. The lubricant attracts grit, which makes it a very effective abrasive compound, wearing away the bar and guide shoe material with every actuation of the lock mechanism, and abrading the bar and socket every time live load causes the span to deflect. Once the clearance at these components has been increased by abrasive wear, impacts at the bearing surfaces from live load add to the rate of increase of the clearance by plastically deforming the shoe and/or bar material.

2.1.4 Tail Locks

Tail locks are used most often when a part of the roadway deck is behind the rotational center of the moving leaf, to provide live load support at the rear of the leaf, forming a shear connection at the rear of the counterweight.

Tail locks usually have no provision for adjustment so they are unlikely to carry any live load reaction, even when newly installed. Tail locks are usually very difficult to reach for maintenance or inspection, and they are consequently usually very worn and out of alignment. Tail locks have frequently been damaged due to actuation when the bridge was not fully closed.

2.1.5 Alignment

Difficulty frequently arises in obtaining proper alignment and effective operation of all span support and stabilization devices. It is a difficult task to achieve proper initial alignment at construction. In-service wear and occasional overloads can cause misalignment of these bridge components even when properly erected. A double leaf bascule bridge with two main girders at each leaf may have as many as eighteen points of support:

- Four trunnions or tracks
- Four live load shoes
- Four live load anchors
- Four tail locks
- Two center locks

2.2 Superstructure

The double leaf bascule superstructure is an important factor in the stability of the bridge. Flexible leaves will deflect more under a given live load than rigid ones, storing more energy as they are bent like a spring under live load. When the live load moves off, the leaf springs back up, imputing a negative impact on the leaf and possibly causing it to lift off its live load supports. For this reason, bridges carrying heavy high speed traffic should be built much stiffer and heavier than bridges carrying light, slow traffic. The bridge should also be carefully designed and constructed to avoid abrupt changes in roadway profile, particularly at the joint between the leaves, as these add to impact forces.

Lifting off under live load and impacting upon the live load supports causes damage to all components, particularly the machinery. The damage is most readily apparent in excessive wear at the rack and pinion teeth, but may also show up as wear at the trunnions or tracks. In more unusual cases wear or damage may show up at other drive components, or on the bridge superstructure or substructure. Frequently, damage is readily apparent at the live load shoes, anchors, and other stabilizing components.

3. BALANCE OF BASCULE BRIDGES

Stability is highly dependent on the balance of the span. It should be slightly "span heavy" when closed, which means that its center of gravity should be toward the navigation channel from the rotating center, when closed to marine traffic. This produces a slight positive dead load reaction at the live load bearings.

Bascule bridges consist of a large moving mass of superstructure, deck, and counterweight, which can be considered balanced for structural purposes. The span can be considered

essentially rigid as it rotates between opened and closed positions. This applies whether it is a simple trunnion leaf, a rolling lift, or an articulated counterweight type. The counterweight gravitational moment is always in a fixed position relative to the bascule span due to the parallelogram arrangement of the pivot points. An exception to this rule is a bascule with operating struts as they move in a different path than the superstructure. The operating strut could be heavy enough to have a noticeable effect on the balance, but this usually only happens with single leaf railroad bridges.

It can be very difficult to achieve a correct balance state, as the amount of imbalance, measured as force at the live load shoes, should be less than 1% of the dead weight. If a bascule bridge leaf had zero imbalance, the machinery would not have to overcome any gravitational loadings while opening or closing the span. The correct balance condition increases the amount of power required to open the leaf because the leaf is actually made to be in a state of unbalance. Opening the span requires lifting the center of gravity through the arc it traverses from the closed to open position. This extra power is a small fraction of the operating cost of a bridge, and the extra machinery strength required is negligible compared to other loadings which should be considered in design.

3.1 Vector Analysis

The position of the center of gravity of the moving leaf can be located so that the span heavy unbalance is at a maximum when the leaf is seated, decreases to zero as the leaf opens, and assumes a negative, "counterweight heavy", condition as the span reaches the open position. This ideal condition of balance provides stable seating in the closed position for live load. It also stabilizes the span in the open position so that a drop of the open leaf would be prevented should there be a mechanical or electrical failure. The ideal condition of balance is illustrated in Figure 1.

The vector "r" from the axis of rotation to the center of gravity should be small, to avoid excessive impact forces on seating, and to minimize power requirements. Hool and Kinne, in "Movable and Long Span Steel Bridges", recommend that the horizontal distance from the axis of rotation to the center of gravity should be just enough to cause a moment sufficient to turn the leaf against friction. The friction factor, k, ranges from 15 percent of

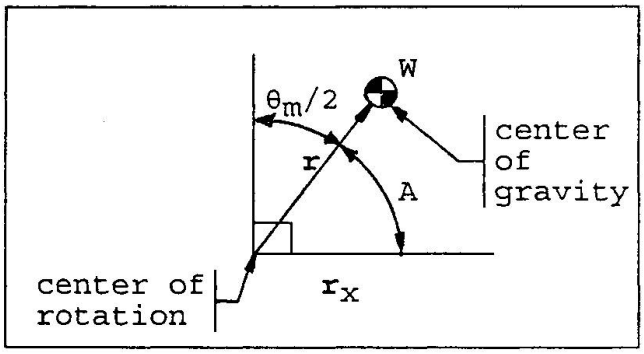

FIGURE 1 - Vector

the total weight of the moving span for a trunnion bascule with friction bearings to 0.9 percent for a rolling lift bridge. These numbers are based on heavy truss type bascule bridges. More flexible leaves, or very low friction trunnions, require the amount of imbalance to be increased somewhat. The friction moment is Wr_tk and this is equated to the span weight times the horizontal component of the vector to the center of gravity, when the leaf is closed ($\theta = 0$).

$$Wr_x = Wr_tk \qquad \text{Eq (1)}$$

W = weight of the moving leaf
r = vector from the axis of rotation to the center of gravity of the moving leaf
r_x = horizontal component of vector r
r_t = radius of the bascule trunnion or rolling lift curved tracks
k = coefficient of friction; 0.15 for friction trunnions, 0.009 for rolling lift or roller bearing trunnion friction
A = angle between r and r_x

θ = opening angle
θ_m = maximum opening angle

For bascule bridges with bronze-journaled trunnions in the 250 to 750 mm diameter range, the distance "r_x", of the horizontal component of "r" would range from 2.25 to 112.5 mm. For rolling lift bridges with curved track radii of 8 meters, the distance, "r_x", would be 72 mm.

The angle "A", should be chosen so that the maximum opening angle, θ_m, is equally divided about the vertical axis.

$$A = 90 - (\theta_m/2) \qquad \text{Eq (2)}$$

This will minimize work and wear of the operating machinery during a complete operating cycle while accomplishing the desired gravitational stabilization. The horizontal component, "r_x", with the leaf closed ($\theta = 0$), determines the gravitational seating force at the live load shoes. "r_x" equals 0.15 times the trunnion radius or 0.009 times the curved track radius, as in equation (1) and equals "r" times the cosine of "A" when $\theta = 0$.

$$Wr_x = Wr_t k = Wr \cos(A+\theta) \qquad \text{Eq (3)}$$

3.2 Balancing

The desired position of the center of gravity should be determined when designing a new bridge. The condition is difficult to achieve due to construction variations, accommodated by pockets in the counterweights where small weights can be added, removed or shifted. The pockets are usually located so that longitudinal and vertical adjustments in the center of gravity can be made. Lateral balance is difficult to measure and does not have as profound an effect on operation.

Not all designers have agreed on the ideal balance condition, resulting in a wide variation in existing bridge balance conditions. Redecking, strengthening, removing overhead trolley wires and supports, painting, moisture absorption and build up of debris can significantly affect the balance condition. The balance condition should be ideal to reduce power requirements and machinery wear and assure safe and reliable operation. Adjustment of the balance condition of existing bridges has frequently involved placements of weights with test openings of the bridge until an acceptable condition of balance was reached. Trial and error methods entail considerable time and expense while never assuring that the balance condition is actually known.

Vector analysis can be used to accurately balance a bascule leaf about the rotational axis. The existing span imbalance vector Wr_i, can be determined by measuring and recording the operating torque at the rack pinion shafts as the bridge is opened and closed under controlled conditions of no wind, snow or ice.

With the initial values of "Wr_i" obtained, and the desired final imbalance value of "Wr_f" assumed, vector analysis can be used to determine the required weight shift (see Figure 2):

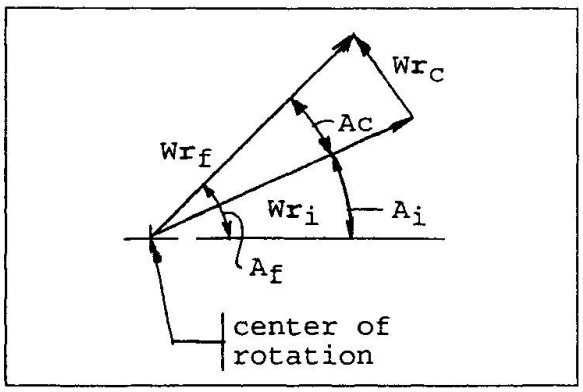

FIGURE 2 - Correction Vector

The correction vector "Wr_C" can be accomplished by shifting small movable weights from the lower to the upper counterweight pockets as shown in Figure 3:

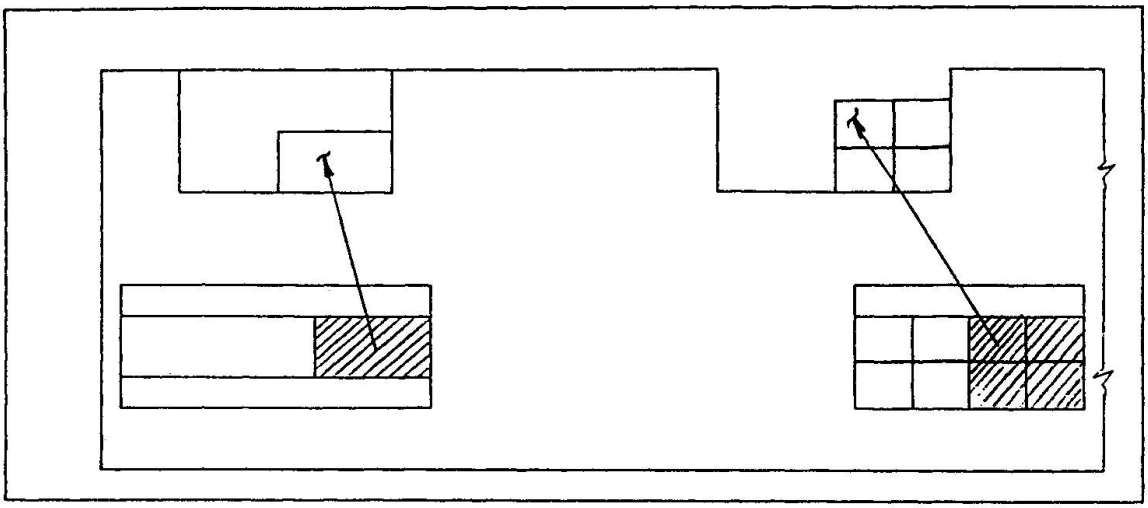

FIGURE 3 - Vertical Section at Counterweight Parallel to Roadway

Many bridges require the addition of weight on the tip of the cantilever arm in order to properly locate the center of gravity.

Friction is canceled out, assuming it is constant, so that the imbalance torques at the rack pinion shafts can be readily derived:

$$(Tup + Tdn)/2 = Wr \cos (A + \theta) \qquad \text{Eq (4)}$$

where: Tup = torques to open
Tdn = torque to close
θ = opening angle at measurement

4. CONCLUSIONS AND RECOMMENDATIONS

Double leaf bascule bridges become unstable because they are poorly designed, poorly constructed, or poorly maintained. They are more susceptible to deficiencies from these causes because they are more delicate than other types of movable bridges.

- Properly designed double leaf bascule bridge should be very rigid.
- The leaves of the double leaf bascule should be firmly supported on very solid live load shoes located adjacent to the pier sea wall, far from the center of rotation.
- The balance of the double leaf bascule should be such that a dead load reaction exists on the live load shoes when the bridge is closed, that is in excess of any negative reaction from live load.
- The roadway surfaces on the double leaf bascule should be formed so that there is no misalignment at the joints, either at the heels of the leaves or at the toes. The vertical curve should be continuous from one leaf to the other and from each leaf to its approach.
- Center locks should minimize the difference in vertical deflection of the tips of the leaves under live load. They should have little or no clearance for free vertical displacement, while allowing longitudinal and rotational displacement due to thermal, live load or other effects.

Deterioration and Evaluation of Chien-Kou Viaduct in Taipei

Détérioration et évaluation du viaduc Chien-Kou à Taipei

Schäden und Zustandsbeurteilung des Chien-Kou-Viadukts in Taipei

Shuh-Juh LIN
Executive Vice President
China Engineering Consultants
Taipei, Taiwan, China

S. J. Lin, born in 1931, received his B.S. degree in civil engineering from National Cheng Kung University, Tainan, Taiwan. Since graduation he has devoted himself to the design and supervision of highway bridges and other structures for 40 years.

Ming-Huang YEH
Manager
China Engineering Consultants
Taipei, Taiwan, China

M.H. Yeh, born in 1942, graduated from Taipei Institute of Technology and did post graduate studies at the Asian Institute Technology. Since graduation he has devoted himself to the design and supervision of highway bridges for 30 years.

Jaw-Lieh WANG
Division Chief
China Engineering Consultants
Taipei, Taiwan, China

J. L. Wang, born in 1953, received his M.S. degree in civil engineering from the National Cheng Kung University, Tainan, Taiwan. Since graduation he has devoted himself to the design of bridges and buildings for 15 years.

SUMMARY

Chien-Kou Viaduct was the first urban expressway built in Taiwan in 1983. The traffic growth increased rapidly since then. Traffic volume of the viaduct had already reached its capacity, and some damages were observed in the past years. This paper focuses on the damage assessment and the safety evaluation of the viaduct, especially, the non-destructive test for the investigation of corrosion rate of steel rebar.

RÉSUMÉ

Le viaduc Chien-Kou a été la première autoroute urbaine construite à Taiwan, en 1983. La croissance du trafic a depuis rapidement augmenté. Le volume du trafic sur le viaduc ayant déjà atteint la capacité du pont, certains dégâts ont pu être observés ces dernières années. Cet article fait le point sur l'évaluation de ces dégâts et de la sécurité du viaduc. L'essai non-destructif pour l'estimation du taux de corrosion de l'acier est exposé.

ZUSAMMENFASSUNG

Die Chien-Kou-Hochstrasse war die erste, 1983 in Taiwan gebaute Stadtautobahn. Seither ist das Verkehrsaufkommen rapide gestiegen. Da die Verkehrsbelastung der Hochstrasse bereits ihr Mass überschritten hatte, kam es in den letzten Jahren zu deutlichen Schäden. Der Beitrag konzentriert sich auf die Schadensaufnahme und die Beurteilung der Tragsicherheit. Insbesondere wird die zerstörungsfreie Prüfung des Bewehrungsstahls auf seine Korrosionsrate hin geschildert.

1. INTRODUCTION

Chien-Kou Viaduct was the first urban expressway built in Taiwan. It was completed in 1983. The total length of the viaduct was more than five kilometers. The viaduct is the main traffic route passing through the north and south parts of the Taipei city, and is connected to the No. 1 National Freeway. The open space under the viaduct was utilized for multi-purposes. It was designed to be gas stations, parking lots or ground roads. The design criteria of structural system of the viaduct were concerned not only the economics and safety, but also the aesthetics and uniformity. The clearance under the viaduct has to fulfil the usage requirements, and also minimize the elevation of viaduct to ease the traffic.

The superstructure of viaduct was continuous prestressed concrete box girders. The standard deck width was 22.6 meters. Two single-cell box girders connected with deck slab were used and transversal prestress was adopted in the deck slab. The construction schemes were ground staging and precast segmental free cantilever methods depending on the traffic detour plan. The ground staging parts were two to four span continuous P. C. box girders with constant cross section as shown in Figure 1. The segmental free cantilever parts had a maximum span length 60 meters and various cross sections as shown in Figure 2. All piers were designed to be single column type without pier caps.

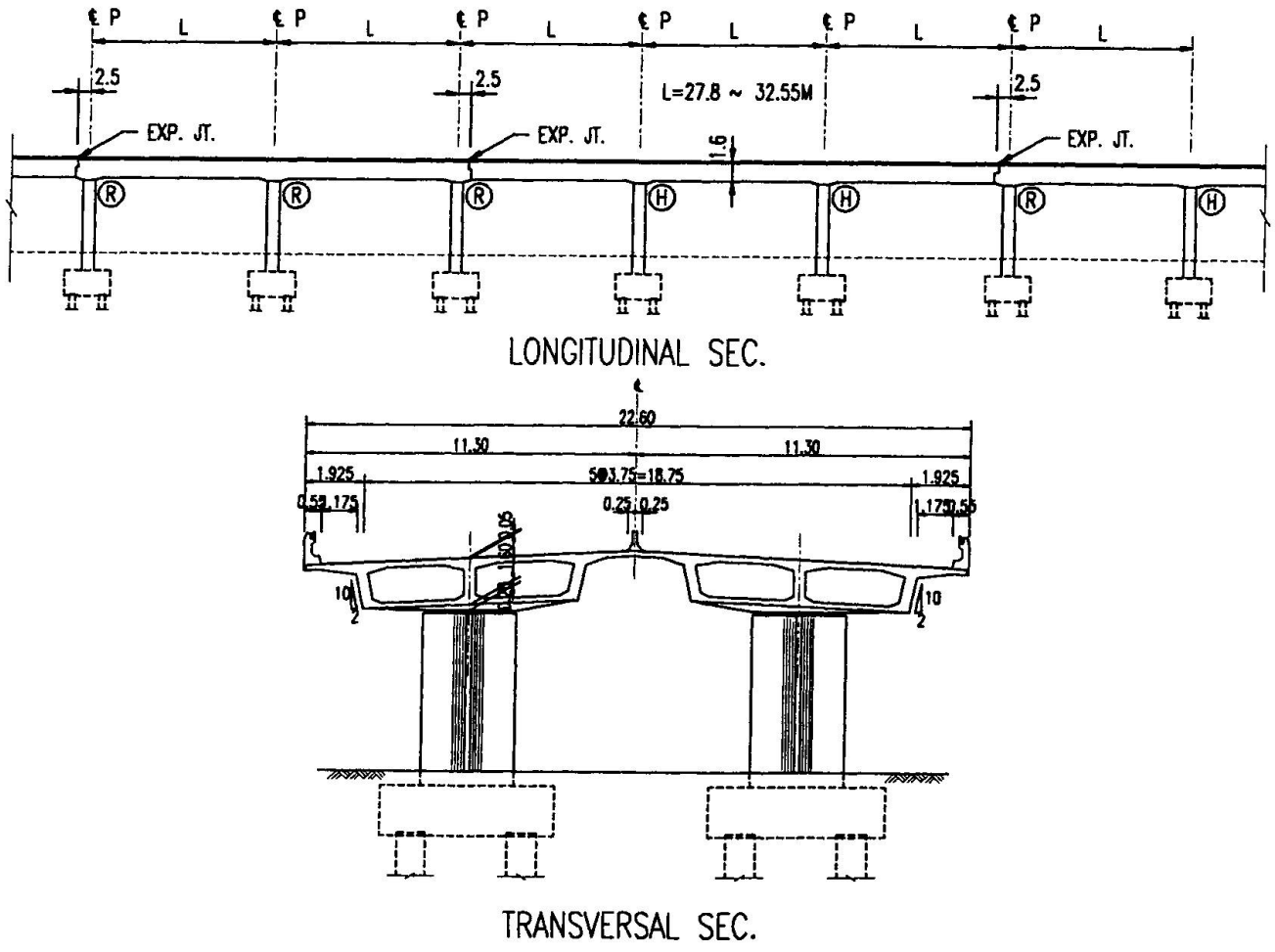

Figure 1. Ground Staging Method

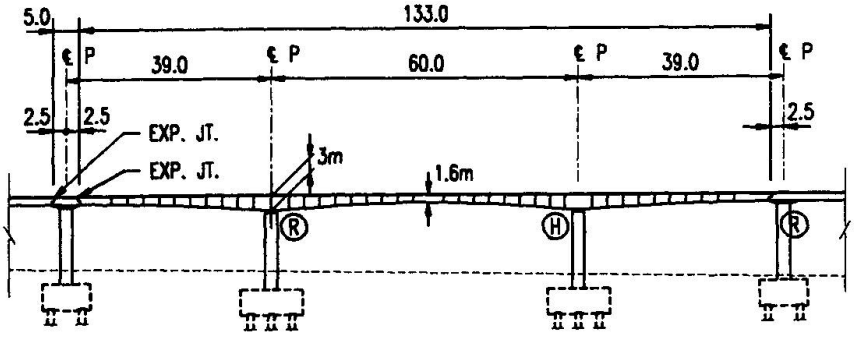

Figure 2. Free Cantilever Method

2. DAMAGE ASSESSMENT

The usage of Chien-Kou Viaduct was already up to its capacity. The traffic volume has reached 7180 PCU per hour which is the highest one of all the viaducts in Taipei. Due to the traffic growth and number increase of heavy vehicles, in addition to occurrences of several earthquakes in the past, there were some damages found in Chien-Kou Viaduct recently. In order to assess the safety and evaluate the remaining loading capacity of the bridge, a series of tests were conducted as listed in Figure 3. The tests included non-destructed test of investigating rebar corrosion and evaluation of concrete protection ability.

The structure of viaduct was mainly P.C. box girders and R.C. piers. The resisting capacity of the viaduct depends mainly on the strengths of concrete and reinforcement. Therefore, the inspections were focus on the damage assessment of these two materials. The checking items were damage assessment on main structure, evaluation of concrete strength and concrete deterioration, and investigation of rebar corrosion.

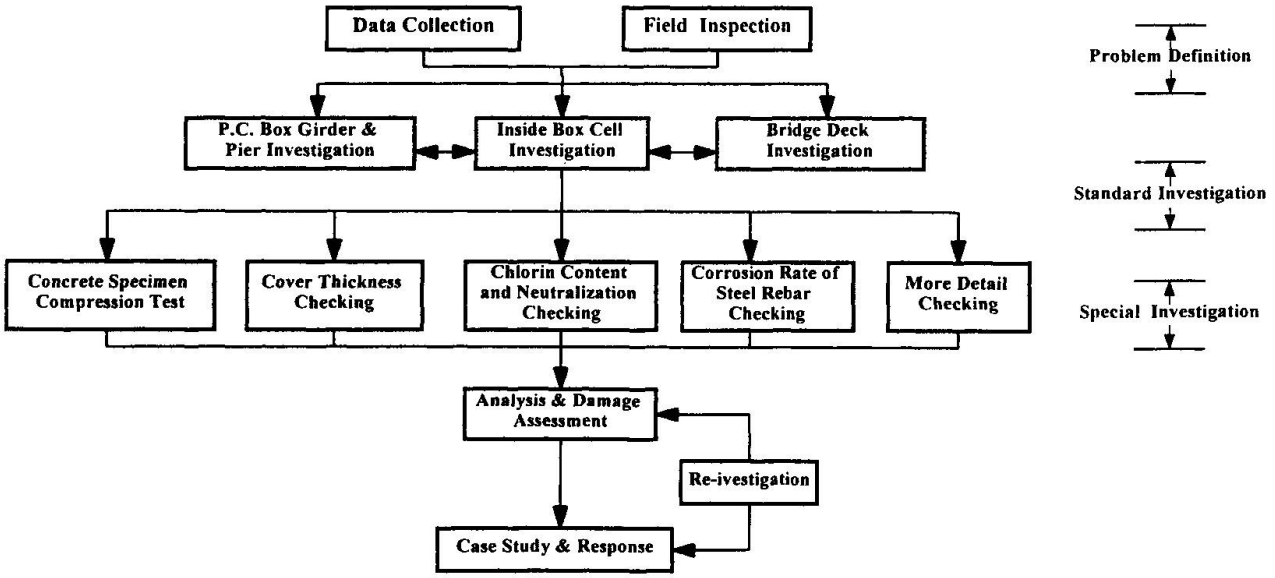

Figure 3. Inpsection of Chien Kou Viaduct

3. INVESTIGATION OF CONCRETE

The take-core tests were done and the specimens showed that there were no deterioration of concrete. There were also no cracks found on the substructure. However, there were several kinds of cracks observed in the superstructure, such as:

(1) Cracks on P.C. box girders : This kind of cracks included three different types - type A crack on the cold joint of bottom slab and web, type B crack on girder web along the strand and type C crack on the bottom slab as shown in Figure 4. There was some water found on type A and C cracks because of the broken drainage pipe. The reason that caused type C crack was related to the service loading.

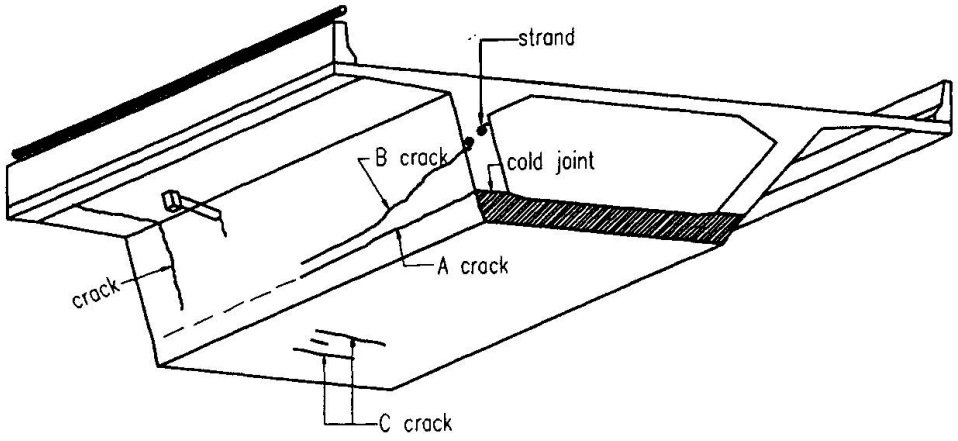

Figure 4. Cracks on P.C. Box Girder

(2) Cracks on connection joint: The main crack on side face of connection joint was alone point a to point b as shown in Figure 5. This kind of crack was caused by differential shrinkage and creep of two different age or strength of concretes. There were also cracks on bottom face of connection joint as shown in Figure 6. This kind of crack was caused by principal stress of bearing reactions as shown in Figure 7. There were no cracks observed on the corner of girder or anchor zone of strand since a detail study was done for the reinforcement design of the connection joint.

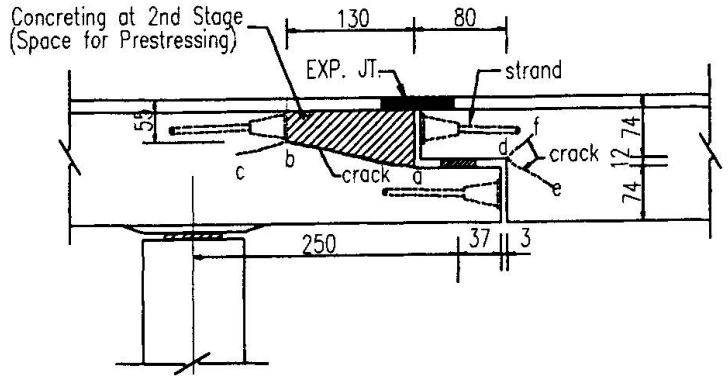

Figure 5. Cracks on Connection Joint

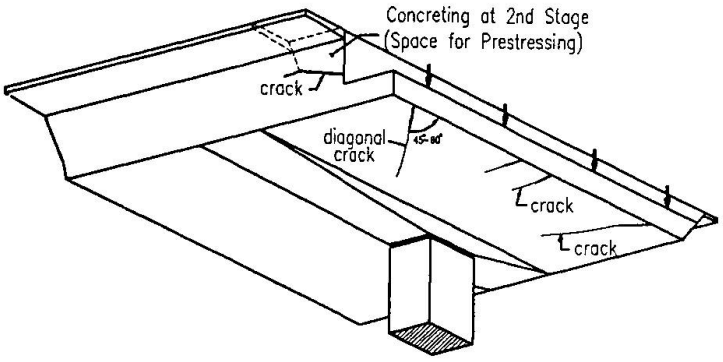

Figure 6. Cracks on Bottom of Connection Joint

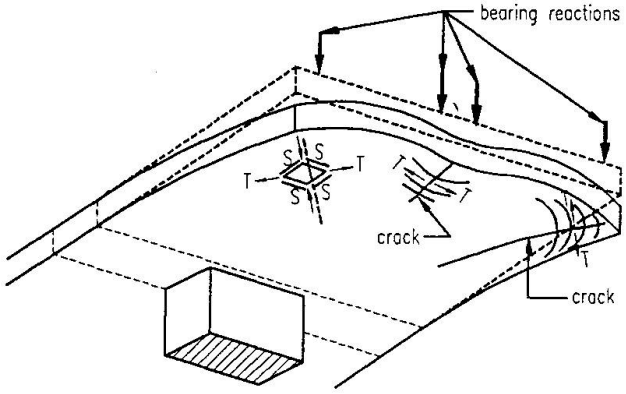

Figure 7. Cracks Caused by Principal Stress of Bearing Reactions

(3) Cracks on diaphragm: There were cracks on the bottom of girder diaphragm as shown in Figure 8.

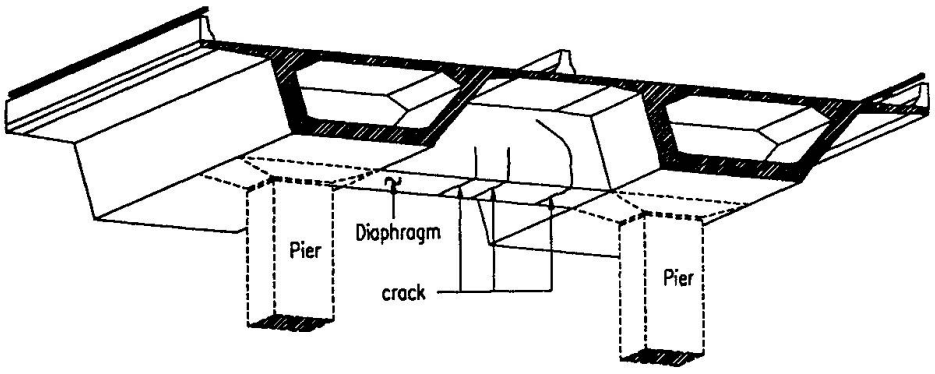

Figure 8 Cracks on Diaphragm

4. INSPECTION OF STEEL REBAR CORROSION

In general, the concrete is an alkali material, the rebar within the concrete should not be corroded unless the concrete is neutralized or the thickness of cover is not enough. The test results showed that the concrete of Chien-Kou Viaduct had a PH value around 10 and the average content of

chloride was below 0.01%. No neutralization was observed and the concrete was sufficient to protect the reinforcement. However, there were still some minor corrosions found on the structure surface. They were summaried as follows:

(1) There were corrosions observed on the parapet and central barrier which and resulted in the concrete deterioration. According to a detail investigation, it can be concluded that the corrosion were caused by no enough cover thickness. One other possible reason was that it might be caused by the exhaust from the vehicles .

(2) Few rebars located on outer edge of bottom slab or middle web were exposed, but they were not serious corroded.

(3) There were large area of corrosion spots observed in the bottom slab of some box girders. An electromagnetic test was conducted to examine the thickness of concrete cover. The test results indicated the thickness was still sufficient to protect the rebar and there was no corrosion developed. The smear might be come from the formwork dirt in construction.

5. EVALUATION OF CORROSION RATE OF REINFORCEMENT

A specially designed corrosion monitoring probe was used to measure the corrosion rate of steel rebar within the concrete. The test was using a special device to measure the electricity in the rebar, and established the deterioration rate of rebar R (μm / year) to electricity I (μA) relationship as shown in Equation 1. Another one was established by using the take-core specimen. The rebar in the specimen was electrified to increase the corrosion rate and observed the crack propagation on the concrete cover. From those experimental data, the relationship among the corrosion quantity Q (μm) which caused the crack on concrete cover, cover thickness C and rebar diameter D can be determined as in Equation 2. According to these two equations, it can be estimated that there will be only few corrosions occurred in next ten years. Especially, no crack will be found in the high stress zone.

$$R = X * I \quad \text{---------- (1)}$$

$$Q = Y (C / D)^m + Z \quad \text{---------- (2)}$$

where X, Y, Z and m are constants

6. CONCLUSION

A series of comprehensive tests were performed to assess the safety and serviceability of Chien-Kou Viaduct. The test results showed that the concrete strength on the main structure was still fulfil the requirement and no severe corrosion was detected. Only some minor damages were found which can be easily repaired and the repairing work is under going now.

The corrosion spots observed on the structure surface was thought as a severe corrosion problem at first time. But after a further investigation, no corrosion was actually found. The test results could clarify the suspicious from the public.

Stability of a Steel Bridge Girder Strengthened by Prestress

Stabilité d'une poutre de pont renforcée par précontrainte

Stabilität eines durch Vorspannung verstärkten Stahlbrückenträgers

Mark A. BRADFORD
Associate Professor
Univ. of New South Wales
Sydney, NSW, Australia

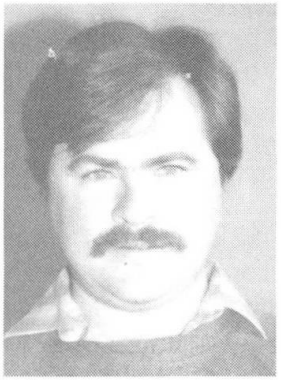

Mark Bradford, born in 1955, received his BSc, BE and PhD degrees from the University of Sydney, Australia. He worked in private practice and in research before joining the University of New South Wales in 1986, where he is an associate professor in the Department of Structural Engineering.

SUMMARY

Steel bridges with plate girder substructures may be strengthened and stiffened during their lifetimes by prestressing the bottom flange. In the absence of live loading, the prestressing operation may produce large compressive stresses in the bottom flange, so that instability of this flange is a necessary design consideration. The paper describes a method of buckling analysis of plate girders during prestressing, and compares the solutions with those of the U-frame approach deployed for assessing the stability of steel through girders.

RÉSUMÉ

Au cours de la vie utile des ponts à poutres métalliques, il est possible de renforcer et augmenter la rigidité de ces dernières par précontrainte de leurs membrures inférieure. La mise en précontrainte en l'absence de surcharge produit d'importantes contraintes de compression dans les membrures inférieures, qui doivent être prises en compte lors du dimensionnement. L'auteur décrit une méthode d'analyse du voilement des poutres métalliques soumises à la précontrainte et compare les solutions obtenues avec celles d'un modèle en cadre en U mis au point pour examiner la stabilité de poutres à âme pleine en acier.

ZUSAMMENFASSUNG

Stahlbrücken mit Blechträgern können während ihrer Nutzungsdauer verstärkt und versteift werden, indem ihr Untergurt vorgespannt wird. Beim Fehlen der Verkehrslast können beim Vorspannprozess grosse Druckspannungen im Untergurt auftreten, so dass die Instabilität des Gurtes ein notwendiges Bemessungskriterium darstellt. Der Beitrag beschreibt eine Methode zum Beulnachweis von Blechträgern unter Vorspannung und vergleicht die Lösungen mit denen eines U-Rahmen-Modells, das zur Stabilitätsuntersuchung von Massivstahlträgern hergeleitet wurde.

1. INTRODUCTION

In many steel bridges whose substructure consists of steel I-section plate girders, the bottom flange and lower portion of the web may yield if the bridge is required to support heavier loads than that for which it was initially designed. The onset of inelasticity may be prevented by welding a steel plate to the bottom flange, but prestressing the girder is a viable alternative since it both delays yielding of the bottom flange and produces a camber in the bridge which may control deflections.

Post-tensioning of steel beams and composite steel-concrete girders has been considered by the author [1,2,3], and it was concluded that instability of the flange which is compressed during prestressing may occur. Although a closed form solution was presented for a composite beam [3], recourse generally has to be made to a computer program for solving the problem. The restraint provided by the superstructure in a steel plate girder bridge means that the buckling mode must necessarily be distortional [4] as shown in Fig. 1. The computer program must therefore be required to account for the distortion or flexing of the web during buckling.

In this paper, an efficient method for the analysis of elastically restrained beam-columns which distort during buckling is modified to incorporate prestressing forces produced by tensioning high strength steel bars or prestressing strand near the bottom flange. The analysis is very efficient computationally, and allows the prestressing force to cause buckling to be calculated for a range of beam geometries, superstructure restraints and prestressing eccentricities. Because of the number of significant parameters involved, an exhaustive parameter study is prohibitive and only a specific girder is examined in detail. The results are compared with a simplified U-frame model used for analysing steel through girders, and the latter approach is shown to be a little conservative.

2. DISTORTIONAL BUCKLING MODEL

An efficient analysis for the distortional buckling of I-section beam-columns with elastic restraints was presented by Bradford [5]. The model assumed that the beam-column was simply supported and subjected to uniform bending and compression, so that the buckling deformations could be represented by a sine curve with a given number of half-wavelengths. In addition, it was assumed that only the web distorted during buckling, with the flanges buckling as rigid bodies. This is applicable to a prestressed plate girder bridge, since the webs are invariably slender and the flanges are stocky.

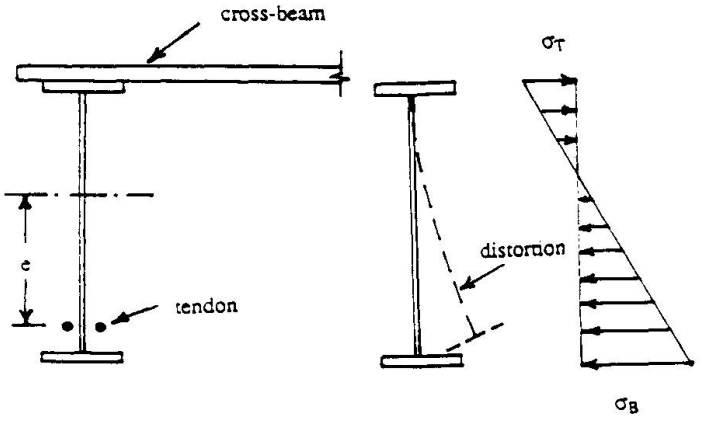

Fig. 1 Prestressed girder and buckling

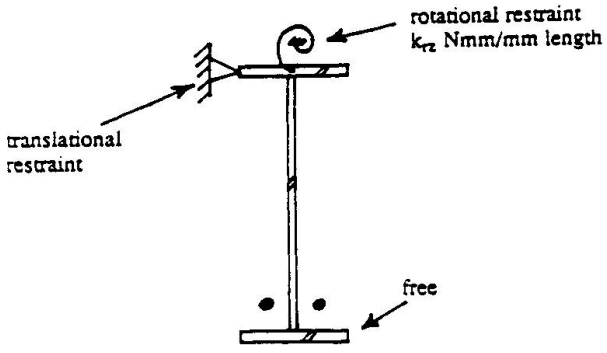

Fig. 2 Top flange restraint model

The distortional buckling analysis was also able to account for elastic restraints at the level of the top or bottom flange. For the problem under consideration, the bridge superstructure effectively prevents lateral buckling displacement and in-plane rotation of the top flange of the plate girder, but provides elastic restraint against twist of the top flange of the girder. This continuous elastic elastic restraint (see Fig. 2) has a stiffness of $k_{rz} = 4EI_s/L_s$ [6], where E is Young's modulus and I_s is the second moment of area of the superstructure per unit length of bridge girder taken about a longitudinal axis parallel to the girder, and L_s is the lateral spacing of the girders.

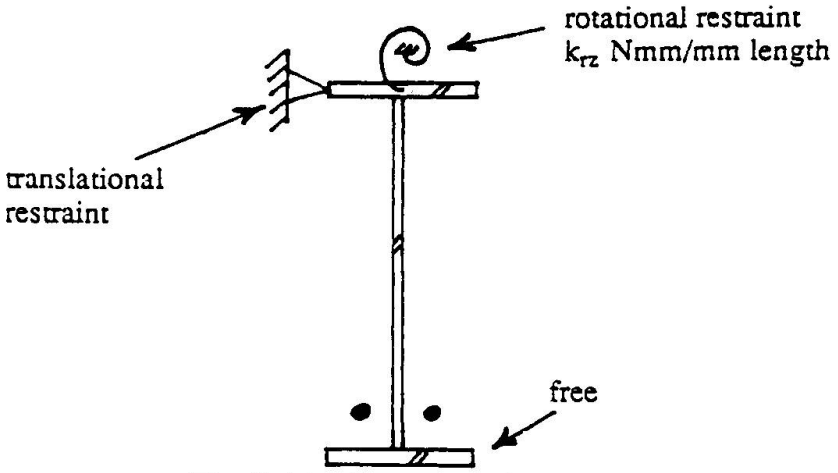

Fig. 2 Top flange restraint model

The vector of the four buckling degrees of freedom { q } consists of the lateral displacements and twists of the top and bottom flanges. The strain energy stored during buckling may then be written as

$$U = \frac{1}{2} \{ q \}^T ([k]+[k_r]) \{ q \} \tag{1}$$

where [k] is the elastic stiffness matrix and $[k_r]$ is the restraint stiffness matrix. These matrices have been derived explicitly by Bradford [5].

The beam-column is assumed to be subjected to a moment M and an axial force N, and factored by the load factor λ until buckling occurs. If the girder is subjected to a prestressing force P, then these actions are clearly

$$\lambda M = \lambda P e \tag{2}$$

and

$$\lambda N = \lambda P \tag{3}$$

where e is the eccentricity of the prestressing force below the centroid of the plate girder. The actions λM and λN do work V during buckling, which can be written as

$$V = \frac{1}{2} \{ q \}^T \lambda [g] \{ q \} \tag{4}$$

where [g] is the stability matrix derived explicitly by Bradford [5].

Invoking the principle of stationary potential energy [7] produces

$$\frac{\partial (U-V)}{\partial \{ q \}} = \{ 0 \} \tag{5}$$

so that, for nontrivial buckling displacements { q },

$$| [k]+[k_r]-\lambda [g] | = 0 \tag{6}$$

Equation 6 may be solved by standard eigenvalue routines for the buckling load factor λ and the mode shape $\{ q \}$. Because the stiffness and stability matrices are only 4 by 4, solution of the eigenproblem in Eq. 6 is instantaneous on a personal computer.

3. THROUGH GIRDER BUCKLING MODEL

Through girders are inverted bridges of the type considered herein, so that the deck is connected to the bottom flange and the top flange is subjected to compression under gravity loading. These through girders may be analysed for instability of their compression flanges by a U-frame approach [8].

The main assumption in the U-frame approach, which is an inverted U-frame for this study, is that the bottom flange is restrained elastically only by the web with a continuous translational restraint stiffness α_t, and furthermore that the bottom flange is a strut subjected to a constant compressive force. The value of α_t may be calculated by applying a pair of equal and opposite unit forces to the girders at the bottom flange level, and calculating the deflection of the bottom flange Δ. The flexibility of the web and the rotation at the attatchment to the superstructure contribute to Δ, so that

$$\Delta = \frac{h^3}{3EI_w} + \frac{h^2}{k_{rz}} \tag{7}$$

where I_w is the second moment of area of the web per unit length of girder ($t_w^3/12$) and h is the distance between the flange centroids. The translational stiffness α_t can then be calculated from the flexibility Δ by

$$\alpha_t = \frac{1}{\Delta} \tag{8}$$

A strut with a continuous elastic translational restraint is analysed in Bleich [9]. Based on this analysis, it is shown in Oehlers and Bradford [8] that the critical force to cause buckling of the bottom flange is

$$N_{cr} = 2\sqrt{EI_F\alpha_t} \tag{9}$$

where I_F is the second moment of area of the bottom flange ($b^3t_f/12$). Equating the critical load in the bottom flange N_{cr} to the force in the bottom flange produced by the prestressing force P at eccentricity e yields

$$P_{cr} = \frac{2\sqrt{EI_F\alpha_t}}{1 + \frac{eh}{2r^2}} \tag{10}$$

where r is the major axis radius of gyration of the plate girder ($\sqrt{I/A}$).

4. BUCKLING STUDY

A steel plate girder bridge with a web depth h = 1700mm and thickness t_w = 15mm and flange widths b = 300mm and thicknesses t_f = 25mm has been studied. The eccentricity of prestress e is at 800mm. Under a prestressing force P (in MN), the stress in the bottom flange will be 64.7P MPa and the camber is $ML^2/8EI = 0.029PL^2$ where L is in metres.

Figure 3 shows the prestressing force to cause buckling versus the buckling half-wavelength as a function of the torsional restraint at the top of the flange for the first harmonic. For all torsional restraint values except zero, the curves have a minimum and are garland shaped. The curves may be plotted for a given length of attachment of tendons to the plate girder L_t by translating the garlands l, $2l$,... to the right to create a series of cusps as are familiar in local buckling studies and presented in Bulson [10].

Consider the plate girders spaced 10m apart with transverse cross beams in the deck, typically each of second moment of area $I_s = 2.5 \times 10^7$ mm^4 spaced at 4m intervals. The torsional restraint is $4EI_s/L_s = 2.0 \times 10^9$ Nmm or $k_{rz} = 5.0 \times 10^5$ Nmm/mm length of girder. A prestressing force P of 2.46 MN in a girder of length L = 35m will produce a precamber of L/400 and a bottom flange compressive stress of 166 MPa. Such a prestressing force is obtainable from tendons of total effective area 2730 mm^2 stressed to 900 MPa. Clearly from Fig. 3, buckling will occur for attachment lengths L_t greater than 7.5m. For a strength analysis using limit states or LRFD principles, this length would have to be reduced even further.

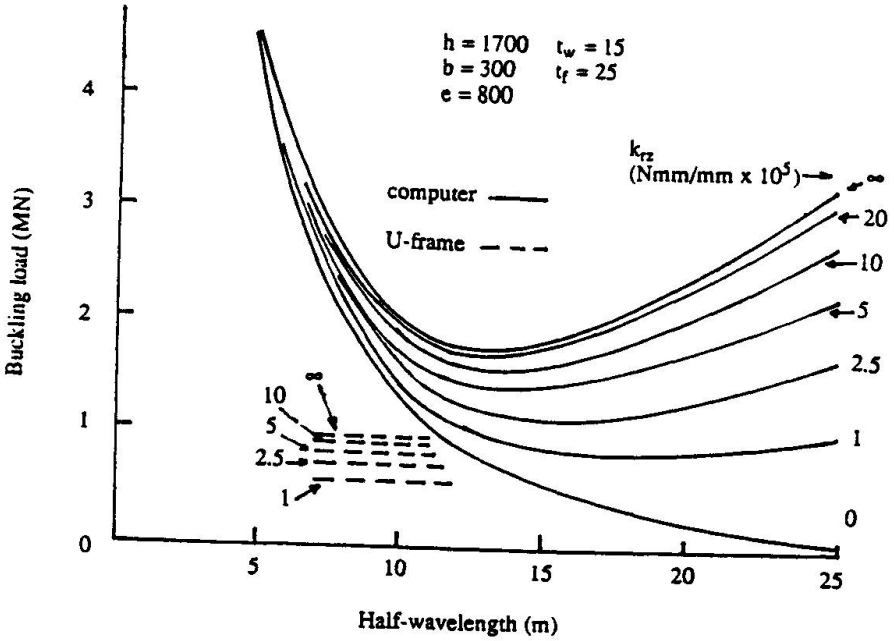

Fig. 3 Buckling loads

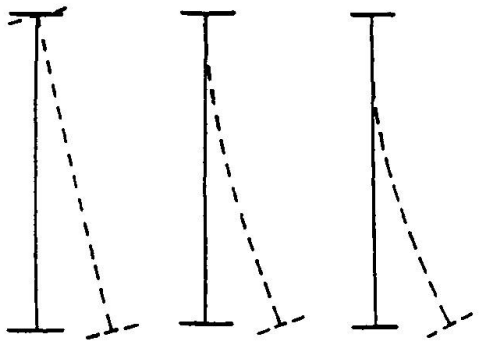

$k_{rz} \times 10^5 =$ 0 5 ∞

Fig. 4 Buckling modes for l = 12.5 m

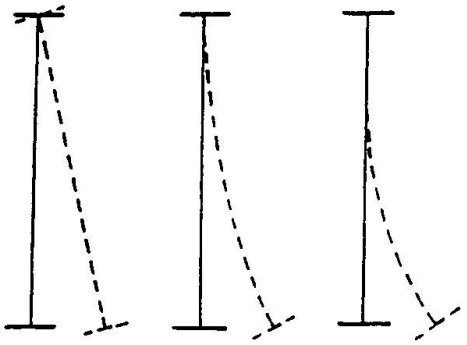

0 5 ∞

Fig. 5 Buckling modes for l = 7 m

Figure 3 also demonstrates the substantial effect that the restraint of the deck has on the minimum buckling load. The effect of this torsional restraint can also be incorporated into the inverted U-frame approach, as noted in the previous section. The buckling loads calculated from Eq. 10 are also plotted in Fig. 3. While being a reasonable and conservative prediction of the nadir of the computer-generated curves, they are quite conservative for the shorter tendon attachment lengths L_t which would be met in practice. The buckling modes are plotted in Fig. 4 at l = 12.5m for $k_{rz} = \infty$, 5×10^5 and 0 Nmm/mm, and in Fig. 5 for l = 7m. The increased cross-sectional distortion as k_{rz} increases is obvious.

5. CONCLUDING REMARKS

A computer-based method for analysing the elastic lateral-distortional buckling of prestressed plate girders in steel bridges has been described. Prestressing is an efficient means of strengthening and stiffening existing steel bridges, and instability of the plate girder during the stressing operation is a necessary consideration in the absence of substantial gravity loads. The effects of the torsional restraint provided to the top flange by the stiffness of the cross beams in the deck was shown to be considerable, but quite less than a rigid torsional restraint.

Because of the large number of significant parameters that affect the buckling solution, only one bridge girder was considered for illustrative purposes. This girder was liable to instability under the quite large prestressing forces required to camber the bridge and to impart practical compressive stresses in the bottom flange. Under this combination of geometry and loading, it was shown that limitations had to be placed on the distance between the attachment of the tendon to the plate girder. The U-frame model affords a convenient, albeit conservative, model of the elastic buckling which can be used in lieu of the computer solution.

REFERENCES

[1] BRADFORD M.A., Buckling of prestressed steel girders. Engineering Journal, American Inst. of Steel Constr., 28, 1991, 98-101.

[2] BRADFORD M.A., Elastic stability of composite tee-beams strengthened by prestress. Proceedings of Instn. of Civil Engrs., London, Part 2, 91, 1991, 975-985.

[3] BRADFORD M.A., Buckling of post-tensioned composite beams. Structural Eng. and Mechancis, 2, 1994, 113-123.

[4] BRADFORD M.A., Lateral-distortional buckling of steel I-section members. Journal of Constr. Steel Research, 23, 1992, 97-116.

[5] BRADFORD M.A., Buckling of elastically restrained beams with web distortions. Thin-Walled Structs., 6, 1988, 287-304.

[6] HALL A.S., and KABAILA A.P., Basic concepts of structural analysis. GreenwichSoft, Sydney, 1986.

[7] TRAHAIR N.S., Flexural-torsional buckling of structures. Chapman and Hall, London, 1993.

[8] OEHLERS D.J., and BRADFORD M.A., Steel-concrete structural members: fundamental behaviour. Pergamon Press, Oxford, 1995.

[9] BLEICH F., Buckling strength of metal structures. McGraw Hill, New York, 1952.

[10] BULSON P.S., The stability of flat plates. Chatto and Windus, London, 1970.

Strengthening of an Externally Prestressed Bridge

Renforcement d'un pont à précontrainte extérieure

Verstärkung einer vorgespannten Brücke

Eric CONTI
Civil Engineer
SETRA
Bagneux, France

Eric Conti, born in 1963, studied engineering at the Politechnic School and at the ENPC. He worked at the SETRA for 6 years and specialised in engineering' structures. Since December 1994, he has been the manager of the public works department in Reunion Island.

Daniel POINEAU
Chief Engineer
SETRA
Bagneux, France

Daniel Poineau, born in 1937, studied engineering at the ENTPE. Throughout his carrier he has worked on engineering structures. For about twenty years, Daniel Poineau specialised in pathology and repair of concrete bridges.

SUMMARY

Recently, on a bridge with totally external prestressing, the end cross-beams became severely cracked before all the prestressing tendons were tensioned. This paper presents the defects observed, their causes and the reinforcement technique applied. It also describes the calculation method, with a strut-and-tie model, developed for the justification calculations of this part of the bridge. Ideas for the design of new externally prestressed bridges are also given.

RÉSUMÉ

Récemment, les entretoises d'about d'un pont à précontrainte totalement extérieure se sont largement fissurées avant l'application de la totalité de la précontrainte. Le présent article présente les désordres constatés, leurs causes et la technique de renforcement qui fut utilisée. Il décrit également la méthode de calcul, basée sur un modèle bielles-tirants, qui a été développé pour le calcul justificatif de cette partie d'ouvrage. Des conseils sont également donnés pour la conception des ponts à précontrainte extérieure.

ZUSAMMENFASSUNG

Vor kurzem traten noch vor Beaufschlagung der gesamten Vorspannung breite Risse in den Endquerträgern einer komplett extern vorgespannten Brücke auf. Vorliegender Artikel erläutert die festgestellten Mängel, deren Ursachen sowie die zur Verstärkung eingesetzte Technik. Er beschreibt weiterhin die Berechnungsmethode auf Basis eines Zugstangenmodells, das zur Nachweisberechnung dieses Bauteils entwickelt wurde. Des weiteren werden Ratschläge zur Konzeption von Brücken mit externer Vorspannung erteilt.

1. INTRODUCTION

In France, external prestressing is now very widely used in large bridge design. Indeed, this technique has many advantages : structures can be lighter in weight, friction prestressing losses are low and, above all, prestressing reinforcements can be replaced if necessary.

The specificity of external prestressing is sometimes forgotten at the design stage, leading in some cases to regrettable design errors. One of its particular aspects, calling for close attention in bridge design, is the diffusion of anchoring loads or external tendon deviation loads through the structure.

In 1983, on the Aiguilly bridge, one of the first French externally prestressed bridges, the anchoring block, broke away several hours after tensioning. Since then, similar incidents have occurred on other externally prestressed bridges. Recently, on a bridge with totally external prestressing, the end cross-beams became severely cracked before all the prestressing tendons were tensioned.

This article presents the case of this bridge, the defects observed, their causes and the reinforcement technique applied. The article also describes the calculation method, with a strut-and-tie model, developed for the justification calculations of this part of the bridge. Advices for the design of new externally prestressed bridges are also given.

2. INITIAL CONSTRUCTION PROJECT AND DEFECTS OBSERVED

2.1 General bridge characteristics

The bridge is a launched structure comprising ten spans with an average length of 52 meters. The deck is a box girder measuring 10 m in width and 3.40 meters in height.

The bridge is entirely prestressed by means of super 19 T 15 external tendons running along one or two spans and which belong to the following families :

- undulating tendons, deviated one-third of the way along each span,
- temporary antagonistic undulating tendons,
- straight tendons running from one support to the next.

Deck prestressing was centered during launching and comprised four deviated undulating tendons, four antagonistic undulating tendons and four straight tendons. At the end of launching, the antagonistic tendons were detensioned and replaced by four normally deviated tendons. A pair of empty ducts was also provided for subsequent prestressing reinforcement.

The following quantities of tendons, anchored at the deck extremities, were thus provided :

- twelve tendons during the launching phase,
- twelve tendons after the launching phase,
- fourteen tendons in the event of tensioning of reinforcement tendons.

The prestressing load to be anchored was therefore very high: each tendon exerted a load of 330 tonnes before deferred losses, making a total load of 4600 tonnes at each end.

2.2 Characteristics of the end cross-beam and defects observed

In the construction project, the designer planned to anchor the extremities of all the tendons in abutment cross-beams with a thickness of no more than 1.70 m (photo 1).

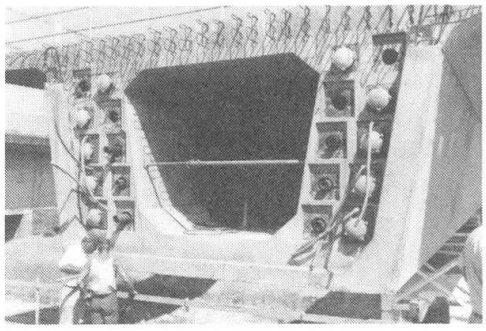

photo 1

The bridge was built according to this design and after casting the formwork was left on the cross-beams to simplify work-site operations. Substantial cracking, localized in two zones (figure 1) was discovered when the formwork was removed :

- on the cross-beam itself, on the lateral faces and on the face opposite of the cross-beam anchorages,
- on the outside of the box girder, along the entire height of the web.

The cracks were mainly horizontal and the largest of them had an opening of 0.2 mm. There was around one crack per prestressing anchorage level. Considering that a reinforced concrete part is liable to rupture when crack opening exceeds 0.4 mm, there was little remaining margin. When these defects were discovered, the final tendons had not yet been tensioned, an action that was bound to further aggravate the situation. Work was therefore suspended and a reinforcement project was devised.

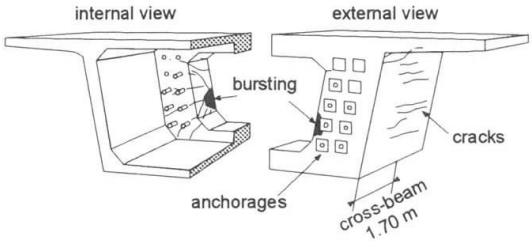

figure 1

2.3 Criticism of initial design

Clearly, the cross-beam on which the tendons were to be anchored was too thin. A length of 1.70 m, corresponding to half the box girder height, is not sufficient to transmit anchoring loads effectively to the box girder. We think that a thickness in the order of magnitude of the deck height (3.40 m) would have been more realistic.

Other factors also had a negative influence. The first problem was the large number of tendons: in general, three to four external tendon pairs are anchored on an end cross-beam. Here there were twice this number.

Secondly, the anchoring points were poorly distributed over the cross-beam: the tendons must be anchored, whenever possible, all around the box girder, as close as possible to the webs and slabs to ensure direct transmission of anchoring loads to the box girder. In this case, the tendons were anchored in two lines arranged at the center of the cross-beam uprights. Some of the anchoring points were thus located almost 90 cm from the box girder walls.

A further aggravating factor was the absence of transverse prestressing - both horizontal and vertical - which would have offset diffusion loads. It is often judicious to use additional prestressing to offset the tensile loads produced by the diffusion of prestressing loads so as to avoid excessive loads on the cross-beam and its subsequent cracking.

Lastly, the quantity of reinforcement required was substantially underestimated, as we will see below.

We wish to point out to designers the importance of taking into account, at the design stage, all these aspects associated with the diffusion of prestressing loads. A number of articles have already discussed this problem [1].

2.4 Criticism of the cross-beam justification in the initial design

In order to design and justify the cross-beam, the designer used the rules given in Appendix 4 of the French prestressed concrete rules [3] concerning "zones of application of concentrated forces". In fact, these rules only cover the case of end members with a cross-section identical to the standard deck cross-section, as is the case for internally prestressed decks. In the present case, the standard deck cross-section is very different from the end cross-section and these calculation models cannot be applied.

By applying Appendix 4, as well as including correct quantities of steel surface and rupture reinforcement immediately behind the anchoring points, the designer provided for "general equilibrium" reinforcement comprising (figure 2) :

- distributed vertical reinforcements: $A_v = 285\ cm^2$
- distributed horizontal reinforcements: $A_t = 345\ cm^2$ (per cross beam)

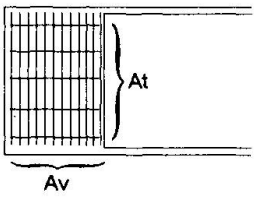

figure 2

We will see below the serious inadequacy of this reinforcement.

3. RECALCULATION OF THE INITIAL DESIGN

In this paragraph, we will examine the various calculation methods used for expert assessment of the defects observed.

3.1 Calculation of the type "deflected wall resting on two supports"

One of the calculation methods applicable is that of Appendix E.5 of the French reinforced concrete rules [4]. This method stems from a strut-and-tie planar calculation model validated by testing.

Here, the cross-beam is considered as a diaphragm attached to the upper and lower slabs (figure 3). In fact, only a part of the prestressing loads are transmitted as shown in the diagram, the rest being diffused directly towards the web. This share of total load can easily be evaluated by assuming that the distribution of stresses leaving the cross-beam is more or less linear. Here, it is 50%, the equivalent of five times 330 tonnes.

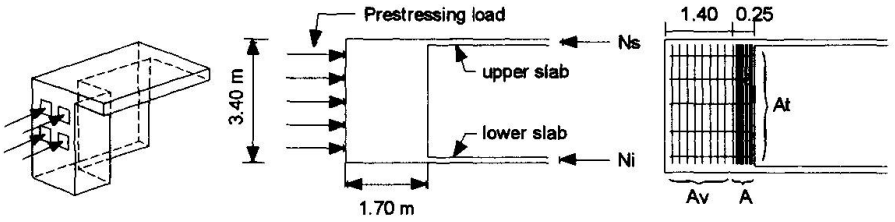

figure 3

The application of Appendix 5 of the BAEL [4] for diffusion in the vertical plane produces the following steel reinforcement requirements:

- principal reinforcement : $A = 235\ cm^2$
- secondary reinforcement : $A_v = 355\ cm^2$
- transverse reinforcement : $A_t = 230\ cm^2$

Comparison with existing steel reinforcement (see paragraph 2.4) reveals a severe lack of vertical reinforcement. Moreover, the vertical reinforcement should have been concentrated on the face opposite the anchoring points, where the cracks were observed.

The simplified calculation model that we have presented cannot be used to determine diffusion in the horizontal plane because the cross-beam is perforated. We therefore developed more representative calculation models to perform this task.

3.2 Finite-elements calculation of the cross-beam

We used a finite-elements method to gain a clearer picture of the cross-beam's mechanical behaviour. The calculation is imperfect, since it is elastic and does not take account of cracks in the concrete, but nevertheless gives a good idea of the loads exerted on the concrete.

Our spatial model concerned a transverse half-deck (symmetrical along the axis). It measured 5.10 meters in length (figure 4). Only the effects of prestressing were considered.

The graphical representation of stress isostatics inside the girder gives a good picture of behaviour (figure 5):

- behind the anchoring plate, loads spread through the cross-beam mass,
- a part of the load, mainly from the lines of anchoring points close to the web, goes directly to the web,
- the other part of the load rises to the upper slab or goes down to the lower slab via the upright.

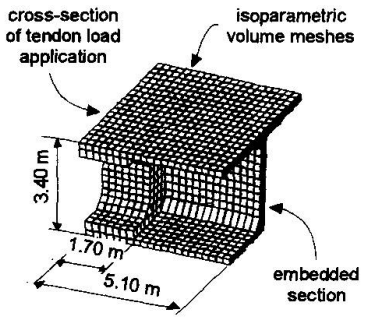

figure 4

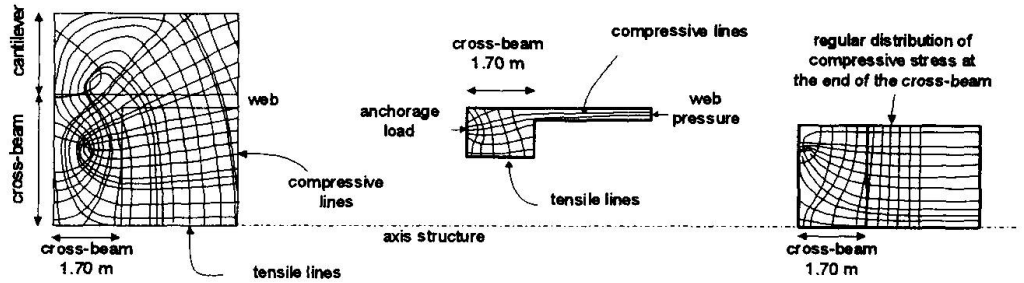

figure 5

When the deformation of the part is visualized, the zones under greatest tension, exactly where the cracks occurred, are revealed. These areas are the back of the upright and the outside of the web (figure 6). We observe a "banana" shaped curvature of the uprights which explains why the web cracks occurred on the outside of the box girder and not the inside. Moreover, on these outer sides, more thermal and shrinkage effects are superimposed, resulting in more extensive cracking.

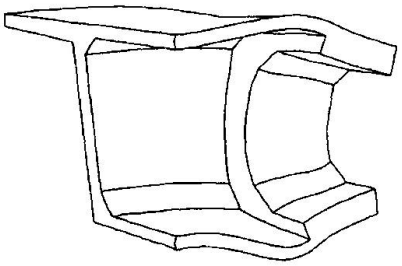

figure 6

The finite-elements model also gives an interesting indication of the tensile loads in the concrete. They reach 7 MPa, three times the tensile strength of concrete. Clearly, the concrete is bound to crack, whatever the quantity of reinforcement used. To prevent this cracking, tensile loads should have been offset by local transverse prestressing of the cross-beams.

As the finite-elements calculation we have just presented is not sufficient to determine stresses in the reinforcements, an additional strut-and-tie model was used.

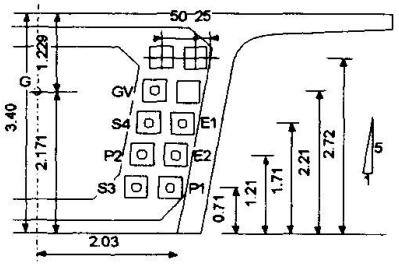

figure 7

3.3 Strut-and-tie model

We chose to build the strut-and-tie model to study the phase of greatest stress, when all the final tendons and the two reinforcement tendons are tensioned, making a total of 7 tendons pairs in all. (figure 7).

A network of principal struts represents the struts transmitting loads from the anchoring points to the box girder. We associated a strut with each anchoring point, and each of these struts goes, via the upright, towards a portion of the box girder whose surface area is chosen to offset exactly the load of an anchoring point in service, i.e. 330 t (figure 8). These struts are balanced transversally by two networks of struts and ties, one on the front face of the upright, on the box girder side, the other on the back face, on the anchoring point side. The organization of these struts stems from information obtained with the finite-elements model. Figure 9 gives a view of the cross-linked model obtained, which is isostatic.

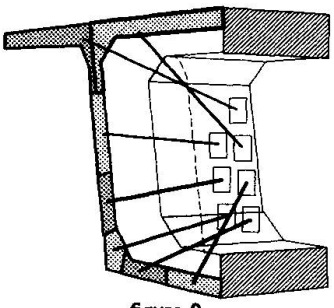

figure 8

The calculation allows to determine the intensity of the general equilibrium loads. The table below gives the quantities of reinforcements needed to ensure overall equilibrium in two situations: a 1.70 m cross-beam (as in the original project), and a 3.20 m cross-beam.

		1.70 m cross-beam	3.20 m cross-beam
Principal reinforcement	A	246 cm^2	133 cm^2
Transverse reinforcement	A_t	255 cm^2	138 cm^2

In both cases, stress in the steel reinforcements was limited to 2/3.f_e, i.e. 267 MPa.

We found once more that the initial vertical reinforcement was greatly under-estimated and that a larger cross-beam would have substantially improved the situation.

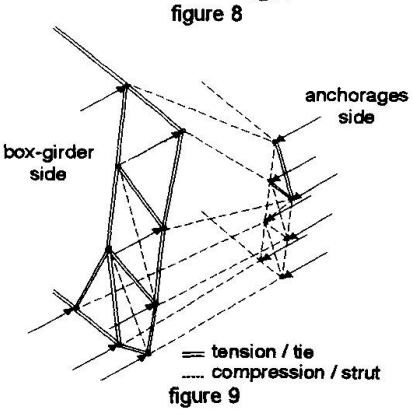

figure 9

4. REINFORCEMENT PROJECT

These calculations clearly indicated that the cross-beam, as originally constructed, would be unable to withstand the loads involved. Reinforcement was therefore necessary.

4.1 Reinforcement principle

A reinforcement block was added in front of the existing cross-beam to take up the loads exerted by the six tendons still to be tensioned.

In order to attach this reinforcement block to the existing box girder, it was necessary to provide:

- additional horizontal transverse prestressing and embedded seam reinforcements for the webs;
- seam reinforcements and four concrete keys in the upper slab;
- seam reinforcements over the entire interface of the lower slab.

Lastly, vertical prestressing was also added to the webs to prevent any extension or cracking.

4.2 Detailed description of the reinforcement block

The cross-beam reinforcement block comprises a U-shaped framework, measuring 1.5 meters in length, added to the inner side of the cross-beam (figure 10). Concreting was carried out from inside the box girder, but also through four openings made in the upper slab which served as a transmission key for loads after hardening of the concrete.

Transverse prestressing is provided by nine 7 T 15 internal tendons, 5 of which pass through the lower part of the reinforcement block and 4 through the upper part. These tendons are curved to create a thrust which partly offsets the thrust of the external longitudinal tendons (figure 10). They are anchored on concrete anchoring blocks outside the box girder.

The seam reinforcements used are as follows:

- 28 bars of 20 mm in diameter on the lower slab,
- 5 bars of 16 mm in diameter on the upper slab,
- 37 bars of 16 mm in diameter in the webs.

These reinforcements are embedded in holes drilled in various parts of the box girder. The depth of embedding is adapted to the steel diameter, in compliance with known test results [5].

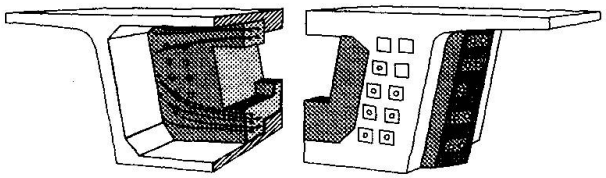

figure 10

4.3 Design of the reinforcement block

Here we will detail the two major points that were examined:

- the inherent strength of the cross-beam reinforcement block and its steel reinforcements;
- the attachment of the block, and the external anchoring blocks, to the box girder.

4.3.1 steel reinforcement of the cross-beam reinforcement block

We calculated the principal steel reinforcement of the block using a strut-and-tie model similar to the one described above.

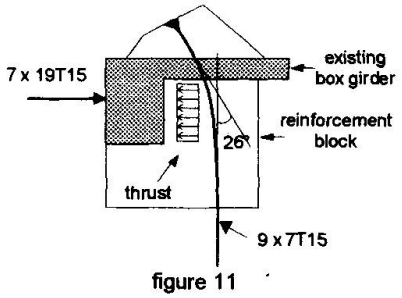

figure 11

To determine the thrust exerted on the block, the two following factors were taken into account:

- firstly, the fact that the longitudinal prestressing already in place before concreting of the block, comprising four 19T15 tendons per web, is already taken up by the existing cross-beam. We nevertheless estimated that 50% of this prestressing, i.e. two tendons per web, would, over the long term, diffuse to the cross-beam reinforcement block, as a result of creep and relaxation;
- secondly, that the thrust of the transverse reinforcement block tendons directly offsets the thrust of one 19 T 15 tendon (figure 11).

Finally, we considered that the reinforcement block supported only 57% of the total thrust of the seven longitudinal tendons per web, i.e. 1300 tonnes.

The quantities of steel reinforcement, positioned on the front face of the reinforcement block (box girder side), are 80 cm^2 per web.

4.3.2 Reinforcement block/ box girder attachment

Loads are transmitted from the reinforcement block to the box girder by concrete-to-concrete friction and by a pin effect of the embedding reinforcements.

To obtain a good friction coefficient, the surfaces were roughened to obtain indentations of at least 5 mm.

Sliding resistance was verified with respect to ultimate limit states using the following generalized seam rule [6]:

$$1{,}35\,P_m \leq \left(0{,}85\,N_P + A_{st}\frac{f_e}{\gamma_s}\right)\frac{\varphi}{1{,}2}$$

where P_m is the sliding load due to longitudinal prestressing, N_p is the normal prestressing load at the slide surface, A_{st} is the total surface area of seam reinforcements, f_e is their elastic limit, γ_s equals 1.15 and φ is the concrete/concrete friction coefficient after setting, fixed at 1.2 in view of the indentations.

It should also be noted that for the upper slab, the shear strength of the keys partly offsets the sliding load.

For verification of external anchoring block bonding, the loads P_m (destabilizing) and N_p (stabilizing) both come from the transverse prestressing. The resistance condition is therefore written:

$$P_m \leq \left(N_P + A_{st}\frac{f_e}{\gamma_s}\right)\frac{\varphi}{1{,}2}$$

4.4 Vertical web prestressing

Of course, the ideal solution would have been to use vertical prestressing, similar to the transverse prestressing, to fix the reinforcement block to the box girder, but this was not possible due to the execution problems involved.
Vertical web prestressing was nevertheless placed at the end of the cracked zone in order to halt the propagation of the horizontal web cracks which would have inevitably occurred as a result of shrinkage, thermal effects and tensioning of the new longitudinal tendons.

Five solutions were considered (see figure 12).

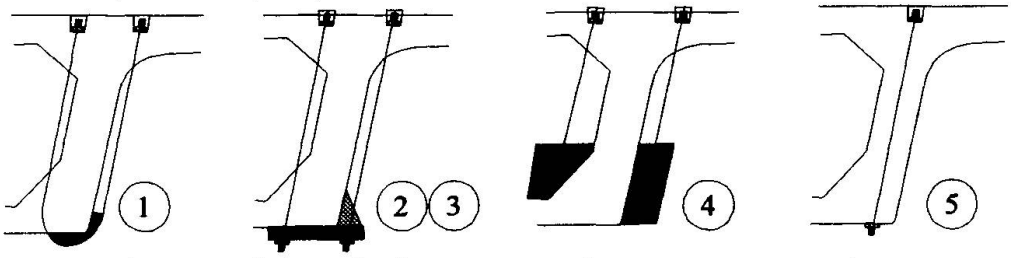

figure 12

Finally, the contractor installed three Ø 36 bars inside the webs, spread longitudinally over a distance of 1.5 m (figure 13). These bars were designed to counteract a stress equal to f_{tj}. To limit the risk of crack propagation during drilling of the web, drilling started at the point farthest from the abutment - above the uncracked zone - and then progressed towards the abutment. Moreover, each bar was tensioned before the next hole was drilled.

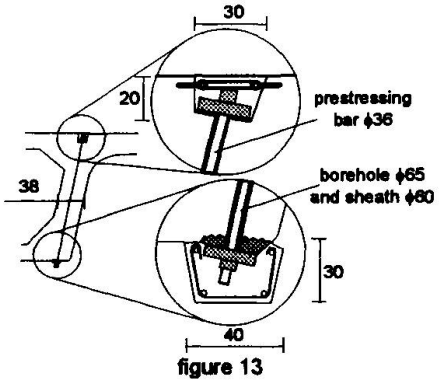

figure 13

5. CONCLUSION

The repair of this bridge cost two million francs (US $ 400,000). It also prolonged construction time by two months. From an aesthetic point of view, the consequences were less dramatic : the external anchoring points were decorated with colored paint and only the twelve covers of the vertical prestressing bars mar the appearance of the deck underside.

It is nevertheless clear that this incident could have been avoided at the project design stage if the designer had respected the following basic rules, specific to external prestressing tendon anchoring zones:

- massive parts should be used to ensure progressive distribution of stresses;
- loads should be transmitted as directly as possible from the anchoring points to the deck;
- diffusion loads should be offset by means of a simple set of struts and ties, avoiding unwanted bending and torsion loads;
- tensile stresses in the concrete should be limited by means of transverse prestressing to minimize the cracking which is inevitable if only ordinary reinforcements are used. Indeed, it is difficult to control cracking in a complex part, designed on the basis of imperfect models, especially with superimposed thermal effects and shrinkage.

ACKNOWLEDGEMENTS

We wish to thank the construction company and the project manager for giving authorization to publish this information. We would also particularly like to thank Rémi Tardy who made a substantial contribution to the writing of this paper.

REFERENCES

[1] M. VIRLOGEUX - La Précontrainte extérieure - *Annales de l'ITBTP - December 1983*

[2] G.P. WOLLMANN, M.E. KREGER, C. ROBERTS-WOLLMANN, J.E. BREEN - External tendon anchorage in diaphragms and intermediate slab blisters - *International Workshop of AFPC - St-Rémy-lès-Chevreuse 1993.*

[3] BPEL 91 : Règles techniques de conception et de calcul des ouvrages et constructions en béton précontraint suivant la méthode des états-limites.

[4] BAEL 91 : Règles techniques de conception et de calcul des ouvrages et constructions en béton armé suivant la méthode des états-limites.

[5] D. POINEAU, J. THEILLOUT, F. CUSIN - Réparation et renforcement des structures de bâtiments et d'ouvrages d'art - Application des techniques de tôles collées et de précontrainte additionnelle - *Annales de l'ITBTP - Febuary 1992.*

[6] Papers cited in the document [5] :
B. FOURE - Surfaces de reprise béton sur béton - *Série essais et mesures n°109 - Annales de l'ITBTP.*
M. VIRLOGEUX - *Document provisoire du CEB.*

Extending the Life of Steel Railway Bridges Using Measure Management

Prolongement de la vie de service des ponts métalliques ferroviaires par gestion des mesures

Verlängerung der Tragfähigkeit für Eisenbahnbrücken mit Vermessung

Yosio TAKAGI
Deputy Manager
East Japan Railway Co.
Tokyo, Japan

Itsuki KOSHIISHI
Deputy Manager
East Japan Railway Co.
Tokyo, Japan

Harumi TABATA
Civil Engineer
East Japan Railway Co.
Tokyo, Japan

Atsushi ICHIKAWA
Chief Engineer
Railway Techn. Res. Institute
Tokyo, Japan

SUMMARY

In order to ensure safety, the East Japan Railway Company evaluates the soundness of its bridge stock and plans necessary repairs by making use of measure management of steel girders. The paper discusses the basis and methodology of this approach, and presents an evaluation case study of the steel girders of in railway bridge built in 1918.

RÉSUMÉ

Il est une règle à la compagnie East Japan Railway d'évaluer l'intégrité d'une structure et de prolonger son utilisation grâce à la gestion des mesures effectuées sur les poutres métalliques. Le rapport décrit les principes de l'évaluation de l'intégrité des poutres en acier, des mesures et contrôles effectués sur des ponts métalliques construits il y a plus de 70 ans en zone urbaine.

ZUSAMMENFASSUNG

Die East Japan Railway Company pflegt mit Vermessung die Mangellosigkeit der Stahlträger zu prüfen und die Tragfähigkeit der Brücke zu verlängern. Der Aufsatz diskutiert die Methodik dieses Ansatzes und zeigt ein Fallbeispiel einer Eisenbahnbrücke aus dem Jahr 1918.

1. Concept of soundness degree evaluation

The soundness degree is defined in the text as the performance in teams of strengthsc oncerning basic safety of the structure like the proof stress durability, etc. Corresponds to "Physical strength" and the itsdecrease an advance of age.

1-1 Proof stress

The proof stress of an existence structure is evaluated as "Existing stress ratio" and its the evaluation formula as follows.

$$\text{Existing stress ratio } (S_R) = \frac{\sigma m}{\sigma} \times 100\%$$

σm is allowable maintenance limit stress used for evaluation of steelgirders in service. The tensile load is decided by the length of the line of influence of the stress generated in the girder and number of train passed.
That is, it is the result of some tiredness having inflenced besides static strength.
σm (tensile stress degree) is shown in Table-1.

Table-1 The maintenance limit stress(tensile stress) unit:(MPa)

tonage	span (m) infulence line length	wrought iron Bessemer steel	SS400		
			before1928	1928~1950	1951~1969
over $20*10^6$ ton	<10	115	140	150	150
	10≦L <20		159	170	170
	≧20				
$10*10^6$ ton $20*10^6$ ton	<10	115	165	176	180
	10≦L <20				
	≧20				
under $10*10^6$ ton	<10	115	165	176	184
	10≦L <20				
	≧20				

The σ is a maximum stress degree the vehicles generarte in the materials when they at the maximum speed. The σ is determinated on an actual section where corrosion was considered.
The measures for the utilization limitation will have to be taken when S_R is larger than 100, because smaller S_R means wider area diminighed through corrosion.
This index is shown in Table-2.

Table-2 Standard for judging the soundness against stress ratio(SR)

S_R (%)	Class
$S_R \leq 100$	AA
$100 < S_R \leq 120$	A_1 or A_2

AA : Repair immediately
A_1 : Repair at an early date
A_2 : Repair when necessary

1-2 Durability

The durability of the structure ranges from the one related to one related to the whole structure. In the text, the dimability of the whole structure is taken up in terms of service life or residual life expectancy.
Therefore, it is decided to expressed the durability of the entire structure as the life of the structure.
However, there are various interpretations about the life of steel bridge.
In general, expresses in the life etc. which are① economical life, ② functional life or③ physical life .
In the text, it refers to physical life, which is supporsed to depend on "Fatigue".
It is thought that physical life is predominantly dependenton "Fatigue" and "Corrosion".
However, corrosion is not caused so long as the painting film

is kept in sound state by proper maintenance.
Therefore, corrosion is decided to be excluded as dimability here.
Figure 1 shows the relation between the residual life expectency and the life from of use to stop of use.
The reason why "Assumed longevity when designing" and "Service life" do not agree is that the condition used for the evaluation is different.
The reasons are that the "Service life" is caluculated baced on thevehicle practically used the distance it run, where "Assumed longevity when designing" is calculated based on the vehicle assumed in design and that the distance it is expected to run.
In general, turns out lower than the weight of the vehicle assumed when the weight of the vehicle which ran actually designs.
Therefore, "Service life" turns out longer than "Assumed longevity when designing".
The fatigue damage degree is obtained in the railway based on the following assumption.

a. The progress of the fatigue damage at a certain stress level is decided solely by the stress and it lineatly accumulates.
b. When the sum total of the fatigue damage at each stress level reaches a constant value, the fatigue failme comese.

Fatigue damage degree $(D) = \Sigma (n_i / N_i)$

N_i : Number of repetitions where crack occurs under a certain stress range is repeated.

n_i : Number of repetitions of the stress range.

That is, it is thought that the fatigue failme comes when the sum of DpT and DaT shown in Figure-1 becomes equal to unity in the girder in service.

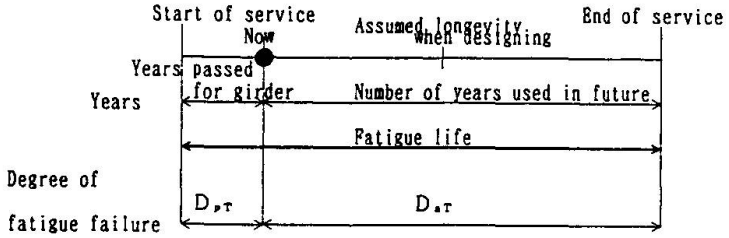

D_{pT} : Degree of fatigue failure in typical train in the past
D_{aT} : Degree of fatigue failure in typical train in futures

Fig-1 Fatigue life of steel girder

The stress is measured in a real bridge and the degree of damage by a train is obtained from the measured more from of the stress.
In addition, time of the crack occurrence is forecast from the result is used is presumed.
The soundness ratings by fatigue are shown in Table-3.

Table-3 Standard for Judging the Soundness against Degree of fatigue failure(D)

D (%)	Class
1.0≦D	A_1
0.8≦D< 1.0	A_2

A_1 : Repair at an early date
A_2 : Repair when necessary

2. Soundness evaluation of real bridge.

2-1 Bridge parameters

Motohashi's crossed angle is narrow as shown in Figure-2.
Therefore, the longitudial gider is directly supported on the abutment, too and it is

a so-called multi point support.

Kind of bridge girder :Through plate girder of two main beam
Span :19.66m*2
Crossed angle :Right 16° 06
Assembly of beams :Rivet
Design train load :Cupar E33 (Figure-3)
Year manufactured :1918

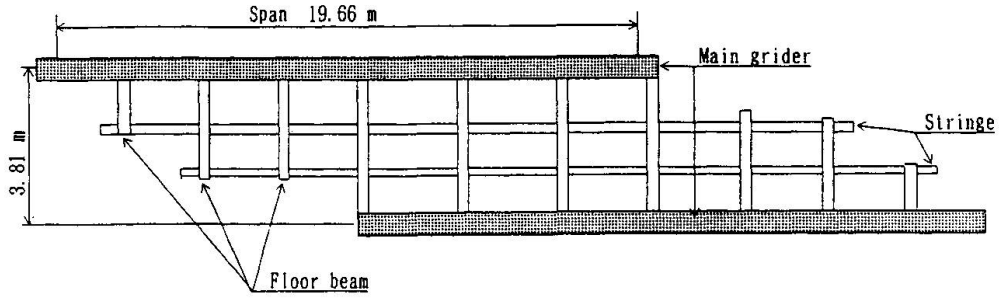

Fig-2 Plain view of Through Plate Girder

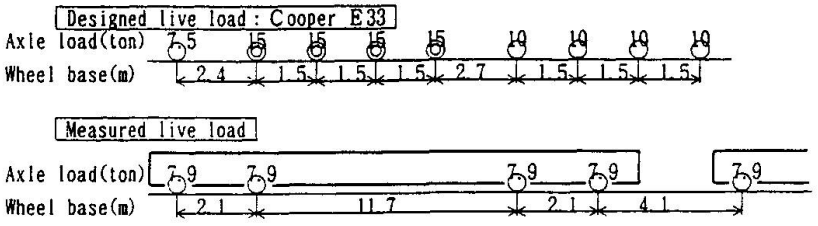

Fig-3 Live load

2-2 Proof stress

Prior calculation each girder section area was measured.
As a result, the section area decrease in upper was lower flange and about 0.5mm even in the girder with remarkable corrosion.
The measured train load is for axle arrangement shown in Figure-3 and the maximum axle load is 7.9 tons.
Minimum existing stress ratio(S_R)of each material calculated for this axle load was 227% in main girders, and 220% in cross girders and 220% in longitudinal girders.
As a result, it was confirmed that the soundness for the proof stress was sutisfactory enough.

2-3 Durability

① Range of permissible joint stress to be used in evaluatoin of fatigue(σ_{fo})
Table-4 shows range (σfo) of the joint stress at to evaluate 2,000,000 times of repetitim used for fatigue evaluation.
The inclination of S-N diagram was assumed three and it was adoptedbecause it is on the safety side even in long life range.

Table-4 Allowable fatigue stress range to be used for fatigue life
Cumulative repeated cycle : 2×10^6 (σ_{r0})

kinds of connection		detail	σ_{r0} (MPa)	sketch
A	connection rivets of flanges	円孔を有する板 slight corrosion	125	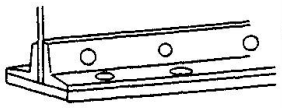
B	flang angle		155	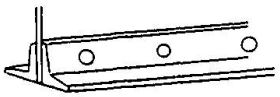
C	base metal wich has clipping gusset plate with fillet	1/5≤r/d	155	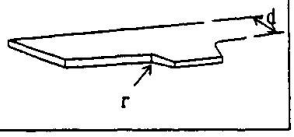

② Fatigue damage degree (D).
It is necessary to investigate the career of the load to calculate D.
It is very difficult to obtain an actual load career.
Motohashi set the following assumption to obtain D.

a. The train, the axle load, the wheel base of the axis, and the travel speed measured this time are the same as those of trains which passed this bridge up this time.

b. In the future, the train, the axle load, the wheel base, the travel speed, and the number of trains measured this time will be same as those of trains which have passed this bridge.

If this is expressed as a formura, becomes as follows.

$$D_{PT}=\frac{n_{eq(1)}\times N_{PT}}{2\times10^6}$$

$n_{eq(1)}$ indicates an equivalent repetition of loading per train measured this time.
N_{PT} indicates the number of accumulated passage of vehicles which passed this bridge up to this time.

$$T_F=\frac{(1-D_{PT})\times2\times10^6}{n_{eq(1)}\times N_{aT}}$$

T_F is residual life expectancy and N_{aT} is the number of vehicles which passed this bridge in one year.
Dating back to the opening of the main lines in the Tokyo metropolitan district where residual life became a problem, the number of the
passed trains was investigated from various documents, and the accumulation of passage vehicles was calculated in each line section.
The accumulation passage of vehicles over this bridge is 45,650,000 as of 1990.

Moreover, the number of passed vehicles in one year is 923,000 vehicles.

③ Analytical result.
A measured result and an analytical result are shown in Table-5.

Table-5 Standard for judging the sundness against stress ratio

member ・place	measured stress(MPa) σ_{max}	σ_{min}	σ^{*1}	σ_{r0} (MPa)	D (%)	class	T_F (years)
center to span of main girders, lower flange	35.1	-1.8	36.9	A / 125	25	–	19
center to track of floor beams, lower flange	22.6	-15.6	38.2	A / 125	28	–	13
center to span of stringers, lower flange	29.8	-0.4	30.2	B / 155	31	–	22
reentrant corner of intermediate stringer*2	29.9	-9.7	39.6	C / 155	82	A_2	1

$\sigma^{*1} = \sigma_{max} - \sigma_{min}$

*2 intersection of stringers and floor beams

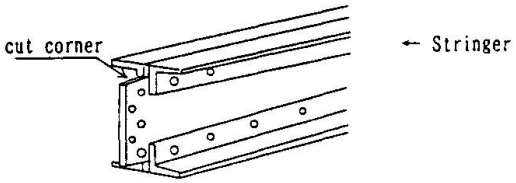

It is judged from this result as follows.
a. The soundness of a main girder is secured.
b. The rating is the notched part of longitudinal girder is A2 and measures will be needed several years later.

Especially, in the notch of the edge longitudinal girder, already, there is the one crack generation already, too.
This is caused is as a result of the damage to the bearing part being reparted because this bridge is a structure of the multi point support.

3. In conclusion

In the evaluation of sondness of this bridge, the physical life referring corrosion and fatigue was determined.
However, it will be necessary to take the following in to consideration besides this before deciding on the replacement of the bridge.
a. When serious deformation overlooked in routine maintenance is anticipated.
b. When a deformation which cannot be tolesated for operation plannig happens.
c. When it costs dear to make repairs.

In our company, the above-mentioned items are judged overall and the best timing for repair and replasement is decided.
The idea is that by doring this, we as a railway operator can ensure safe transport.

Monitoring of Railway Bridges in Poland

Surveillance des ponts de chemins de fer en Pologne

Kontrolle der Bahnbrücken in Polen

Jan BIEN
Dr. Eng.
Wroclaw Technical University
Wroclaw, Poland

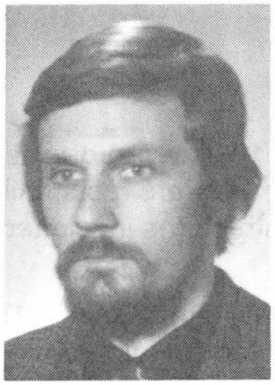

Born 1950, received his C.E. degree and Ph.D. at Wroclaw TU. For 20 years he has been involved in computer applications in bridge engineering. He is project manager in the field of railway bridge management.

Maciej SAWICKI
Civil Engineer
Polish State Railway
Warsaw, Poland

Born 1959, received his C.E. degree at Wroclaw Technical University. On the board of Polish State Railways he is responsible for implementation of bridge management system.

SUMMARY

New computer-aided system of bridge condition monitoring has been implemented by Polish railway administration. Main elements of the system, such as bridge inspection, condition rating, computer software, inspector training, are presented in the paper.

RÉSUMÉ

Aidé par l'ordinateur, un nouvel système d'évaluation et de contrôle est introduit par l'administration des chemins de fer polonais. Les principaux éléments du système, tel qu'inspections de ponts, estimation de l'état des ponts, programmation, instruction pour les inspecteurs, sont présentés dans cet article.

ZUSAMMENFASSUNG

Das neue rechnerisch unterstützende Beurteilungs- und Kontrollsystem des Brückenzustandes wird von der polnischen Bahnverwaltung eingeführt. Im vorliegenden Aufsatz werden die Grundelemente des Systems, sowie die Brückeninspektion, die Zustandsbeurteilung, die Computerprogramme und die Inspektorsausbildung, dargestellt.

1. INTRODUCTION

Polish State Railway (PKP) is one of the biggest railway companies in Europe. In 1993 PKP transported 530 million passengers what gives fourth place in Europe and 213 thousand tons of goods - second place in Europe. Railway infrastructure of PKP is third in Europe: 23.250 km of railway lines (48.000 km of trucks), 1.050 square km of area (0.33 % of Poland), 34.000 civil structures (about 10.000 bridges).

Condition of bridges and other civil structures can be described by following data:

- 65 % of structures is more than 80 years old,
- only 1 % of structures is less than 10 years old,
- weighted mean of civil structures age is about 90 years,
- during last 25 year's maintenance funds were less than 20 % of needs.

2. BRIDGE MONITORING SYSTEM

2.1 General remarks

Taking into account large needs in bridge maintenance PKP decided in 1994 to reorganise the management system and to form new units - Bridge Divisions. New units are responsible for management and maintenance of all bridges and other railway civil structures in allotted areas.

Simultaneously to the reorganisation, the Railway Bridge Management System "SMOK" [1], has been elaborated as computer-aided management system. One of the most important parts of the RBMS "SMOK" is a uniform bridge monitoring system that consists of:

- system of inspections,
- system of bridge condition rating,
- computer system for data storage and processing,
- training system for bridge inspectors.

2.2 Bridge inspections

Bridge inspections are the most important part of the monitoring system because they are source of information on a real condition of the structures. In Poland five levels of railway bridge inspections are distinguished in the monitoring system. Characteristics of the inspections are presented in Table 1.

2.3 Bridge condition rating

Condition of railway bridges is evaluated taking into account two aspects:

- ***technical condition*** - defined as conformity between designed and current technical parameters (properties) of the structure,
- ***serviceability*** - defined as conformity between current service parameters of the structure and service parameters (speed limit, load capacity, clearance) required by the railway network.

Technical condition and serviceability of the bridge are evaluated in the 6-level scale, from 5 (full conformity between current and required parameters) to 0 (serious damages of the structure, bridge out of use).

No	Name	Frequency	Executor	Type
1.	General overview	every day	truck inspector	visual inspection
2.	Current inspection	3 months	bridge inspector	visual inspection
3.	Basic inspection	1 year	bridge inspector	visual inspection & simple tests
4.	Detailed inspection	5 years	division inspector & bridge inspector	visual inspection & advanced tests
5.	Special inspection	if any needs	consultants & division/bridge inspector	high-tech tests, proof loads, etc.

Table 1 Bridge inspections

Technical condition is evaluated separately for 10 main elements of the bridge, divided into 4 groups according to an importance of the elements:

- group 1: 1.1. supports, 1.2. main girders, 1.3. deck, 1.4. bearings;
- group 2: 2.1. waterproofing, 2.2. drainage, 2.3. accessories;
- group 3: 3.1. approaches, 3.2. non-bridge installations;
- group 4: 4.1. underpass.

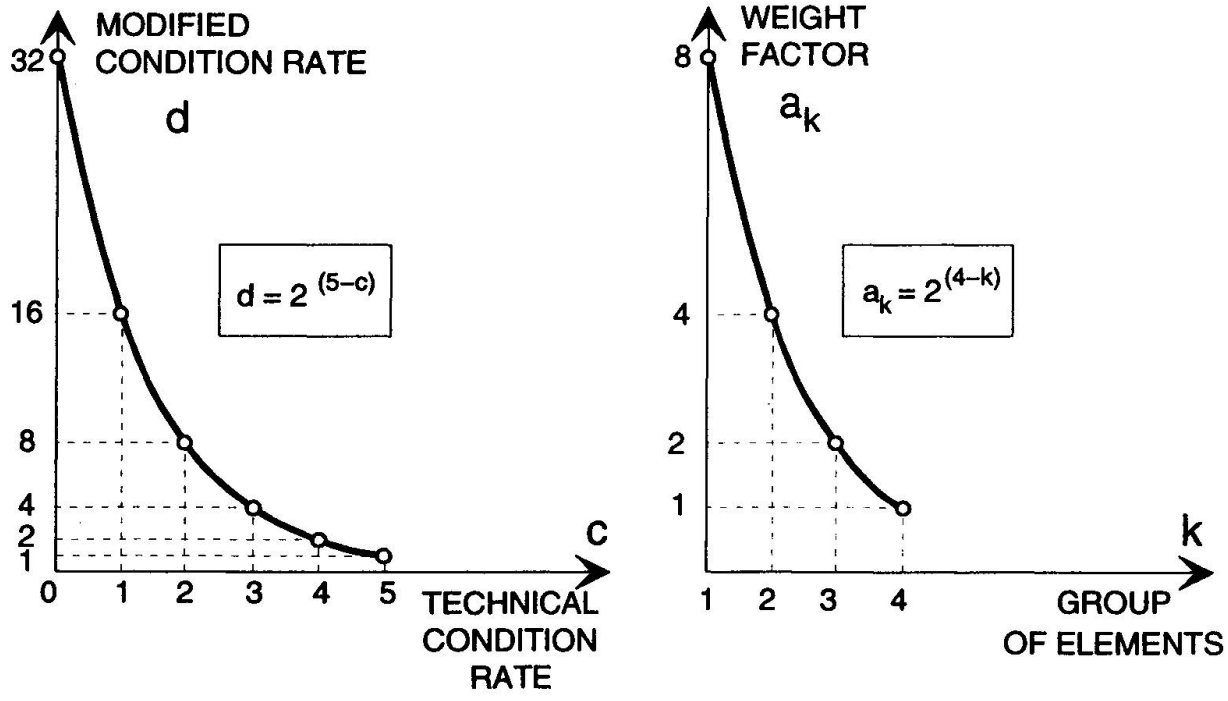

Fig. 1 Modification of technical condition rate [2]

Technical condition of the whole structure is calculated on the basis of element condition as:

(1) **B**ridge **SA**fety index (**BSA** index)

$$BSA = min\ (c_{11}, c_{12}, c_{13}, c_{14}) \tag{1}$$

where c_{ik} is the technical condition rate of element *"i"* in the group *"k"*;

(2) **B**ridge **T**echnical **C**ondition index (**BTC** index) calculated by means of the WRAM method [2] in the following steps:

- calculation of modified rate d_{ik} for each evaluated element *"i"* in each group of elements *"k"* (Fig.1a),
- on the basis of an arithmetic mean of d_{ik} for each group *"k"* is calculated weighted rate of technical condition for the group c_k,
- BTC index for the whole structure is calculated as a weighted mean of c_k for all groups of elements

$$BTC = \sum_{k=1}^{4} a_k \times c_k \Big/ \sum_{k=1}^{4} c_k \tag{2}$$

where a_k is the weight for the group *"k"* (Fig. 1b). Values of both indices (BSA and BTC) are in the range 0 to 5.

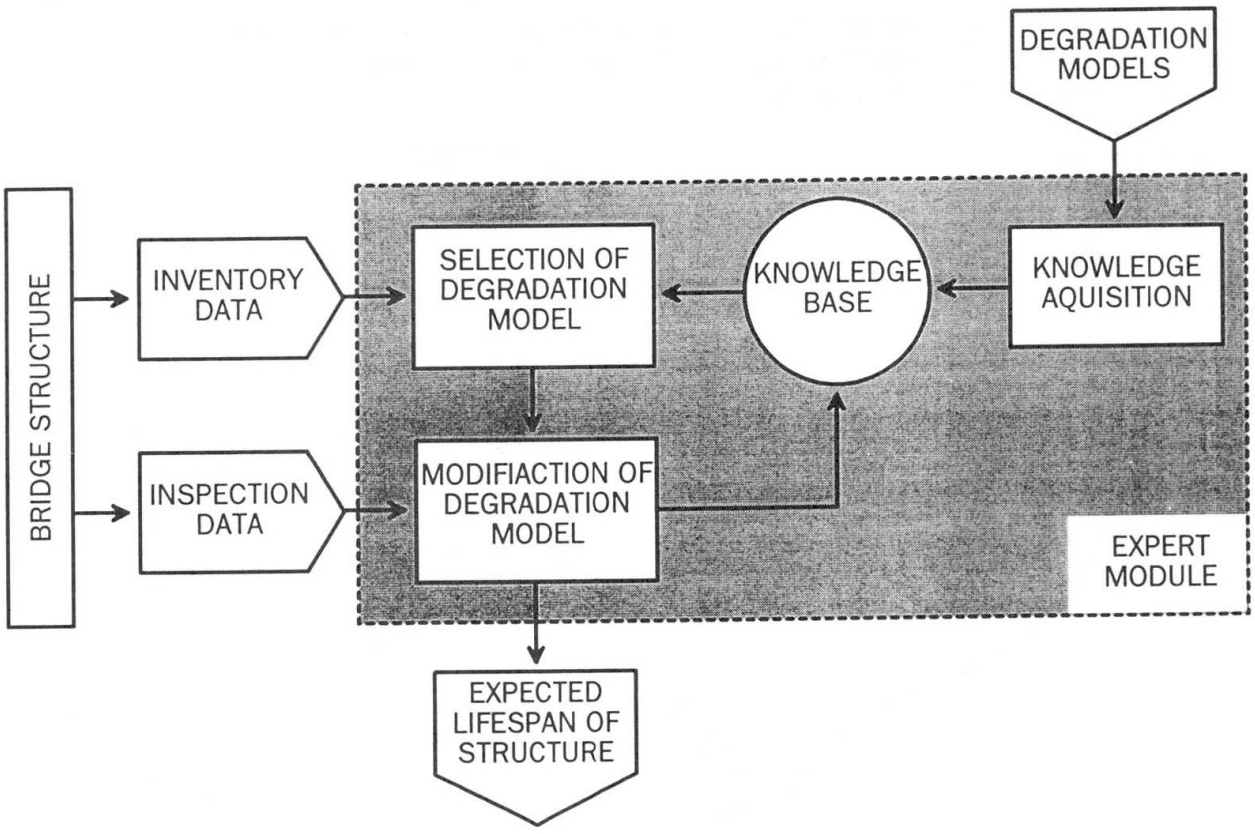

Fig.2 Expert module in computer system

Serviceability of the structure is represented by the **B**ridge **SE**rviceability index (**BSE** index). BSE index is calculated like BSA index as a weighted mean of serviceability rates for service parameters: speed limit, load capacity, clearance, etc.

2.4 Computer system

Bridge monitoring is aided by computer system, part of the "SMOK" system. Prediction of bridge condition and service life is supported by expert module (Fig. 2). This part of the system is based on fuzzy logic and neural network technique [3], [4].

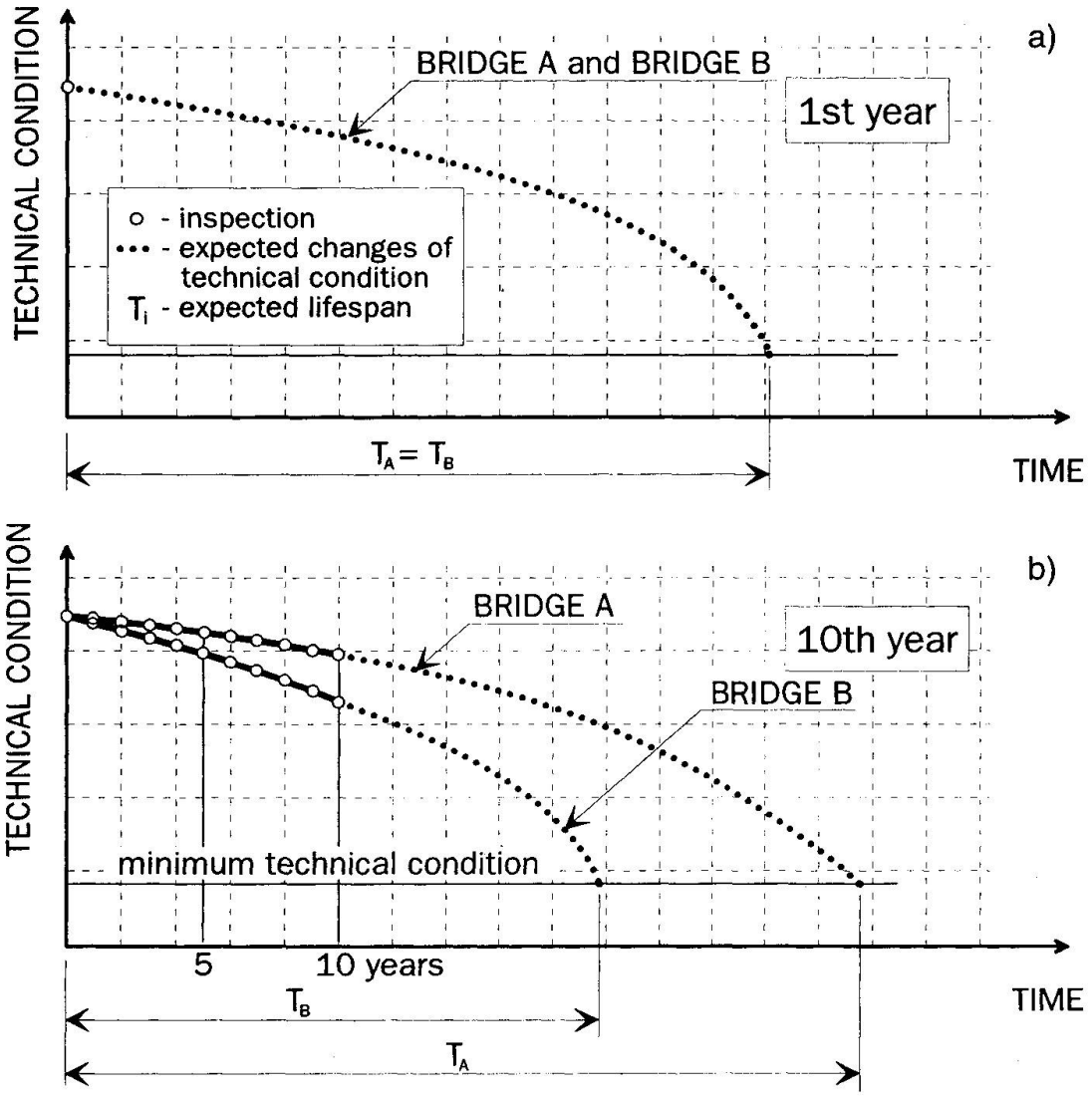

Fig. 3 Self-modification of deterioration model

For various types of bridges special deterioration models are elaborated. Proper model for each bridge is selected (see Fig. 2) taking into account inventory data such as: material, construction, age, etc. During implementation of the system (first year) for all bridges of the

same type there is applied the same deterioration model (Fig. 3a). Considering bridge condition evaluated by inspection's, deterioration model will be modified in the next years and individual model for each structure will be created (Fig. 4b).Such individualisation enables very exact prediction of bridge condition and lifespan.

2.5 Bridge inspectors training

Bridge inspectors (about 200 in the entire country) play very important part in the monitoring system and they should be trained permanently. In the training system there are two phases distinguished:

(1) training during system implementation (2-3 weeks courses): "Bridge inventory", "Evaluation of bridge condition and maintenance planning", "Economic aspects of bridge management";

(2) training after implementation of the system - 2 or 3-day meetings once a year.

3. CONCLUSIONS

The railway bridge monitoring system is designed and developed at Wrocław Technical University (WTU) for the Polish State Railway (PKP). The conceptual design study was prepared in 1993 and now the system is being implemented.

New computer-aided system of bridge condition monitoring should give more efficient allocation of limited maintenance funds. It is estimated that profits from the system should cover its costs within 1-2 years.

REFERENCES

1. BIEŃ J., KMITA J., REWIŃSKI S., Scientific and technical basis of the Railway Bridge Management System "SMOK". Part 4. Detailed conception of the system (in Polish). Wrocław Technical University, Inst. of Civ. Eng., Report SPR-59/93, 1993.
2. BIEŃ J., BIENIEK K., RAWA P., REWIŃSKI S., ROWIŃSKA W., Scientific and technical basis of the Railway Bridge Management System "SMOK". Part 9. Evaluation of technical condition and serviceability of bridge structures (in Polish). Wrocław Technical University, Inst. of Civ. Eng., Report SPR-64/94, 1994.
3. REWIŃSKI S., BIEŃ J., Expert systems in bridge safety management. Proc. Conf. : Safety of Bridge Structures, pp. 325-330, Wrocław, 1992.
4. BIEŃ J., REWIŃSKI S., SAWICKI M., System-based strategy of railway bridge maintenance in Poland. Proc. Conf. : Maintenance of Bridges and Civil Structures, pp. 373-382, Paris, 1994.

Preventive Measures for Reducing the Seismic Risk of Bridges

Mesures pour la réduction du risque sismique des ponts

Massnahmen für die Reduzierung des Erdbebenrisikos von Brückenbauten

Giuliano AUGUSTI
Professor of Structural Mechanics
Università di Roma "La Sapienza"
Roma, Italy

Giuliano Augusti, born in 1935, received his honors degree in Civil Engineering from the Univ. of Napoli and his Ph.D. from the Univ. of Cambridge, UK. His main interests have been in plasticity, instability, earthquake and wind engineering.

Marcello CIAMPOLI
Researcher
Università di Roma "La Sapienza"
Roma, Italy

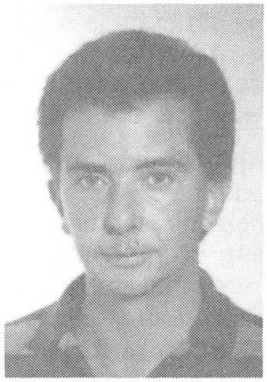

Marcello Ciampoli, born in 1956, received his honors degree in Civil Eng. from the Univ. of Bologna, and his Ph.D. from the Univ. "La Sapienza". His main interests have been in seismic design and reliability of structural systems, assessment of existing structures, repair of damaged HRC structures.

SUMMARY

With specific reference to the seismic reliability of existing bridges and highway networks, the design of preventive upgrading interventions is discussed. Results are presented of a numerical analysis of the seismic response of multispan bridges, aimed at evaluating the efficiency of different upgrading techniques. A procedure is illustrated for assigning priorities among the bridges included in a highway network, allocating the available resources in an optimal way. Three possible objective functions are considered, namely the reliability of the network, the time-effciency of the interventions and the out-of-service time of the network in case of a severe earthquake.

RÉSUMÉ

Les problèmes d'intervention en vue du renforcement sismique des ponts sont présentés. Les résultats d'une analyse numérique concernent la réponse sismique des ponts avec tablier en béton armé; elles permettent d'évaluer la validité de différentes techniques de renforcement. La définition des priorités d'intervention sur les ponts situés dans un réseau autoroutier permet d'optimaliser les ressources disponibles. Trois objectifs sont fixés: la fiabilité du réseau, l'efficacité temporelle des interventions et la durée hors de service du réseau en cas de séisme.

ZUSAMMENFASSUNG

Es wird die Planung von Verbesserungsmassnahmen präsentiert, die besonders den Fall der seismischen Zuverlässigkeit von existierenden Brücken bzw. des Autobahnnetzes betreffen. Als erstes werden die Ergebnisse einer ausführlichen numerischen Analyse der seismischen Antwort von Stahlbetondurchlaufträger (Brückenträger) dargestellt. Eine Prozedur wird dann eingeführt, die die Prioritäten innerhalb der im Netz befindlichen Brücken zuordnet; hierzu werden die verfügbaren Ressourcen so zugewiesen, dass einige Funktionen maximiert werden. Folgende drei Funktionen werden in Betracht gezogen: die Zuverlässigkeit des Netzes zu garantieren, die zeitliche Effizienz der Eingriffe, und die Dauer der Ausfallszeit des Netzes im Falle eines starken Erdbebens.

1. INTRODUCTION

Apart from conservation of architectural heritage, there are several motivations for extending the lifespan of a constructed facility: from economic convenience to the minimization of environmental impact (to restore a structure is usually less traumatic than to demolish and rebuild), to the need of maintaining continuously effective a lifeline or service network.

To tackle rationally the problem it is necessary to assess the present strength of the structure, the foreseeable evolution of its reliability and, if either are deemed unsatisfactory, the feasibility and costs of repair/upgrading interventions versus the availability of economic resources. In fact, the design of preventive interventions is (or at least should be) the result of a decisional process involving a cost-benefit analysis of the possible interventions on the considered structure: from this viewpoint, the decisions would be - in principle - immediate. However, account should also be taken of the fact that often the structure is an element of a system (in full rigour, this is always the case) and that the available resources are usually limited: therefore the interventions must be planned in function of their costs and effectiveness with regard to the reliability of each structure and of the system as a whole, that is, the available resources must be allocated in an optimal way.

Both aspects are dealt with in this short paper. In Section 2, the effectiveness of alternative upgrading interventions is studied with reference to typical reinforced concrete girder bridges, through an extensive numerical investigation on the consequent reduction of their fragility. Then, Section 3 tackles the planning of interventions on bridges considered as critical elements of a highway network, in such a way that, for a given amount of available resources, an appropriate objective function is maximized. More details on assumptions, procedures and results can be found in the References listed at the end of the paper.

2. SEISMIC UPGRADING OF R.C. GIRDER BRIDGES

The investigation summarized here is aimed at optimizing the choice and the design of the interventions for seismic upgrading of existing r.c. bridges: this information is missing from current codes, that do not supply neither general concepts nor special provisions for retrofitting.

A specific structural type is investigated [4][5]: namely, multispan r.c. girder bridges made by a simply-supported (s.s.) or continuous (cnt.) horizontal deck and vertical piers of different height and section.

The layouts of the case examples are shown in Table 1. It can be noted that almost all bridges are characterized by piers with strongly different stiffnesses: indeed, such bridges are very vulnerable to seismic action and also prone to degradation, due to the major demand for ductility in the critical sections of the stiffest piers (the 4th, 8th and 11th cases are introduced for comparison). Three cross sectional shapes of the piers are assumed: two hollow rectangular (A and B) [4] and one hollow circular (C) [5].

Two techniques for upgrading are examined: the first one (J) consists in jacketing the piers with a shotcrete cover and adding steel reinforcement (Table 2); the second (IS) modifies the structural response by replacing the existing girder bearings with isolation/dissipation (i/d) devices.

In the design of IS interventions, two main problems arise: (a) the optimal balance between the yielding forces of the devices and their deformability; (b) the choice of the most suitable location and orientation of the devices, and in particular whether these devices should be arranged on all piers or only on the stiffest piers. Several solutions are tried, as described in detail in [4][5].

Among the possible causes of failure, only structural damage is considered. It is assumed that the piers are the critical elements of the structural systems, and that the failure of only one pier determines the failure of the bridge. A damage and a collapse limit state condition are considered, respectively identified with the attainment of the values 0.4 and 1.0 of the damage indicator proposed by Ang (1987) [4]. If the bridges are retrofitted by the second technique, another constraint is introduced, that is, the maximum required displacement ductility in the i/d device is limited below a threshold value (10 in the specific case).

The seismic fragility (i.e., the probability of attaining a limit state vs. the intensity of the action) of

the assumed existing and retrofitted bridges is obtained numerically by applying an improved MonteCarlo procedure; artificial accelerograms, consistent with the spectrum S2 of Eurocode N.8 and scaled to a peak ground acceleration a_g in the range 0.10-0.45 g, are assumed as inputs.

Bridge	*Deck*	*Span*		*Piers*	
		number	*length (m)*	*type*	*height (m)*
1	s.s.	4	50	A	10 - 30 - 20
2	s.s.	5	50	B	40 - 10 - 10 - 40
3	s.s.	5	50	A	10 - 20 - 20 - 10
4	s.s.	9	40	A	10 - 20 - ... - 20 - 10
5	s.s.	4	40	B	20 - 40 - 20
6	s.s.	4	50	C	10 - 30 - 20
7	s.s.	4	50	C	40 - 10 - 20
8	s.s.	4	50	C	20 - 20 - 20
9	cnt.	4	50	C	10 - 30 - 20
10	cnt.	4	50	C	40 - 10 - 20
11	cnt.	4	50	C	20 - 20 - 20

Table 1 *Layout of examined bridges*

Intervention type	*Pier section*	*Cover thickness (m)*	*Ratio between added and existing reinforcement (%)*
J1	A / B	0.08	50
J2	A / B	0.16	100
J3	C	0.10	50
J4	C	0.15	75

Table 2 *Characteristics of jacketing interventions*

Inspection of the fragility curves of the piers in their present conditions shows that damage and collapse probabilities are rather large, especially for the stiffest piers (10 m tall) and for $a_g > 0.25g$.

The effects of jacketing interventions of types J1-J4 are shown in Fig. 1, in which the ratio ξ between the probability of attaining the damage limit state and the corresponding value for the assumed existing piers is plotted in a semi-logarithmic scale. It can be noted that the effects of the J1 and J3 interventions are comparatively small: the mean value of ξ (ξ_{avg}) is equal to 0.6. ξ decreases with a_g and is practically equal to 1 if $a_g > 0.3g$. J2 intervention is slightly more effective ($\xi_{avg} = 0.3$). J4 intervention worsens the structural response, because it reduces excessively the curvature ductility of the pier section (therefore, J4 is not reported in Fig. 1). The effects of interventions J1-J2-J3 are larger for taller piers, whose influence on the structural safety is smaller. Similar results are obtained with regard to the collapse limit state: ξ_{avg} is equal respectively to 0.35 and 0.1 for interventions J1-J3 and for intervention J2.

Analogous results are also obtained when the failure of the bridge schemes of Table 1 are considered instead of failure of the individual piers.

It may be concluded that:

- strengthening the piers by concrete jacketing has a limited effect (the damage probability is reduced no more than by one or two orders of magnitude; the collapse probability remains practically unchanged if $a_g > 0.25g$);
- these interventions are convenient when the piers are highly ductile, and the expected seismic intensity is low;
- the expansion joint in the s.s. deck cannot be eliminated, since this intervention would involve an increase in the forces acting on the stiffest piers and in the ductility demand; indeed, the joint can be eliminated only in the case of bridges characterized by piers of the same height.

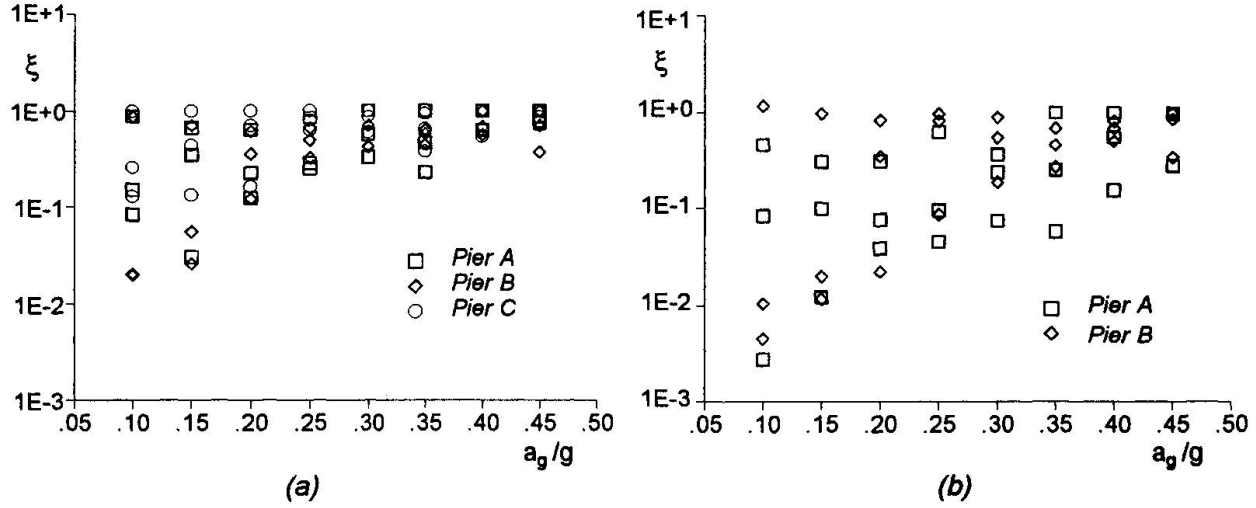

Fig. 1 *Ratio ξ between damage probabilities of the individual piers (upgraded/existing piers) vs. peak ground acceleration: (a) intervention types J1, J3; (b) intervention type J2.*

As for IS interventions, the i/d devices on rectangular piers (bridges 1-5) have been designed with yield strength equal to 50% (Case 1) of the pier limit strength in the transversal direction, and those on circular piers (bridges 6-11) with yield strength equal to 50% (Case 1), 75% (Case 2) and 85% of the pier limit strength. Fig. 2 shows that in this way the damage probability of bridges is usually reduced by one or two orders of magnitude up to the largest values of a_g (ξ_{avg} is equal to 0.056 for Case 1 and to 0.014 for Case 2), even if the devices are placed only on the two stiffest piers; the reduction is much larger for lower values of a_g. If the seismic action acts in the longitudinal direction, the most effective intervention consists in placing only one device on the abutment.

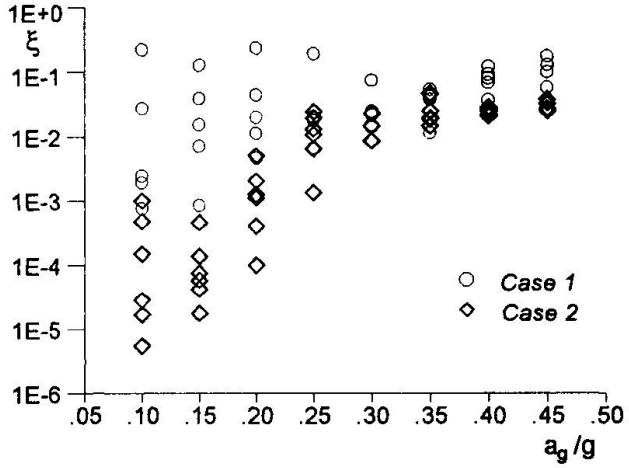

Fig. 2 *Ratio ξ between damage probabilities of the bridges vs. peak ground acceleration (seismic action acting in transversal direction), as a function of the yield strength of the i/d devices .*

From the results of the numerical analyses, it can be inferred that:

- the replacement of existing bearings with i/d devices can eliminate the need for strengthening the piers, but the stiffnesses and strengths of the restraints must be calibrated in such a way that a favourable redistribution of seismic forces between piers and abutments is obtained;
- this intervention is very effective also if the expected seismic intensity is very high and the bridges are characterized by piers of different height: as a matter of fact, it makes more regular the nonlinear response of the whole structural system;
- the yield strength of the i/d devices should be limited to 50 - 75% of the pier limit strength (the lower value apply if the force-displacement relationship of the i/d device may present a signifi-

cant hardening);

- the i/d devices can be placed on the stiffest piers only;
- this intervention permits to eliminate the expansion joints.

3. SEISMIC UPGRADING OF A HIGHWAY NETWORK

Specific reference is made to the seismic reliability of existing road networks, a system modelled in general as a redundant network, comprising a number of critical elements, identified with the bridges in this study.

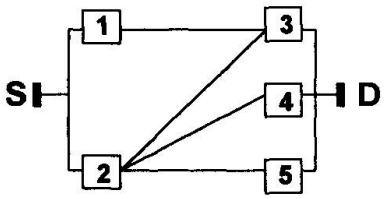

Fig. 3 *Example network*

If C_{max} is the total amount of resources available, its optimal allocation corresponds to the set of interventions (each with a cost H_i) which maximizes the chosen objective function when the network is subjected to an earthquake of intensity a_g, under the constraint

$$\Sigma_i H_i \leq C_{max}$$

As a case example, the bridges 1-5 (Table 1) are located in the five nodes of the network represented in Fig. 3, that is assumed to fail when the connection between the nodes S and D is severed (i.e., the *reliability* R of the network is defined as the probability of maintaining a connection between a *source* and a *destination* node).

Reasonable construction costs of the five bridges, costs and times required by three types of interventions on each bridge (J1, J2, IS, indicated as I, II, III in this Section) and *out-of-service times* (i.e., times required to restore a bridge hit by an earthquake) have been assumed; all costs have been expressed in terms of an ideal *resource unit* (r.u.) equal to 1/100 of the construction cost of bridge 4 [1][2][3].

On the basis of the results summarized in Sec. 2 with regard to the decrease of fragility, the interventions have been optimized with respect to three alternative objective functions [3], namely:(i) the decrease of the above defined probability P_f of network failure (i.e., the increase ΔR of the network reliability); (ii) the ratio (defined *time-efficiency*) $\eta = \Delta R/T^*$ between the increase of network reliability ΔR yielded by a set of interventions and the time T^* that its execution requires; (iii) the length of time (*out-of-service time*) in which an upgraded network remains out of service after an earthquake, i.e., the time necessary to restore at least one S-D path.

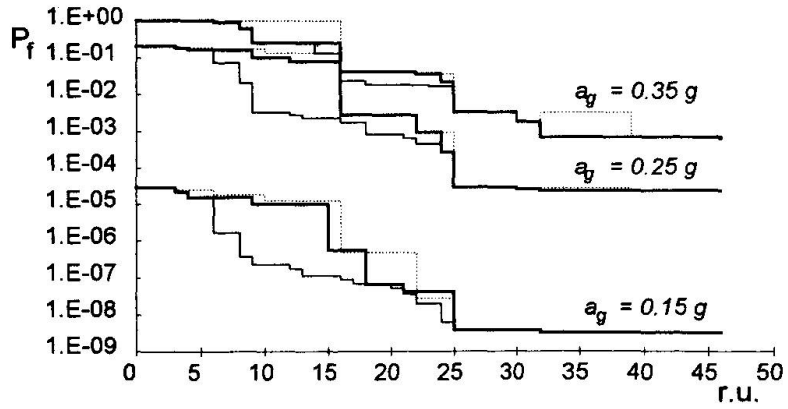

Fig 4 *Probability of failure P_f of example network vs. employed resources, optimized with respect to the probability of network failure itself* (thin lines), *to the time-efficiency of the interventions* (thick lines) *and to the out-of-service time* (dotted lines)

The distributions of the interventions optimized with respect to the three objective functions for a_g = 0.35g are reported in Table 3, while the three sets of lines in Fig. 4 show, for three values of a_g,

the corresponding probability of network failure P_f, versus the total amount C_{max} of available resources (note that 46 r.u. are sufficient to perform intervention III on the five bridges of the network).

The first optimization yields of course the lowest probabilities of failure P_f, but all P_f plotted in Fig. 4 can be shown [2] to be much lower than the probabilities obtained with the same amount of resources allocated without optimization. Thus, Fig. 4 proves that alternative optimizations yield comparable results and therefore suggests to find a compromise solution to take account of different exigencies.

	C_{max}	3	6	9	12	15	18	21	24	27	30	33	36	39	42	45	46
(i)	1	-	-	-	-	-	-	-	-	III	III	III	III	III	III	III	III
	2	-	I	III	III	III	III	III	III	III	III	III	III	III	III	III	III
	3	-	-	-	-	-	III	III	III	III	III	III	III	III	III	III	III
	4	-	-	-	-	-	-	-	-	-	-	-	-	III	III	III	III
	5	-	-	-	-	I	-	-	I	-	I	III	III	-	-	I	III
(ii)	1	-	-	-	-	-	III	III	III	III	III	III	III	III	III	III	III
	2	-	-	-	-	-	-	-	II	III	III	III	III	III	III	III	III
	3	-	-	-	-	-	-	-	III	III	III	III	III	III	III	III	III
	4	-	-	-	-	-	-	-	-	-	-	-	-	-	-	-	III
	5	-	-	-	-	-/I	-	-	-	-	I	III	III	III	III	III	III
(iii)	1	I	I	I	III	III	III	III	III	III	III	III	III	III	III	III	III
	2	-	-	-	-	-	-	-	I	III	III	III	III	III	III	III	III
	3	-	I	I	I	I	III	III	III	III	III	III	III	III	III	III	III
	4	-	-	-	-	-	-	-	-	-	-	I	I	I	I	I	III
	5	-	-	-	-	-	-	-	-	-	I	-	-	III	III	III	III

Table 3 *Interventions on each bridge (1-5) vs. employed resources (3-46 resource units) optimized for a_g = 0.35g with respect to (i) reliability, (ii) time-efficiency, (iii) out-of-service time of the network.*

4. CONCLUDING REMARKS

Two different aspects of the same problem have been briefly tackled in this paper. To improve the exploitation of available resources for reducing the seismic risk (like any other risk) of the constructed world, it is indeed necessary on the one side to understand better the effects and efficiency of upgrading interventions applied to individual structures, on the other side to know how to distribute these interventions among the elements of a system. To give some contributions to this double need has been the object of this and previous papers.

ACKNOWLEDGEMENT Research supported by a grant from the (Italian) National Research Group for Earthquake Effects Mitigation (G.N.D.T.).

REFERENCES

1. AUGUSTI G., BORRI A., CIAMPOLI M., Seismic protection of constructed facilities: optimal use of resources, *Structural Safety*, Vol. 16, 1994, pp. 91-109.
2. AUGUSTI G., BORRI A., CIAMPOLI M., Optimal allocation of resources in the reduction of the seismic risk of highway networks, *Engineering Structures*, Vol. 16, N. 7, 1994, pp. 485-497.
3. AUGUSTI G., CIAMPOLI M., Optimal allocation of resources for increasing the seismic reliability of lifelines, *CERRA-ICASP7*, 7th Intern. Conf. Applications of Statistics and Probability in Civil Engineering, Paris, July 1995.
4. CIAMPOLI M., AUGUSTI G., Seismic reliability assessment of retrofitted bridges, *Structural Dynamics*, Proc. 2d European Conference on Structural Dynamics *EURODYN'93*, Trondheim, Norway, July 1993, Balkema Publ., Vol. 1, pp. 193-200.
5. CIAMPOLI M., Upgrading r.c. bridges for seismic risk reduction, *10th ECEE*, Tenth European Conf. Earthquake Engineering, Wien, August/September 1994 (in print).

Seismic Damage Evaluation of a Conventional Highway Bridge

Evaluation des dégâts causés par un séisme sur un pont-route conventionnel

Seismische Zerstörungsuntersuchung einer konventionellen Autobahnbrücke

C. L. MULLEN
Research Assistant
Princeton University
Princeton, NJ, USA

A. S. CAKMAK
Professor
Princeton University
Princeton, NJ, USA

SUMMARY

As part of a larger project to improve seismic retrofit guidelines for conventional highway bridge structures in the United States, a two-dimensional finite element analysis has been performed for a typical structure configuration. Damage of a vulnerable single-column central pier is modelled using a nonlinear-dynamic hysteretic program, and damage indices are computed based on both hysteretic energy and maximum softening concepts. The interaction of the flexible column with the stiff deck is examined for measured and simulated seismic events.

RÉSUMÉ

Élément d'un large projet visant à améliorer les directives pour les modifications des structures des ponts-routes aux États-Unis, un calcul par différences finies bidimensionnel a été exécuté pour un cas de structure typique. Les dégâts provoqués à un pilier central composé d'une colonne est modélisé en utilisants à la fois des concepts d'énergie hystérétique et de tolérance maximum. L'interaction de la colonne flexible avec le tablier rigide est examinée pour des cas de charges sismiques réels et simulés.

ZUSAMMENFASSUNG

Als Teil eines grösseren Projekts, die seismische Richtlinie für konventionelle Autobahnbrücken in den Vereinigten Staaten zu verbessern, wurde eine zweidimensionale Finite-Element-Analyse für einen typischen Bauwerk ausgeführt. Schäden für eine verwundbare Einzelsäule, bestehend aus einem zentralen Pfeiler, ist ausgeführt mit einem "non-dynamic hysteric" Programm, und Schadenindexe sind basierend auf "hysteric" Energie berechnet und auch auf maximale Erweichungskonzepte. Die Wechselwirkung von der biegsamen Säule mit dem steifen Deck ist für gemessene und simulierte seismische Vorfälle untersucht worden.

1. INTRODUCTION

Important modes of seismic damage have been identified from a literature review [1] of observed damage to existing structures in the United States constructed in the last 25 years. With a few exceptions, all major damage occurred in continuous-span, prestressed or reinforced concrete, multi-cell box-girder bridges having one of three basic configurations:

1. Curved multi-span, single-column bent
2. Skewed short-span, multi-column bents
3. Straight double-deck viaducts with hinged columns

In this study, we focus on the simplest form of the first type, a straight two-span overpass with a single-column bent. In particular, we select the Meloland Road Overpass (MRO), located in El Centro, California, which has been instrumented extensively enough to monitor the primary global vibration modes. A schematic view of the MRO configuration and the instrumentation layout is shown in Figure 1. The MRO has been reported by Werner *et al* [2] for a nondamaging event of M_L= 6.4. Our goal is to calibrate a dynamic model to the undamaged state and then to simulate damaged states using hysteretic models. Unfortunately, calibration against observed damaged states is not yet possible for lack of data.

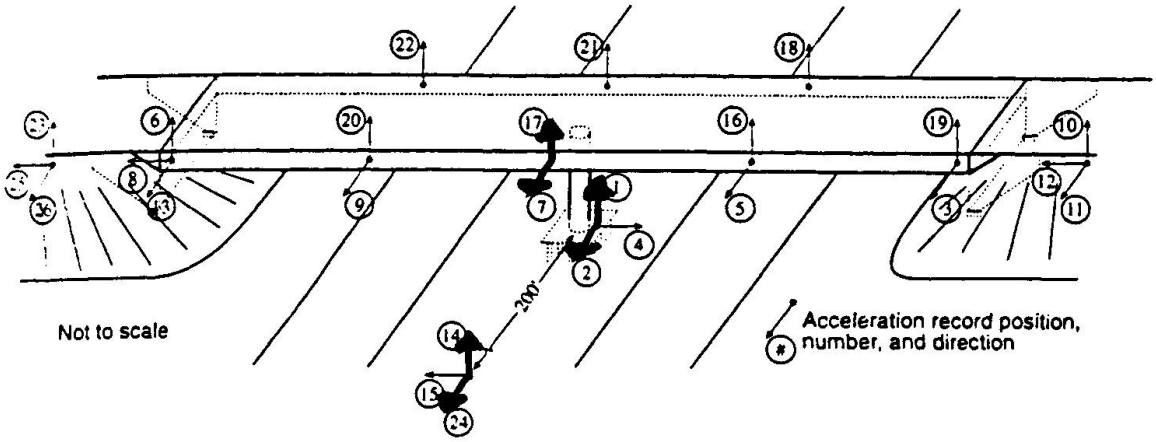

Fig. 1 Schematic MRO configuration and instrument array

The literature review has indicated that, broadly speaking, damage is concentrated in columns and their connections to footings and cap-beams. Failure occurs at varying heights of the column and in both short and tall columns. Combinations of bending and shear failure modes are apparent in many cases with axial force contributing to the damage mode. Shear failures at midheight also occurs at the end of flared sections of short columns.

The factors affecting damage modes have both demand and capacity aspects. Key capacity factors have been identified by Chai *et al* [3] who point to the role of reinforcement detailing and the effects of confinement on strength of concrete. Simplified procedures for capacity and demand analysis have been proposed based on static or pseudo-static procedures. These procedures have recently been applied in failure assessments of bridges damaged during the Northridge earthquake. Priestley *et al* [4] provide moment-curvature and shear-strength analyses and Buckle *et al* [5] compute vulnerability ratings to show the expected distribution of damage in different locations of a structure.

The pseudo-static procedures, however, do not adequately account for the complex influence on column demands that occur dynamically in the presence of damage. The relationship between relative stiffness, mass distribution, restraints at supports and connections, and global modes of vibration, need closer examination so that the key parameters may then be identified. Calvi *et al* [6] attempt this but with design in mind rather than retrofit. Our study attempts to examine the above relationships for the MRO column/deck system using a simplified representation of the structural dynamic system.

2. IDARC MODEL OF THE MRO

The most vulnerable region of the MRO is the central pier which consists of a single pile-supported column and a solid beam made integral with the box-girder deck. Figure 2 shows the basic configuration taken from as-built drawings and the IDARC beam-column element idealization. Also shown are the locations where the participating deck mass has been lumped and where accelerations have been monitored. For simplicity, the base is fixed and the measured horizontal and vertical accelerations are applied as inputs. The rotational flexibility of the footing and piles is therefore neglected. This flexibility will tend to lower the natural frequency

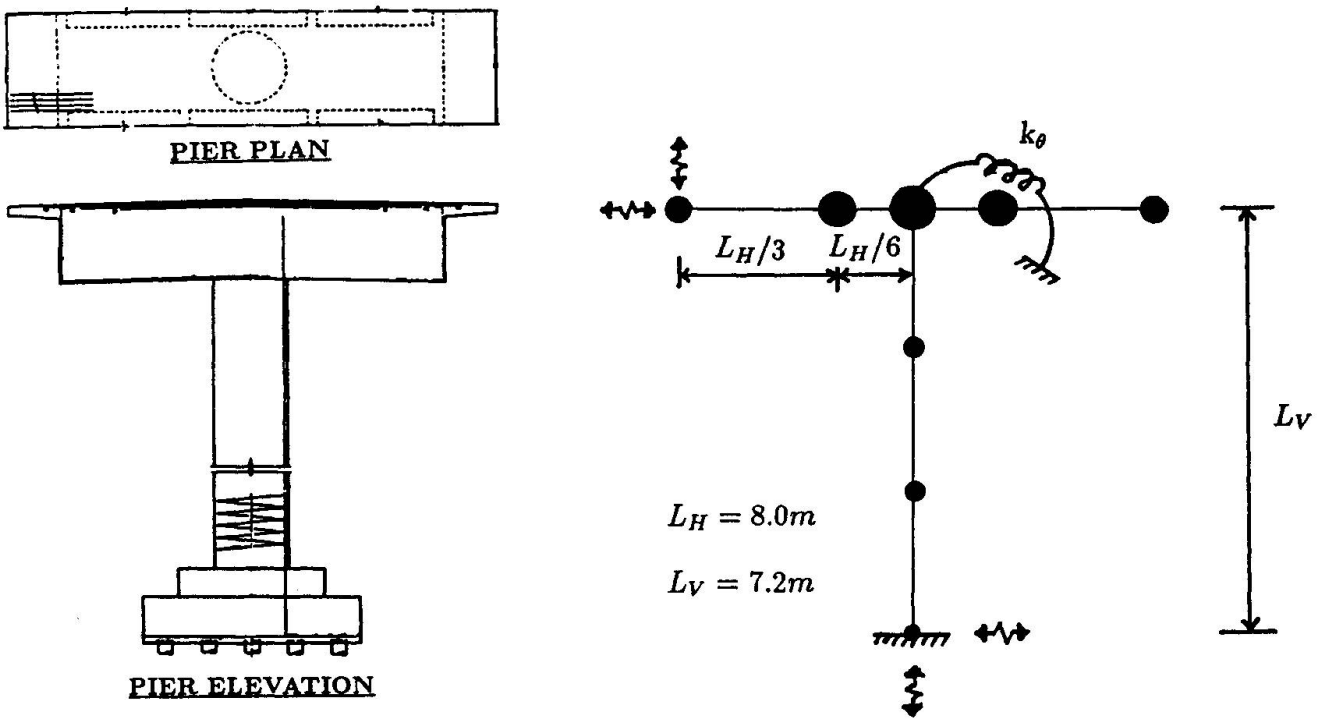

Fig. 2 IDARC model of single-column central pier

of the system relative to that of the fixed base model. All geometric data were selected to be consistent with the as-built drawings and the in-situ values of material properties reported in Werner *et al* [7]. Key data for the model are summarized in Table 1 which indicate relative values of stiffness, rigidity, and bending moments.

Description	Quantity	Value or Ratio
deck rot. stiffness	$k_\theta = (GJ/L)_{eq}$	11.29 GN-m/rad
deck lat. stiffness	$k_{HD} = c_H\ (EI/L^3)$	175.1 MN/m
col. flex. rigidity	EI_C	7.314 MN-m^2
col. yield. moment	M_{YC}	+/−121.2 kN-m
dead load reaction	$P_0 = c_V\ (wL)$	5.338 MN
meas. freq.-1st transv.	f_{1T}	2.47 Hz
col. lat. stiffness	k_{HC}/k_{HD}	0.5
col. crack. moment	M_{CC}/M_{YC}	+0.26 /−0.26
capbm. flex. rigidity	EI_B/EI_C	1.05
capbm. yield. moment	M_{YB}/M_{YC}	+0.18 /−1.27
capbm. crack. moment	M_{CB}/M_{YC}	+0.18 /−0.25
dead load reaction	$P_0/A_g f'_c$	.0828
model freq. @ $W/P_0 = 0.25$	f_1/f_{1T}	1.03
model freq. @ $W/P_0 = 0.50$	f_1/f_{1T}	0.85

Table 1 Key data for MRO IDARC model

Interaction of the pier with the deck cannot be neglected. If no interaction is present, the solid capbeam collapses because of the heavy deck masses that are cantilevered. Concentrating all the mass at the beam-column connection is not realistic either. A compromise has been made here by distributing a fraction of the estimated dead load reaction, W/P_0, along the beam with highest concentration at the connection. The distribution and dead load fraction have been selected by tuning the fundamental period to that identified by measurements of Werner *et al* [2].

The torsional and lateral stiffness of the deck have been modeled through a linear rotational spring applied at the beam-column connection. A separate lateral spring is not necessary, because the resisting moment developed by the rotational spring produces shears which resist lateral displacement at the deck level. Beam theory has been used to estimate the spring constant with rigidities corresponding to the ATC-32 recommendations described in Werner *et al.* [7].

3. MODEL CALIBRATED RESPONSE

Time histories were computed of response at the deck level to inputs at the footing level using acceleration records measured [2] at the site during the $M_L = 6.4$ Imperial Valley earthquake of 1979. Figure 3 shows a comparison of the measured and computed responses. No damage is predicted nor was observed in this case having a horizontal peak ground acceleration, PGAH= 0.32 g. The horizontal response is predominantly in the first two modes shown in Figure 4. The vertical response is predominantly in the third and fourth modes. The 2-D model is capable of representing the horizontal response adequately, but cannot capture the vertical response which is response which is associated with deck behavior that is 3-D in nature.

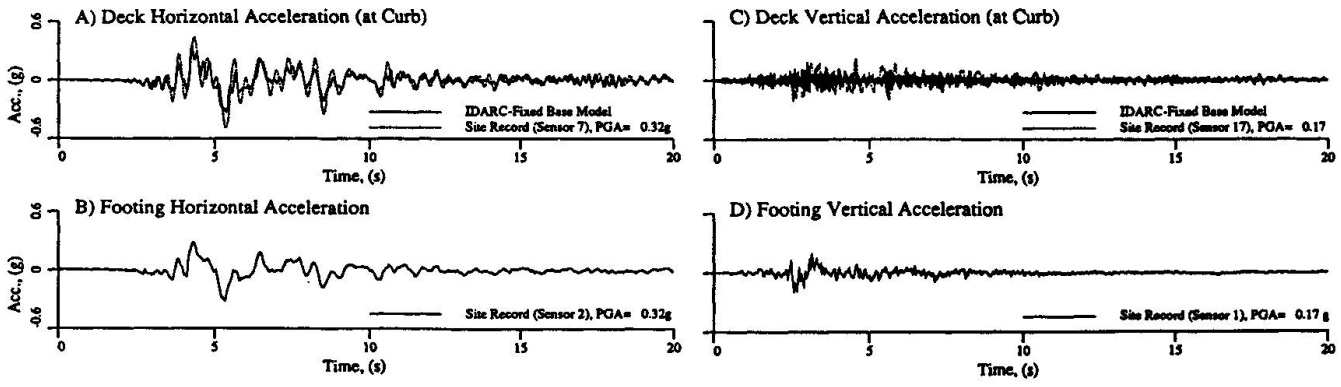

Fig. 3 Response time histories for 1979 Imperial Valley earthquake

4. MODEL DAMAGED RESPONSE

Damage was studied by scaling the records uniformly to higher PGAH. The results were highly sensitive to the assumed participation level of the dead load fraction, its distribution, and the spring constant level. Leaving the spring constant at the value estimated by beam theory and using default values of tri-linear hysteresis parameters set by the program, the remaining parameters with the most uncertainty were the mass level and distribution. A dead load fraction of 1/3 was required to tune the fundamental frequency to the measured value of 2.47 Hz. This fraction is too low to introduce significant damage even at extremely high accelerations. A fraction of 2/3 and higher introduced unrealistically high response accelerations and damage states at moderate input accelerations. A fraction of 1/2 was therefore used in the damage analysis.

Figures 4 and 5 shows two manifestations of the damage from an input event scaled to PGAH= 1g. Figure 4 shows the time-varying softening (increase in) modal periods during the event and Figure 5 the moment-rotation hysteresis. The softening was used to compute a Maximum-Softening (M-S) damage index, δ_M= 0.30. The hysteresis was used to compute a Park-Ang (P-A) damage index, δ_{P_A}= 0.40. Figure 4 also shows the computed variation of the respective indices with PGAH. It should be noted that the upper bound for the M-S index is 1.0.

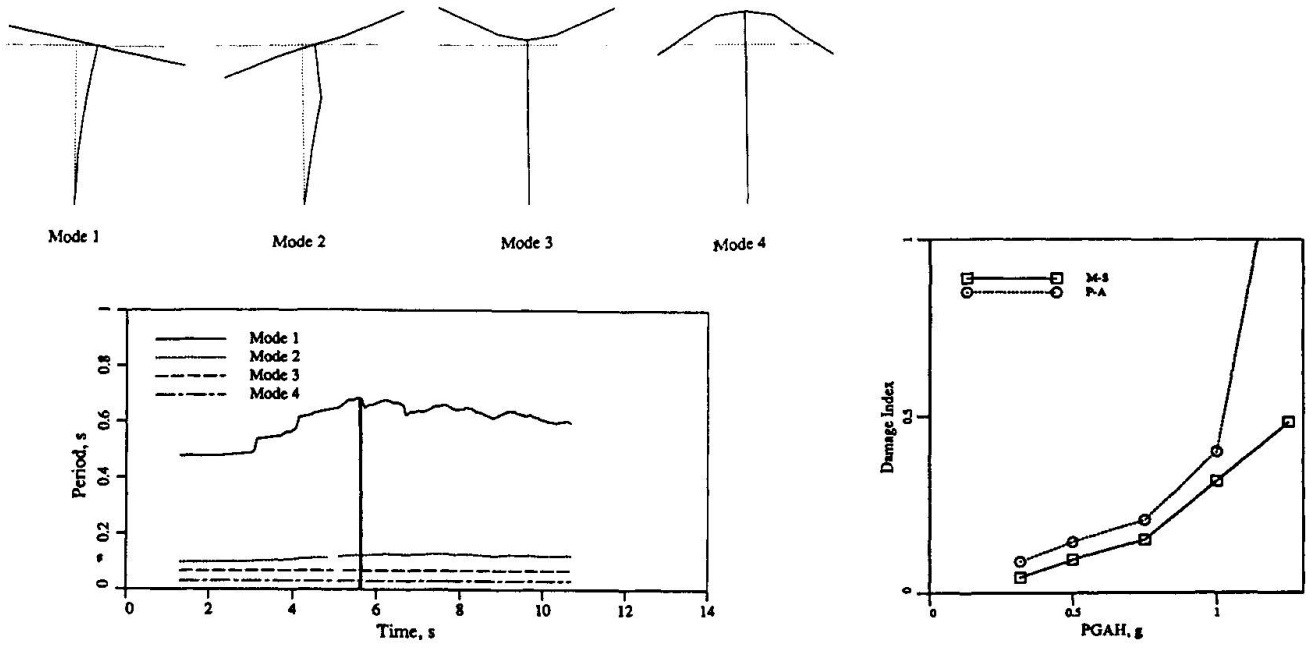

Fig. 4 Modal softening damage for scaled PGAH= 1g event

5. CONCLUSIONS

A simple 2-D analysis of a well-instrumented bridge of simple configuration reveals the complexities of response features governing damage in a nonlinear-dynamic setting. It is clear that 2-D models are not capable of representing damage behavior reliably because of 3-D interaction and global modes of vibration. They may be useful for linear analysis and design based on such analysis, but may be unconservative if used to predict damage without applying considerable judgement to the results. Research is needed to develop efficient and reliable analysis tools and simplified relationships to support damage assessment and retrofit design of existing conventional highway bridge structures. Of particular importance is the modeling of flexure and flexure/shear failure in the presence of realistic representations of axial and biaxial bending forces.

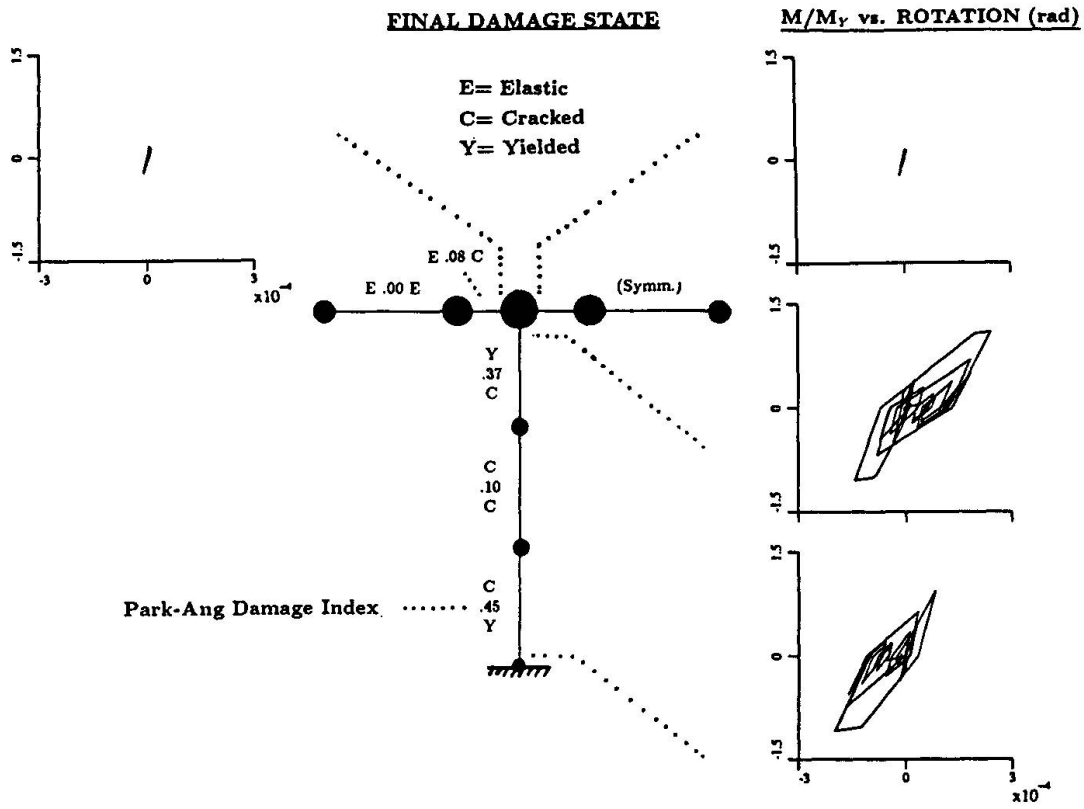

Fig. 5 Hysteresis damage for scaled PGAH= 1g event

REFERENCES

1. CAKMAK A. S., MULLEN C. L. AND BLOCK J., Vulnerability Assessment-Structure Fragility. Task E.7-1 Interim Report, NCEER/FHWA Highway Project 106, Princeton University, 1994.

2. WERNER S. D., BECK J. L. AND LEVINE M. B., Seismic Response Evaluation of the Meloland Road Overpass, using 1979 Imperial Valley Earthquake Records. Earthquake Engineering and Structural Dynamics, 1987, Vol. 15, pp. 249-274.

3. CHAI Y. H., PRIESTLEY M. J. N. AND SEIBLE F., Seismic Retrofit of Circular Bridge Columns for Enhanced Flexural Performance. ACI Structural Journal, 1991, Vol. 88, No. 5, pp. 572-584.

4. PRIESTLEY M. J. N., SEIBLE F. AND UANG C. M., The Northridge Earthquake of January 17, 1994: Damage Analysis of Selected Freeway Bridges. University of California at San Diego Report No. SSRP-94/06, 1994.

5. BUCKLE I., ed., The Northridge, California Earthquake of January 17, 1994: Performance of Highway Bridges. NCEER Technical Report NCEER-94-0008, 1994.

6. CALVI G. M., CIAMPOLI M. AND PINTO P. E., Reliability of Seismic Design and Analysis Procedures for Bridges. Proc. 4th U. S. National Conf. on Earthquake Engineering, Palm Springs, EERI, 1990, pp. 977-986.

7. WERNER S. D., CROUSE C. B., KATAFYGIOTIS L. and Beck J. L., Model Identification and Seismic Analysis of Meloland Road Overcrossing. Dames and Moore Technical Report to CalTrans, 1993.

Models to Evaluate Flutter Instability of Cable-Suspended Pipelines

Évaluation de l'instabilité de conduites suspendues dues à des oscillations

Modelle zur Bestimmung der Schwingungsinstabilitäten von aufgehängten Pipelines

Giuseppe CREAZZA
Professor
I.U.A.V.
Venice, Italy

Carmelo MAJORANA
Researcher
Universita di Padova
Padua, Italy

Anna SAETTA
Researcher
I.U.A.V.
Venice, Italy

Renato VITALIANI
Associate Professor
Universita di Padova
Padua, Italy

SUMMARY

Flutter instability of cable-suspended pipelines is investigated by means of two different approaches. The first one is based on use of hyper-elastic beams in finite strains, whose motion is governed by non-commutative Lie groups for rotations, parallel transport and exponential mapping. The second one uses eigenvalue analyses of deformed configurations, achieved by means of the finite element method, under both conservative and non-conservative forces and allows to evaluate the instability load for a given structure. The methods are applied to a real test case.

RÉSUMÉ

L'instabilité de conduites suspendues dues à des oscillations est examinée selon deux approches différentes. La première est basée sur l'utilisation de poutres super élastiques avec déformations finies dont le mouvement est régi selon les groupes Lie. La seconde utilise des analyses par valeurs propres des configurations déformées, réalisées au moyen de la méthode des éléments finis, à la fois sous l'action de forces conservatrices ou non; elle permet d'évaluer l'instabilité de charge pour une structure donnée. Les méthodes sont appliquées à des situations réelles et sont comparées.

ZUSAMMENFASSUNG

Die Instabilität der Schwingungen der Kabel, an denen die Pipelines hängen, wird mit zwei verschiedenen Versuchen untersucht. Der Erste basiert auf dem Gebrauch von hyperelastischen Trägern mit massiger Spannung, deren Bewegungen von einer nicht kommutativen Lie-Gruppe für Rotationen, parallelem Transport und eine Exponentialkarte geleitet wird. Der Zweite benutzt Eigenwertbetrachtungen von verformten Strukturen, ausgeführt durch die Methode der finiten Elemente unter konservativen, sowohl nicht konservativen Kräften, und erlaubt die Bestimmung der unstabilen Last für eine gegebene Konstruktion. Die Methoden sind an einem reellen Fall angewendet.

1. INTRODUCTION

Cable suspension pipelines subjected to wind loads can suffer flutter instability. Turbulence phenomena may rise around suspension pipelines with mechanisms like the Von Karman's one. Hence a corresponding structural evaluation is needed for this purpose. In literature such a study is performed by means of eigenvalue analyses since coincidence of exciting force frequency with one or more natural frequencies gives rise to resonance phenomena [e.g. 1,2]. In this paper, an investigation of instability phenomena of suspension pipelines is proposed by means of two different procedures. The first procedure is based on the use of a geometrically exact approach to analyse deformable beams in large motions [3,4,5]. Main features of the formulation are the SO(3) noncommutative Lie group employed to follow the rotation of the beam transverse section and the concepts of exponential mapping and parallel transport for numerical integration of the involved equations. Hence elastic instability problems like flutter are treated in a natural way, achieving exact consistent linearized results with quadratic rate of convergence. The second procedure is based on a nonlinear finite element analysis of elastic structures subjected to conservative as well as nonconservative forces [6,7,8]. The stability of the structural system is checked by means of eigenvalue analyses of the deformed configurations. Modes of instability, flutter and divergence, together with values of critical loads are identified both in presence and in absence of damping. This approach appears direct and effective. It is also usefull if compared with general purpose F.E. codes, since nonconservative forces coupled with eigenvalue analysis are not included in usual nonlinear dynamic analyzers. Comparisons between the two approaches are carried out as evaluation procedures to determine the structural performances. The case of a real cable suspension pipeline [2] is considered as example.

2. MATHEMATICAL APPROACHES

2.1 First method.

The analysis is carried out within a general approach, based on the beam model due to J.C. Simo [3,4,5]. This allows to investigate the mechanical behaviour of structural elements in the framework of large strains, displacements and rotations. Moreover, the wide application spectrum of the stated mathematical approach allows to analyse in this context any problem involving elastic stability or non conservative loads. The effect of finite rotations is analysed within the orthogonal SO(3) Lie group. The formulation incorporates as essential concepts those of exponential mapping (for the configuration update) and of parallel transport. The theory can be applied both in analytical form, for calibration purposes, and in a discrete one by means of finite element technique. In the latter case, the update is performed exactly, since Rodrigues' formula is applied to update rotations. After posing the equilibrium in functional form, linearization procedures are employed, leading to geometrical and material tangent stiffnesses. Consequently quadratic convergent rates are achieved within a solution alghoritm of Newton-Raphson type, allowing efficient analysis of a wide range of problems, like finite vibration or dynamic stability and motions implying finite displacements and rotations of flexible beams. In the following a brief account of the governing equations is given.

2.1.1 Reference systems. Kinematic assumptions.

The actual configuration of the beam is described introducing the following objects:

1. A curve defined within an open interval $\Sigma \subset R$, $S \in I \rightarrow \varphi_0(S) \in R^3$, called centre line.
2. A family of planes defined by the unit vector field, $S \in I \rightarrow \mathbf{n}(S) \in R^3$. Planes through $\varphi_0(S)$ orthogonal to $\mathbf{n}(S)$, $S \in \mathbf{I}$, are defined as beam sections.
3. A fiber inside each section defined by the unit vector field, $S \in I \rightarrow \mathbf{t}_I(S) \in R^3 \quad I = 1,2.$
   As a consequence, each point of the curve $S \rightarrow \varphi_0(S)$ can be associated to an orthogonal reference system $\{\mathbf{t}_1(S), \mathbf{t}_2(S), \mathbf{n}(S)\}$, called the intrinsic or convected system.

2.1.2 Exponential map

The rotations $\theta \in so(3)$ (space of emisymmetric tensors) are treated by means of the explicit Rodrigues formula:

$$\exp[\theta] = 1 + \frac{\sin\|\theta\|}{\|\theta\|}\theta + \frac{1}{2}\frac{\sin^2(\|\theta\|/2)}{(\|\theta\|/2)^2}\theta^2 \tag{1}$$

which allows the exact updating of the rotation tensor pertaining to a given transverse section of the beam. The above formula is fundamental with respect to the next developments.

2.1.3 Forces and couples. Equations of motion.

Given a section $A_t = \varphi_t\big|_{s=fixed}(A)$ in the current configuration and defining $\mathbf{P}(\xi,t)$ as the first Piola-Kirchhoff stress tensor, a two-point tensor given by

$$\mathbf{P}(\xi,s) \equiv \mathbf{T}_1(\xi,s)\otimes\mathbf{E}_1 + \mathbf{T}_2(\xi,s)\otimes\mathbf{E}_2 + \mathbf{T}_3(\xi,s)\otimes\mathbf{E}_3 \tag{2}$$

with $\mathbf{T}_3(S,\xi) = \mathbf{P}(S,\xi)\mathbf{E}_3$ the stress vector acting on the section $\mathbf{A} \subset \mathbf{R}^2$, the resultant contact force by unit reference arc-length $\mathbf{n}(S,t)$ on the section A_t of the current configuration is given by

$$\mathbf{n}(\xi,S) \equiv \int_A \mathbf{P}(\xi,S)\mathbf{E}_3 d\xi = \int_A \mathbf{T}_3(\xi,S)d\xi \quad , \tag{3}$$

and similarly the resultant couple by unit reference arc-length $\mathbf{m}(S,t)$ on the section A_t of the actual configuration is represented by

$$\mathbf{m}(S,t) = \int_A [\mathbf{x} - \varphi_0(S,t)]\times\mathbf{T}_3(\xi,S)d\xi \,. \tag{4}$$

2.1.4 Internal energy. Strain measures.

The internal energy, in terms of spatial forces and moments $\mathbf{n}(S,t)$ and $\mathbf{m}(S,t)$ takes the form [4]:

$$\Pi \equiv \int_{A\times I} \mathbf{P} : \mathbf{F}d\xi dS = \int_I (\mathbf{n}\cdot\tilde{\gamma} + \mathbf{m}\cdot\tilde{\omega})dS \tag{5}$$

where $\tilde{\omega}(S,t)$ is the spatial vector related to the curvature, $\tilde{\gamma}(S,t)$ is the spatial strain vector:

$$\tilde{\gamma}(S,t) \equiv \frac{\partial\varphi_0}{\partial S}(S,t) - \mathbf{n}(S,t). \tag{6}$$

$\Psi(\Gamma,\kappa)$ is the properly invariant internal energy function, which can be represented in the material form as

$$\Psi(\Gamma,\kappa) = \frac{1}{2}[\Gamma_t,\kappa_t]\,\mathrm{Diag}[GA_1, GA_2, EA, EI_1, EI_2, GJ]\begin{Bmatrix}\Gamma\\ \kappa\end{Bmatrix} \tag{7}$$

with Γ and κ the material forms of the linear and angular deformations.

2.1.5 Weak form. Inertia operator.

Given $\varphi=(\varphi_o,\Lambda)\in C$, the current configuration and $\eta \equiv (\eta_0,\psi)$, a kinematic admissible variation in the spatial reference, with $\eta\in T_\varphi C$, multiplying the spatial form of the local equilibrium equations reported in Table I, times an arbitrary admissible variation η the nonlinear functional is obtained

$$G_{dyn}(\varphi,\eta) := \int_0^L \left\{A_\rho\ddot{\varphi}_0\cdot\eta_0 + \left[I_\rho w + w\times(I_\rho w)\right]\psi\right\}dS + G(\varphi,\eta) = 0 \tag{8}$$

where $G(\varphi,\eta)$ represents the weak form of the local static equilibrium equations,

$$G(\varphi,\eta) := \int_{[0,L]}\left\{\frac{\partial\psi(S,\Gamma,\Omega)}{\partial\Gamma}\cdot\Lambda^t\left[\frac{\partial\eta_0}{\partial S} - \psi\times\frac{\partial\varphi_0}{\partial S}\right] + \frac{\partial\psi(S,\Gamma,\Omega)}{\partial\Omega}\cdot\Lambda^t\frac{\partial\psi}{\partial S}\right\}dS - \int_{[0,L]}(\mathbf{n}\cdot\eta + \mathbf{m}\cdot\psi)dS\,, \tag{9}$$

with respect to an arbitrary $(\eta_0,\psi\Lambda)\in T_\varphi C$. Homogeneous boundary conditions (Dirichlet's conditions) are chosen as example.

(1) **Material** deformations and **spatial** stresses

$$\Gamma = \Lambda^{t}\frac{\partial \varphi_0(S,t)}{\partial S} - \mathbf{E}_3, \qquad \Omega = \Lambda^{t}\omega, \qquad \mathbf{n} = \Lambda\frac{\partial \psi(S,\Gamma,\Omega)}{\partial \Gamma}, \qquad \mathbf{m} = \Lambda\frac{\partial \psi(S,\Gamma,\Omega)}{\partial \Omega}. \tag{10a,b,c,d}$$

(2) **Spatial** local linear and angular equilibrium

$$\frac{\partial \boldsymbol{n}}{\partial S} + \tilde{\boldsymbol{n}} = A_\rho \ddot{\varphi}_0 \qquad \frac{\partial \mathbf{m}}{\partial S} + \frac{\partial \varphi_0}{\partial S} \times \mathbf{n} + \mathbf{m} = \mathbf{I}_\rho \mathbf{w} + \mathbf{w} \times \left[\mathbf{I}_\rho \mathbf{w}\right] \tag{11a,b}$$

Table I

2.1.6 Tangent stiffnes

The consistent linearization of the weak form allows to find the tangent stiffness matrix defined as:

$$\boldsymbol{K}_{IJ}\left(\Lambda_n, \varphi_{n+1}^{(i)}\right) = \boldsymbol{M}_{IJ}\left(\Lambda_n, \Lambda_{n+1}^{(i)}\right) + \boldsymbol{S}_{IJ}\left(\varphi_{n+1}^{(i)}\right) + \boldsymbol{G}_{IJ}\left(\Lambda_{n+1}^{(i)}\right) + \boldsymbol{L}_{IJ}\left(\Lambda_{n+1}^{(i)}\right) \tag{12}$$

The discrete tangent dynamic operator $\kappa_{IJ}(\Lambda_n, \varphi_{n+1}^{(i)})$ coupling the degrees of freedom of node I with those of node J is the assembling of the following tangent matrices: i) the inertia matrix, ii) the material stiffness matrix, iii) the geometric stiffness matrix, iv) the matrix due to follower forces. The application of eq. (12) to stability problems in presence of follower forces can be found in [5].

2.2 Second approach

2.2.1 Finite element formulation

Within a Total Lagrangian approach, the Green's strains and the Piola Kirchhoff's stresses are used to approximate the non linear 3D beam element presented in [7]. By using the theory of geometrically nonlinear analysis within the classical finite element method, the global stiffness matrix $\boldsymbol{K}_T$ of the structure can be written as in eq. (12), by the addition of the Cartesian elastic, the initial displacement and the initial stress stiffness matrices: $\boldsymbol{K}^0$, $\boldsymbol{K}^L$ and $\boldsymbol{K}^S$ respectively. Nonconservative forces of the follower type lead to non-self-adjoint boundary value problems. Within the finite element formulation, the effect of such forces is in fact to produce a non-symmetric load correction matrix $\boldsymbol{K}^{nc}$ which has to be added to the total tangent stiffness matrix [6,7,8]. Therefore the total tangent matrix becomes non-symmetric and can be expressed by:

$$\mathbf{K}_T = \mathbf{K}^0 + \mathbf{K}^L + \mathbf{K}^S - \mathbf{K}^{nc} \tag{13}$$

2.2.2 Problem of elastic stability

The tangential equation of motion in the finite element formulation can be written as follows:

$$\boldsymbol{M}\ddot{\boldsymbol{u}} + \boldsymbol{C}_T\dot{\boldsymbol{u}} + \boldsymbol{K}_T\boldsymbol{u} = \boldsymbol{0} \tag{14}$$

where $\boldsymbol{M}$, $\boldsymbol{C}_T$, and $\boldsymbol{K}_T$ are respectively the global mass matrix, the tangential damping matrix and the tangential stiffness matrix, $\boldsymbol{u}$ is the displacement vector. The eigenvalue problem related to eq. (14), transformed by using the phase space is the following one [7]:

$$\left(\begin{bmatrix}\mathbf{M} & \mathbf{0}\\ \mathbf{0} & \mathbf{K}_T\end{bmatrix} - \lambda\begin{bmatrix}\mathbf{0} & \mathbf{M}\\ -\mathbf{M} & -\mathbf{C}_T\end{bmatrix}\right)\begin{bmatrix}\lambda\mathbf{u}_0\\ \mathbf{u}_0\end{bmatrix} = 0 \tag{15}$$

Eq. (15), assuming regularity and positive definiteness for the mass matrix ($detM \geq 0$ and $M > 0$), becomes:

$$\mathbf{A}_T\mathbf{X}_0 = \lambda\mathbf{X}_0 \qquad \text{where} \qquad \mathbf{A}_T = \begin{bmatrix}-\mathbf{M}^{-1}\mathbf{C}_T & -\mathbf{M}^{-1}\mathbf{K}_T\\ \mathbf{I} & \mathbf{0}\end{bmatrix} \tag{16}$$

The stability behaviour of systems governed by equation (14) can be studied by examining the nature of the eigenvalues of the problem, in the neighbourhood of the current equilibrium solution. Therefore the eigenvalues λ_k of (16a) at each load step have to be computed by means of a

numerical procedure for unsymmetric matrices and the stability conditions [7] become: a)if all $Re(\lambda_k) = \alpha_k$ are negative, the position is asymptotically stable; if at least one $Re(\lambda_k) > 0$ exists, the position is unstable; If some eigenvalues have negative real parts, while the others have zero real parts, the position is weakly stable.

These are the stability assessments of Ljapunov, where the real part of the characteristic exponents are the well-known Ljapunov exponents. Moreover, the *divergence critical load* occurs when at least one eigenvalue λ_{ki} vanishes and the conjugate λ_{kj} becomes negative real, while the remaining eigenvalues are complex conjugate with negative real parts. If the load slightly increases over the critical load, the zero eigenvalue becomes one, with positive real parts, showing that the trivial state becomes locally unstable. The *flutter critical load* occurs when at least one pair of eigenvalues λ_k become pure imaginary eigenvalues, while the remaining eigenvalues are complex conjugate with negative real parts. If the load slightly increases over the critical load, the zero real parts of the pure imaginary eigenvalues become positive, showing that the trivial state is locally unstable and also that there is an oscillatory motion with increasing amplitude.

For undamped systems, usually the stability behaviour is studied by considering the square of the eigenfrequencies of the system, defined as $\omega^2 = -\lambda^2$. Therefore the divergence critical load is the value of the load to which the smallest square of the eigenfrequencies becomes equal to zero, while the flutter critical load is the value of load to which the two smallest eigenvalues approach each other until they coalesce.

3. NUMERICAL EXAMPLE

Some preliminary investigations with the proposed procedures are carried out, with reference to the case of a cable suspension pipeline. Using the first approach, stability diagrams are built-up to show stability conditions under exciting wind load. Moreover the values of the critical loads are found by means of the second approach. The geometric configuration is shown in Fig. 1. It is taken from Ref. [2], where the case was originally investigated, finding the first eigenfrequencies and eigenmodes. A symply supported tube-beam of circular cross section is considered for this purpose, together with a suspension cable of parabolic shape, connected to the former with vertical rods. Four lenghts are taken into account for the beam, from 50 m to 200 m with maximum height to span ratio of 1/6, 1/8, 1/10. The investigated outer diameters are 250, 400 and 560 mm, with thicknesses of 10, 10.3, 11.9 mm, respectively. The Young's modulus of the material used is equal to 160 Gpa. Periodic wind actions are applied, which have the well known self-exciting character. The research is here limited, as example, to the first resonance fequency. According to the beam motion, see Ref. [2], the load has a "following" character. For comparison, also the case of "non-following" forces has been taken into account. With the above indicated procedure, it was possible to find the stability diagrams of the cable suspended pipeline, as function of the span, height to span ratio, tube diameters and thicknesses. As usually, the diagrams are represented in non-dimensional form. As a results of the analyses, it was found that the boundaries of the principal regions of instability in nondimensional representation appears quite similar for the investigated cases. One of them is reported in Fig. 2 as example. In this representation, the ratio of the amplitude of the periodic load to the critical load is reported in the abscissa and the ratio of the exciting frequency to the first natural frequency is reported as ordinate. It can be observed the norrowing effect of the follower forces with respect to the unstable region. The values of the critical load found with the second approach are in agreement with those predicted in Ref. [2].

4. CONCLUSIONS

As a conclusion, it can be stated that the computational approaches here presented allow to gain a thorough understanding of the nonlinear geometrically behaviour of complex systems like the one taken into account in this paper. The research will be extended to include viscous damping effects.

REFERENCES

1. Creazza G., Mele M. (eds.), *Advanced problems in bridge construction,* CISM courses, 1991
2. Vitaliani R., Self-excited vibrations of cable suspension pipelines under constant wind loads, *C.T.A. Conference,* october 1977, (in italian).
3. Simo J.C., A finite strain beam. Part I, *Comput. Meths. Appl. Mech. Engrg,* 1985, 55-70
4. Simo J.C., Vu-Quoc L., Three-dimensional finite strain rod model. Part II:Computational aspects, *Comput. Meths. Appl. Mech. Engrg.*, 1986, 79-116
5. Simo J.C., Vu-Quoc L., On the dynamics in space of rods undergoing large motions- a geometrically exact approach, *Comput. Meths. Appl. Mech. Engrg.*, 1988, 125-161
6. Argyris, J.H, Symeondis, S., Nonlinear finite element analysis of elastic systems under nonconservative loading. Natural formulation. Part I Quasistatic problem, *Comput. Methods Appl. Mech. Engrg.* **26**, 1981, 75-123.
7. Gasparini, A., Saetta, A., Vitaliani, R. On the stability and instability regions of nonconservative continuous system under partially follower forces, in press, *Comput. Meths. Appl. Mech. Engrg.*
8. Zienkiewicz O. C., Taylor R. L., *The Finite Element Method,* vol I-II, McGraw-Hill, 1989.

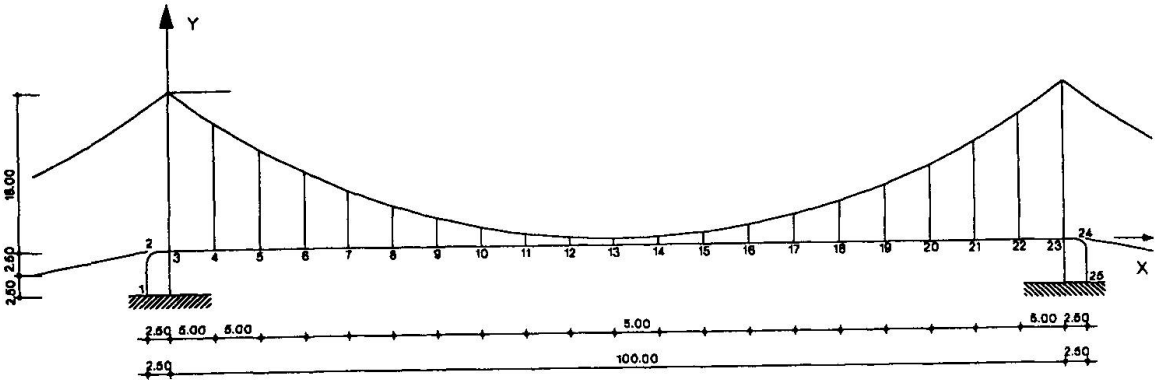

Fig. 1 - Model problem

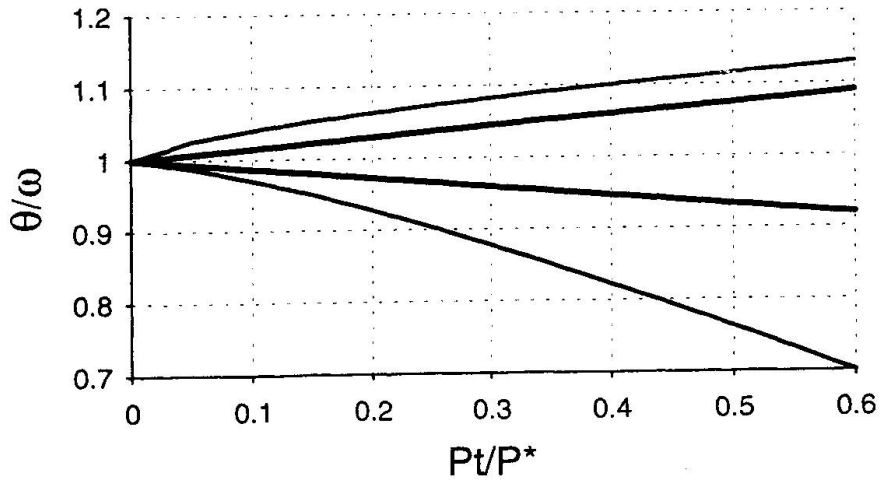

Fig. 2 - Stability diagram (bold line: follower forces)

Safety of Suspension Cables of the Williamsburg Bridge

Sécurité des câbles du pont suspendu de Williamsburg

Sicherheit der Hängeseile der Williamsburg Brücke

George DEODATIS
Assistant Professor
Princeton University
Princeton, NJ, USA

George Deodatis received his diploma in civil engineering from the National Technical University of Athens in 1982 and his Ph.D. from Columbia University in 1987. His research interests are in the area of probabilistic mechanics and earthquake engineering.

Roger Q. HAIGHT
Graduate Student
Princeton University
Princeton, NJ, USA

Roger Haight received his chemical engineering degree from Virginia Polytechnic Institute in 1982, and studied also at the Univ. of Exeter and Technical Univ., Delft. He was expert for caprolactam production in North America after working in Belgium from 1986-89. He came to Princeton University in 1992.

David P. BILLINGTON
Professor
Princeton University
Princeton, NJ, USA

David Billington received his civil engineering degree from Princeton University in 1950. He received a Fulbright Fellowship to study in Belgium from 1950-52. He was a structural engineer for Roberts & Schaefer before returning to Princeton University as Engineering Professor in 1960.

SUMMARY

The Williamsburg Bridge spanning New York City's East River has been attacked by salt air, which has corroded its steel main suspension cables. In 1988, the bridge was judged to be in need of replacement. Later, another study concluded the bridge was structurally sound. Methods are presented to estimate the current safety factor of the main cables, based on wire samples tested for tensile strength. The method uses the Ductile Wire Model and the Extreme Value Distribution approach and gives estimates for the cable safety factor.

RÉSUMÉ

Le Pont de Williamsburg sur le East River à New York a subi les attaques de la corrosion. En 1988, on estimait que le pont devait être remplacé. Puis une autre étude a montré qu'il était possible de garder le pont. Quelques méthodes utilisées pour l'évaluation des câbles sont présentées. Des essais sur des torons ont permis d'en estimer la résistance. Les méthodes, utilisant le "Ductile Wire Model" et "Extreme Value Distribution" donnent les facteurs de sécurité du câble.

ZUSAMMENFASSUNG

Die Williamsburg Brücke über den East River der Stadt New York war der Manhattaner Salzluft ausgesetzt, welche die Stahl-Haupthängekabel korrodiert hat; 1988 wurde beschlossen, die Brücke zu ersetzen. Später hat eine andere Untersuchung ergeben, dass die Brücke baulich sicher war. Basierend auf für Zugfestigkeit geprüften Drahtproben sind hier Methoden vorgestellt, den gegenwärtigen Sicherheitsfaktor des Hauptkabels abzuschätzen. Die Methode benutzt das Ductil Wire Model und gibt Schätzungen für den Kabelsicherheitsfaktor.

1. INTRODUCTION

Nearly a quarter of a million people a day cross New York City's Williamsburg Bridge via car, truck, train, bicycle, and on foot [1]. At its opening in 1903, engineers and media hailed its record 488 m main span. Considered in 1988 structurally unfit for future use, it is now under large-scale rehabilitation after a later study concluded that the bridge was structurally sound. [5]. On the basis of previous work [4], this study re-evaluates the current strength of the main cables. By opening up the cables for inspection and wire sampling, inspectors visually evaluated and physically tested the cable wires. This study uses the existing data base and a new approach based on the Type I Asymptotic Distribution of the Smallest Value [2] to estimate the current value for the safety factor of the main cables.

2. CABLE ANALYSIS OF THE WILLIAMSBURG BRIDGE

7,696 parallel wires with diameters of 0.0049 m comprise each of the four main cables of the bridge. 32 wire lengths were removed from each of five locations to estimate the current cable capacity and predict its reliability; data were collected from April to June of 1988. Engineers then cut each of the 32 wire samples into ten 0.3048 m segments to be tested in tension for breaking strength [1]. Figure 1 shows the locations of the 32 wire samples within the cable cross-section. The wire sample indicated by the shaded dot in Figure 1 is labeled B2 and will serve as an example in the following sections. For each one of the 32 wire samples, a mean and a standard deviation were computed for the tensile strength based on the ten 0.3048 m segments. The investigators assumed that the tensile strength follows a Gaussian distribution, with each wire sample having a different mean and standard deviation for each of these two parameters.

Fig. 1: Wire sample positions in cable cross-section (Location I at mid span)

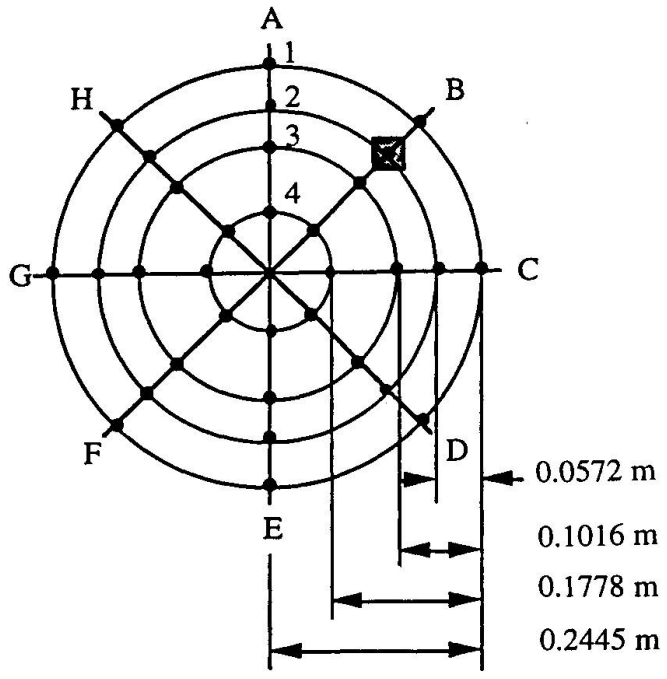

The data were used to develop contour maps depicting wire minimum breaking strength over the entire cable cross-section. The objective of this paper is to estimate the current safety factor of the main suspension cable, which is the ratio of its predicted strength divided by its ultimate load. The predicted strength is determined using the test results to estimate the average break load of the cable wires and then multiplying by the number of unbroken, ductile wires in the cross-section. The ultimate load is the maximum expected load and is calculated using structural analysis. The strength of the main cable is estimated using the Ductile Wire Model and an Extreme Value Distribution method, which can be implemented without using a computer.

The Ductile Wire Model is based on the assumption that all wires within the cable cross-section, when over-stressed, have sufficient ductility to elongate plastically before breaking. On-site investigations produced clear indications of general ductile wire behavior and load redistribution among the cable wires. This model assumes elastic-perfectly plastic behavior and uses the tensile strength results to estimate the cable strength.

2.1 Average Wire Break Load: Extreme Value Distribution

The mean values and standard deviations are computed for each one of the 32 wires using ten 0.3048 m segments. Consequently, these values for the tensile strength and the elongation are valid only for wire segments that are 0.3048 m in length. Assuming, in each row vector of ten tensile strengths, the test results are arranged from smallest to largest (i.e., $X_{11} < X_{12} < X_{13} < \cdots < X_{110}$), the first column of the matrix of test results (i.e., $X_{11}, X_{21}, X_{31}, \cdots, X_{321}$) automatically provides the values of the break loads for the 32 wires.

However, the issue of the break load for a longer wire segment in the cable must be addressed using the idea of effective clamp length. Because of the clamping effect of cable bands and wrapping on the wires, the load of the broken wire is channeled to the remaining intact wires in the vicinity of the break and is channeled back to the broken wire as its ability to carry loads is regained away from the break location. It is this phenomenon that allows taking wire samples from the main cable without risking a significant drop in the cable load-carrying capacity over its full length. This indicates that the weakest point in each wire should not be sought over the cable's full length, but over a limited length known as the effective clamp length.

Retractions were measured for cut wires to estimate the effective clamp length. By measuring the retraction length after cutting a wire under tension, it is possible to compute the amount of tensile force carried by the wire at any location away from the cut. From these computations it is reasonable to estimate that a broken wire contributes only partially to the load-carrying capacity of the main cable for three panel lengths (or 18.3 m) in the vicinity of the break (a panel length is the horizontal distance between two successive cable bands). Outside this 18.3-meter zone, the wire regains nearly its full initial load carrying ability. Therefore the cable bands produce an effective clamp length of 18.3 m. The wrapping of wires, which is continuous along the entire length of the main suspension cable, applies additional pressure to the wires and produces friction. Theoretical values for similar cables are as low as 1.5 m [3]; however as a conservative measure, the influence of cable wrapping is neglected, and the effective clamp length for this study remains 18.3 m [4].

Denoting now by $X_{(1)}$ the random variable describing the wire break load, its probability distribution function will be given by the Type I Asymptotic Distribution of the Smallest Value:

$$F_{X_{(1)}}(x) \approx 1 - \exp\left(-e^{\alpha_1(x-u_1)}\right) \tag{1}$$

where u_1 and α_1 are calculated from:

$$F_X(u_1) = \frac{1}{N} \tag{2}$$

$$\alpha_1 = N \cdot f_X(u_1) \tag{3}$$

In Equations (2) and (3), F_X and f_X are respectively the probability distribution and probability density functions of the initial distribution of random variable X; the value of N corresponds to the number of 0.3048 m segments in the effective clamp length of 18.3 m, or 60 units. Recall that X is a Gaussian random variable describing the tensile strength of 0.3048 m wire segments:

$$f_X(x) = \left(\frac{1}{\sqrt{2\pi}\cdot\sigma_X}\right)\cdot\exp\left[-\frac{(x-\mu_X)^2}{2\sigma_X^2}\right] \qquad -\infty < x < \infty \tag{4}$$

with μ_X and σ_X the mean value and standard deviation of X, respectively, and:

$$F_X(x) = \int_{-\infty}^{\infty} f_X(u)\,du = \Phi\left(\frac{x-\mu_X}{\sigma_X}\right) = \Phi(z) \tag{5}$$

with $\Phi(z)$ denoting the Standard Normal Distribution. The average wire break load is the mean value of random variable $X_{(1)}$, since $X_{(1)}$ describes the wire break load. The mean value and standard deviation of $X_{(1)}$ are given by:

$$E[X_{(1)}] = u_1 - \frac{0.57721}{\alpha_1} \tag{6}$$

$$\sigma_{X_{(1)}} = \sqrt{\frac{\pi^2}{6\alpha_1^2}} \tag{7}$$

The average wire break load is now computed for wire B2 using the Extreme Value Distribution. For wire type B2, the mean value and the standard deviation of the initial distribution are:

$$\mu_X = 28{,}976 \text{ N} \quad \text{and} \quad \sigma_X = 262.9 \text{ N} \tag{8}$$

Considering that the effective clamp length is 18.3 m, the value of N is 60. Using now Equations (2) through (5), the numerical values of parameters, u_1 and α_1 are:

$$u_1 = 28{,}416 \text{ N} \quad \text{and} \quad \alpha_1 = 0.0094 \tag{9}$$

Having computed u_1 and α_1, the probability distribution function, the mean value and the standard deviation of the wire break load are:

$$F_{X_{(1)}}(x) \approx 1 - \exp\left(-e^{0.0094(x-28{,}416)}\right) \tag{10}$$

$$E[X_{(1)}] = 28{,}355 \text{ N} \tag{11}$$

$$\sigma_{X_{(1)}} = 136.3 \text{ N} \tag{12}$$

2.2 Number of Unbroken Wires in the Cable Cross-Section

The broken wires must be discounted from the main cable cross-section. The bottom surface of the main cable contained the greatest number of wire breaks, where water infiltrating into the cable wrapping tended to collect [4]. The wires in the cross-section are divided into two groups: (A) the 78 surface wires of the bottom quadrant (where corrosion and wire breaks occurred to a high degree), and (B) the remaining 7,618 interior and surface wires. These two groups are shown in Figure 2.

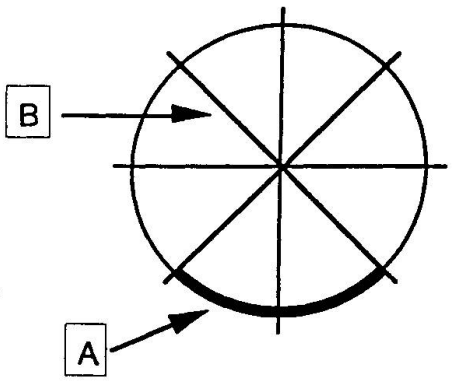

Fig. 2: Two wire groups in cable cross-section

A 78 surface wires in bottom quadrant

B 7,618 remaining interior and surface wires

The probability that a wire will be broken in either one of the two groups is based upon on-site inspections. The investigators found 15 broken wires among the 78 wires inspected in group A. Three broken wires were found in group B; although there are 7,618 wires in group B, only 1,057 could actually be inspected from the limited number of wedged cable openings. Therefore,

$$p_A = \frac{15}{78} \quad \text{and} \quad p_B = \frac{3}{1{,}057} \tag{13}$$

The number of broken wires in groups A and B are two random variables, NBW_A and NBW_B, respectively. Following the Binomial Distribution with the number of trials $N_A = 78$ and $N_B = 7{,}618$, respectively, the corresponding mean values and variances are:

$$E(NBW_A) = N_A \cdot p_A = 15 \tag{14}$$
$$E(NBW_B) = N_B \cdot p_B = 21.62 \tag{15}$$
$$Var(NBW_A) = N_A \cdot p_A \cdot (1 - p_A) = 12.12 \tag{16}$$
$$Var(NBW_B) = N_B \cdot p_B \cdot (1 - p_B) = 21.56 \tag{17}$$

The sum of these two random variables is a new random variable, NBW_{tot}, representing the total number of broken wires in the cable cross-section:

$$NBW_{tot} = NBW_A + NBW_B \tag{18}$$
$$E(NBW_{tot}) = E(NBW_A) + E(NBW_B) = 36.62 \approx 37 \tag{19}$$
$$Var(NBW_{tot}) = Var(NBW_A) + Var(NBW_B) = 33.68 \approx 34 \tag{20}$$

In view of the fact that the values of p_A and p_B shown in Equation (13) are estimated from the inspection of a single cable cross-section along the length of the main suspension cable, it is necessary to establish a sufficiently conservative value for the total number of broken wires in the cable cross-section. This is achieved using Chebyshev's inequality:

$$P\left\{\left|NBW_{tot} - E[NBW_{tot}]\right| \geq \delta\right\} \leq \frac{Var(NBW_{tot})}{\delta^2} \tag{21}$$

and an upper bound of 1% yielding the following value for δ:

$$\frac{Var(NBW_{tot})}{\delta^2} = 0.01 \quad or \quad \delta = 58.31 \tag{22}$$

Consequently, a sufficiently conservative value for the total number of broken wires in the cable cross-section is estimated as:

$$E[NBW_{tot}] + \delta \approx 96 \text{ broken wires} \tag{23}$$

The corresponding number of unbroken wires is 7,600.

3. SAFETY FACTOR ESTIMATION

The procedure to compute the safety factor of the main suspension cable using the Ductile Wire Model is described using an effective clamp length of 18.3 m (or 60 units).

(1) The average wire break load for the cable cross-section is estimated as 26,751 N.
(2) The conservative value for the total number of broken wires in the cable cross-section is estimated as 96 (Equation 23). The corresponding number of unbroken wires is 7,600.
(3) The strength of the main cable is the average wire break load multiplied by the number of unbroken wires, or 203,307,600 N.
(4) The ultimate load, or maximum expected load, on the main cable was determined as 48,485,400 N using structural analysis.
(5) Finally, the safety factor is the ratio of the cable strength divided by the ultimate load:

$$\text{Safety Factor} = \frac{203{,}307{,}600\ N}{48{,}485{,}400\ N} = 4.19$$

Table 1 displays the corresponding safety factor values for effective clamp lengths of 6.1 m (20 units) and 12.2 m (40 units).

Table 1: Safety Factors of Main Suspension Cable using the Ductile Wire Model

Effective Clamp Length	**6.1 m (20 units)**	**12.2 m (40 units)**	**18.3 m (60 units)**
Safety Factor	4.23	4.21	4.19

Note: 1 unit = 0.3048 m.

4. CONCLUSIONS

Wire break loads are directly described by Type I Asymptotic Distributions of the Smallest Value with parameters that can be easily determined from the test data. The assumptions considered in the computation of the safety factor of the main cable are generally conservative. Recall, for example, that the influence of cable wrapping on the effective clamp length was neglected and that Chebyshev's inequality was used to estimate a conservative value of the total number of broken wires.

When using the Ductile Wire Model, the effect of the effective clamp length on the value of the safety factor is minimal (see Table 1). On-site investigations produced clear indications of general ductile wire behavior and load redistribution among the cable wires. Consequently, engineers concluded that all unbroken wires should be considered ductile. The values for the safety factor of the main suspension cable shown in Table 1 indicate a range between 4.19 and 4.23. These values are sufficiently high to support the conclusion to rehabilitate, and not replace, the main suspension cables of the Williamsburg Bridge.

REFERENCES

1. LEVINE, R. and JOHNSON, K. Chronicle of City's Neglect of Williamsburg Bridge, The New York Times, June 10, 1988, pp. A1 and B4.

2. MATTEO, J. A., DEODATIS, George, and BILLINGTON, D. P. Safety Analysis of Suspension-Bridge Cables: Williamsburg Bridge, Journal of Structural Engineering, ASCE, Vol. 120, No. 11, 1994, pp. 3197-3211.

3. RAOOF, M. and HUANG, Y. P. Wire Recovery Length in Suspension Bridge Cable, Journal of Structural Engineering, ASCE, Vol. 118, No. 12, 1992, pp. 3255-3267.

4. STEINMAN BOYNTON GRONQUIST & BIRDSALL in association with COLUMBIA UNIVERSITY. Williamsburg Bridge Cable Investigation Program: Final Report, submitted to the New York State and New York City Departments of Transportation, October 1988.

5. WILLIAMSBURG BRIDGE TECHNICAL ADVISORY COMMITTEE. Technical Report to the Commissioners of Transportation of the City and State of New York, June, 1988.

Reliability of a Concrete Railway Bridge

Fiabilité d'un pont-rail en béton

Zuverlässigkeit einer Betoneisenbahnbrücke

R. RANGANATHAN
Professor
Indian Inst. of Technolgy
Bombay, India

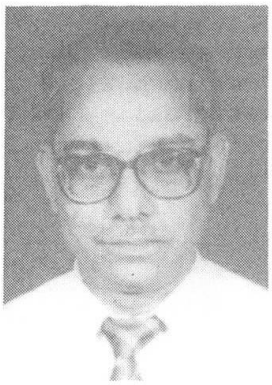

R. Ranganathan, born in 1939, received B.E. and M.Sc. (Struct. Eng.) degrees from Madras University and Ph.D. from Indian Institute of Technology, Kanpur, India. His main areas of research are reliability analysis and design of structures.

S.N. PATWARDHAN
Design Engineer
Stup Consultants Ltd
Bombay, India

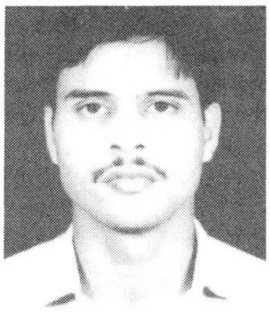

S.N. Patwardhan, born in 1967, received B.E. (Civil) degree from Bombay Univ. and M.Tech. (Struct.) from Indian Institute of Technology, Bombay, India. He is involved in design of bridges and consultancy services for Nuclear Power Corp., Department of Atomic Energy, India.

SUMMARY

The paper deals with the reliability analysis of short span concrete bridge commonly used in Indian railways. Available load spectrum based on actual field data is used for the analysis. Based on the experimental work, values of constants in Paris crack growth equation are fixed. Using Monte Carlo technique, fatigue crack growth reliability is calculated for different desired remaining cycles and initial depth of crack. Even after a crack is detected, it is observed that there is sufficient remaining life for the bridge to serve. Calculated reliability may be useful in development of inspection strategy.

RÉSUMÉ

L'étude traite de la fiabilité des ponts en béton à faible portée, tels que ceux couramment utilisés par les chemins de fer en Inde. Il se base sur des spectres de charges provenant de données d'exploitation réelles. A partir de données expérimentales, les paramètres sont déterminés sur la base de la formule de propagation des fissures d'après Paris. Le calcul de fiabilité prenant en compte la progression des fissures superficielles à la fatigue se fait au moyen de la méthode de simulation de Monte Carlo, cela pour différentes fréquences des cycles de charges désirées ainsi que des longueurs initiales de fissures. De tels calculs de fiabilité peuvent servir à la mise au point de stratégies de contrôles.

ZUSAMMENFASSUNG

Der Beitrag behandelt die Zuverlässigkeitsuntersuchung kurzer Betonbrücken, wie sie bei den Indischen Eisenbahnen häufig anzutreffen sind. Für die Untersuchung stehen Lastspektren aus echten Betriebsdaten zur Verfügung. Anhand experimenteller Daten werden die Parameter in der Risswachstumsformel nach Paris bestimmt. Die Zuverlässigkeit gegenüber Fortschreiten von Ermüdungsrissen wird für verschiedene gewünschte Lastwechsel und Anfangsrisslängen mittels Monte-Carlo-Simulationen berechnet. Selbst nach Sichtbarkeit eines Risses besteht demnach eine ausreichende Restlebensdauer für die Brücke. Solche Zuverlässigkeitsberechnungen können für die Entwicklung von Inspektionsstrategien nützlich sein.

1. INTRODUCTION

Short span reinforced cement concrete (RCC) bridges are common in Indian Railways. Safety of a bridge is to be evaluated against different failure criteria. Significant work has been done in the evaluation of a concrete bridge at the strength limit states viz. limit states of collapse in flexure and shear. Evaluation of reliabilty of a bridge under fatigue is one of the important factor. Though much work has been done on fatigue reliabilty of steel offshore structures and bridges, no significant work is reported in the case of concrete structures especially evaluating fatigue crack growth reliability. Under the action of fluctuating loads, crack initiates, propogates and may cause the final failure. To avoid such failures, it is necessary to know the behaviour of crack propogation in a bridge during lifetime of the structure. Knowledge of crack propogation also, may be useful for preparing maintenance and inspection schedule. In this paper, a method to determine behaviour of a crack in RCC bridge is presented by making use of fracture mechanics. Use of Paris equation is made to determine the depth of a crack at a given time. The empirical constants involved in the Paris equation are established by subjecting RCC test specimens to constant amplitude fatigue load. A typical RCC railway bridge under Indian Railway conditions is taken for present study. Fatigue reliability of the bridge is evaluated.

2. DETAILS OF THE BRIDGE AND LOAD SPECTRUM

Details of a typical short span RCC railway bridge commonly used in Indian Railways are shown in Fig.1. It consists of precast RCC units placed side by side and simply supported at its ends. The span of the bridge is 6.1 m. There are two broad gauge railway tracks. Concrete mix M 20(cube strength 20 N/mm^2) and high yield strength deformed bars(yield strength 415 N/mm^2) are used for tension steel and vertical stirrups.

Detailed traffic survey has been carried out and based on this a load spectrum has been developed [1]. This consists of eleven load categories, first ten for freight traffic and the last one for passenger train loading. The same is used in the present study.

3. DETERMINATION OF CONSTANTS c AND m IN PARIS EQUATION

To establish the empirical constants involved in the Paris crack growth equation[2], six RCC test specimens have been tested under constant amplitude fatigue loading. Size of the specimen used is 150 x 300 x 2300mm. Ordinary portland cement and aggregate with maximum size 12mm, have been used. Beams have been cured for minimum 28 days before testing. Fe 415 grade steel(yield strength 415 N/mm^2) has been used for tension steel and stirrups. Details of tested six specimens are given in Table 1. The beams have been tested after 28 days of curing. Beam is simply supported with 2000mm effective span and loads are applied at 1/3 rd spans. In the beginning of the test each beam has been subjected to monotonically increasing load, till the visible crack develops. Then the beam has been subjected to dynamic loading. In all the cases, the minimum load has been maintained as 18 KN and maximum load has been maintained equal to or less than the load corresponding to the first crack. Constant amplitude fatigue load at frequency 8 hertz has been applied. Beams have been observed physicaly frequently throughout the test. Crack growth has been continuously monitored. Each beam has been subjected to 2 million load cycles.

At the end of the test, a plot of depth of crack and number of cycles is obtained (Fig.2). Exponential best fit is drawn. From the graph a plot of crack growth rate, da/dN, and stress intensity factor range, ΔK, is obtained by adopting the procedure given in ASTM standard[2]. Plot of log(da/dN) and

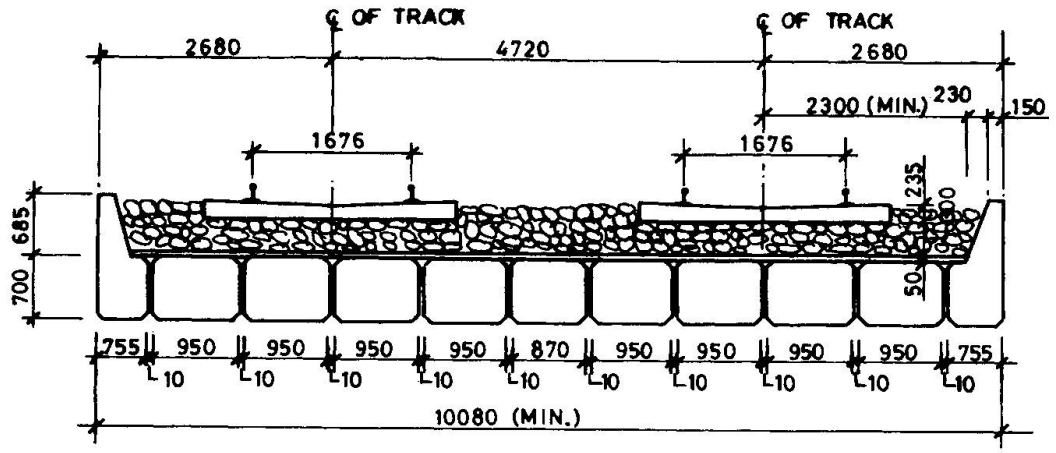

a) CROSS SECTION

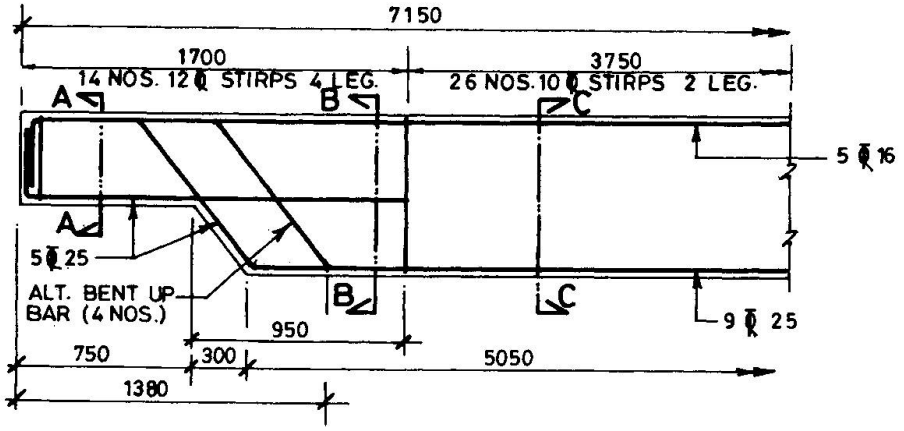

b) SECTIONAL ELEVATION

Fig.1 Details of a typical short span RCC railway bridge

$\log(\Delta k)$, shown in Fig.2 is a straight line. Slope and intercept on vertical axis of this line gives values of m and c in Paris equation. For each beam, two curves are studied one on eitheer side of the beam. From the test results, it is observed that the variation in the value of m is negligible and is found to be equal to 2.

Beam No.	28 days Cube Strength (MPa)	Tension Steel (per cent)	Maximum Applied Load (KN)
1	23.200	0.38	33.0
2	23.200	0.38	35.0
3	35.704	0.38	35.0
4	35.704	0.38	35.0
5	36.593	0.74	55.0
6	36.593	0.74	70.0

Table 1 Details of Test Specimens

4. FATIGUE RELIABILITY

If the flaws which exist in the structure are nearly planer, then the crack growth starts from the first load application. From the experimental studies, crack growth rate da/dN is given by the following equation, knwon as Paris crack growth equation [3].

$$\frac{da}{dN} = c(\Delta k)^m \qquad \ldots(1)$$

Where, $$\Delta k = k_{max} - k_{min} \qquad \ldots(2)$$

Stress intensity factor K, is expressed as

$$k = F(a)\ S\ \sqrt{\pi a} \qquad \ldots(3)$$

Where, F(a) is finite geometry correction factor, S is stress range and a is crack depth. For concrete structures, it can be expressed as [4]

$$F(a) = \frac{1}{\sqrt{\Pi}} \frac{1.99 - A(1-A)(2.15 - 3.93A + 2.7A^2)}{(1+2A)(1-A)^{1.5}} \qquad \ldots(4)$$

where, A = a/d and d is depth of beam. To calculate the number of cycles to failure when crack propogates from initial depth a_i to final depth a_f, Eq.1 is integrated from limit a_i to a_f.

$$N = \int_{a_i}^{a_f} \frac{da}{c(\Delta k)^m} \qquad \ldots(5)$$

For available load spectrum the equivalent stress range, s_{re}, is computed by the following equation [5].

$$S_{re} = [\Sigma P_i\ S^n_{ri}]^{\frac{1}{n}} \qquad \ldots(6)$$

Where, P_i is the frequency of occurance of the ith stress range, S_{ri}, and n is slope of cyclic crack growth rate curve.

To calculate reliability in fatigue crack growth, Monte Carlo simulation technique is used. From the Paris equation, the number of cycles required to propogate the crack from initial depth a_i to final depth a_f is calculated by making use of Eqs. 3, 4 and 5. Equation 3 is modified as,

$$\Delta k = B_m\ F(a)\ s_{re}\ I_f\ \sqrt{\pi\ /\ a} \qquad \ldots(7)$$

Where, B_m is model uncertainty parameter, S_{re} is equivalent stress range, and I_f is impact factor. Bridge is analysed for the load spectrum consisting eleven load categories as mentioned in Sec.2 and equivalent stress range is obtained as 162.514 MPa, by taking n = 2 in Eq.6. Failure function is written as,

$$Z = N - n \qquad \ldots(8)$$

Where, n is desired number of cycles (say 2 million cycles) and N is number of cycles required to reach the crack from a_i to a_f. While generating number of samples of Z by using Monte Carlo technique, a counter is made when $Z < 0$. Then the reliability is given by,

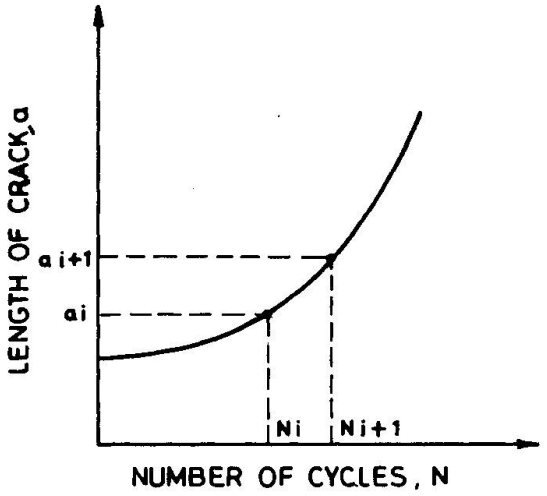

Fig.2 Typical crack growth curve

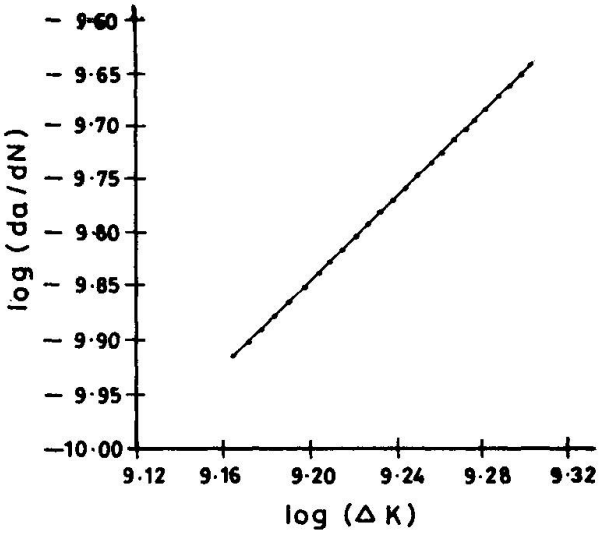

Fig. 3 Typical crack growth rate curve

$$R_s = 1 - p_f = 1 - \frac{n_f}{n_s} \qquad \ldots(9)$$

where, n_f is number of times value $Z < 0$ and n_s is total number of samples generated. Reliability index, β_s is given by

$$\beta = -\Phi^{-1}(p_f) \qquad \ldots(10)$$

Where Φ is cumulative probability of standard normal variable.

From the test results it is observed that the variation in the value of m is negligible and hence it is assumed to be deterministic. From the analysis of the bridge for eleven load categories it is found that equivalent stress range is approximately equal to 70.0 per cent of the permissible stress in steel. Corresponding to this stress range the mean value of c, from test results, is obtained as 0.442×10^{-12} with coefficient of variation 75 per cent for present case. Statistics of variables used in fatigue reliability analysis are given in Table 2. Using the same and the method explained earlier, fatigue crack growth reliability is calculated for various values of a_i and N. The results are shown in Table 3.

5. CONCLUSION

An attempt has been made to evaluate fatigue crack growth reliability of a concrete bridge used in Indian railways. Within the limitations of the experimental programme, it is observed that (i) value of m in Paris equation is 2 and statistical variation in m is negligible and (ii) lower values of c in Paris equation are obtained for higher values of initial depth of crack, percentage of steel and magnitude of loads. Parameter c is subjected to considerable statistical variation and is observed to be 75 per cent for applied stress range equal to 60 per cent of permissible stress in steel. It is observed also that experimental and theoretical results by making use of Paris crack growth equation are in good agreement. From Table 3 it is noted that fatigue relibility is sensitive to initial depth of crack and it is observed that fatigue crack growth reliability index β is equal to 2.32 corresponding to

Variable	Mean	Coefficient of Variation in Percentage	Distribution
Initial depth	25.0,50.0,100.0, 150.0 mm	15.0	Truncared lognormal
Final depth	525.0 mm	15.0	Truncated lognormal
c	0.442×10^{-12}	75.0	Lognormal
Equivalent stress range	162.514 MPa	15.0	Type 1 extremal (largest)
Model parameter	1.01	20.0	Lognormal
Impact factor	1.70	20.0	Lognormal

Table 2 Statistics of variables for fatigue reliability analysis

the desired remaining life of 2 million cycles with initial depth of crack equal to 25 mm. This means that there is sufficient capacity(remaining life) for the bridge to serve even after a crack is detected and there is sufficient time available to carry out repair work. Calculated fatigue crack growth relibility may be useful for developement of inspection strategy.

Initial depth of crack (mm)	Values of β (corresponding p) for			
	$N = 2.0 \times 10^6$	$N = 1.5 \times 10^6$	$N = 1.0 \times 10^6$	$N = 0.5 \times 10^6$
25.0	2.32(0.0102)	2.50(0.0062)	2.82(0.0024)	3.37(0.0004)
50.0	2.16(0.0156)	2.35(0.0094)	2.64(0.0041)	3.19(0.0007)
100.0	1.67(0.0048)	1.89(0.0029)	2.22(0.0013)	2.75(0.0029)
150.0	0.53(0.2960)	0.53(0.2223)	1.27(0.1025)	1.88(0.0299)

Table 3 Results of fatigue reliability analysis

REFERENCES

1. Ravi,G,Fatigue Reliability Analysis and Design Approach to Railway Rivetted Steel Bridges, Ph.d Thesis Report, Civil Engineering Department, I.I.T., Bombay, July, 1993.

2. ASTM Committee E-24, Standard Test Methods for Measurement of Fatigue Crack Growth Rate, ASTM Standard, E-647, V03.01, pp.646-666.

3. The Committee on Fatigue and Fracture reliability, Fatigue Reliability: Introduction, Journal of Struct. Engg. ASCE, 108 (1), Jan.1982, pp. 3-24.

4. Jenq., Y., and Shah, S.P., Two parameter Fracture Model for Concrete, Journal of Engineering Mechanics, III (10), October 1985, pp. 1227-1241.

5. Schilling, C.G., Stress Cycle for fatigue Design of Steel Bridges, Journal of Struct. Engg. Div., ASCE, 110 (6), June, 1984, pp.1222-1234.

Long-Term Behaviour of Continuous Prestressed Composite Bridges

Comportement de longue durée des poutres mixtes continues précontraintes

Langfristiges Verhalten von vorgespannten kontinuierlichen Balken mit Verbundquerschnitt

Franco MOLA
Professor
Politecnico di Milano
Milan, Italy

Franco Mola, born 1946, is active in research concerning creep, structural analysis, instability and rehabilitation of concrete structures. Member of the Editorial Group of the FIP CEB Manual "Structural Effects of Time Dependent Behaviour of Concrete". In 1985 he was conferred the IABSE Prize.

SUMMARY

The long-term analysis of continuous prestressed composite steel-concrete beams is presented. Referring to beams with thin slabs, the problem is solved in the viscoelastic domain by using a feasible algebraic formulation for the concrete creep constitutive law. In this way simple moment-rotation relationships, very useful for design, can be deduced. A case study considers the basic aspects of the problem, in particular the different structural responses to external loads and to prestressing.

RÉSUMÉ

L'analyse de longue durée des poutres continues précontraintes avec section mixte acier-béton est présentée. La résolution du problème est déterminée pour les poutres avec ta-bliers de faible épaisseur dans le domaine de la viscoélasticité linéaire en utilisant une formulation algébrique pour la loi de fluage du béton. L'application à un cas réel permet de discuter les aspects fondamentaux du problème, en particulier le comportement de la structure lors de l'application des charges ou de la précontrainte.

ZUSAMMENFASSUNG

Gegenstand der Arbeit ist die Analyse von vorgespannten kontinuierlichen Balken mit Verbundquerschnitt. Mit Bezug auf Balkenplatten mit geringer Dicke wird das Problem im Rahmen der linearen Viskoelastizität gelöst durch Anwendung von algebraischen Formulierungen des Zustandsgesetzes des Betons, die ein schnelles Abfassen der Verträglichkeitsgleichungen erlauben. Das Beispiel einer Anwendung gestattet es, die wichtigsten Aspekte des Problems zu erörtern, insbesondere die unterschiedliche Reaktion des Bauwerks auf äussere Kräfte und auf Vorspannung.

1. INTRODUCTION

Steel-concrete composite beams represent an efficient and economical choice for the construction of short or middle-span bridges. In design practice the simply supported scheme is commonly adopted in order to assure compressive stresses in the concrete slab which considerably increases the strength and the rigidity of the transverse sections. The simply supported scheme does not represent the most feasible choice for multispan bridges as it introduces some disadvantages exerting a marked negative influence on structural durability. The unreliability of the simply supported scheme is mainly connected to the presence of a large number of support devices and of elastic joints representing one of the most important factors of structural degrading. On the contrary, the scheme of continuous beam allows to considerably reduce the number of supports and to eliminate the elastic joints, assuring in the same time favourable moment redistributions at ultimate significantly increasing the structural bearing capacity. The main drawback of continuous beams is the presence of tensile stresses in the concrete slab in the zones near to the interior supports which can produce diffuse cracking and generate structural damaging to which a lifespan reduction is generally connected. In order to maintain the statical and economical advantages of continuous beams, contemporaneously eliminating cracking phenomena in the support zones, a feasible technique consists in prestressing the concrete slab. In this way we can guarantee the presence of only compressive stresses in the slab during the service stage, significantly improving the structural lifespan. On the other hand the evaluation of the prestressing effects has to be performed by means of a refined structural analysis in order to correctly compute the stresses connected to the presence of parasitic moments which markedly reduce the efficiency of prestressing. Moreover, steel-concrete composite beams exhibit a marked rheological inhomogeneity so that the state of stress produced by permanent loads varies in time as a consequence of the creep and shrinkage deformations arising in the concrete slab. In particular the mutual interaction existing between the stress distribution in the transverse sections and the moment distribution along the beams, has to be accurately investigated. A general and reliable procedure of structural analysis for continuous steel-concrete composite beams has not yet been satisfactorily developed so that, even if the Codes [1], [2], [3], give exhaustive informations about the creep constitutive laws for concrete, a reliable design procedure for the analysis of continuous composite steel-concrete beams is still lacking. This item is the main goal of the present paper, where the general formulation for the analysis of the state of stress in continuous prestressed steel-concrete beams is derived. The problem is approached in the linear viscoelastic domain, assuming for concrete the algebraic creep law proposed by Trost, [4] which drives, as widely proven in other works [5], [6], to very reliable results, allowing in the same time, to state simple design formulas which can be easily used in design practice. In order to avoid useless complications in developing the analytical process we shall assume that the slab can be regarded as perfectly flexible. This hypothesis, which is more realistic when the depth of the slab is small with respect to the height of the beam, does not represent a limitation for the solution, as its generalization to the case of deep slabs is a trivial task. On the contrary it allows to deal with simpler formulas which can be discussed in a direct and immediately understandable way.

2. PROBLEM FORMULATION

2.1 Sectional Analysis

Let us consider the section of Fig. 1.a, subjected to a bending moment M varying in time, and to an initial prestressing force N_{op}, applied by means of a steel cable having area A_{sp}. Assuming for concrete the subsequent algebraic creep law

$$\epsilon_c=\lambda\sigma_c/E_c+\mu\sigma_{co}/E_c+\epsilon_{sh} \quad (1)$$

with

$$\lambda=-\phi/\rho, \qquad \mu=[\rho(1+\phi)+\phi]/\rho \quad (2)$$

where $\phi>0$, $\rho<0$, ϵ_{sh}, are respectively the creep coefficient, the relaxation coefficient, and the shrinkage deformation, the compatibility equations between the slab and the cable and between the slab and the beam according to Fig 1.b assume the form

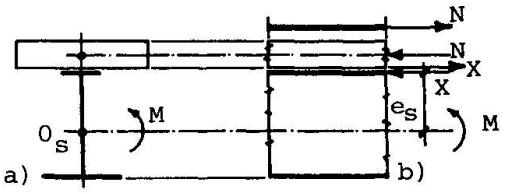

Fig.1 Composite section

$$(N-X)\omega\lambda+(N_o-X_o)\omega\mu+N\alpha(1-\omega)=\epsilon_1E_cA_c\omega \quad (3)$$

$$(N-X)\omega\lambda+(N_o-X_o)\omega\mu-X(1-\omega)=\epsilon_2E_cA_c\omega+M\beta(1-\omega)/e_s$$

In eqs. (3) the subscript o is applied to the initial quantities (time t_o) and the subsequent parameters have been defined

$$\omega=[1+(1/np_s)(1+e_s^2/r_s^2)]^{-1}; \quad n=E_s/E_c; \quad p_s=A_s/A_c;$$
$$\alpha=(p_s/p_{sp})(1+e_s^2/r_s^2)^{-1}; \quad p_{sp}=A_{sp}/A_c; \quad \beta=(1+r_s^2/e_s^2)^{-1} \quad (4)$$

Finally for ϵ_1, ϵ_2 representing the relative deformations imposed between the cable and the slab and between the slab and the beam the subsequent expressions hold

$$\epsilon_1=(N_{op}/E_cA_c)[(\alpha/\omega)(1-\omega)+(1-X_o/N_{op})]-\epsilon_{sh}; \quad \epsilon_2=-\epsilon_{sh} \quad (5)$$

where the first term at second member of the first of eqs. (5) is related to the relative deformation between cable and slab imposed by prestressing. At initial time t_o, we have $\epsilon_{sh}=\phi=\rho=0$, and from eqs. (2) $\lambda=1$, $\mu=0$, so that eqs. (3) become

$$(N_o-X_o)\omega+N_o\alpha(1-\omega)=\epsilon_{1o}E_cA_c\omega; \quad (N_o-X_o)\omega-X_o(1-\omega)=\epsilon_{2o}E_cA_c\omega+M_o\beta(1-\omega)/e_s \quad (6)$$

The solutions of eqs. (6), (3) drive to the subsequent expressions

$$N_o=-\beta\omega M_o/[e_s(\omega+\alpha)]+N_{op}; \quad X_o=-(\beta M_o/e_s)[1-\alpha\omega/(\omega+\alpha)]+N_{op} \quad (7)$$

$$N=-X/\alpha-\beta M/\alpha e_s; \quad X=F_MM/e_s+F_M'M_o/e_s+F_pN_{op}+F_SN_s \quad (8)$$

where $N_s=\epsilon_{sh}E_cA_c$ and functions F are given by the following relationships

$$F_M=-\beta[1-\alpha\omega\lambda/G]; \quad F_M'=\beta\alpha^2\omega\mu(1-\omega)/[(\alpha+\omega)G]$$
$$F_p=\omega[1+\alpha(1-\omega)\phi/G]; \quad F_S=\alpha\omega/G; \quad G=(1+\alpha)\omega\lambda+\alpha(1-\omega) \quad (9)$$

The solution of eqs. (6), (3) for the unprestressed sections ($p_{sp}=0$) can be obtained from eqs. (7), (8), (9) by assuming, according to eqs. (4), $\alpha=\infty$. In this way we obtain

$$N_o=N_{op}=0; \quad X_o=-\beta(1-\omega)M_o/e_s; \quad N=0; \quad (10)$$

$$X=\bar{F}_MM/e_s+\bar{F}_M'M_o/e_s+\bar{F}_SN_s \quad (11)$$

$$\bar{F}_M=-\beta[1-\omega\lambda/\bar{G}]; \quad \bar{F}_M'=\beta\omega\mu(1-\omega)/\bar{G}; \quad \bar{F}_S=\omega/\bar{G}; \quad \bar{G}=1+\omega(\lambda-1) \quad (12)$$

The absolute values of functions F versus ω are reported in Fig. 2 for $t=\infty$, $\beta=0.55$ assuming α as parameter. The function $|F_M|$ is decreasing as it points out the effect of the viscoelastic restraint represented by the slab in reducing the bending stresses in the steel beam. High α values are related to high deformabilities of the slab and consequently to small values of F_M. In particular for $\alpha=\infty$, $\omega=1$ the slab is perfectly deformable so that no restraints are applied to the beam and consequently $F_M=0$. Functions F_P and F_S are increasing as they are connected to the effect of the elastic restraint represented by the beam in preventing the slab deformations due to prestressing and shrinkage. For $\omega=0$ the beam is perfectly deformable making the slab unrestrained

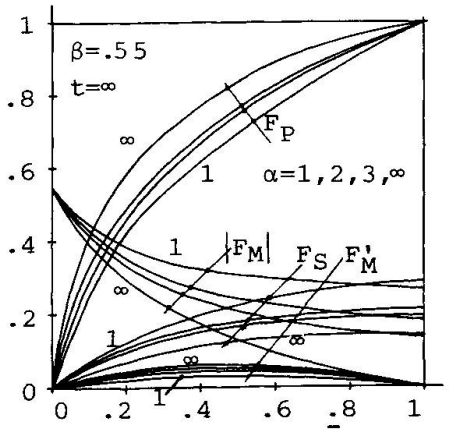

Fig.2 Functions F,$\bar{F}$

so that $F_P=F_S=0$, while for $\omega=1$ the beam is rigid and the functions F_P, F_S take their maximum values. It is interesting to observe that for $\omega=1$ we have $F_P=1$ whatever is α, while F_S takes values which are increasing with α. This can be explained taking into account that the imposed prestressing force N_{op} does not depend from the cable deformability while the shrinkage effects in the slab are increased by increasing the cable deformability. Finally function F_M' which is related to the algebraic form assumed for the creep law takes zero values for $\omega=0,\omega=1$ independently on α as these two cases, related to a perfectly deformable or to a perfectly rigid slab do not require the definition of creep deformations for evaluating the problem solution. The parameter α affects the functions F in a not negligeable way. We can see that the functions $\bar{F}$, represented in Fig. 2 by the diagrams with $\alpha=\infty$, cannot be assumed as representative of the totality of the obtained results so that in performing the structural analysis we have to take into account that the transverse sections of the beams have to be considered variable, by using for the calculation of the F functions $\alpha=\infty$ in the unprestressed zones and the proper value of α, depending on p_{sp} in the prestressed zones.

2.2 Structural Analysis

The evaluation of the moment distribution in continuous beams can be conveniently performed by means of the moment-rotation relationships. Referring to Fig. 3, indicating by g the uniformly distributed load and by N_{op} the common prestressing force acting in the two zones $0\le z\le z_1$, $z_2\le z\le 1$, for the moment M, the curvature 1/r and the end rotations Θ_1, Θ_2 of the steel beam we can write

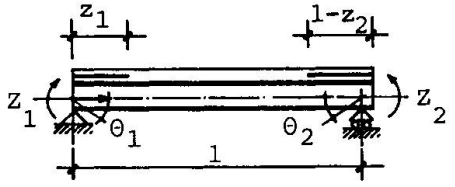

Fig.3 Rotations at beam edges

$$M=Z_1(1-z/1)+Z_2z/1+M_g;\quad 1/r=(M+Xe_s)/E_sJ_s;\quad \Theta_1=\int_1 (1-z/1)\frac{1}{r}dz;\quad \Theta_2=\int_1 (z/1)\frac{1}{r}dz \qquad (13)$$

Combining eqs. (8), (9), (12), (13), for the left edge rotation Θ_1 we derive

$$\Theta_1=\delta_{11}Z_1(c_{11}+\bar{c}_{11})+\delta_{12}Z_2(c_{12}+\bar{c}_{12})+\delta_{11}Z_{10}(d_{11}+\bar{d}_{11})+\delta_{12}Z_{20}(d_{12}+\bar{d}_{12})+$$
$$+3/2\delta_{11}N_{op}e_sp_{11}+3/2\delta_{11}N_se_ss_{11}+gl^3/24E_sJ_s(c_{10}+\bar{c}_{10});\quad \delta_{11}=2\delta_{12}=1/3E_sJ_s \qquad (14)$$

$$c_{11}=(1+F_M)[1+f_{11}(\zeta_1)-f_{11}(\zeta_2)];\quad \bar{c}_{11}=[1-c_{11}/(1+F_M)](1+\bar{F}_M);$$
$$c_{12}=(1+F_M)[1+f_{12}(\zeta_1)-f_{12}(\zeta_2)];\quad \bar{c}_{12}=[1-c_{12}/(1+F_M)](1+\bar{F}_M);$$
$$c_{10}=(1+F_M+F_M')[1+f_{10}(\zeta_1)-f_{10}(\zeta_2)];\quad \bar{c}_{10}=[1-c_{10}/(1+F_M+F_M')](1+\bar{F}_M+\bar{F}_M')$$
$$d_{11}=c_{11}F_M'/(1+F_M);\quad d_{12}=c_{12}F_M'/(1+F_M); \qquad (15)$$
$$\bar{d}_{11}=\bar{c}_{11}\bar{F}_M'/(1+\bar{F}_M);\quad \bar{d}_{12}=\bar{c}_{12}\bar{F}_M'/(1+\bar{F}_M)$$
$$f_{11}=\zeta(\zeta^2-3\zeta+3);\quad f_{12}=\zeta^2(3-2\zeta);\quad f_{10}=\zeta^2(6-8\zeta+3\zeta^2)$$
$$p_{11}=F_P[\zeta_1(2-\zeta_1)+(1-\zeta_2)^2];\quad s_{11}=\bar{F}_S[\zeta_2-\zeta_1][2-(\zeta_1+\zeta_2)]+p_{11}F_S/F_P;\quad \zeta=z/l$$

The rotation Θ_2 can be obtained from eq. (14) by changing Z_1 with Z_2 and putting $\zeta_1=1-\zeta_2$ in eqs. (15). Applying eq. (14) at time $t=t_0$ ($\lambda=1$, $\mu=0$) we obtain the initial elastic moment rotations relationships which allow to write the compatibility equations of the continuous beam and to perform the structural analysis at initial time evaluating the moments Z_{10}, Z_{20}. As a second step we apply eq. (14) and calculate the moments Z_1, Z_2 at time t. The problem is so reduced to the execution at different stages of two elastic structural analyses, the first, at initial time t_o connected to the actual values of the elastic parameters of the various parts, the second, at time t, connected to a varied value of the elastic modulus of the concrete part, taking also into account the effects produced by the time variability of the state of stress connected to the initial values Z_{10}, Z_{20} entering in eq. (14).

3. NUMERICAL EXAMPLE

The preceding relationships have been applied for the analysis of the continuous

beam of Fig. 4, for which we have α=3.02; ß=0.683; ω=0.2556 together with the subsequent values for the various parameters: ϕ=3; ρ =-0.88; μ=0.6; $\epsilon_{sh}=20\cdot10^{-5}$; N_{op}=8500 kN; g=53.3 kN/m. In Fig. 5 the relative moments $M/(gl^2/8)$ are represented for various loading conditions at time t_o and for t=∞. We observe that the moment M_g produced by external load is scarcely influenced by creep so that we can consider it constant in time without significant error. On the contrary the parasitic moment due to prestressing which is about -0.52 $gl^2/8$ at initial time grows up to -0.81 $gl^2/8$ with an increase of 55%. This fact, together with the developing of the moment produced by shrinkage, produces an increase of about 22% of the initial total moment on the central support. The time variability of the absolute values of the stresses acting in the continuity and in the span sections is reported in Fig. 6, where an increase of the beam stresses together with a marked decrease of the slab stress can be observed. In order to simplify the plotting of the diagrams, the stresses have been normalized to their maximum value 184.2 MPa, coinciding with the compressive stress σ_{s2} acting

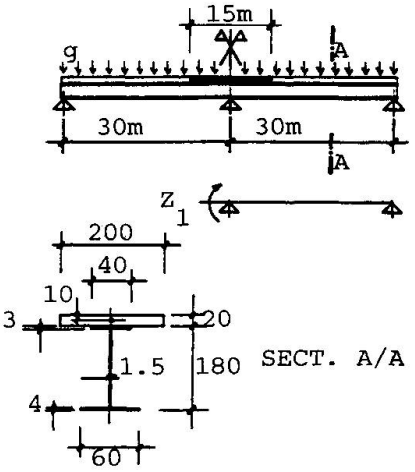

Fig.4 Case study

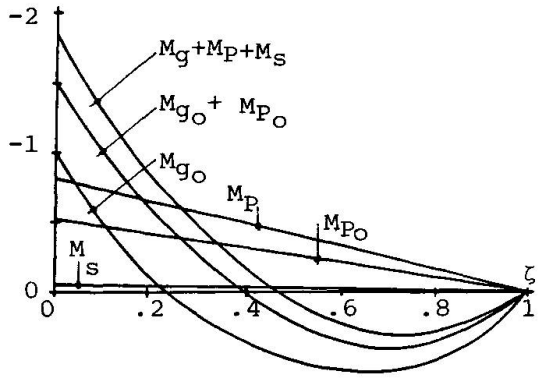

Fig.5 Bending moments at initial and final time

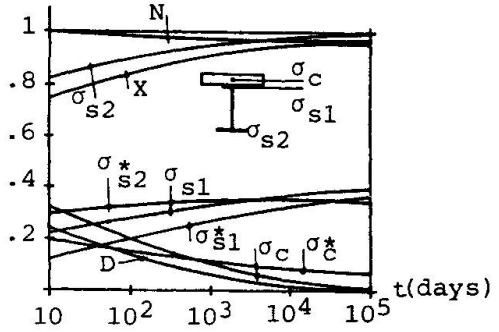

Fig.6 Stresses in transverse sections

at time t=∞ at the lower edge of the beam in the continuity section. The stresses in the concrete slab have been amplified by the factor 10 to obtain a clearer representation. In the same figure the values of the prestressing force N, of the shear force X and of their diference D=N-X are reported using N_{op} as normalization factor. The stresses in the beam are greater in the continuity section, in particular the highest value is reached by σ_{s2} as at the lower edge of the beam both the prestressing force and the bending moment generate compressive stresses. The reduction of the stress in the concrete slab is quite higher in the continuity section where the prestressing produces a marked increase of the shear X strongly reducing the slab compressive stress which is practically vanishing for t=∞. On the contrary in the span section the reduction of the concrete stress is connected to the increase of the slab deformation produced by creep and is governed by the functions $\bar{F}_M$, $\bar{F}_M'$ which have finite values for t=∞. Regarding the prestressing and the shear forces N, X we can observe that the first is practically constant in time (N/N_{op}=0.97) as the presence of the elastic restraint represented by the steel beam drastically reduces the creep deformations of the slab together with the loss of the prestressing force. For the same reason X markedly increases in time reaching the final ratio X/X_o=1.30=0.96 N_{op}, so that the difference D=N-X representing the total axial force acting in the slab is practically vanishing at final time together with the final concrete stress.

4. CONCLUDING REMARKS

The scheme of continuous beam, reducing the number of supports devices and the elastic joints between adjacent decks represents a favourable choice in preventing the risks of structural damaging. The prestressing of the slab in the continuity zones, avoiding the developing of cracking phenomena allows to significantly increase the structural durability and the related lifespan. The behaviour of continuous steel-concrete prestressed beams is markedly influenced by concrete creep producing notable variations in the state of stress and in the moment distribution acting along the beams. In order to correctly design the various structural elements a reliable procedure for the long term structural analysis is consequently needed. The procedure developed in the present work, based on an algebraic formulation of the creep law represents an useful tool for the analysis and the design of continuous prestressed beams as it allows to obtain good results by means of simple calculations very similar to the ones governing the elastic structural analysis. The application to an actual case study has shown that the parasitic moment produced by the prestressing force significantly increases in time, together with the shear force acting between the slab and the beam, so that the compressive stress in the concrete slab is highly reduced in time. This fact clearly states the need of proceeding by means of a refined long term structural analysis in order to evaluate in a reliable way the final stress in the concrete slab and to check the structural safety regarding the efficiency of prestressing in preventing cracking effects and in improving structural lifespan.

REFERENCES

1. CEB/FIP Model Code for Concrete Structures 1990, Bulletin d'Information CEB No.195-196,1990.
2. Eurocode N. 2 Design of Concrete Structures.
3. Eurocode N. 4 Design of Composite Steel and Concrete Structures.
4. TROST M., Auswirkungen des Superpositionprinzips auf Kriech und Relaxation Probleme bei Beton und Spannbeton. Beton und Stahlbetonbau, H. 10, 1967.
5. MOLA F., Structural Effects of Time Dependent Behaviour of Concrete. Advanced Problems in Bridge Construction, Springer-Verlag, New York, 1991, pp. 176-221.
6. MOLA F., Creep Analysis of Composite Steel Concrete Members with Deformable Connectors. Proceedings of the ASCE Structures Congress XII, Atlanta, USA, 1994, Vol. 1, pp. 737-742.

System Performance of Two Prestressed Concrete Bridges

Comportement de deux ponts en béton précontraint

Verhalten von zwei vorgespannten Betonbrücken

Michel GHOSN
Associate Professor
The City College of New York
New York, NY, USA

Michel Ghosn, born in 1956, studied at Case Western Reserve Univ. in Cleveland, OH, where he completed his Ph.D. in 1984. He is Assoc. Prof. of Civil Eng. at The City College of New York. His research interests include bridge load modelling, structural reliability and code calibration.

Juan R. CASAS
Associate Professor
Technical Univ. of Catalunya
Barcelona, Spain

Juan R. Casas, born in 1960, received his civil eng. degree from the Techn. Univ. of Catalunya (UPC) in 1984, where he completed his doctorate in 1988. He has been Assoc. Prof.of bridge engineering at UPC. His research interests include design, dynamic analysis & field testing of bridges.

SUMMARY

A non-linear analysis of the behaviour of two alternate bridge designs with the same simple span length of 25 m is performed. The first configuration has 11 parallel prestressed I-beams. The alternate design consists of three spread box beams. The two configurations are designed to satisfy the same Spanish bridge code requirements. Results of the deterministic non-linear analysis are used to calculate member and system reliability indices for both bridges. Redundancy indexes are calculated to compare the system safety performance to the member performance of each bridge configuration.

RÉSUMÉ

On analyse le comportement non linéaire de deux ponts isostatiques de 25 m de portée. Le premier pont est formé de 11 poutres en I en béton précontraint, l'autre par trois poutres-caissons, les deux ayant été calculés pour satisfaire aux conditions des normes espagnoles. Les résultats de l'analyse non linéaire servent à calculer les indices de sécurité des éléments et de l'ensemble des deux ponts. On calcule les indices de "redondance" qui permettent la comparaison entre le comportement et la sécurité de chaque système et celui de ses éléments.

ZUSAMMENFASSUNG

Inhalt des Artikels ist eine nichtlineare Untersuchung des Verhaltens von zwei verschiedenen Brückenkonstruktionen mit der gleichen Spannlänge über 25 m. Die erste Brükkenkonstruktion enthält 11 parallel vorgespannte I-Balken. Die andere Konstellation besteht aus drei gespreizten Hohlkastenträger. Beide Entwürfe sind nach den spanischen Richtlinien für Brücken konstruiert. Die Ergebnisse der deterministischen, nichtlinearen Untersuchung werden verwendet, um Zuverlässigkeitsindizes beider Brücken zu bestimmen. Redundanzindizes vergleichen die Systemsicherheitsleistungen mit den Leistungen einzelner Brückenelemente.

1. INTRODUCTION

Prestressed concrete I-girder bridges have had a long history of excellent performance under regular truck traffic loads as well as overloads. In addition, I-girder bridges are economical and easy to construct and are known to have high levels of system reserve strength and redundancy. On the other hand, the use of spread box girder bridges is becoming more common because, in addition to their good structural performance, they are more aesthetically pleasing than I-girder bridges. For this reason, the spanish bridge authorities have abandoned the use of parallel prestressed concrete I-girder bridges in favor of spread box beam bridges for all overcrossings in new highway constructions.

The object of this paper is to compare the structural performance and the safety levels of these two bridge types. To perform such a comparison, two example bridges with the same span length of 25 m are designed to satisfy the same spanish code requirements. Figures 1 and 2 describe the two alternate bridge configurations.

2. LIMIT STATES AND ANALYSIS PROCEDURE

Although widely used in design codes, it is generally accepted that the linear analysis of a bridge structure is not sufficient to verify the safety and the functionality of a bridge structure: It is also important to verify the adequacy of its ultimate capacity for intact as well as damaged conditions and to verify its system serviceability. For concrete bridges, ultimate capacity is reached when a mechanism forms or when unloading begins due to excessive concrete damage. It has been observed that unloading begins at a load level close to the point when concrete crushing in a main longitudinal member occurs [1,2]. Therefore, this point is used herein to define system failure. It appears that the most suitable serviceability limit state for bridges is a deflection to span length ratio limit [3]. A displacement limit equal to the span length/200 was proposed in reference [2] and is used herein as a system serviceability limit state. In addition, the capacity of the structure to carry load after the complete damage or ductile failure of a main load carrying member should also be performed.

A nonlinear bridge analysis program NONBAN developed in references [2] and [4] is used for the analysis of the two alternate bridge configurations for the four limit states described above. The program uses a grillage (grid) discretization of a bridge structure to model its linear and nonlinear behavior in the longitudinal and transverse directions including the effect of the slab and diaphragms.

Flexural nonlinearity occurs when the loads applied on a beam element are incremented until the internal moments exceed their linear elastic limits. At this point the beam undergoes plastic end rotations. These plastic end rotations are related to the section curvature and the plastic hinge length. To perform the nonlinear analysis using NONBAN, moment versus curvature relationships are obtained using the basic principles of equilibrium. Estimates of the plastic hinge length for are obtained from empirical equations such as the ones proposed by Park and Pauley [5].

3. RESULTS OF DETERMINISTIC ANALYSIS

To perform the nonlinear analysis, the two bridge systems described above are discretized as grillages as outlined by Hambly [6]. Reference [4] demonstrated that this scheme was sufficiently accurate to study the global linear and nonlinear behavior of typical I-beam as well as box beam bridge configurations. The nonlinear incremental analysis is performed under the effect of two side-by-side trucks with a minimum lateral distance of 1.2 m between the axles of the adjacent trucks. Each of the applied trucks is assumed to have the configuration of a typical 5 axle semi-trailer observed over the spanish road network with an average total weight equal to 407 kN. Both bridges are assumed to have elastomeric supports at the ends of every longitudinal beam such that vertical displacements are restrained but all end rotations are free. For the box beams this assumes a single support at the center of each end section under the existing diaphragm.

In a first step, a linear elastic analysis of the two structures is performed. First member failure is assumed to occur when the most heavily loaded longitudinal member reaches its maximum capacity. The concrete stress-strain relationships used for the derivation of the nonlinear material properties assume that concrete crushes when the compression strain is equal to 0.0035. It is found that first longitudinal member failure would occur in the 11-girder bridge when the weights of the two side-by-side trucks are incremented by a load factor of 8.98. For the three-box girder bridge, this value is 8.53. For both bridges, the most critical loading position was obtained when the two trucks are transversely placed on the extreme edge of the bridge and the rear tridem axle placed at the middle of the span. In both cases, failure occurred at the midpoint of the external longitudinal girder.

In a second stage, a complete nonlinear analysis is performed for the same trucks and loading positions described above. For the 11-girder bridge, system failure occurred at a load factor of 10.40. In this case, failure occurred when the exterior girder under the load reached its maximum plastic rotation at the middle of the span. For the three-box girder bridge, system failure occurred at a load factor of 9.18. At this load factor, failure occurred transversely in the slab section joining the web of the exterior box girder and the middle box girder. Because of the known limitations of the grid model to simulate the actual behavior of the deck slab, another analysis is performed assuming that the slab

will continue to carry loads beyond the level at which the strain in the transverse slab elements reaches the value of 0.0035. In this case, system failure is assumed to occur at the point at which concrete crushes in a main longitudinal member. This level was reached at a load factor equal to 10.92 for the three-cell bridge.

System serviceability limit, i.e. when girder deflection equals span length/200, is reached at a load factor equal to 9.03 for the 11 girder bridge and at a load factor of 9.17 for the box girder bridge. Figure 3 shows a comparison between the load factor versus maximum displacement curve for the two bridge configurations analyzed.

To study the effect of the boundary conditions of the box-girder bridge, two elastomeric supports are placed at the beams' end sections under each web to restrain its torsional rotation. First member failure assuming linear elastic response occurs in the external member at a load factor equal to 9.08. Accounting for the nonlinear behavior, slab crushing in the transverse direction occurs at a load factor equal to 10.41. If the nonlinear analysis is continued beyond this load level then the load factor at system failure is equal to 12.67 when the exterior longitudinal member crushes. The serviceability displacement limit is reached at a load factor equal to 10.43.

Damaged conditions assume that the external member of the 11-girder bridge is completely damaged. The nonlinear analysis shows that failure of the slab occurs at a load factor of 1.91. If the slab is assumed to be able to sustain this load, crushing in a main longitudinal member would then occur at a load factor of 6.92. Damage to the three-box girder bridge is simulated by assuming complete damage of the external web of the external girder. For the box girder with only one support at each section end, the slab would fail under the effect of the dead load alone. If loading is continued assuming that slab failure is only a local failure, then system failure would occur at a load factor of 5.67. For the box girder bridge with supports under each web, the load factor at which transverse slab failure occurs is 1.3 and the load factor at which longitudinal member failure occurs is 6.21. The load factors calculated for the damaged box girder bridge are lower than those observed for the 11-girder bridge because damage to one web will not only reduce the external box's moment capacity by one half but will also reduce the torsional rigidity of the member to a practically negligible level. The results of all the analyses performed herein are summarized in table 1.

4. RELIABILITY AND SYSTEM SAFETY

To account for bridge strength and load uncertainties, a reliability analysis is performed. The safety margin Z for a bridge system is defined as:

$$Z = (R - D) - (L + I) = LF - LL \tag{1}$$

where the incremental load factor, LF, is equal to the resistance R minus the dead load D (LF=R-D). LF determines the capacity of a bridge system to support the applied live load. LL is the maximum applied live load effect expected in a given return period. LL depends on the static truck load effects L and the dynamic effect I. Since in this study the calculation of the bridge system capacity is presented as a function of the typical average truck configuration, both LF and LL are herein normalized with respect to the effect of that truck. Both LF and LL are random variables. LF is random due to the uncertainties in determining the system resistance R and the dead load D. A deterministic estimate of LF for each of the four limit states previously identified is obtained using the nonlinear analysis program as seen in section 3. LL is random due to the uncertainties associated with predicting the maximum expected load in a given return period. It is a function of the number of trucks that cross the bridge during the return period, the number of trucks that are simultaneously on the bridge when the maximum load effect is measured, the positions of the trucks on the bridge deck, the weights of the trucks, the distribution of the weights to the individual axles and the axle configurations. In addition, the load effect is a function of the dynamic impact. All these factors are random and produce high levels of uncertainty. Reference [7] provides a simple truck live load model which has been proven to be valid for the spanish truck traffic [8]. The model gives the maximum expected lifetime load effect as a function of a typical truck configuration with a characteristic weight. The total truck load effect L+I is given as:

$$L + I = amW_{95}Hi \tag{2}$$

where "a" is the effect of a representative truck configuration with a one unit total load. "m" is factor representing the variation of the random trucks from the configuration of the representative truck. W_{95} is the chracteristic 95 percentile value of the truck weight histogram for a given jurisdiction. H is the headway factor representing the number of representative trucks of weight W_{95} that will produce the same effect as the maximum expected lifetime load effect. "i" is the impact factor. When normalized with respect to the effect of the typical spanish semi-trailer truck equation 2 becomes:

$$LL = \frac{mW_{95}Hi}{407kN} \tag{3}$$

Since the analysis performed in the previous section uses an average truck configuration "m" is herein assumed to be equal to 1.0 and its coefficient of variation (COV) is assumed to be equal to 8 % [7]. W_{95} for typical spanish truck gross weights is given as 559 kN [9]. A COV of 10 % is used to account

for the uncertainty and site to site variability of W_{95} [7]. The dynamic impact factor for two trucks is shown to be about 1.10 with a COV of 8 % [10].

H is a function of the return period. Two different loading conditions are identified: Extreme loading condition and regular truck traffic condition. Extreme loading condition is defined as the maximum expected lifetime load. The expected bridge lifespan is usually around 50 to 75 years. The extreme loading condition is normally used in the evaluation of member safety and for the safety for the ultimate limit state. Reference [7] shows that for 25 m spans and for a 50-year return period H is on the order of 2.78 times the effect of one representative truck (or 1.39 times the effect of two side-by-side trucks). Regular traffic condition is defined as the recurrent load expected to be regularly applied on the bridge. A two-year exposure period is used herein to define the maximum load expected under regular traffic conditions. This condition is used for the analysis of the serviceability limit state and for the analysis of damaged bridges. Reference [10] shows that the expected 2 year load is about 93% of the maximum lifetime load. Thus, H becomes equal to 1.30 times the effect of two side-by-side trucks. Reference [7] recommends a COV equal to 7 % for H. In addition, a COV of 10 % is added to LL to account for possible future changes in truck traffic patterns and growth in truck traffic rates. The final COV obtained for the normalized live load effect LL is then equal to 20 %.

According to reference [10] prestressed concrete member capacities are on the average higher than the nominal or code specified resistances by a factor of 1.05 with a COV of 7.5 %. Actual dead load values are on the average 1.04 times higher than the estimated values obtained from bridge plans with a COV of 9 %. For the bridges studied in this paper, this would produce a bias of 1.05 on LF (LF=R-D) and a COV of 10 %. In addition, a COV of 8 is added herein to account for the variablity in the lateral and longitudinal positions of the trucks. The final bias on LF is then equal to 1.05 and the final COV is equal to 13 %. Cornell [11] explains that such a COV on member capacity would result in a lower COV (on the order of about 10 %) for the complete system. However, in this study it is proposed to use the same COV for member capacity as well as system capacity to account for the uncertainties associated with modeling the nonlinear behavior and predicting the system capacity. Thus, it is herein assumed that a bias of 1.05 and a COV of 10 % are valid for all four limit states studied.

Knowing the mean values and the COV of LF and LL and assuming that LF follows a lognormal distribution while LL follows an extreme type I distribution, the probability of failure P_f and the safety index β can be calculated using a first order reliability program [12].

Redundancy is defined as the capability of a bridge system to continue to carry load after the failure of its most critical member. Hence, to study the redundancy of a system, it is useful to examine the difference between the safety indices of the system and the safety index of the most critical member. If the safety index of the system for the ultimate limit state is defined as $\beta_{ult.}$, the safety index of the system for the serviceability limit state is $\beta_{serv.}$, the safety index for the damaged condition is $\beta_{damaged}$ and the safety index for member failure assuming linear elastic response is β_{member}, then the redundancy indices for the ultimate limit state, $\Delta\beta_u$, the serviceability limit state $\Delta\beta_s$ and the damaged condition $\Delta\beta_d$ are defined as:

$$\begin{aligned} \Delta\beta_u &= \beta_{ult.} - \beta_{member} \\ \Delta\beta_s &= \beta_{serv.} - \beta_{member} \\ \Delta\beta_d &= \beta_{damaged} - \beta_{member} \end{aligned} \tag{4}$$

Reference [2] proposed a set of reliability conditions that adequately redundant bridge systems should satisfy. For example, to be clasified as adequately redundant, a bridge system must produce $\Delta\beta_u$, $\Delta\beta_s$ and $\Delta\beta_d$ values respectively equal to or higher than +1.0, -1.0 and -0.5.

The results in table 1 show that in all the cases analyzed, the safety index for member is above 5.38. Knowing that a target member safety index of 3.5 was used in North America for the development of bridge design and evaluation codes, the member safety index values obtained herein indicate that these bridges provide highly conservative levels of safety. This however does not necessarily mean that these bridges are adequately redundant. In fact it is observed that only the bridge with end torsional rotations restrained provide an adequate level of redundancy for the ultimate limit state. None of the bridge configurations studied provide adequate redundancy for the damaged condition. However, it is observed that the 11-girder bridge shows the best performance for this case. On the other hand, all the bridges provide adequate levels of system serviceability performance.

The same calculations are repeated assuming that the COV of LF is equal to 10 %. The effect of the change in this COV is relatively small because this produces a change in the system safety indices as well as a change in the member safety indices such that the net effect on the redundancy indices is small. Similar observations are also made in reference [2] indicating that the measures of redundancy proposed in equation (4) are robust and not very sensitive to variability in the data base.

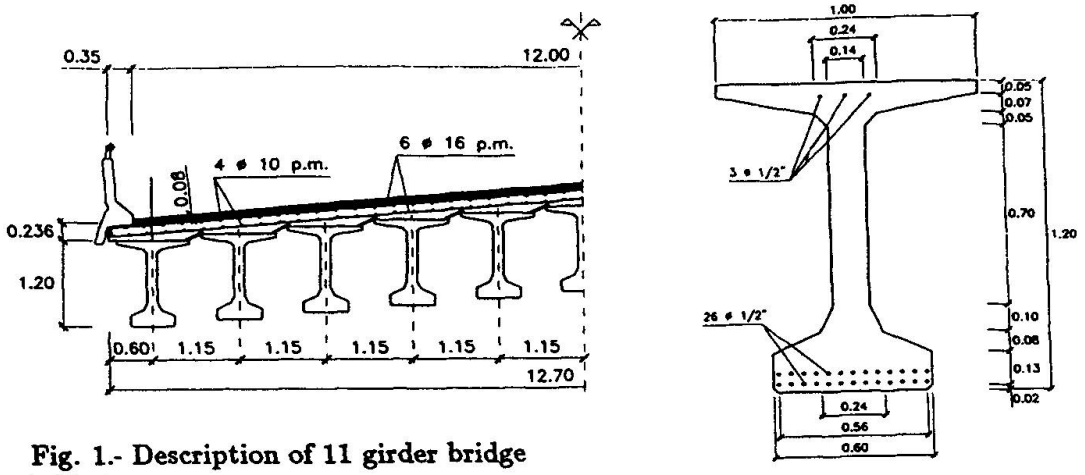

Fig. 1.- Description of 11 girder bridge

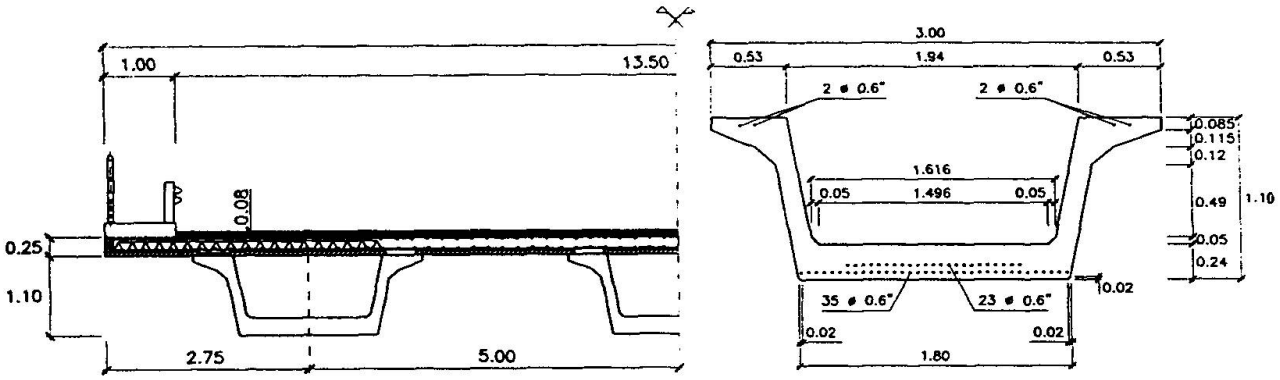

Fig. 2.- Description of 3 box-girder bridge

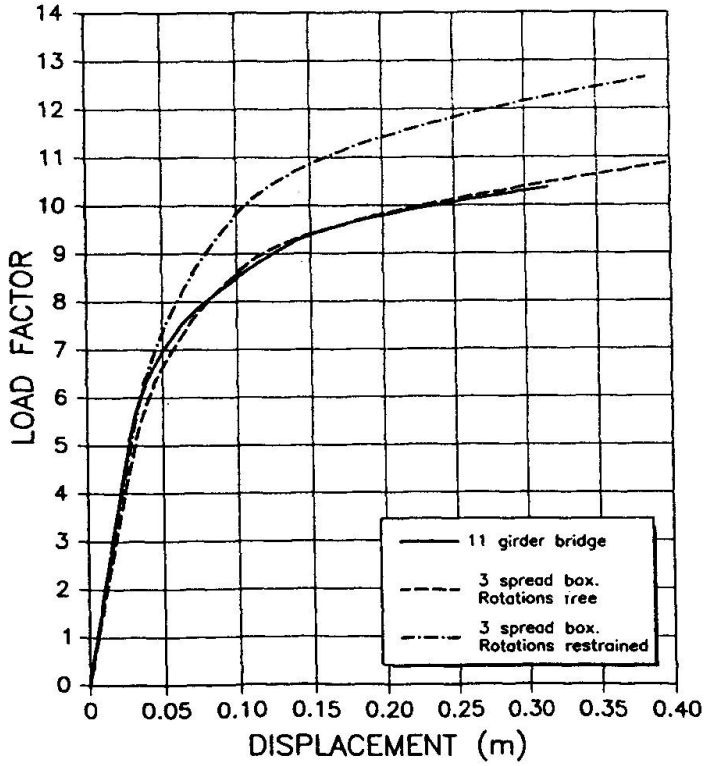

Fig. 3.- Load factor versus maximum deflection for the 3 cases analysed

Table 1. Summary of results.

			LF COV = 13%			LF COV = 10%		
CONFIGURATION	LIMIT STATE	LF	Beta	Delta beta	target	Beta	Delta beta	target
11-GIRDER BRIDGE	1 st member - Linear elastic	8,98	5,56	x	x	5,84	x	x
	Transverse slab failure	x	x	x	x	x	x	x
	Longitudinal member failure	10,40	6,09	0,53	1,00	6,41	0,57	1,00
	System serviceability	9,03	5,84	0,28	-1,00	6,14	0,30	-1,00
	Damaged condition	6,92	4,90	-0,66	-0,50	5,13	-0,71	-0,50
3-SPREAD BOX BEAM BRIDGE	1 st member - Linear elastic	8,53	5,38	x	x	5,64	x	x
one support at center	Transverse slab failure	9,18	5,64	0,26	x	5,92	0,28	x
of end section	Longitudinal member failure	10,92	6,27	0,89	1,00	6,60	0,96	1,00
	System serviceability	9,17	5,90	0,52	-1,00	6,20	0,56	-1,00
	Damaged condition	5,67	4,22	-1,16	-0,50	4,41	-1,23	-0,50
3-SPREAD BOX BEAM BRIDGE	1 st member - Linear elastic	9,08	5,60	x	x	5,88	x	x
one support under each	Transverse slab failure	10,41	6,09	0,49	x	6,41	0,53	x
web of end section	Longitudinal member failure	12,67	6,82	1,22	1,00	7,20	1,32	1,00
	System serviceability	10,43	6,36	0,76	-1,00	6,70	0,82	-1,00
	Damaged condition	6,21	4,53	-1,07	-0,50	4,74	-1,14	-0,50

5. CONCLUSIONS

The system performance of two alternate bridge configurations is analyzed. The results indicate that the three-cell bridge configuration provides the best system performance for the ultimate limit state. However, it is the 11-girder bridge that provides the best system performance in case of damage to one critical member. Although, the redundancy indices obtained are relatively low, the values of the system safety indices obtained are high (greater than 4.2 even for the damaged condition), indicating that these bridges are conservatively designed and provide overall high levels of system safety.

ACKNOWLEDGEMENT

This paper was written during the sabbatical stay of the first author at the Technical University of Catalunya in Barcelona, Spain. The financial support provided by the Generalitat of Catalunya is greatly appreciated.

REFERENCES

1. BURDETTE, E.G., and GOODPASTURE, D.W., "Tests of Four Highway Bridges to Failure", ASCE Journal of the Structural Division, vol. 99, No. ST3, March 1973.
2. GHOSN, M. and MOSES, F., "Redundancy in Highway Bridge Superstructures", NCHRP 12-36, Final Report, Washington DC, March, 1994.
3. Ad Hoc Committee on Serviceability Research, "Structural Serviceability: A Critical Appraisal and Research Needs", ASCE Journal of Structural Engineering, Vol. 112, No. 2, December, 1986.
4. GHOSN, M. and CASAS, J.R., "Evaluation of Highway Bridge Systems", Draft Report, Department of Construction Engineering, Technical University of Catalonia Barcelona, December, 1994.
5. PARK, R. and PAULEY, T., Reinforced Concrete Structures, Wiley and Sons, New York, 1975.
6. HAMBLY, E.,C., "Bridge Deck Behavior", Chapman and Hall, London, 1976.
7. MOSES, F. and GHOSN, M., "A Comprehensive Study of Bridge Loads and Reliability", Report FHWA/ODOT/ 85-005, 1985.
8. CASAS, J.R., and GHOSN, M., "Comparison between Live Load Models for Highway Bridges", in progress, 1994.
9. SOBRINO, J.A., "Evaluacion del Comportamiento Funcional y de la Seguridad Estructural de Puentes Existentes de Hormigon Armado y Pretensado", Tesis Doctoral, Departament d'Enginyeria de la Construccio, Universitat Politecnica de Catalunya, Barcelona, Diciembre de 1993.
10. NOWAK, A.S., "Calibration of LRFD Bridge Design Code", NCHRP project 12-33, December 1993.
11. CORNELL, C.A., "Risk-Based Structural Design", Proceedings of a Symposium on Risk Analysis, Department of Civil Engineering, University of Michigan, Ann Arbor, MI,August, 1994.
12. RACKWITZ, R., and FIESSLER, B., "Structural Reliability under Combined Random Load Sequences", Computers and Structures, No. 9, 1978.

Simulation and Consulting System for Bridge Construction

Système de simulation et de conseils pour la construction des ponts

Ein Simulations- und Beratungssystem für den Brückenbau

David C. EKCHIAN
Civil Engineer
Swiss Fed. Inst. of Technology
Zurich, Switzerland

David C. Ekchian, born in 1966, studied Structural Engineering at EPF, Lausanne. He worked as a research engineer for the firm Hilti before joining the ETH at Zurich to prepare a Ph.D. thesis in computer sciences.

Edoardo ANDERHEGGEN
Professor
Swiss Fed. Inst. of Technology
Zurich, Switzerland

Edoardo Anderheggen, born in 1939, received his diploma in civil eng. and his Ph.D. from ETH Zurich. Since 1976, he is Prof. of Applied Computer Sciences. His main interests concern program development in the field of finite element analysis with applications to civil eng.

Pieter E. ROELFSTRA
Dr. Eng.
INTRON S.M.E.
Yverdon, Switzerland

Pieter E. Roelfstra, born in 1946, studied struct. eng. at Delft Univ., and obtained his Ph.D. from EPF Lausanne. He worked for 12 years at the Dutch Ministry of Public Works. He is now director of INTRON S.M.E., specialised in computational physics and mechanics.

SUMMARY

The computer program *Bridges* is used to determine the optimum shuttering geometry and predict the long-term displacements of long multispan concrete bridges. *Bridges* simulates each single construction step. When used during the design phase, *Bridges* is expected to help improve construction quality, extend the lifespan of the structure and reduce maintenance costs. The program, however, is also to be used in the construction phase as a consulting system. Each measured quantity, like displacement, temperature, humidity, etc. as well as unforeseen events, causing changes in the construction schedule can be taken into account at any time.

RÉSUMÉ

Le programme de calcul *Bridges* s'emploie à déterminer la géométrie optimale des coffrages et prévoir les déformations à long terme des grands ponts en béton armé et précontraint à travées multiples. Toutes les étapes de la construction sont intégrées dans un planning, puis simulées. Exploité durant la phase de projet, *Bridges* permet d'améliorer la qualité de la construction, d'assurer une plus longue durée de vie de l'ouvrage et de réduire les coûts d'entretien. Tout au long de la construction, le programme supervise son évolution et guide l'ingénieur dans les phases critiques sur la base des mesures effectuées sur l'ouvrage.

ZUSAMMENFASSUNG

Das Computerprogramm *Bridges* dient zur Bestimmung der optimalen Schalungsgeometrie und allfälliger Auflageranpassungen bei grossen vorgespannten und schlaff bewehrten Stahlbetonbrücken unter Berücksichtigung der zu erwartenden Langzeitverformungen. Dabei wird jede Phase des Bauprozesses simuliert. Eingesetzt bereits in der Projektierungsphase, erlaubt *Bridges* eine Erhöhung der Ausführungsqualität, eine Verlängerung der Lebensdauer und eine Reduktion der Unterhaltskosten. Während der Ausführungsphase steht dem Bauingenieur ein Beratungssystem zur Verfügung, welches den Baufortschritt überwacht und in kritischen Bauphasen Unterstützung leistet.

1 INTRODUCTION

The computer program *Bridges* is used to determine the optimum shuttering geometry and predict the long-term displacements of long multispan concrete bridges. These are strongly influenced by time-dependent deformations such as creep and shrinkage, temperature gradients and the stress relaxation of prestressing cables. *Bridges* simulates each single construction step taking into account all these effects.

The simulation program consists of three modules. The first one, the schedule manager, handles the timing of all building operations. The planned schedule can be updated at any time to accommodate unexpected events. The second module determines the distribution of the temperature and moisture in the transverse direction of the structure, under stationary and transient conditions. A set of state parameters defining the concrete's delayed behaviour are computed at each cross-section for each event defined in the schedule. The third module is a finite element code for the analysis of the structural deformations. Based on simple beam theory, the rates of change of physical and mechanical concrete properties are determined as a function of the state parameters mentioned above and included in the material laws. The resulting displacements can be compared with the deflections of the girders measured during construction.

The program is intended to be used daily on site. A consulting system is therefore coupled to the simulation module. If unexpected events occur (changes in the schedule, low material quality, special weather conditions, settlement of a pier, etc.) and the predicted displacements reveal unacceptable differences compared to the ideal state, the program suggests the required support adjustments, or even changes in the shuttering geometry, to be applied in order to achieve the desired final state.

When used during the design phase, *Bridges* is expected to help improve construction quality, extend the lifespan of the structure and reduce maintenance costs. Throughout the construction, the program monitors its evolution and guides the site engineer in the critical phases.

2 GEOMETRICAL DISCRETISATION

A unique geometrical description of the bridge is used throughout the 3 modules of the program. This discretisation has to consider the construction method in the definition of the girders and supports. The girders are described by a succession of beam elements, each being defined by two sections. These are generally different, thus the beam length has to be chosen so that a linear interpolation of all relevant section properties between them is a reasonable simplification. Each section is subdivided into subsections. The subsections are domains where the material parameters computed with a fine mesh can be assumed to be constant. The sections, consisting of subsections, generate subbeams which are assembled to build the beam elements (Fig. 1).

The geometry of the prestressing cables is defined by points in 3D space. The coordinates of the points are given by the construction plans. The high number of points generally needed to describe the exact cable position allows the use of a linear interpolation between them.

A 3D viewer allows the user to define the geometry of the bridge and check the accuracy of the consecutive construction steps.

3 A SIMULATION TOOL

In *Bridges*, each single construction step is simulated. To handle this, a schedule manager coordinates the time-step decomposition of the whole construction process to be simulated by the two following modules: a finite element code for 2D analysis in the transverse direction for determining the temperature and moisture diffusion in the cross-sections and a finite element code for longitudinal 1D analysis of the structural deformations at each stage of the construction.

3.1 The schedule manager

The schedule manager keeps track of the timing of all the casting operations, removal of formwork (shuttering), tensioning of prestressing cables, special time-dependent load definitions, changes of support conditions, etc. A preliminary schedule is generally established by the

contractor. This is the reference schedule, used to define the shuttering geometry. Due to unexpected events (e.g. strikes, lack of materials, extreme weather conditions, part of the construction area damaged), this schedule will inevitably evolve during the construction process. Therefore, the schedule manager, through an interactive graphical user interface, allows both for changes in the sequence of *events* and for modifications or definitions of new construction steps.

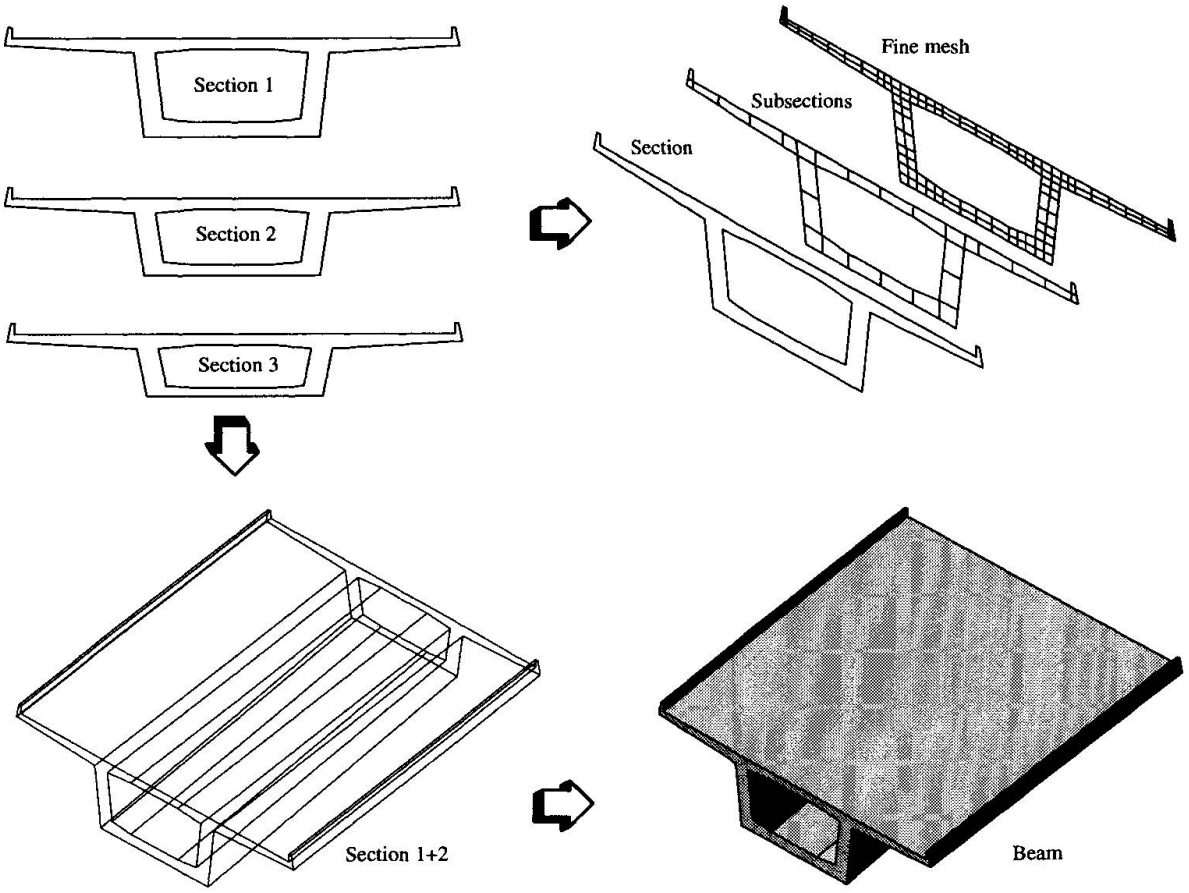

Fig. 1: Geometrical description of the bridge

The user does not have to define all the details of every construction operation. Since many procedures are repetitive, macro-events called *stages* are declared with starting and ending dates. The stages can be chained with several kind of relations such as "start n hours before end of stage B", "end with end of stage B", etc. If an absolute date of a stage is moved, all the relative stages are moved accordingly. Conflicts are automatically detected. Each stage is built of local events with a corresponding application date and a list of *actions*. At the beginning of a simulation, the stages are expanded and the global events are generated. For each local event's date mentioned, a global event is created, if necessary, and the local list of actions is appended to the global list for that event. This global event list determines the dates to be considered during the simulation process. The time-step values to be used later in the incremental equations are directly generated from this list.

3.2 The diffusion module

In this module, the bridge is analysed in the transverse direction for simulating transport phenomena such as mass flow (gas, liquid) and energy (heat) diffusion under stationary and transient conditions. The analysis is applied at each previously defined cross-section defining a beam's end for each event defined in the schedule. The time-dependent temperature distributions due to the liberation of concrete hydration heat is predicted. Nonlinear moisture transport as a function of time is also simulated. In this way shrinkage-induced deformations

and stresses can be computed and assessed. Phenomena like internal and external condensation can also be taken into account.

The concrete model implemented [1] is based on the following set of so-called state parameters at the microstructural level:
- degree of hydration α (describes the chemical hydration process)
- maturity M (describes the time-dependence of the mechanical properties)

and at the physical level:
- temperature T
- relative humidity H

It is assumed that the rates of change of physical and mechanical properties of concrete are fully determined by these parameters. A second fundamental assumption is that the thermo-mechanical coupling, such as the liberation of thermal energy in the fracturing process, can be neglected. This means that the evolution of the state parameters can be determined independently of the mechanical behaviour of the structure.

The evolution of these state parameters is computed by solving a set of coupled nonlinear differential equations modelling temperature and humidity diffusion.

The program then builds a state parameter table at each construction stage (*event*) for all subsections.

3.3 The simulation module

This module is called to compute the structural deformations according to the material data and loading at each *event*. From the schedule manager, the program fetches the external and internal loads as well as the corresponding state parameters and computes the deformations incrementally. Both ordinary reinforcement and prestressing are included in this computation.

All physical and mechanical properties depend on the state parameters determined in the previous module, each providing its own contribution to the total strain rate.

In this last module, the program follows the whole process of the construction and delivers the deformations of the bridge after each *event*. The result is a simulated deflection line (profile) which can be compared with the measured deflections of the girders (i.e. the effective construction state) and the ideal line. Changes in the schedule, settlements and others unexpected events, as well as the introduction of material data based on in-situ tests influence the deflections. If the predicted deflection line reveals unacceptable differences compared with the ideal one, the user can assign special degrees of freedom to some girders or supports (rotation of the girder, adjustment of the bridge bearing) and ask for a (computer) consulting session. The longitudinal analysis is started again and, taking into account the new degrees of freedom, the program attempts to:
- determine the required rotations of the girder in order to obtain the best possible deflection line without any changes in the shuttering geometry
- propose the required adjustments of the bridge bearing (e.g. after a settlement) to obtain the optimum deflection line (in spite of this settlement)
- suggest the minimum corrections to the shuttering geometry

At the end of the session, a new simulated deflection line is presented with the corrections used to obtain it (Fig. 2).

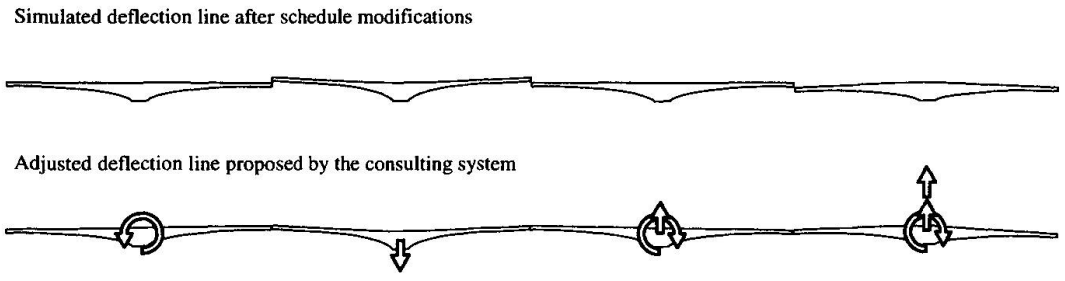

Fig. 2: Result of a consulting session

4 THE CONCRETE MODEL

As mentioned in section 3.2, the concrete model used in *Bridges* depends on the evolution of a set of microstructural and physical state parameters. The value of these parameters along the whole construction process is calculated by solving a set of coupled nonlinear and nonstationary differential equations [2] modelling temperature and humidity diffusion:

The energy (thermal) balance is expressed by:

$$C_{TH}\,\dot{H} + C_{TT}\,\dot{T} - C_{Ta}\,\dot{a} = \nabla(k_{TH}\,\nabla H + k_{TT}\,\nabla T) \tag{1}$$

The mass (hydrous) balance is given by:

$$C_{HH}\,\dot{H} + C_{HT}\,\dot{T} + (C_{Ha} + P)\,\dot{a} = \nabla(k_{HH}\,\nabla H + k_{HT}\,\nabla T) \tag{2}$$

The hydration rate is evaluated using:

$$\dot{a} = F_1\left(a, \tfrac{w}{c}\right) F_2(H) \exp\left(\frac{Q}{R}\left(\frac{1}{T_0} - \frac{1}{T}\right)\right) \tag{3}$$

where ∇ represents the gradient operator; a dot indicates differentiation with respect to time; C_{HH} and C_{TT} are the hydrous and thermal capacity; C_{Ta}, C_{Ha} and P are material parameters which depend essentially on the type of cement; a is the degree of hydration; k_{HH} and k_{TT} are the hydrous and thermal permeability coefficients; C_{TH}, C_{HT}, k_{TH} and k_{HT} are the coupling matrices. The function F_1 takes the influence of the degree of hydration and the concrete composition into consideration; F_2 describes the influence of pore humidity on the rate of hydration. The influence of the degree of hydration, temperature and relative humidity on the hydration rate is given by (3). The parameters of these equations are extensively discussed in the reference [1].

An average value for each state parameter is evaluated at each subsection for each event. For the longitudinal analysis, these parameters are integrated for determining the strains and stresses. Thus, the following contribution to the total strain rate can be described, with c_1, c_2 and c_3 representing known constant values:

$$\dot{\varepsilon}_{Total} = \dot{\varepsilon}_T + \dot{\varepsilon}_H + \dot{\varepsilon}_{CH} + \dot{\varepsilon}_{VE} \tag{4}$$

Thermal deformation: $\dot{\varepsilon}_T = c_1\,\dot{T}$ (5)

Hygral shrinkage: $\dot{\varepsilon}_H = c_2\,\dot{H}$ (6)

Chemical shrinkage: $\dot{\varepsilon}_{CH} = c_3\,\dot{M}$, if $M \leq 24$ *hours* (7)

$\dot{\varepsilon}_{CH} = 0$, if $M > 24$ *hours*

Viscoelastic deformation: $\dot{\varepsilon}_{VE} = \boldsymbol{C}^*\,\dot{\sigma}$ (8)

The shrinkage and thermal dilatancy rate are directly computed from the physical state parameters. The rate of elastic and creep strain are combined and related to the stress rate by means of specially developed constitutive relations $\boldsymbol{C}^*$ [1]. The stress evolution is then obtained by time integration.

5 A DESIGN TOOL

Most computer programs in the construction industry are dedicated to the structural safety (i.e. calculation of the ultimate load, simulation of the collapse mode, etc.). Today, however, a substantial and increasing amount of money is invested for maintaining and repairing poorly designed structures. These costs can be drastically reduced if more care is taken during the design phase. It has become increasingly apparent over the last decade that temperature effects due to the hydration of cement contribute substantially to the early-age cracking of

concrete. These cracks can result in a serious decrease of the load-bearing capacity of unreinforced concrete elements (e.g. breakwater blocks). They can also have a major impact on the serviceability and durability of reinforced concrete structures through a lack of watertightness and corrosion of the reinforcement, respectively. *Bridges* is capable of predicting the time-dependent temperature distributions due to the release of concrete hydration heat with a high degree of accuracy. The deformations are computed and the risk of cracks due to arbitrarily restrained volume changes is efficiently detected. As a result, damage cases can be studied and the effects of structural or technological measures for improving the structure (e.g. artificial cooling system) can be investigated. With the implemented concrete model, the temperature influence on the development of structural concrete properties can be predicted. When used during the planning of construction work, *Bridges* helps the designer make decisions for critical phases and determine the suitable times for prestressing and removal of formwork.

6 CONCLUSION

An early version of this program has been successfully used on the Størebælt West Bridge in Denmark [3][4][5]. It was used daily on site and exhibited a high degree of accuracy for the predicted girder deflections. *Bridges* is able to help the site engineer make decisions and suggest the required adjustments throughout the construction process. As a design tool, *Bridges* is a useful adviser to reduce both construction and maintenance costs, and thus to enhance the quality of the structure.

REFERENCES

[1] ROELFSTRA P.E., A numerical approach to investigate the properties of concrete – Numerical Concrete, Ph.D. thesis 788 EPF–Lausanne, 1989.

[2] ARGYRIS J.H., WARNKE E.P., WILLAM K.J., Berechnungen von Temperatur- und Feuchtefeldern in Massivbauten nach der Methode der Finiten Elemente, Deutscher Ausschuss für Stahlbeton, Heft 278, Berlin, 1977.

[3] SALET T.A.M., ROELFSTRA P.E., Computersimulaties op de bouwplaats. In: Civiele Techniek, nr. 2, 1993.

[4] VISSER J., BILDERBEEK D.W., SERLE J.P., Westelijke brug over Størebælt (I), ontwerp en prefabricage. In: Cement, nr. 12, 1990.

[5] VISSER J., SALET T.A.M., ROELFSTRA P.E., Temperatuurbeheersing van jong beton op basis van computermodellen. In: Cement, nr. 9, 1992.

Generalised Collapse Analysis Method for Concrete Bridge Assessment

Mécanismes d'écroulement pour l'évaluation des ponts en béton

Kollapsanalyse zur Beurteilung von Betonbrücken

Tim IBELL
Research Associate
University of Cambridge
Cambridge, United Kingdom

Tim Ibell completed his Ph.D. at Cambridge University in 1992. He worked as a team-leader on a petro-chemical plant erection project. He returned to Cambridge University in 1994 to work on non-flexural strength assessment of existing concrete bridges.

Campbell MIDDLETON
A/Director of Research
University of Cambridge
Cambridge, United Kingdom

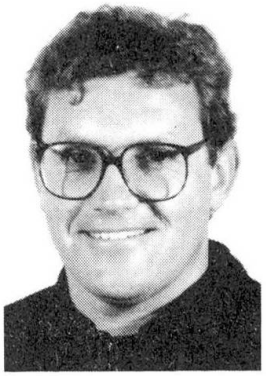

Campbell Middleton joined Cambridge Univ. in 1989 after 10 years in bridge and highway construction and design. He holds an M.Sc from Imperial College, London and a Ph.D. from Cambridge Univ. Research areas: bridge assessment methods, rationalisation of computer modelling techniques

SUMMARY

A generalised collapse analysis method for evaluating the ultimate load capacity of concrete bridge decks in flexure has been developed. By using computer graphics and solid-modelling concepts, many of the existing difficulties with plastic collapse and yield-line methods, which previously limited their application to simple slab and road configurations, have been overcome. In addition, work has progressed on incorporating a plasticity-based shear failure mechanism into the analysis. This additional module will generalise this concrete bridge assessment package still further.

RÉSUMÉ

Une méthode généralisée d'analyse des mécanismes de ruine a été développée dans le but d'évaluer la capacité de charge maximale des ponts en béton. Grâce à l'infographie, beaucoup de problèmes ayant trait à l'effondrement plastique et aux méthodes d'écoulement, problèmes qui jusqu'à alors avaient une application limitée à des simples configurations, ont été résolus. Par ailleurs, un mécanisme de rupture plastique par cisaillement a été introduit. Ce module supplémentaire permettra de généraliser l'application de ces programmes d'évaluation des ponts en béton.

ZUSAMMENFASSUNG

Eine verallgemeinerte Methode der Kollapsanalyse zur Abschätzung der maximalen Lastkapaziät von Betonbrücken unter Biegung wurde entwickelt. Durch Anwendung von Computergrafik konnten viele der bestehenden Schwierigkeiten im Zusammenhang mit plastischem Versagen und Grenztragfähigkeits-Theorien der Platten ausgeräumt werden. Darüber hinaus wurde die Analyse durch einen auf der Plastizitätstheorie basierenden Versagensmechanismus für Schubbelastung erweitert. Durch dieses zusätzliche Modul wird das Programmpaket zur Abschätzung der Lastkapazität von Betonbrücken weiter verallgemeinert.

1. BACKGROUND TO THE PROBLEM AND SOLUTION

1.1 The U.K. Bridge Assessment Programme

In the U.K., assessment of all bridges is being undertaken to check their strengths. With over 50,000 bridges, of which more than 9000 are concrete, this is indeed a major task. Preliminary estimates[1] suggest that around 35% of the concrete bridges will need strengthening or replacement, costing of the order of $1.2 billion.

1.2 The yield-line method as assessment tool

In order to assess this vast number of bridges, an automated, quick and accurate method of analysis is required. Unfortunately, up until recently, this goal has been elusive. The reason is that there are three main analysis techniques available to the engineer for assessing the strength of existing concrete bridges, all of which have limitations. The three methods are elastic, non-linear finite element and yield-line techniques. Elastic methods, although quick and in widespread use, are inherently conservative. This could have severe cost implications in such a large assessment programme. Non-linear finite element analysis is complicated and expensive. Further, it is excessively time-consuming. Yield-line analysis is tedious by hand and relies on the optimum failure geometry being known for the analysis to provide a safe result.

The work which has been conducted at Cambridge University over the past 5 years has been to develop a generalised flexural yield-line analysis package, called **COBRAS**, which overcomes the above disadvantages associated with yield-line analysis[2]. A concrete bridge may now be analysed by **COBRAS** and assessed for flexural load-carrying capacity within a couple of minutes.

2. THE GENERALISED COLLAPSE ANALYSIS METHOD

2.1 The basis of the method

Traditionally, automated yield-line analysis by computer has been carried out by programming the mathematical relationships amongst several variables and allowing the computer to optimise the solution in some way for one or more failure patterns. Complicated, but practical, failure patterns (such as fanning mechanisms) have been avoided due to the excessively complicated mathematical relationships which have had to be developed for each individual case.

The approach used here, however, has been to seek a general solution. It was recognised that any collapse mechanism can be reduced to what is fundamentally a problem of geometry. Using relatively recent developments in *computer graphics* and *solid modelling* theory, an analysis technique has been developed which can derive all the required geometrical relationships for the mechanisms, whilst incorporating features describing the component material properties and the applied loads. This is achieved as follows.

The bridge is considered to be made up in plan of polygonal areas, each one of which has associated attributes. These attributes, or features, would include a concrete layer, a dimension layer, steel reinforcement layers, loading layers, and so on. See Figure 1.

Having modelled the bridge in this way, these polygons may be *intersected* to provide a distinct 'patchwork' on the bridge of areas where all attributes are identical. Then, a 3-dimensional failure mechanism is applied to the model and the deformed shape of the structure is found. See figure 2. Contained within this new solid bridge model are full details of all the information necessary to describe the structural parameters of the material components and dimensions of the bridge, the external loading acting on the bridge, and the required geometric information needed for the collapse mechanism analysis using the work method. This includes the location of all the yieldlines, the details of fixity at each of the boundaries and the relative rotations between adjacent rigid plate elements of the failure

surface. Further details of this approach are presented in Reference 2.

By changing the position of some of the solid-model vertices, a rapid "step-like" iteration of the solid failure mode shape can be performed in a search for the critical global collapse mechanism with the lowest factor of safety.

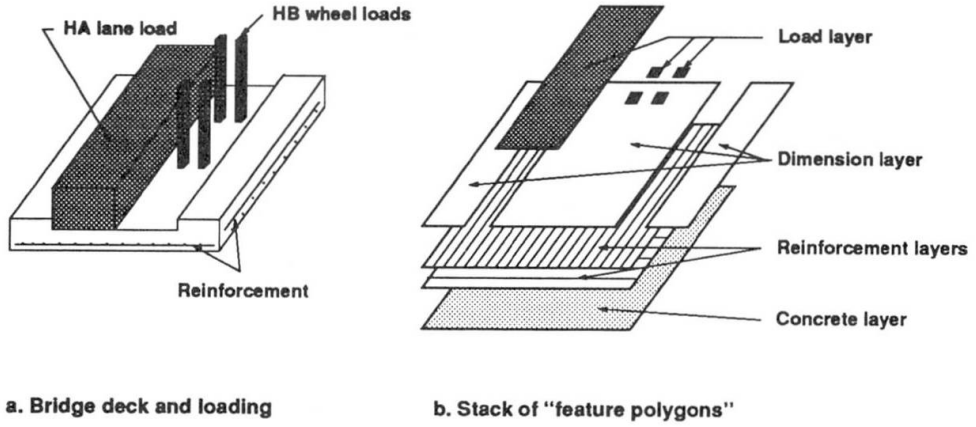

Figure 1: Bridge feature polygons

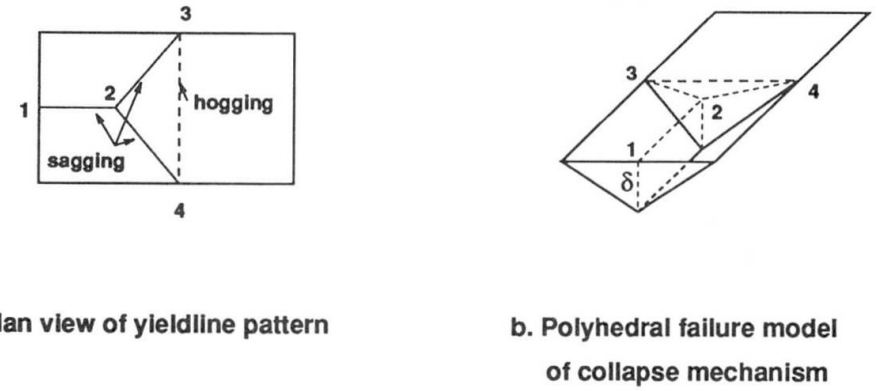

Figure 2: Modelling the failure mechanism

2.2 Other program features

The **COBRAS** program calculates the "theoretical" moment capacity of the actual section allowing for all the orientations, depths and types of reinforcement that cross the selected yieldline overcoming the need to adopt Johansen's stepped yield criterion and also avoiding any necessity to use the affinity theorems to account for orthotropic reinforcement layouts.

Since most code measures of ductility are related to the geometry and material components along the yieldlines of the structure, each of which is fully defined in the solid bridge model in the **COBRAS** program, the rotation capacity at all yieldline sections can be checked directly.

2.3 Testing of the **COBRAS** program

COBRAS has been tested against a wide variety of theoretical, numerical and test data. Details of these favourable correlations are to be found in Reference 2. It is noteworthy that

in comparison with theoretical textbook solutions, where simplifications for ease of hand-calculation have been made, more critical failure mechanisms than the 'critical' one assumed in the textbook, have been found[2].

3. SHEAR FAILURE MODEL

3.1 Justification for the model

The above yield-line analysis package is aimed at determination of the flexural failure capacity of existing concrete bridges. However, there exists the need to carry out checks on the shear capacity of concrete bridges for a full assessment. If the flexural check has been carried out by realistic yield-line analysis, then it is reasonable to use a similar approach for the shear analyses, lest conservative shear checks should condemn the bridge.

For this reason, it was decided to incorporate a shear checking module into **COBRAS**. This shear model is based on a plasticity approach, so that the actual collapse mechanism is modelled in a compatible manner with the flexural analysis.

3.2 Shear model details

Figure 3 shows a possible shear failure mechanism for a concrete beam, loaded by any P(x). A bi-linear yield-line is permitted to occur, with relative rotation between the two rigid blocks causing compressive and tensile yield-lines. Relative vertical and horizontal translation between the two rigid blocks also occurs. This model can therefore cover the range from pure flexure (relative translations are zero) to pure shear (relative rotation is zero) in the beam.

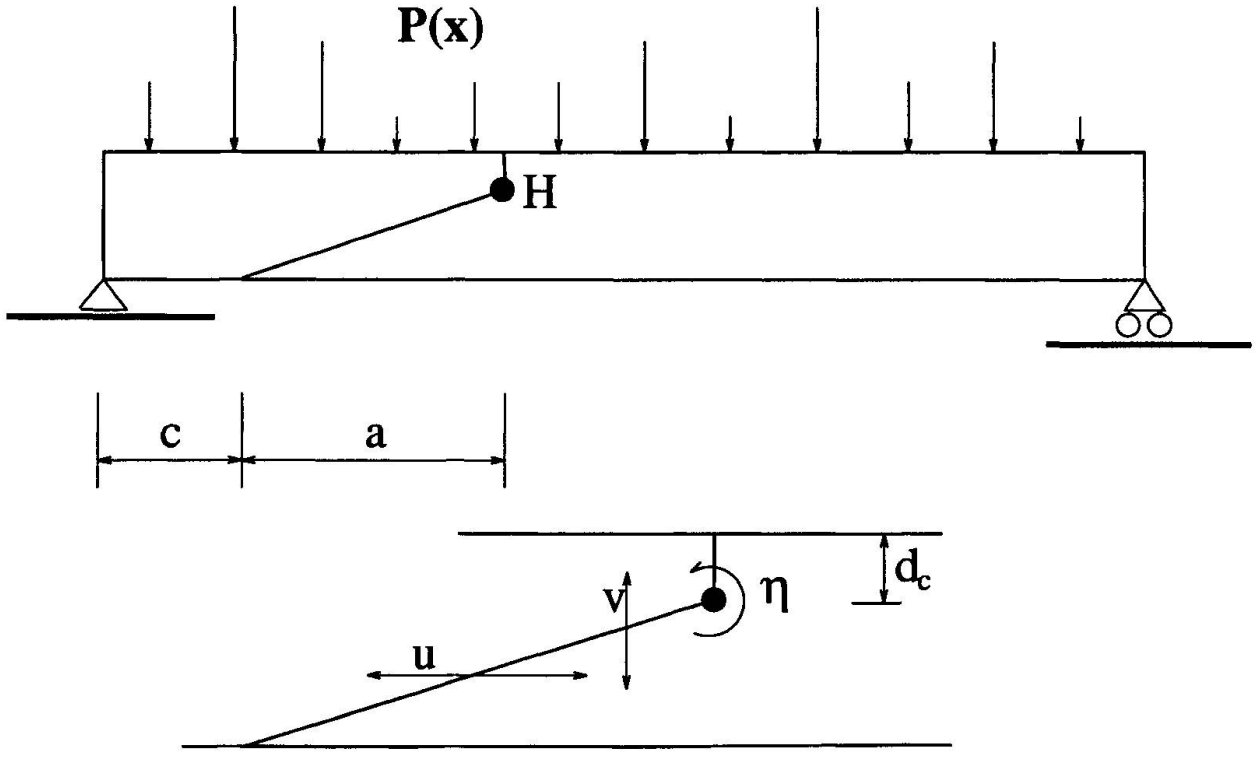

Figure 3: **Possible shear failure mechanisms for a beam under general loading.**

The variables which are to be optimised in each case are

1. The horizontal distance to the base of the inclined shear crack, c,
2. The horizontal length of the inclined crack, a,

3. The depth into the beam of the hinge, d_c,
4. The rotation applied to the hinge, η,
5. The relative vertical translation, v, and
6. The relative horizontal translation, u.

3.3 Internal energy dissipation

3.3.1 General dissipation formulation

It may easily be shown[3] that the energy dissipation rate per unit length in the concrete along a yield-line under generalised (compatible) motion between two rigid blocks is given by

$$\dot{D} = \frac{1}{2} f_c \delta (1 - \sin \alpha) \tag{1}$$

in the range $0 \leq \alpha \leq 2\pi$, where f_c is the *effective* compressive strength of concrete, δ is the instantaneous relative displacement between the two rigid blocks and α is the angle that this displacement vector makes with the yield-line. Note that the tensile strength of concrete is considered negligible in this particular case.

Where steel bars cross a line of discontinuity, the internal energy dissipated in the steel (which is assumed to be yielding), W_s, is given by

$$W_s = A_s f_y \delta |\cos(\alpha - \gamma)| \tag{2}$$

where A_s is the area of steel crossing the yield-line, f_y is the yield strength of the steel and γ is the angle the steel makes with the yield-line.

3.3.2 Energy dissipation in the concrete

Let us consider the yield-line portion above the hinge point, H, in Figure 3. The combined relative displacement vector, δ, will vary along the length of this yield-line, as will the angle it makes with the yield-line, α. As an illustration of how the calculations would be carried out, consider a point half-way along this yield-line (that is, a point $d_c/2$ in depth into the beam). At this point, the horizontal displacement vector has magnitude $(\frac{1}{2} d_c \eta + u)$ and the vertical displacement vector is v. The relative displacement vector, δ, is

$$\delta = \sqrt{(\frac{1}{2} d_c \eta + u)^2 + v^2} \tag{3}$$

at an angle to the yield-line of

$$\alpha = \arctan\left(\frac{\frac{1}{2} d_c \eta + u}{v}\right). \tag{4}$$

The instantaneous energy dissipation, $\dot{E}_c$, at this point is then

$$\dot{E}_c = \frac{1}{2} b \delta (1 - \sin \alpha). \tag{5}$$

The total energy dissipation in the concrete along this yield-line will then be given by

$$E_c = \int_0^{d_c} \dot{E}_c dx. \tag{6}$$

In order to carry out this integration, Simpson's Rule with four intervals is used for each line.

In order to calculate the energy dissipation in the concrete along the tensile (sloping) yield-line, a similar approach is used.

3.3.3 Energy dissipation in the steel

All steel will undergo stretching due to the three relative displacements occurring. Energy in the longitudinal (flexural) steel will be dissipated as follows.

$$E_s = \sum_{i=1}^{ns} A_s f_y |d_i - d_c| \eta \; + \; \sum_{i=1}^{ns} A_s f_y u \tag{7}$$

where ns is the number of flexural steel bars crossing the yield-line and d_i is the depth from the top surface to the steel bar.

Where steel shear stirrups are present, additional energy E_{ss} will be dissipated, calculated in a similar way.

The final energy dissipation in the system is then found to be

$$ED = E_c + E_s + E_{ss}. \tag{8}$$

3.3.3 External work done by the loads

The external work done by the loads is calculated based upon the vertical distances through which the various loads on the bridge move. This is easily calculated as

$$WD = \int_0^\ell P(x) w(x) dx \tag{9}$$

where $w(x)$ is the variation along the beam in notional displacement, as defined by the particular combination of variables specified above.

3.4 Comments on the shear analysis

This shear analysis method is presently being implemented into the **COBRAS** package. Included in the features are provisions for the curtailment of reinforcing bars and multiple beam-and-slab portions failing in a single mechanism.

Comparisons with existing test data for simple beams have been promising. Generally, the correct failure type (pure or flexural shear) is predicted. However, the quantitative predictions for shear capacity are (as usual in plasticity theory) heavily dependent on the 'effectiveness factor' chosen for the strength of the concrete. This calibration work continues at present.

4. CONCLUSIONS

A new generalized collapse mechanism analysis method for evaluating the *ultimate strength* of concrete bridges has been developed. Computer graphics and solid modelling techniques have been employed to overcome many of the existing difficulties with traditional yieldline theory.

This program provides a means by which researchers, designers and highway authorities can more effectively assess the strength of concrete bridges under the influence of overload and/or deterioration of the material components.

More recently, the problem of shear failure in beam-and-slab bridges has been addressed by considering a plasticity-based shear failure mechanism for a concrete bridge. The model has been preliminarily shown to be suitable for such analysis, although work on its implementation continues.

REFERENCES

1. DEPARTMENT OF TRANSPORT. The assessment of highway bridges and structures. Bridge census and sample survey. London, January, 1987.
2. MIDDLETON C.R., Application of new analysis techniques to the strength and safety assessment of existing concrete bridges. University of Cambridge. January 1994.
3. NIELSEN M.P., Limit analysis and concrete plasticity. Prentice-Hall, USA. 1984.

Evaluation of a Bridge Using Simplified Finite Element Modelling

Evalutation des ponts à l'aide d'un modèle simplifié par éléments finis

Evaluation von Brücken durch vereinfachte FE-Modellierung

Charles R. FARRAR
Team Leader
Los Alamos National Laboratory
Los Alamos, NV, USA

Charles Farrar obtained his Ph.D. in Civil Engineering from the University of New Mexico, Albuquerque, NM, in 1988. For the past 10 years, he has been involved in the static and dynamic testing and analysis of civil engineering structures.

Thomas A. DUFFEY
Visiting Professor
New Mexico Highlands University
Las Vegas, NV, USA

Thomas Duffey received his Ph.D. in Civil Engineering from the University of New Mexico, Albuquerque, NM, in 1974. For the past 29 years he has primarily been involved in the experimental, theoretical and numerical study of dynamic structural response.

SUMMARY

An experimental-numerical comparison of the forced and ambient vibrations of a multi-span composite plate-girder bridge was performed. The bridge was modelled using a finite element program at three levels of complexity, including a simple 250 degrees-of-freedom model that utilises a single beam element to represent the entire bridge cross section. Difficulties encountered in the development of the simple model are discussed. The dynamic properties predicted by the simple model were consistent with those measured on the bridge and computed using more detailed finite element models.

RÉSUMÉ

Une comparaison expérimentale et de type numérique sur les vibrations forcées et naturelles d'un pont-poutre composite à plusieurs travées a été effectué. Un programme d'élé-ments finis à trois niveaux de complexité, et un modèle simple à 250 degrés de liberté ne comprenant qu'une seule poutre comme élément pour représenter la coupe transversale du pont ont été réalisés. Les difficultés rencontrées lors du développement du modèle simplifié sont commentées. Les propriétés dynamiques prédites par le modèle simplifié se sont avérées concorder avec les propriétés mesurées sur le pont et calculées en utili-sant des modèles d'éléments finis plus détaillés.

ZUSAMMENFASSUNG

Ein experimentell-numerischer Vergleich der gezwungenen und natürlichen Schwingungen einer Plattenbalkenbrücke wurde durchgeführt. Die Brücke wurde durch ein FE-Programm auf drei Komplexitätsniveaus modelliert, insbesondere als ein einfaches Modell mit 250 Freiheitsgraden, welches einen einzelnen Balken benutzt. Die Schwierigkeiten bei der Entwicklung des einfachen Modells werden beschrieben. Die vorhergesagten dynamischen Eigenschaften stimmten sowohl mit den Messungen auf der Brücke als auch mit der Berechnung eines komplexeren FE-Modells überein.

1. INTRODUCTION

In the 1960's and 1970's over 2500 bridges were built in the U.S. with a design similar to those on Interstate 40 over the Rio Grande in Albuquerque, New Mexico, Fig. 1. Because the bridges over the Rio Grande were to be razed during the summer of 1993, the investigators were able to perform extensive dynamic testing on the bridges using both ambient and forced vibration techniques. This paper summarizes the numerical models of the bridge and compares results obtained with these models to the measured dynamic properties of the bridge. A primary purpose of the work reported herein is to determine if a very simple beam element representation of the bridge could be developed that would accurately predict the global dynamic response of the bridge. Such models would be very useful for designers because they would provide a simplified PC-based computational tool with which to examine the dynamic response of the bridges to a wide variety of load conditions. First, a brief description of the bridge and summary of experimental results is presented, followed by a summary of numerical calculations and correlations with experimental results.

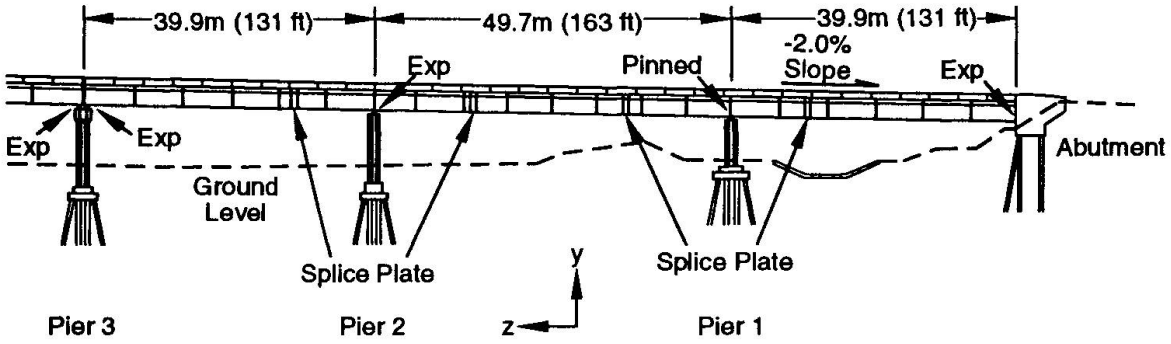

Fig. 1. I-40 Bridge Over The Rio Grande

2. DESCRIPTION OF THE I-40 BRIDGES

The existing I-40 bridge over the Rio Grande consists of twin spans made up of a concrete deck supported by two welded-steel plate girders and three steel stringers, Fig. 2. Each bridge is made up of three identical sections. All testing was performed on a single, three-span section.

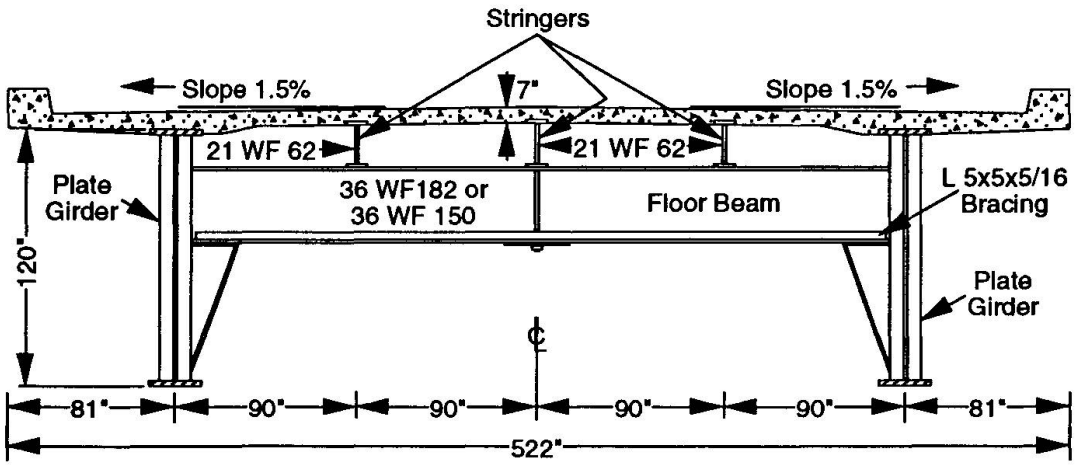

Fig. 2. I-40 Bridge Cross- Section

Drawing not to scale
1 in. = 2.54 cm

3. SUMMARY OF EXPERIMENTAL RESULTS

3.1 Ambient Vibration Testing

Ambient (traffic) vibration tests were conducted to identify the structure's resonant frequencies, modal damping, and the corresponding mode shapes. Testing was performed both with and without traffic on the tested section of the bridge. In the latter case, excitation was induced by traffic on the adjacent bridge transmitted through the ground. To circumvent the drawbacks of the methods used in previous ambient vibration tests [1], an ambient vibration system identification method [2] was applied to the measured response data. Ambient vibration from traffic was found to provide an adequate source of input for identifying the dynamic properties of the bridge. Integrated circuit piezoelectric accelerometers were used for vibration measurements. The data acquisition system, consisting of 29 input modules and a signal processing module, is described elsewhere [3].

3.2 Forced Vibration Testing

A series of forced vibration tests was conducted on the same bridge section using a hydraulic actuator and large reaction mass. Traffic was removed from the bridge during testing. A random signal generator was used to produce a uniform random signal. Force input to the bridge was determined using an accelerometer mounted on the reaction mass. The level of excitation during the forced test was on the same order as provided by direct traffic ambient excitation. All instrumentation used for the forced vibration test was identical to that used for the ambient vibration tests.

3.3 Data Reduction

Resonant frequencies, mode shapes, and modal damping values were determined by fitting analytical models to the measured frequency response function data using a commercial curve fitting algorithm. Dynamic properties measured during the forced vibration test fall within the range of those measured during the various ambient vibration tests.

4. DETAILED FINITE ELEMENT ANALYSIS

Two detailed finite element models of the bridge were developed. The first model utilizes eight-node shell elements to model the web of the plate girder and the concrete deck. Three-node beam elements were used to model the stringers, floor beam, and flanges of the plate girder. Twenty-node continuum elements were used to model the concrete piers. This model had approximately 4500 degrees of freedom describing the bridge structure above the pier. Fixed boundary conditions were specified at the base of the piers. No attempt was made to model the soil medium underneath these piers.

A second more detailed model was constructed, similar to the first, but with a more refined mesh. This more detailed model uses approximately 25,000 degrees of freedom to model the bridge deck and supporting steel structure. Comparisons of modal analyses for the 25,000 and 4,500 degree-of-freedom models revealed almost identical dynamic properties, indicating convergence.

5. SIMPLIFIED FINITE ELEMENT MODEL

When compared with experimental results (subsequently discussed), it is evident that the detailed finite element models of the I-40 Bridge described in the previous section provide an accurate model for calculating the dynamic response of the bridge. However, the detailed models suffer from complexity and size, as structural elements are intricately modeled using shell elements. A

more simplified and practical model using a single beam element to represent the cross-section of the bridge would be desirable. However, certain confounding factors make the representation of the bridge by simple beam elements somewhat difficult. These factors include the composite (steel and concrete) nature of the bridge construction, the presence of but a single axis of symmetry in the cross section, and the dynamic nature of the bridge response. Implications of the above factors are that some flexural and torsional modes of response will be coupled[4] and that determination of the shear center and the torsional constant of a non-circular composite cross section will be required.

The ABAQUS Finite Element Program [5] was selected for both the refined shell element models of the I-40 Bridge as well as for the simplified beam element model. The program is representative of a class of high quality general purpose finite element packages commercially available to the technical community. Therefore, the development which follows regarding consistent input for the simplified beam model is representative of the input considerations needed for most other finite element software packages as well.

5.1 Modeling Flexural Behavior

The cross-section of the I-40 bridge shown in Fig. 2 has been idealized as consisting of the following components: A concrete slab of constant thickness with a cross-sectional area equivalent to that of the actual slab shown in Fig. 2; two steel plate girders; and three steel stringers. The procedures for representing the composite bridge cross section as a simple beam for the purpose of calculating the dynamic flexural response of the beam are based on well known methods for transformation of a composite cross section into an equivalent single material [6]. An equivalent mass density of the bridge is then determined such that the transformed section will have the same mass per unit length as the original section.

5.2 Modeling Torsional Behavior

The I-40 Bridge cross section is composed of steel and concrete members. It can be shown that the total torsional stiffness of the n individual members are

$$\frac{T}{\theta} = \sum_{i=1}^{n} G_i J_i , \qquad (1)$$

where G_i and J_i are the shear modulus and torsional constant for the i^{th} material. Individual torsional constants are determined using handbook values or well-known formulas for rectangular sections.

5.3 Shear Center Location

The general problem of non-uniform torsion of open, thin-walled members composed of any number of different materials is addressed in [7]. Unfortunately, application of the method to the I-40 bridge cross section was not straight forward. Instead, the shear center for the I-40 bridge was located numerically using the ABAQUS shell model described in Section 4. The procedure used is to apply a static force to the bridge cross section using effectively a rigid link offset from the center of the concrete slab by a distance e. By calculating the rotation of the cross section about the z-axis for two different values of e, an extrapolation was made to determine the value of e that results in no net rotation of the cross section.

5.4 Modeling the Mass Distribution

For the torsional portion of the coupled beam response to be correct, the generalized torsional mass must be input properly. This implies that the mass polar moment of inertia about the center of mass must be correct. The area polar moment of inertia. I_p, in ABAQUS is internally computed from the user-supplied area moments of inertia. The quantity $\mu L I_p$, where L is the length of the beam, then provides the generalized torsional mass necessary to correctly model the torsional vibration response. A confounding factor is the area moments of inertia are input about the centroid of the cross section which, in general, is not coincident with the center of mass.

The procedure utilized is to calculate the center of mass of the composite steel/concrete beam cross section, determine the polar moments of inertia about the center of mass for both steel and concrete components in the cross section and then use the following equation to determine an equivalent mass density, μ_{eq}, for torsional vibrations,

$$\mu_{eq} = \frac{\mu_c I_{pc} + \mu_s I_{ps}}{I_{11} + I_{22}}, \tag{2}$$

where I_{11} and I_{22} are the moments of inertia supplied to ABAQUS, μ_S is the mass density of the steel, μ_C is the mass density of concrete, I_{ps} is the polar area moment of inertia of the steel cross section about the center of mass, and I_{pc} is the polar area moment of inertia of the concrete cross section about the center of mass. Finally, the area of the equivalent beam is specified such that the mass density given by Eq. 2 produces the correct mass per unit length of bridge cross-section to model torsional and flexural behavior. Specifying the area in this manner will produce errors in the axial response of the beam, but such response is unimportant for the I-40 Bridge.

6. RESULTS AND CONCLUSIONS

Results of the finite element analyses are compared to experimental results in terms of resonant frequencies and mode shapes in Table I.

TABLE I

Comparison of Analytical and Experimental Modal Analysis Results

		Resonant Frequency (Hz)		
	Mode Type	Experimental	Detailed FEM	Simplified FEM
Mode 1	Bending	2.48	2.59	2.85
Mode 2	Torsion	2.96	2.78	3.01
Mode 3	Bending	3.50	3.71	4.28
Mode 4	Bending	4.08	4.32	5.55
Mode 5	Torsion	4.17	3.96	4.56
Mode 6	Torsion	4.63	4.50	5.11
Ave. % Diff. from experimental		--	5.08%	15.8%

Examination of the mode shapes predicted by both the detailed and simplified finite element models shows that the measured mode shapes are being accurately predicted by both numerical simulations. The detailed model accurately predicts the measured resonant frequencies with an average percent difference of 5.08% from the measured values. The larger discrepancy between the measured resonant frequencies and those calculated by the simplified model are attributed to the inability to model three dimensional features such as cross beams and the plate girder - pier supports.

The major contribution of this study is a simple 250 DOF model that uses a single beam element to represent the entire bridge cross-section. This model required the development of a method for analyzing the torsional response of an open thin-walled cross-sectional of two materials. Because the finite element code used does not allow the polar area moment of inertia to be specified explicitly, methods of calculating an equivalent mass density and cross-section area had to be developed to accurately model both the flexural and torsional response. Because of the limited numbers of DOFs, this type of model can be exercised extensively on a PC (typical of the computing environment at most smaller consulting engineering firms) to study the response of the bridge to time-varying inputs such as seismic or wind loading. The mode shapes predicted by this simple model were consistent with those measured on the bridge. Resonant frequencies, however, show more error because of the inability to model certain three dimensional effects associated with the supports and with out-of-plane structural members. Further refinements to simplify the modeling of these three dimensional effects are needed. The location of the shear center and specification of cross-section warping properties are important input parameters for modeling the dynamic response of a cross-section where the centroid, center of mass, and shear center are not coincident, hence further work is needed to develop a simple method for approximating these properties. Work in both these areas is currently being pursued at Los Alamos National Laboratory.

7. ACKNOWLEDGMENTS

The authors acknowledge the cooperation of all parties involved in the I-40 bridge project including engineers from Sandia National Laboratory; faculty, technicians and students from New Mexico State University; faculty from Texas A&M University, personnel of the New Mexico State Highway and Transportation Department; and the staff at the Alliance for Transportation Research.

REFERENCES

1. ABDEL-GHAFFAR, A. M. and G. W. HOUSNER, "Ambient Vibration Tests of Suspension Bridge," ASCE Journal of the Engineering Mechanics Division, **104**, 1978, pp. 983-999.

2. JAMES, G. H., T. G. CARNE, and J. P. LAUFFER "The Natural Excitation Technique (NExT) for Modal Parameter Extraction From Operating Wind Turbines," Sandia National Laboratory report SAND92-1666, 1993.

3. FARRAR, C. R., et al., "Dynamic Characterization and Damage Detection in the I-40 Bridge over the Rio Grande," Los Alamos National Laboratory report LA-12767-MS, 1994.

4. GERE, J. M., "Torsional Vibrations of Beams of Thin-Walled Open Section," Journal of Applied Mechanics, 1954, pp. 381-387.

5. ABAQUS User's Manual, Hibbitt, Karlsson and Sorensen, Inc., Providence RI, 1989.

6. POPOV, E. P., *Introduction to Mechanics of Solids*, Prentice-Hall, Inc., Englewood Cliffs, NJ., 1968.

7 MCMANUS, P. F., and C. G. CULVER, "Nonuniform Torsion of Composite Beams," Journal of the Structural Division, ASCE, **95**, 1969, pp. 1233-1256.

Updating of Existing Structures' Models Based on Modal Testing

Optimalisation de modèles de structure basée sur des essais modaux

Optimierung von Tragwerksmodellen auf der Basis von modalen Versuchen

Reto CANTIENI
Dr. sc. techn.
EMPA
Dübendorf, Switzerland

Stanislaw PIETRZKO
Dr. sc. techn.
EMPA
Dübendorf, Switzerland

Yasar DEGER
Dr. sc. techn.
EMPA
Dübendorf, Switzerland

SUMMARY

Strengthening or rehabilitation of existing structures are common tasks of the civil engineer today. Successful planning of the related work has to be based on a sound knowledge of the structure's actual properties. First, a modern method combining analytical and experimental investigations is described. A preliminary Finite Element Model is updated based on the results of Modal Testing. This updated model can be assumed to be as close to reality as possible. Two examples of the method's application are then discussed: Investigation of the effects of strengthening measures for the bridge on the Aare River at Aarburg and the Westend Bridge, Berlin.

RÉSUMÉ

Le renforcement et l'assainissement des ouvrages d'art font aujourd'hui partie des tâches courantes de l'ingénieur civil. Le succès de la planification des travaux exige une connaissance approfondie des caractéristiques actuelles de l'ouvrage. L'article décrit une méthode moderne qui associe les résultats d'études analytiques et expérimentales: optimalisation d'un modèle de structure porteuse obtenu par la méthode des éléments finis au moyen des résultats d'une analyse modale expérimentale. Cette méthode est illustré à l'aide de deux exemples: ponts sur l'Aar à Aarburg et de Westend à Berlin.

ZUSAMMENFASSUNG

Verstärkung und Sanierung von Bauwerken gehören heute zu den täglichen Aufgaben des Bauingenieurs. Um diese Aufgabe zweckmäßig lösen zu können, muss ein möglichst wirklichkeitsnahes Bauwerksmodell erarbeitet werden. Zunächst wird eine moderne Methode beschrieben, die zu diesem Zweck die Resultate analytischer und experimenteller Untersuchungen kombiniert: Optimierung eines Finite Element Modells des Tragwerkes aufgrund der Resultate einer experimentellen Modalanalyse. Die Anwendung der Methode wird dann anhand zweier Beispiele illustriert: Untersuchung der Auswirkung von Verstärkungen der Aarebrücke Aarburg und der Westend-Brücke Berlin.

1. INTRODUCTION

Establishing a proper model of an existing structure is not always an easy task. Drawings and design calculations may no longer exist, the actual static and kinematic boundary conditions as well as the effective structural mass and stiffness may be uncertain. However, the first step of the method to determine a realistic structural model described in this paper is always generating of a preliminary Finite Element (FE) model based on all the information available. As a second step, a modal test is performed on the structure. The results of this modal test are then used to update the preliminary FE model. This updating procedure (also referred to as LINK) yields an FE model being as close to reality as possible. Within the boundaries of linearity, this model can then be used to perform analytical studies of any type like e.g. determining of the structural response to a static or dynamic input function or, as will be the case here, to calculate the effects of possible strengthening or rehabilitation measures.

2. MODAL TESTING

2.1 General

Modal Testing means determination of a structure's modal parameters, e.g. natural frequencies as well as associated mode shapes and damping coefficients, from its Frequency Response Matrix. This matrix is derived from tests where the structure's response to controlled dynamic excitation is measured. The time signals simultaneously acquired for input force $x_i(t)$ and response $y_k(t)$ are transformed into the frequency spectra $x_i(\omega)$ and $y_k(\omega)$ by applying the Fast Fourier Transformation. From this, the Frequency Response Function (FRF) between points i and k, $H_{ik}(i\omega)$, and the Frequency Response Matrix $H(i\omega)$ for the whole structure can be determined.

Two items are important here:

- The larger the number of response measurement points the better the information on the structure's modal parameters especially the mode shapes.
- Dealing with linear structures means that $H(i\omega)$ is symmetric to its diagonal. This is of considerable practical importance because it is then possible to keep the point of excitation k constant and to hover the measurement points i over the structure.

2.2 Excitation

From the several possibilities to efficiently excite a structure like a bridge, bandlimited burst random excitation making use of a servohydraulic actuator has proven to be the most suitable one. Impulse-type excitation using some hammer-like instrument may be much cheaper to apply but experience shows that the quality of the results is not sufficient for large structures. Narrow-band excitation using e.g. mechanical actuators with unbalanced masses is very time-consuming since only one frequency can be investigated at a time.

The heart of the servohydraulic actuator used in the tests described later is a 10 kN cylinder with a 100 mm stroke. A 500 kg mass is fixed to the tip of its piston rod so that the cylinder produces a maximum force amplitude of 5 kN. To drive the cylinder a suitable electronic circuitry, an air-cooled hydraulic power pack (40 l/min, 280 bar) and a diesel generator (45 kW) are necessary. The driving signal is provided by the Modal Analysis System described later on. To allow measurement of the force introduced into the structure the actuator is placed on three load cells (Fig. 1).

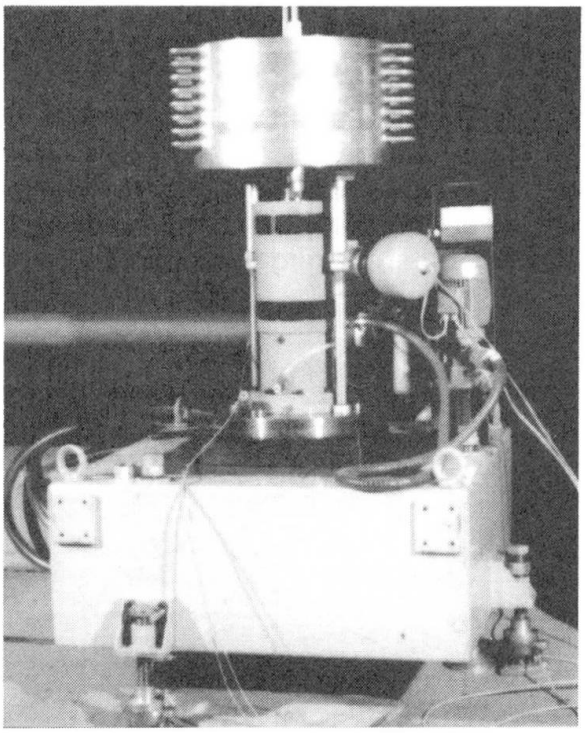

Fig. 1 The vibration generator.

2.3 Response Measurement

The standard instruments used with Modal Testing at EMPA are accelerometers Brüel & Kjær 8306. These have a measurement range of ±1 g, a sensitivity of 10 V/g and a resolution of 10^{-6} m/s^2. Usually, the structural response is determined in every measurement point in three directions. Hence, three of these accelerometers are orthogonally fixed to a supporting device. Stiffness of the connection between structure and transducers is ensured by firmly screwing the supports to the bridge pavement or concrete. Depending on the equipment and time available, EMPA uses two to four of these three-dimensional set-ups simultaneously. Testing of a bridge typically requires five to ten minutes per measurement cycle or up to two working days for 150 to 250 measurement points.

2.4 Signal Acquisition and Processing

The measured force and acceleration signals are passed through a front end where they are filtered, amplified and digitized. Signal processing requires a computer and Modal Analysis software packages. The time signals are first transformed into the frequency domain. All Frequency Response Functions response/force are then calculated, averaged over a reasonable number of FRF's and stored on hard disk. Depending on the quality of the signals acquired, "reasonable" may be a number between 5 and 15.

Calculation of the modal parameters from the FRF's is the second processing step. Determination, or, as the process is of an iterative and therefore not of a mathematically exact nature, estimation of the modal parameters is a two-stage procedure. With the CADA-X software package used by EMPA pole values (damped natural frequencies, damping ratios) and modal participation factors are firstly calculated using the Least Squares Complex Exponential Algorithm. In the second stage the modal vectors or mode shapes are calculated using the Least Squares Frequency Domain Technique.

3. FINITE ELEMENT MODELING, MODEL UPDATING

Application of the LMS Link model updating software based on CADA-X modal test results is possible for MSC/NASTRAN FE-models only. To later allow model updating, the modal test measurement point grid has to be a sub-quantity of the grid used for the FE-model. The crucial part of the Link-software is the Sensitivity Analysis routine which gives indications where mass and/or structural stiffness should be changed to optimally adapt the FE-model to the experimental results. However, the engineer can fortunately enough not be fully replaced by the computer: His judgement is very much sought after here. The result of the updating efforts is presented graphically in form of the so-called MAC-Matrix (Modal Assurance Criterion).

4. EXAMPLES

4.1 Bridge on the Aare River at Aarburg

The Bridge on the Aare River at Aarburg was built by Robert Maillart in 1911/12. It consists of a clamped-in concrete arch with a 72 m span, a bridge deck and originally a significant number of columns between the two. The latter two elements mentioned having been subject to severe deterioration, they were removed and replaced by a prestressed concrete bridge deck slab with two longitudinal main girders but without any columns between deck and arch in 1969 (Fig. 2).

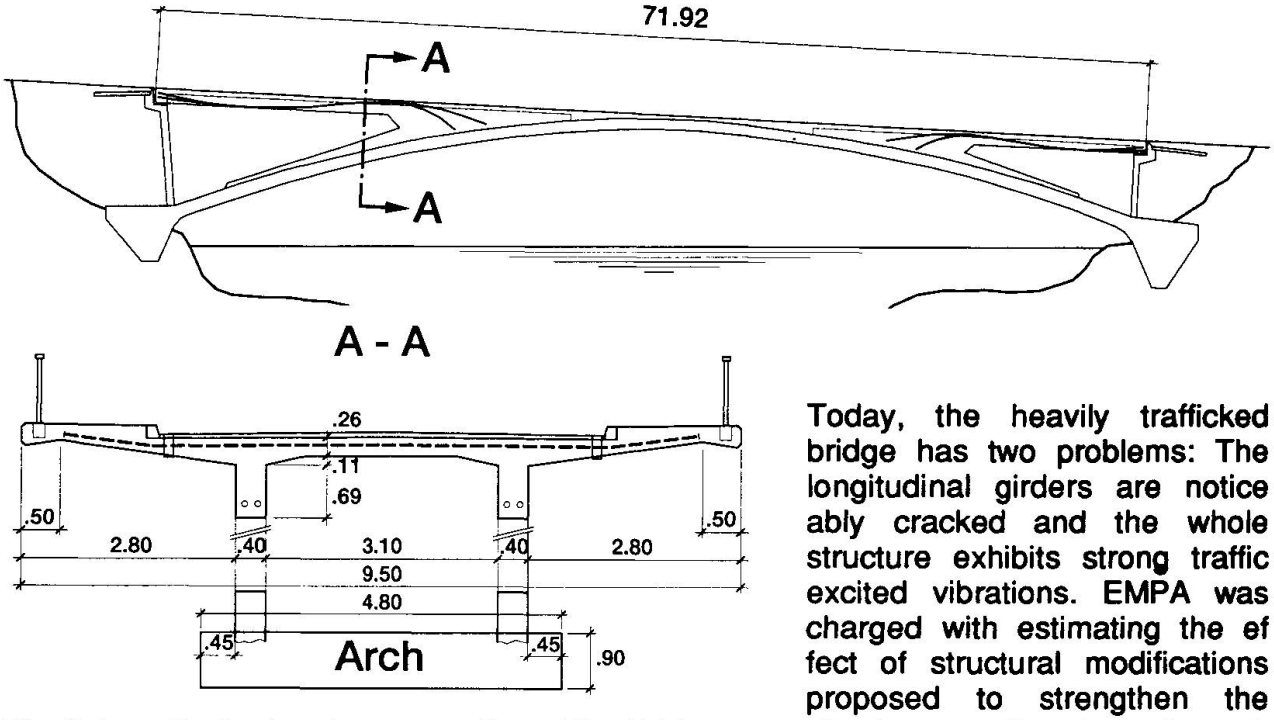

Fig. 2 Longitudinal and cross section of the Bridge on the Aare River at Aarburg (dimensions in m).

Today, the heavily trafficked bridge has two problems: The longitudinal girders are noticeably cracked and the whole structure exhibits strong traffic excited vibrations. EMPA was charged with estimating the effect of structural modifications proposed to strengthen the structure on the dynamic and, subsequently also on the static bridge behavior.

A modal test was performed on the bridge in April 1992. The structure was excited using the abovementioned servohydraulic vibration generator. The bridge response was acquired in a total of 142 measurement points in three directions each, 106 and 36 of them distributed over the bridge deck and arch respectively. The initial FE-model of the bridge consisted of roughly 200 CQUAD4 quadrilateral plate elements. It was refined after having performed the modal test finally consisted of 304 plate and beam elements. Figure 3 gives the comparison of frequency and mode shape as determined experimentally and analytically for the first three of the total of seven natural vibrations identified in the range f = 3...9 Hz. Coincidence can be described as being good.

Subsequent investigations using the updated FE-model showed that strengthening of the longitudinal bridge deck girders solves the static problems. The dynamic problem of shifting the fundamental frequencies out of the critical range of heavy vehicles dynamic wheel loads, $f \approx 3$ Hz, can however be achieved through fixing of the horizontal longitudinal mobility of the bridge at one bridge deck abutment only. This suppresses the first two natural modes of the bridge and yields a fundamental frequency of f = 4.54 Hz. Studies are now performed to develop shock absorbers suppressing the vibrations but ensuring the mobility for longterm deformations due to e.g. temperature effects.

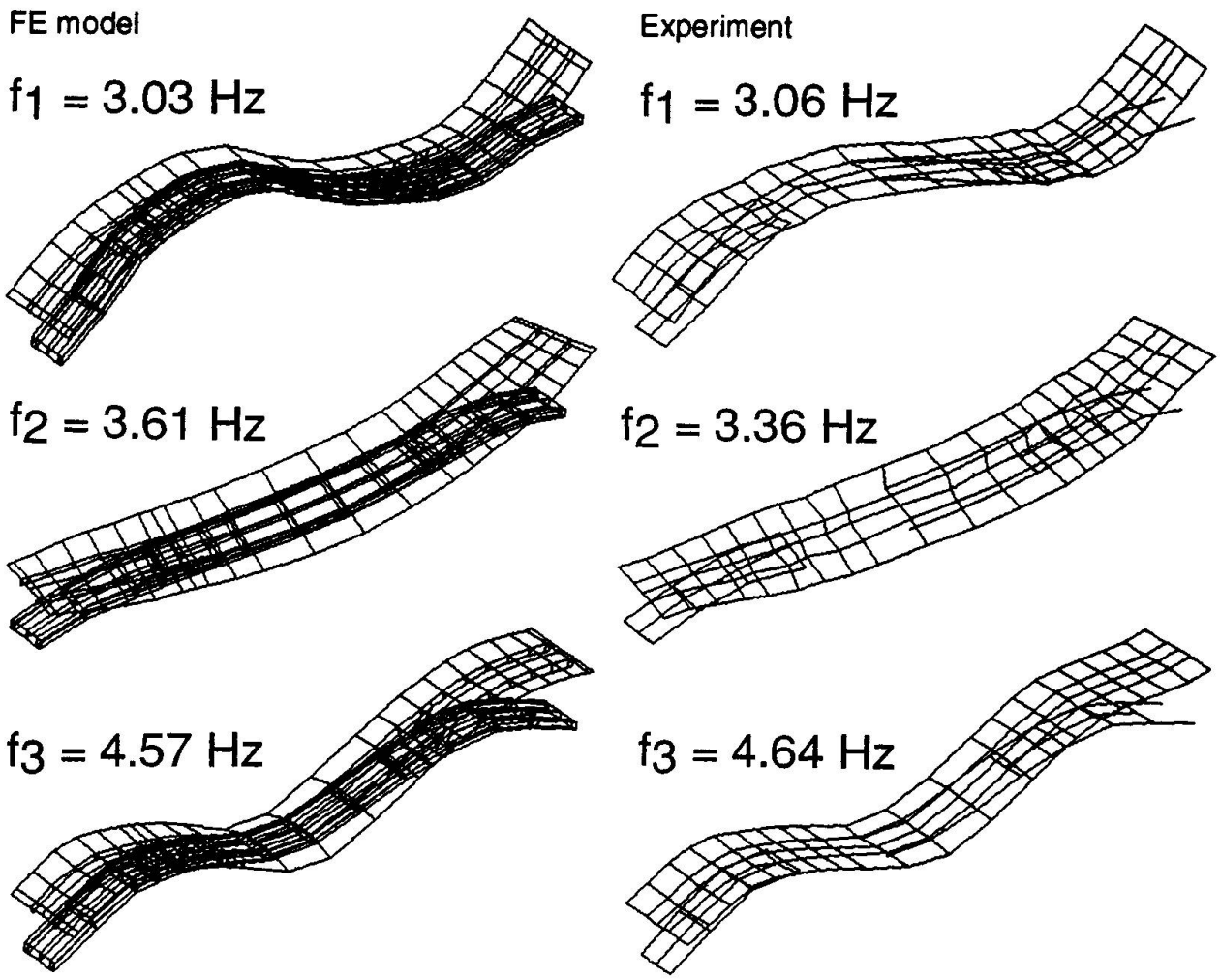

Fig. 3: Aare Bridge: Frequencies and mode shapes: Updated FE-model vs. experiment.

4.2 Westend Bridge Berlin

The Westend Bridge is a part of the Berlin City Highway Belt where it connects downtown Berlin and Tegel Airport. This 242 m long and roughly 30 years old bridge is a prestressed concrete girder continuous over eight spans with lengths between 5 m and 38 m. The cross section is a 14 m wide three-cell box. The bridge is exposed to relatively dense heavy commercial traffic and does no longer match today's requirements. It has therefore been strengthened by means of of longitudinal prestressed steel plates being added externally to the box girder bottom flange in 1993. To assess the effectiveness of the structural modifications, two test series have been planned, one before and one after strengthening. This report covers the test performed in autumn 1993. The project is a joint venture encompassing EMPA and BAM (Bundesamt für Materialprüfung- und -Forschung, Berlin, Germany) and is also financially supported by the Berlin Senate.

The modal test measurement point grid consisted of 215 points on the bridge deck and 18 points on piers and abutment walls. The modal test's results were not of same high quality as for the Aare Bridge. This is on the one hand due to the vibraton generator's energy being limited for $f < 2$ Hz, on the other hand to the relatively short middle span which cuts the bridge into two dynamically rather weakly coupled parts and makes it hence very difficult to identify all bridge modes with using one exciter only. Attempts will be made to use two shakers simultaneously for the second test in 1995 (Multiple Input Method).

The FE-model of the bridge was built up from 1000 CQUAD4 quadrilateral plate elements and 28 CBEAM beam elements (Fig. 4). Comparison of the experimental and analytical results is given in Figure 5 for the first four of the total of 25 identified modes between f = 1.7 Hz and f = 16 Hz.

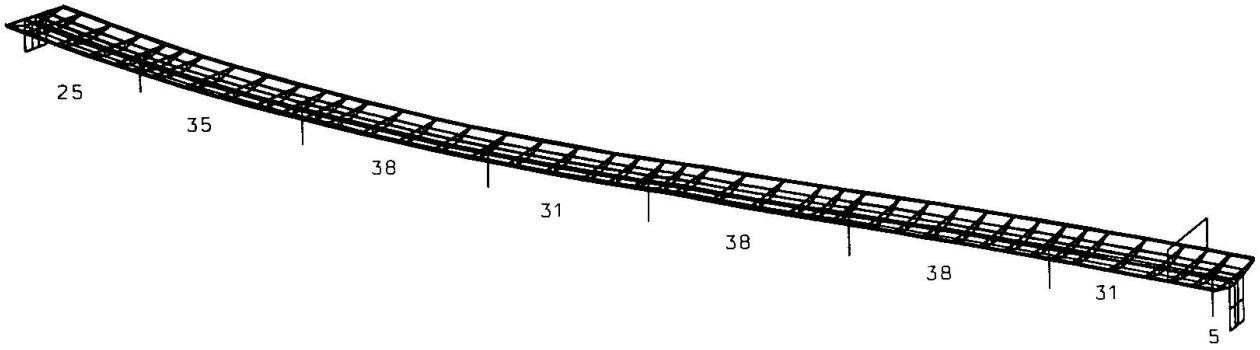

Fig. 4 Westend Bridge: Finite Element model. Span lengths are indicated in m.

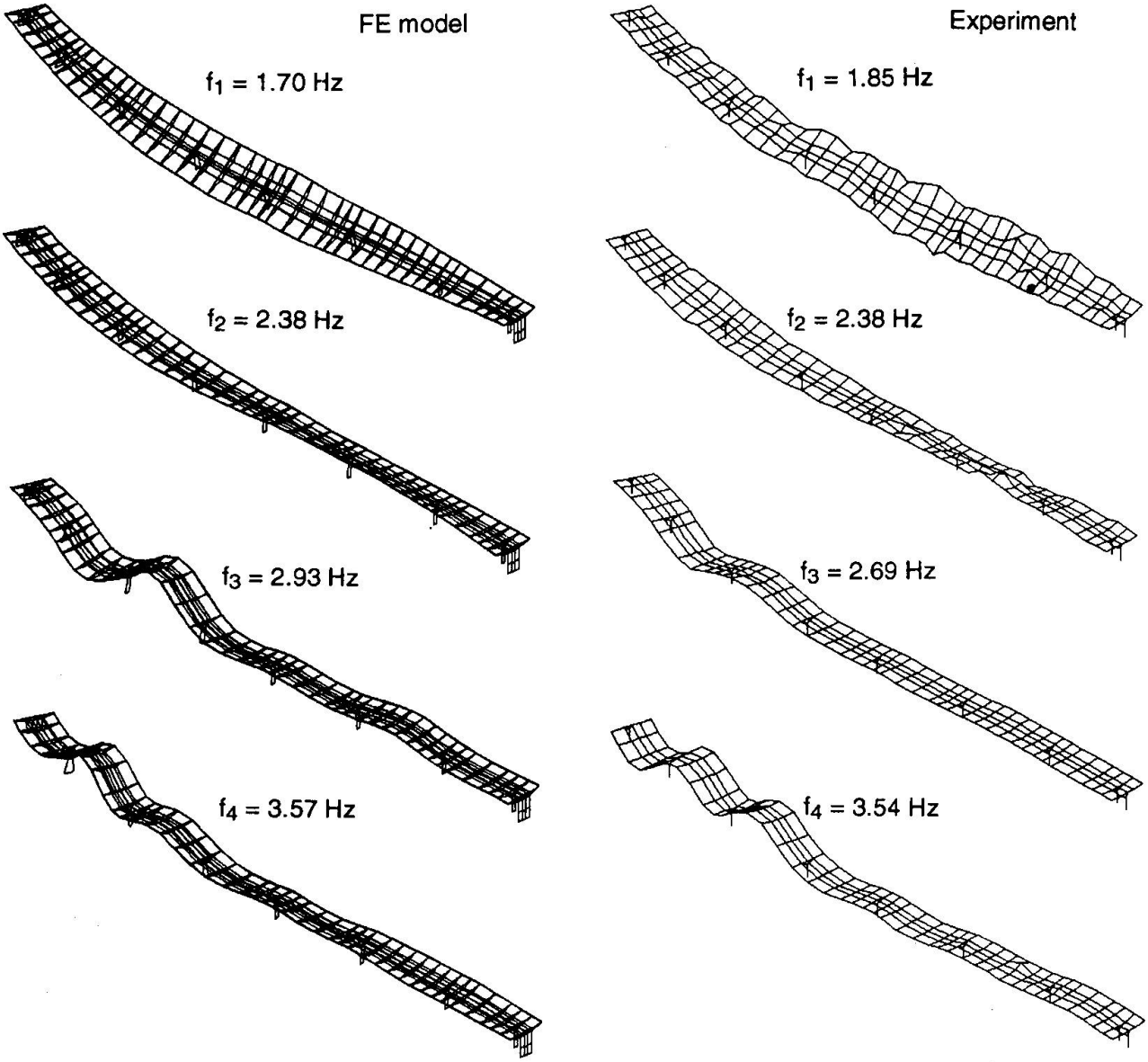

Fig. 5 Westend Bridge: Frequencies and mode shapes: FE-model vs. experiment.

Thermal Deformations in Segmental Concrete Structures

Déformations thermiques des voussoirs en béton armé

Temperaturdeformationen in segmentweisen Betonkonstruktionen

Michail GRANOVSKY
Civil Engineer
Research Inst. of Transp. Constr.
Moscow, Russia

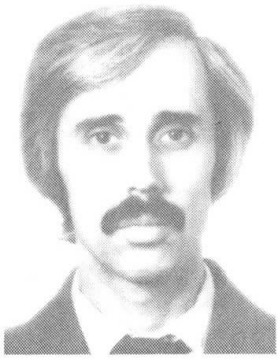

Michail Granovsky, born 1960, graduated from Moscow Railway Engineers Institute, received his Cand.Sc. degree at the Research Institute of Transport Construction where he was involved in the analysis of temperature regimes in transportation structures.

SUMMARY

The paper deals with the development of a procedure for the analysis of temperature fields, stresses and deformations in segmental concrete structures in the course of their fabrication. Application of the procedure is demonstrated by the example of analysis of three-dimensional deformations of segments fabricated by the match casting method for bridge superstructures.

RÉSUMÉ

Le rapport traite de la méthode de calcul des champs thermiques de contraintes et de déformations dans les voussoirs en béton armé en cours de fabrication. L'application de la méthode est illustrée par l'exemple du calcul des déformations des éléments de voussoirs préfabriqués en béton.

ZUSAMMENFASSUNG

Im Vortrag wird die Entwicklung eines Verfahrens zur Berechnung von Temperaturfeldern, Spannungen und Verformungen in segmentweisen Betonkonstruktionen während der Herstellung behandelt. Eine Anwendung dieses Verfahrens wird am Beispiel der Berechnung von dreidimensionalen Verformungen bei Brückensegmenten gezeigt.

1. METHOD OF ANALYSIS

Lengthy segmental concrete structures are being widely used nowadays for construction industry as a whole and for bridge building in particular. They are, first of all, bridge superstructures and piers field erected from separate segments with usage of reinforcing steel and glued joints. The abovesaid segments are precast constructions which fabrication is carried out by match casting method using purpose-designed forms. According to this method, which is rather popular in the USSR, end face of the earlier built segment is used instead formwork for concreting and hardening of the next segment, which would provide ideal coincidence of segments end faces when erecting a structure. In this case in the course of fabrication fresh concrete, in which intensive heat release due to cement hydration takes place, comes into contact with the "old" concrete of the previously fabricated structure. Similar situation occurs when erecting superstructure by cantilever method and constructing high bridges piers and pylons in a slipform, etc.

As a result of intensive processes of heat release and heat exchange, complicated spatial temperature fields, continuously varying with time, are being formed in the structures under fabrication, which induce growth of temperature stresses and strains. In some cases they may be of critical value and lead to cracks occurence, structure's axis deviation from the design position and other negative post-effects. This is why prediction of such temperature fields and thermostressed state is considered to be challenging engineering problem, especially when designing extraordinary structures.

It should be noted that the problem under consideration, i.e. investigation of thermostressed state of various structures, has been a subject of extensive research and its results are available in the literature. But for our case, the problem seems to be specific, presenting significant difficulties for its solution and requiring development of purpose-designed procedure.

First of all should be considered the effect of cement exothermicity, which conditions largely temperature field to be formed. The intensity of cement heat release is known to have rather sophisticated dependence both on concrete temperature at a given moment and on all the previous "temperature history" beginning from concrete mix placing. This factor necessitates solution of two problems: that of heat conductivity and heat release one, being described by interdependent differential equations.

The structures to be constructed have often rather complex cross-sectional profile (box segments, slab-ribbed structures, etc.). On the other hand, the length of a segment to be cast has sizes, comparable with those of cross-section. All this requires the problem solution in three-dimensional formulation, otherwise it is of no avail.

And the last. It is evident that every time when concreting the next segment increment of design area takes place. When fabricating segments by match casting method the process seems to be more complex, as first takes place increment of design area when concreting a new segment in contact with the previous one, and then its decrease when separating segments. Temperature fields in a "new"segment and earlier built section of the structure have

strong reciprocal effect. The latter should be taken into consideration in the design scheme and analysis procedure.

This complicated problem may be more effectively solved by means of temperature fields and stresses simulation on the basis of advanced numerical methods and use of computering devices.

As a result of investigations conducted, special procedure and programs package related have been developed, which make possible calculation of three-dimensional non-stationary temperature field and spatial stress-strain state, induced by change of the field by the structure volume. The procedure is based on plotting of discrete design diagram and use of relevant numerical methods. Digitization is carried out by division of the design area into finite elements in the form of rectangular prisms. Calculation is performed in two stages. First the problem of non-stationary heat conductivity with internal heat sources is solved to determine temperature fields for the time of our interest. Afterwards thermoelasticity is determined and stresses and deformations (displacements), occured under changed temperature field are calculated, assuming structure elastic behaviour.

Programs package featurescombination of two various numerical methods - finite difference method, being used for solution of heat conductivity problem and finite element method, being used for that of thermal conductivity. In our opinion it makes it possible to realize the both methods advantages and to obtain optimal complex, combining high effectiveness, simplicity and applicability. Finite element's simple form selected allows preservation of the same discrete scheme when changing thermal analysis for thermoelastic one. The difference is in unknown parameters: in the first case they are temperatures in the elements centres, while in the second one-their nodes displacements.

Significant advantage of the complex over the other ones is involvement of the procedure of cement heat release consideration. Advancements in the field of investigations of hardening concrete heat release phenomenon have been used for this complex development. The studies conducted showed that intensity of elementary volume heat release was proportional to maximum heat release by cement weight unit, to cement consumption per 1 m^3 of concrete mix, to portion of the cement, unreacted by the given time and to coefficient, depending on the given point temperature. In its turn, the quantity of unreacted cement depends, in a rather complicated way, on "temperature history" of elementary volume, beginning from the moment of concrete mix placement. So, when solving heat conductivity problem, for every time step is first determined heat release in every element, then change of its heat content due to released heat and heat exchange with the adjacent elements and, finally, change of temperature; afterwards the process is repeated by cycles.

The procedure allows consideration of nonuniform heat release by the structure volume, change of its time intensity and interdependence with temperature field.

The program developed makes it possible to change design area geometry by increasing or decreasing its dimensions, which allows development of mathematical model, featuring adequately technological process, consideration of temperature fields reciprocal effect in structure various sections, being cast at different time.

The programs package developed, not being universal, is meanwhile rather useful and effective means for calculation of temperature fields, stresses and strains in reinforced concrete structures, constructed by concreting by lifts, match casting or some other methods, when change of design area geometry should be considered for calculation. The program requires minimum of initial data, allows partial computerization of their preparation process, has high internal performance and quantitative capabilities. It has easy information input and exchange with external memory. Its programming language is FORTRAN.

2. ANALYSIS OF THERMAL DEFORMATIONS OF REINFORCED CONCRETE BOX SEGMENTS FOR HIGHWAY BRIDGES SUPERSTRUCTURES

On the basis of the procedure developed and program package there has been conducted a series of calculations to determine thermal regime and thermostressed state of reiforced concrete box segments, being constructed by match casting method, for highway bridges superstructures. The purpose of the calculations was to define the effect of thermal treatment various regimes on the mode and size of deformations, developing after segments cooling. Segments had 3,4 m depth, 12,5 m width of upper plate and 2 m length along the axis.

The problem is that coincidence of adjacent end faces of neighbouring segments, which should be provided by the technology used, i.e. due to matching of every next segment to be cast on the end face of the previously cast one, is frequently disturbed in practice. To a considerable extent it is related to thermal deformations growth. The matter is that in the course of hardening on a mould there are being formed temperature fields, which are significantly nonuniform by volume, as a result of thermal treatment as well as concrete self-heating due to cement exothermicity. Segment being at various stages of hardening, those fields are different.Complicated spatial stress-strain state is being developed in segments after their separation and temperatures gradual equalization. The abovementioned state induces, in particular, deformation of end faces, leading to disturbance of segments coincidence. When erecting a superstructure this results in segments turn relatively to each other, structure's axis deviation from the design position and differential size of a gap between adjacent faces. All the said effects negatively on the quality of glued joints used, aggravating their physical and mechanical properties.

To improve the quality of segments production optimal technological regimes should be selected, which would provide minimum thermal deformations or would compensate their growth by structural means. To this end, should be studied the nature of various thermal regimes effect on segments deformation, developing after cooling.

We set the problem basing on the assumption that after thermal treatment, i.e. by the moment of segments separation, their adjacing faces coincide completely. To find out mutual arrangement of segments during structure assemblage, first of all we have to obtain spatial pattern of deformed end faces. This pattern would be dependent on the thermostressed state, developing in every segment under change of temperature field - from that for separation moment to some constant by volume (equal to am-

bient air temperature). It should be noted that the absolute value of that constant is of no importance, as change of temperature by the whole volume of a free body by the same value results in the only uniform change of its linear dimensions, but doesn't change its stress-strain state. Besides, accounting for the assumption accepted, the problem of initial stresses by the separation moment, being rather complicated, may not be considered as a solved one. The object of our interest should be alteration of thermostressed state within two specified periods of time, leading to occurence of deformations under consideration. The problem was formulated for elastic behaviour, without consideration of reinforcement. Concrete was considered as homogeneous isotropic medium with constant mechanical and thermophysical characteristics.

As per the procedure developed, analysis of temperature fields, being generated in segments by the moment of their separation, was conducted in several phases with alteration of design scheme when changing one phase for the other according to technological cycle stages. The said allowed consideration of mutual effect of segment-matrix and segment-match temperature fields. Various thermal treatment regimes were considered for the analysis. Temperature of heating, conditions of thermal exchange on the surface, etc. varied. (In all the cases heating formwork was on the segment's exterior surface, except the upper slab).

As a result of calculations data have been obtained on temperature distribution by the volume of each of two segments by the moment of their separation. Data on the magnitudes of thermoelastic displacements of points, being on the segments end faces, have been obtained as well. The latter characterize the nature and extent of end faces deformation after complete cooling of segments up to ambient air temperature, providing that temperature field at the separation moment is taken as initial state. Just those values show the possible degree of non-coincidence of adjacent segments end faces, resulting from temperature deformations, induced in the course of cooling. Here, the final objective of the calculations was determination of surface points displacement, but not stresses field, which is typical of the most problems.

Analysis of the results obtained showed that temperature fields in segments after thermal treatment completion have complicated non-uniform and pronounced three-dimensional mode, conditioned, to a considerable extent, by segments reciprocal effect. Here, temperature fields of the segment-matrix and segment-match differ significantly, which is obvious in Fig.1 and 2. As the structure and boundary conditions are symmetrical relatively to vertical plane, passing through segment's axis, then all the fields of temperatures and displacements appear to become symmetrical as well. That's why the fields, given below, are plotted for the half of a segment cross-section.

The results of thermoelastic analysis evidence that after segments cooling their end faces are being deformed and have complicated curved shape. Here, adjacent end faces of the neighbouring segments deform differently, which results in their non-coincidence. It should be noted that though analysis data describe completely three-dimentional mode of segments deformation, they don't give answer to the question about the position of

segments and gap size between them, when trying to assemble those segments with deformed end faces, joining them by means of cantilever method. To answer the above question complicated geometrical problem on tangency of two curved faces should be solved. We managed to obtain rather simple solution of the problem on the basis of graphoanalytical methods used. But its description cannot be presented because of the paper content limitation. Use of this procedure made it possible to determine for all the variants considered the angle of segments turn relatively to one another, which is the result of non-coincidence of end faces during segment assemblage, and to define deviation of superstructure's axis from the design position. Besides, fields have been plotted, featuring distribution of gap size (glued joint thickness)on the latter surface, one of which is given in Fig.3. Attention should be paid to the fact that there are given not absolute values of joint thickness, but values for this thickness excess over some minimum one, which would be in "tangential points, marked by circles.

As a result of investigations conducted all the necessary conclusions have been drawn and measures have bee proposed to improve the technology for superstructure segments fabrication by match casting method.

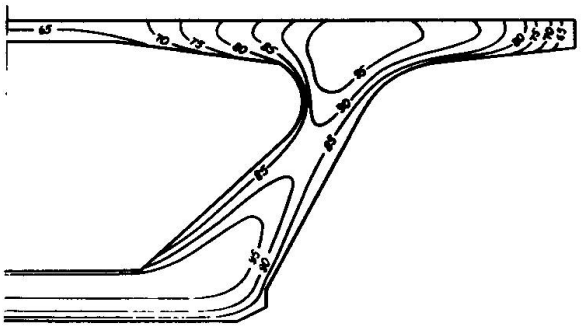

Fig.1 Temperature field in the middle section of a segment-matrix (isolines values are given in °C)

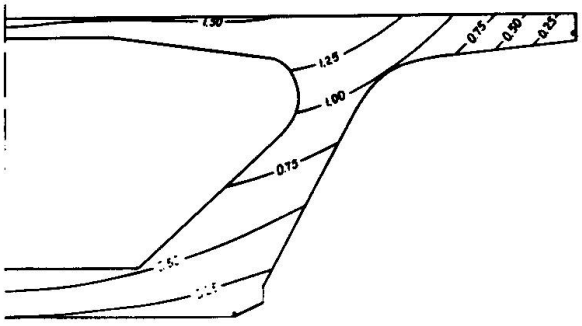

Fig.3 Distribution of glued joint thickness along its surface (isolines values are given in mm)